

STAGED FIELD EXPERIMENT NO. 3

*Application of Advanced
Technologies in
Tight Gas Sandstones -
Travis Peak and Cotton
Valley Formations,
Waskom Field,
Harrison County,
Texas*



GAS RESEARCH INSTITUTE

GRI DISCLAIMER

LEGAL NOTICE: This publication was prepared as an account of work sponsored by the Gas Research Institute (GRI) and other organizations. Neither GRI, members of GRI nor any person acting on behalf of either:

- makes any warranty or representation, express or implied, with respect to the accuracy, completeness, or usefulness of the information contained in this report, or that the use of any information, apparatus, method or process disclosed in this report may not infringe privately-owned rights; or
- assumes any liability with respect to the use of, or for damages resulting from the use of, any information, apparatus, method or process disclosed in this report.

Reference to trade names or specific commercial products, commodities or services in this report does not represent or constitute an endorsement, recommendation or favoring by GRI of the specific commercial product, commodity or service.

STAGED FIELD EXPERIMENT NO. 3

*Application of Advanced
Technologies in Tight
Gas Sandstones -
Travis Peak and Cotton Valley
Formation, Waskom Field,
Harrison County, Texas
Reservoirs*

Report No. GRI-91/0048

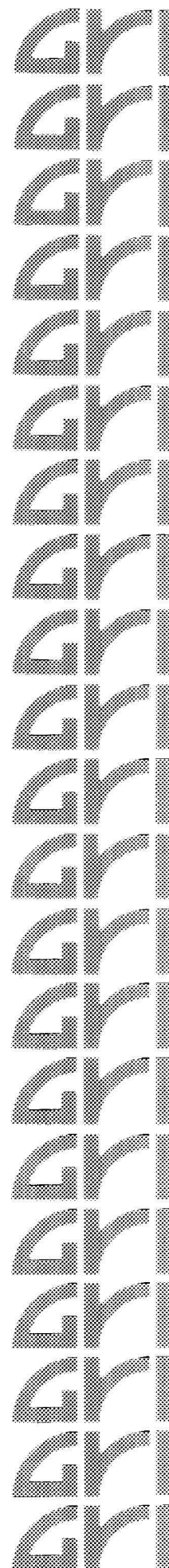
Compiled and Edited by
CER CORPORATION
950 Grier Drive
Las Vegas, NV 89119

and

S.A. HOLDITCH & ASSOCIATES, INC.
900 Southwest Parkway East
College Station, TX 77840

Prepared For
GAS RESEARCH INSTITUTE
8600 W. Bryn Mawr Avenue
Chicago, Illinois 60631

FEBRUARY 1991



REPORT DOCUMENTATION PAGE	1. REPORT NO. GRI-91/0048	2.	3. Recipient's Accession No.
4. Title and Subtitle		5. Report Date February 1991	
7. Author(s)		6.	
9. Performing Organization Name and Address <i>Compiled and Edited By:</i> CER Corporation 950 Grier Drive Las Vegas, NV 89119		8. Performing Organization Rept. No.	
S.A. Holditch & Associates 900 Southwest Parkway East College Station, TX 77840		10. Project/Task/Work Unit No.	
12. Sponsoring Organization Name and Address Gas Research Institute 8600 West Bryn Mawr Avenue Chicago, IL 60631		11. Contract(C) or Grant(G) No. (C) 5090-211-1940 (G)	
15. Supplementary Notes Principal contributing organizations include Bureau of Economic Geology, University of Texas at Austin; CER Corporation; Resources Engineering Systems; ResTech Houston; S.A. Holditch & Associates; and Teledyne Geotech		13. Type of Report & Period Covered Topical Report	
16. Abstract (Limit: 200 words) Staged Field Experiment No. 3: Application of Advanced Technologies in Tight Gas Sandstones - Travis Peak and Cotton Valley Formations, Waskom Field, Harrison County, Texas The Gas Research Institute has sponsored research directed towards improving the recovery efficiency and reducing the cost of producing gas from tight reservoirs. To more effectively acquire data and perform research experiments, the concept of Staged Field Experiments (SFEs) was developed. SFE No. 3 is the third well in a series of four SFEs. The well is located in the Waskom Field in Harrison County, Texas. Engineering and geologic data were measured and analyzed on the Travis Peak and Cotton Valley Formations. SFE No. 3 provided a field laboratory site to test technology on in-situ stress profiling, fracture diagnostics, real-time fracture analysis, and pre- and post-fracture well performance analysis. This report documents the detailed information and results from GRI's research efforts in SFE No. 3.		14.	
17. Document Analysis a. Descriptors Tight Gas Sandstones In-Situ Stress Testing Fracture Diagnostics Hydraulic Fracturing b. Identifiers/Open-Ended Terms East Texas, Travis Peak Formation, Cotton Valley Formation Staged Field Experiment No. 3 c. COSATI Field/Group			
18. Availability Statement Release Unlimited		19. Security Class (This Report) Unclassified	21. No. of Pages 253
		20. Security Class (This Page) Unclassified	22. Price

Research Summary

Title Staged Field Experiment No. 3: Application of Advanced Technologies in Tight Gas Sandstones - Travis Peak and Cotton Valley Formations, Waskom Field, Harrison County, Texas

Contractors Bureau of Economic Geology, University of Texas at Austin
CER Corporation
Resources Engineering Systems, Inc.
ResTech, Inc.
S.A. Holditch & Associates, Inc.
Teledyne Geotech

Objectives A major objective of the GRI Staged Field Experiment Program has been to develop technology using experiments conducted in field laboratories. To test technology on in-situ stress profiling, real-time hydraulic fracture analysis and pre- and post-fracture well performance analysis. In particular, SFE No. 3 provided the opportunity to perform experimentation designed to verify hydraulic fracture height.

Technical Perspective Significant amounts of potentially recoverable natural gas exist in low-permeability sandstone formations located in sedimentary basins throughout the United States. However, a combination of technical and economic constraints prevents the widespread commercial exploitation of these resources. These constraints include (1) uncertainty as to the parameters critical to gas production from tight sands and (2) lack of a consistently effective hydraulic fracturing treatment method that allows economic gas production from tight gas sands. GRI analyses indicate that evolutionary improvements in technologies and practices could significantly increase the amount of cost-competitive gas recoverable from tight sands.

The major focus of GRI's strategy to improve technology is to conduct an integrated program emphasizing three major R&D needs: (1) improved geology and resource parameter quantification; (2) enhanced stimulation techniques including real-time analysis and control of hydraulic fracturing parameters; and (3) improved fracture diagnostics for determining fracture azimuth, fracture height and overall fracture dimensions.

Technical Approach To effectively acquire data, perform research experiments and validate models and technology in a relatively unrestricted environment, a research well drilled and completed under the supervision and control of GRI contractors was required. With a GRI-controlled well, more intensive open-and cased-hole data acquisition programs could be implemented, and a completion program could be structured around the acquisition and evaluation of research data. In drilling and completing the SFE No. 3 well, each of the GRI Tight Gas Sands Program

Contractors could field their technologies with extended time and risk allocations. The high-quality data set collected would be analyzed and subsequently integrated into a complete characterization of the Travis Peak low permeability reservoirs. These characterizations, in turn, would support the reservoir testing and fracture stimulation programs designed to improve gas recovery from tight sandstone reservoirs.

Results

Between September 1988 and March 1989, the Taylor Sandstone in the lower Cotton Valley Formation was drilled, tested and fracture treated in the SFE No. 3 well. Initially, an extensive open-hole data acquisition program was implemented in SFE No. 3. This program included coring, MWD logging, wireline logging (multiple passes) and open-hole stress testing. Using the recovered core, comprehensive geologic analyses and extensive routine and special core analyses in the Travis Peak and Cotton Valley Formations were performed. After casing was set, the data acquisition program included wireline logging to estimate fracture height and evaluate cement bond and cased-hole stress tests.

An extensive data set was also collected during well testing and fracture treatments performed in the Taylor Sandstone. Pre-fracture flow and pressure buildup testing were performed and resulted in estimates of formation properties. Two mini-fracs were also performed to gather data for estimating fracture height and azimuth and to acquire information to calibrate the fracture propagation model. Interpretation of passive seismic data indicated that the mini-frac had a height of approximately 300 ft and strike of N77°E.

The main hydraulic fracture treatment consisted of over 1.1 million pounds of proppant and 9,500 barrels of fluid. All of the important fracture treatment data were monitored, measured and recorded during the treatment. Post-fracture well testing was performed, and the data were analyzed using a three-phase, three-dimensional reservoir simulator. A history match resulted in estimates of fracture and formation properties. On the basis of the post-fracture data, it is estimated that SFE No. 3 will produce 1.14 BCF over a 20-year period from the completed interval.

Contents

EXECUTIVE SUMMARY	E-1
1.0 INTRODUCTION AND SUMMARY	1
1.1 Concept of Staged Field Experiments	1
1.2 SFE No. 3 Site Selection Criteria	1
1.3 Principal Advancements Resulting from SFE Research	4
1.3.1 In-Situ Stress Profiling	4
1.3.2 Fracture Height Analysis	4
1.3.3 Hydraulic Fracture Analysis	7
1.3.4 Post-Fracture Performance Analysis	8
2.0 SFE NO. 3 DATA ACQUISITION OBJECTIVES AND RESULTS	11
2.1 Open-Hole Data Acquisition	11
2.1.1 Drilling Operations Summary	11
2.1.2 Coring Objectives and Results	11
2.1.3 Core Orientation Objectives and Results	15
2.1.4 Geophysical Wireline Logging Objectives and Results	15
2.1.5 Downhole Measurements-While-Drilling	17
2.1.6 Surface Measurements-While-Drilling	18
2.1.7 Open-Hole Stress Testing	19
2.2 Cased-Hole Data Acquisition	21
2.2.1 Cased-Hole Logging	21
2.2.2 In-Situ Stress Testing	22
2.3 Summary of Well Testing and Completion Operations	23
2.3.1 Pre-Fracture Tests	23
2.3.2 Fracture Treatments	24
2.3.3 Post-Fracture Tests and Production History	25

3.0	GEOLOGICAL ANALYSIS OF THE TRAVIS PEAK FORMATION AND COTTON VALLEY SANDSTONE	27
3.1	Geologic Setting	27
3.1.1	Regional Structural Setting of the East Texas Basin	27
3.1.2	Local Structural Setting of Waskom Field	27
3.1.3	Regional Stratigraphy and Depositional Systems of the Travis Peak Formation and Cotton Valley Group	30
3.1.4	Local Stratigraphic Setting of Waskom Field	30
3.2	Sedimentological Analyses - Summary and Conclusions	31
3.2.1	Stratigraphy of Travis Peak and Cotton Valley, Waskom Field	32
3.2.2	Macroscopic Core Descriptions and Interpreted Depositional Environments	33
3.2.3	Petrographic Description	40
3.3	Structural Geology Analysis of SFE No. 3 Data - Objectives and Conclusions	54
3.3.1	Analysis of Natural Fractures	55
3.3.2	Drilling-Induced Fractures and Direction of S_{Hmax}	63
3.3.3	Open-Hole Stress Test Fractures and Direction of S_{Hmax}	65
3.4	Application of Geological Analyses to the SFE No. 3 Completion Strategy	65
4.0	WELL LOG AND CORE ANALYSES IN THE COTTON VALLEY FORMATION	67
4.1	Results of Well Log Analyses and Selection of Completion Intervals	67
4.1.1	Log Analysis Methodology and Petrophysical Modeling	67
4.1.2	Interpretation Techniques and Application of Acoustic Well Log Data to Calculations of Rock Mechanical Properties and In-Situ Stress	74
4.2	Results and Application of Core Analysis	82
4.2.1	Routine core Analysis Measurements	82
4.2.2	Special Core Analysis Measurements	84

4.2.3	Effects of Clay Dehydration on Core Analysis	98
5.0	IN-SITU STRESS TESTING AND STRESS PROFILING	107
5.1	In-Situ Stress Testing	107
5.1.1	Introduction	107
5.1.2	Open-Hole Stress Tests	107
5.1.3	Cased-Hole Stress Tests	107
5.2	Vertical Stress Profiling Through Integration of Log-Derived Rock Mechanical Properties and In-Situ Stress Tests	109
5.2.1	Introduction	109
5.2.2	Review of SFE No. 1 and SFE No. 2 Results	111
5.2.3	Permeability and Stress Profiles for SFE No. 3	113
5.2.4	Summary of In-Situ Stress Profiling	115
6.0	ANALYSES AND INTERPRETATIONS OF PRE-FRACTURE DATA	121
6.1	Production and Pressure Buildup Tests	121
6.2	Execution and Analysis of Mini-Frac Treatments	124
6.2.1	Mini-Frac No. 1	124
6.2.2	Mini-Frac No. 2	126
6.2.3	Microseismic Analysis of Mini-Frac No. 1: Azimuth and Height	129
6.2.4	Analysis of Mini-Frac No. 1 With 3-D Fracture Simulator	144
6.2.5	Analysis of Mini-Frac No. 2 With 3-D Fracture Simulator	151
7.0	HYDRAULIC FRACTURE TREATMENT OF THE LOWER COTTON VALLEY FORMATION (TAYLOR SANDSTONE)	155
7.1	Treatment Objectives and Design	155
7.2	Treatment Monitoring and Quality Control	158
7.2.1	Quality Control of the Fracturing Fluids	158
7.2.2	Measurement of Fracture Treatment Data	160
7.3	Analysis with 3-D Fracture Simulator	162

7.3.1	Net Pressure Analysis	162
7.3.2	Main-Fracture Dimensions	164
8.0	POST-FRACTURE ANALYSIS	171
8.1	Production Performance	171
8.2	Conventional Well Test and Pressure Buildup Analysis	171
8.3	Reservoir Simulation	175
8.3.1	Description of Models	175
8.3.2	Analysis Using Type I Model	178
8.3.3	Analysis Using Type II Model	178
8.3.4	Analysis Using FAST	181
8.3.5	Analysis Using Type III Model	181
8.4	Microseismic Analysis of the Treatment-Induced Fracture After Four Months of Production	190
8.4.1	Objectives	190
8.4.2	Field Operations and Data Acquisition	190
8.4.3	Hydraulic Fracture Orientation	191
8.4.4	Hydraulic Fracture Height	194
8.5	Fracture Height Proof-Of-Concept Experiment	194
8.5.1	Experiment Design	195
8.5.2	Results and Interpretation	196
9.0	REFERENCES	201
	NOMENCLATURE	207
	APPENDIX 1	
	Logging Operations	209
	APPENDIX 2	
	Well Test Analysis and Fracture Treatment Summary	225
	APPENDIX 3	
	Routine Core Analysis Results	243

Figures

Figure E-1	Pre-Fracture Analysis Results for the Completion Interval, SFE No. 3	E-2
Figure E-2	Permeability-Thickness Profile and Stress Profile of the Completion Interval in SFE No. 3	E-2
Figure E-3	Proppant Concentrate Profile at Treatment Shut-In Using Log-Derived Stresses	E-5
Figure E-4	Reservoir Model for Final History Match, SFE No. 3	E-6
Figure 1-1	Regional Location of the SFE No. 3 Well	5
Figure 1-2	Location of SFE No. 3 Well in the Waskom Field	6
Figure 2-1	Time Versus Depth Drilling Curve for SFE No. 3	13
Figure 2-2	SFE No. 3 Wellbore Schematic Showing Casing and Cementing Record	13
Figure 3-1a	Structural Setting of the Study Area in the Northern Gulf of Mexico Basin	28
Figure 3-1b	Location of Gas Research Institute Research Wells in East Texas	28
Figure 3-2	Structure Map of the Top of the Lower Cotton Valley Taylor Sandstone, Waskom Field	29
Figure 3-3	Gamma Ray and Resistivity Logs of Lower Travis Peak, SFE No. 3	32
Figure 3-4	Gamma Ray and Resistivity Logs of Lower Cotton Valley Sandstone and Upper Bossier Shale, SFE No. 3	32
Figure 3-5	Cross Section of Lower Cotton Valley Taylor Sandstone Interval in the Area Around the SFE No. 3	34
Figure 3-6	Net Sandstone Isolith Map of Upper Taylor Sandstone, Waskom Field	35
Figure 3-7	Net Sandstone Isolith Map of Lower Taylor Sandstone, Waskom Field	36

Figure 3-8a	Freeze-Dried Sample in Which Fibrous Illite Has Replaced Feldspar Grain, SFE No. 3	48
Figure 3-8b	Freeze-Dried Sample Which Lacks Significant Illite Growth, SFE No. 3	48
Figure 3-8c	Freeze-Dried Sample With Fibrous Illite Coating Quartz Grain, SFE No. 3	49
Figure 3-8d	Freeze-Dried Sample With Bladed Illite Morphology, SFE No. 3	49
Figure 3-9a	Delicate Illite Fibers in Freeze-Dried Sample from 7,388.8 ft, SFE No. 3	50
Figure 3-9b	Collapsed Illite Fibers in Extraction-Dried Part of Sample from 7,388.8 ft, SFE No. 3	50
Figure 3-9c	Illite Fibers in Freeze-Dried Part of Sample from 7,382.7 ft, SFE No. 3	51
Figure 3-9d	Matted and Collapsed Illite Fibers in Air-Dried Part of Sample From 7,382.7 ft, SFE No. 3	51
Figure 3-10	Photomicrograph of Quartz-Cemented Sandstone from 9,275.6 ft	53
Figure 3-11	Ferroan-Calcite Cement Filling Primary Pores and Intragranular Secondary Porosity	53
Figure 3-12	Photograph of Natural Extension Fractures in the Taylor Sandstone at a Depth of 9,246 to 9,251 ft	61
Figure 3-13a	Vertical Fracture Length (Height) of Natural Fractures in Travis Peak and Cotton Valley Core Plotted Against Depth, SFE No. 3	62
Figure 3-13b	Vertical Fracture Length (Height) of Natural Fractures in Taylor Sandstone Plotted Against Depth, SFE No. 3	62
Figure 3-14	Examples of BHTV and FMS Logs Imaging Fractures in the Taylor Sandstone	63
Figure 3-15	Lengths of Drilling-Induced Fractures in SFE No. 3 Core	64
Figure 3-16	Drilling-Induced Fracture Strike in SFE No. 3 Core	65

Figure 4-1	Presentation of the Log Results Over the Completed Interval in SFE No. 3 Displayed With Core Analysis	68
Figure 4-2	Comparison of Log-Derived Clay Volume and Thin-Section Clay Volume	71
Figure 4-3	Comparison of Log-Derived Lithology and Thin-Sections	72
Figure 4-4	Comparison of Log-Derived Porosity and Core Porosity Measured at Net Overburden Pressure	73
Figure 4-5	Comparison of Log-Derived Permeability and Water Saturation to Core Data	75
Figure 4-6	Computed Closure Stress Gradient Versus Measured Closure Stress Gradient in the Cotton Valley Formation of SFE No. 3	77
Figure 4-7	Pre-Fracture Analysis Results for the Completion Interval, SFE No. 3	80
Figure 4-8	Frequency Percent of Klinkenberg-Corrected Gas Permeability at 800 psi Stress Measured from Routine Core Analysis in the Cotton Valley, SFE No. 3	85
Figure 4-9	Frequency Percent of Porosities Measured from Routine Core Analysis in the Cotton Valley, SFE No. 3	85
Figure 4-10	Frequency Percent of Grain Density Measured from Routine Core Analysis in the Cotton Valley, SFE No. 3	86
Figure 4-11	Formation Resistivity Factor Versus Porosity Measured at NOB Stress for Cotton Valley, SFE No. 3	93
Figure 4-12	Resistivity Index Versus Water Saturation Measured at NOB Stress for Cotton Valley, SFE No. 3	95
Figure 4-13	Typical Set of Gas and Water Relative Permeability Curves for Cotton Valley Sandstone, Sample Depth 9,295.0 ft	95
Figure 4-14	Klinkenberg-Corrected Gas Permeability Versus Porosity Measured at NOB Stress for Cotton Valley, SFE No. 3	96
Figure 4-15	Brine Permeability Versus Klinkenberg-Corrected Gas Permeability at NOB Stress for Cotton Valley, SFE No. 3	97
Figure 4-16	Gas Relative Permeability With Normalized Gas Saturations for Cotton Valley, SFE No. 3	97

Figure 4-17	Water Relative Permeability Correlated with Normalized Water Saturation for Cotton Valley, SFE No. 3	98
Figure 4-18	Typical Air-Brine Capillary Pressure Behavior for Cotton Valley Sandstone, Sample Depth 9,295.0 ft	99
Figure 4-19	Comparison of Effective Permeability to Gas and Water of Preserved Versus Extracted/Restored Core at 7,387.8 ft at Various Gas Saturations	102
Figure 4-20	Comparison of Capillary Pressure Behavior of Core Sample at 7,387.7 ft, Preserved Versus Extracted/Restored	104
Figure 4-21	Comparison of Electrical Resistivity of Core Sample at 7,383.3 ft, Preserved Versus Extracted/Restored	104
Figure 5-1	Log-Log Plot of Cased-Hole Stress Test No. 1	110
Figure 5-2	Linear Flow Analysis of Cased-Hole Stress Test No. 1	110
Figure 5-3	Measured Closure Stress Versus Poisson's Ratio Function for SFE No. 2	112
Figure 5-4	Preliminary Stress Profile Calibrated With Open-Hole Test Data From SFE No. 3	114
Figure 5-5	Measured Closure Stress Versus Poisson's Ratio Function	115
Figure 5-6	Comparison of Measured Stress With Stress Profile Generated Using Elastic Model	16
Figure 5-7	Final Correlation Between Log-Derived Closure Stress Gradient and Measured Closure Stress Gradient	117
Figure 5-8	Permeability-Thickness Profile and Stress Profile of the Completion Interval in SFE No. 3	118
Figure 5-9	Computed Values for Poisson's Ratio and Young's Modulus for the Completion Interval in SFE No. 3	119
Figure 6-1	Horner Analysis of the Pressure Buildup Test Conducted Before Mini-Frac No. 1	122
Figure 6-2	Type Curve Analysis of the Pressure Buildup Test Conducted Before Mini-Frac No. 1	122
Figure 6-3	Horner Analysis of the Pressure Buildup Test Conducted After Mini-Frac No. 1	123

Figure 6-4	Type Curve Analysis of the Pressure Buildup Test Conducted After Mini-Frac No. 1	123
Figure 6-5	Bottomhole Pressure History During Mini-Frac No. 1	127
Figure 6-6	Treatment Data History During Mini-Frac No. 1	128
Figure 6-7	Pressures Measured During Mini-Frac No. 2, SFE No. 3	129
Figure 6-8	Low-Frequency Signals Recorded at 9,000 ft and 9,100 ft During Shut-In Stages of Mini-Frac No. 1	131
Figure 6-9	Upper Hemisphere Stereographic Projection of Particle Motion Orientations for Low-Frequency Signals Recorded at 9,000 ft, 9100 ft and 9,590 ft During Shut-In	132
Figure 6-10	Comparison of Low-Frequency Signals Recorded at 9,590 ft During Flowback to Typical High-Frequency Signals Recorded at 9,590 ft During Shut-In	133
Figure 6-11	Typical Low-Frequency Signals Recorded at 9,590 ft During Flowback Following Stage 9 of Mini-Frac No. 1	134
Figure 6-12	Amplitude and Interval Distributions of Low-Frequency Signals Recorded at 9,590 ft During Flowback Following Stage 9 of Mini-Frac No. 1	135
Figure 6-13	Upper Hemisphere Stereographic Projection of Particle Motion Orientations for Low-Frequency Signals Recorded at 9,590 ft During Flowback	136
Figure 6-14	Total Background Particle Velocity Before and During Mini-Frac No. 1 Versus Depth	140
Figure 6-15	Total RMS Background Particle Velocity After Main Fracture and Production Versus Depth	140
Figure 6-16	Pre-Perforation H/Z Ratio Using Unfiltered Motion Data and Stress Profile Versus Depth	142
Figure 6-17	Pre-Perforation H/Z Ratio With 75 Hz High-Pass Filter Versus Depth	142
Figure 6-18	Pre-Mini-Frac, Post-Perforation H/Z Ratios Versus Depth	143
Figure 6-19	Mini-Frac Stage 3 H/Z Ratios Versus Depth	143
Figure 6-20	Mini-Frac Stage 9 H/Z Ratios Versus Depth	144

Figure 6-21	Mini-Frac No. 1 Pressure Match With Stresses From Logs	145
Figure 6-22	Mini-Frac No. 1 Pressure Match With Modified Stresses	145
Figure 6-23	Mini-Frac No. 1 Dimensions With Stresses From Logs	149
Figure 6-24	Mini-Frac No. 1 Dimensions With Modified Stresses	149
Figure 6-25	Net Pressure Prediction for Main Frac Based on Early Treatment Design	151
Figure 6-26	Dimensions Prediction for Main Frac Based on Early Treatment Design	152
Figure 6-27	Propped Dimensions Prediction for Main Frac Based on Early Treatment Design	152
Figure 7-1	Viscosity of Pre-Mixed 50-lbm Gel at Downhole Temperature, SFE No. 3	159
Figure 7-2	Viscosity of Pre-Mixed 40-lbm Gel at Downhole Temperature, SFE No. 3	159
Figure 7-3	Viscosity of 40-lbm Gel at Downhole Temperature, SFE No. 3	160
Figure 7-4	Profile of Bottomhole Treating Pressures, Casing Pressures and Tubing Pressures During Treatment	161
Figure 7-5	Profiles of Proppant Concentration and Cross-Linker, LGC, Slurry and Diesel Flowrates During Treatment	161
Figure 7-6	Profiles of the Base Gel Viscosity, the Clean and Slurry pH Levels, and the Downhole and Fluid Temperatures During Treatment	162
Figure 7-7	Net Pressure Match of Mini-Frac No. 2 and Main Fracture Using Log-Derived Stresses	163
Figure 7-8	Net Pressure Match of Mini-Frac No. 2 and Main Fracture Using Modified Stresses	163
Figure 7-9	Profiles of Slurry Rate, Measured Net Pressure Without Erosion Correction, and Model Net Pressure Using Modified Stresses	165
Figure 7-10	Main Fracture Created Dimensions During Treatment Using Log-Derived Stresses	166

Figure 7-11	Main Fracture Created Dimensions During Treatment Using Modified Stresses	166
Figure 7-12	Main Fracture Propped Dimensions During Treatment Using Log-Derived Stresses	167
Figure 7-13	Main Fracture Propped Dimensions During Treatment Using Modified Stresses	167
Figure 7-14	Proppant Concentration Profile at Treatment Shut-In Using Log-Derived Stresses	168
Figure 7-15	Proppant Concentration Profile at Treatment Shut-In Using Modified Stresses	169
Figure 7-16	Volume Fraction of Proppant in Slurry at Treatment Shut-In Using Log-Derived Stresses	169
Figure 7-17	Volume Fraction of Proppant in Slurry at Treatment Shut-In Using Modified Stresses	170
Figure 8-1	Post-Fracture Production History	171
Figure 8-2	Cinco Type-Curve Analysis Assuming Finite Conductivity Hydraulic Fracture	172
Figure 8-3	Ramey-Barker Type-Curve Analysis Assuming Infinite Conductivity Hydraulic Fracture With Wellbore Storage	173
Figure 8-4	Linear Flow Analysis of Post-Fracture Buildup Test	174
Figure 8-5	Horner Analysis of Post-Fracture Buildup Test	175
Figure 8-6	Reservoir Simulation Model Types	177
Figure 8-7	Results of 1-D, Single-Phase, Radial Model History Match	179
Figure 8-8	Results of 2-D, Single-Phase, Areal Model With Single- Conductivity-Function History Match	180
Figure 8-9	Results of 2-D, Single-Phase, Areal Model With Variable- Conductivity-Function History Match	182
Figure 8-10	Results of Semi-Analytic Reservoir Model History Match	183
Figure 8-11	Model Grid System for Analysis of SFE No. 3	184
Figure 8-12	Production History of SFE No. 3	185

Figure 8-13	Relative Permeability Curves for SFE No. 3	186
Figure 8-14	History Match of Water Production Prior to PBU Test, SFE No. 3 . .	186
Figure 8-15	History Match of Flowing Bottomhole Pressures, SFE No. 3	187
Figure 8-16	History Match of Post-Fracture PBU Tests, SFE No. 3	187
Figure 8-17	Reservoir Model for Initial History Match, SFE No. 3	188
Figure 8-18	History Match of Water Production After PBU Test and Cleanup Treatment, SFE No. 3	189
Figure 8-19	Flowing Pressure Match After PBU Test and Cleanup Treatment, SFE No. 3	189
Figure 8-20	Reservoir Model for Final History Match, SFE No. 3	190
Figure 8-21	Very Large Signals With Apparent Precursors Recorded at 8,925 ft and 9,400 ft Approximately Four Months After Main Fracturing Operation	192
Figure 8-22	Unprocessed Apparent Precursors After Use of Noise- Conditioned Pure-State Filter	193
Figure 8-23	Upper Hemisphere Stereographic Projection of Particle Motion Orientations of Precursors to Very Large Signals Recorded at 8,925 ft and 9,400 ft	194
Figure 8-24	H/Z Ratios After Main Fracture Treatment Versus Depth	195
Figure 8-25	Summary of Mini-Frac Top and Bottom Interpretations From Proof-Of-Concept Experiment	198
Figure 8-26	Summary of Main Frac Top and Bottom Interpretations From Proof-Of-Concept Experiment	198

Tables

Table E-1	Summary of SFE No. 3 Production Tests	E-7
Table 1-1	Contractors Involved in SFE No. 3 Research Programs	2
Table 1-2	SFE No. 3 Well Information	7
Table 2-1	Operations Summary, SFE No. 3, Harrison County, Texas	12
Table 2-2	Results of SFE No. 3 Coring Operations	14
Table 2-3	Data Measured by Surface Transducers During Drilling	19
Table 2-4	Summary of Open-Hole Stress Tests	20
Table 2-5	Summary of Cased-Hole Stress Tests	23
Table 3-1	Petrographic Analyses of SFE No. 3 Core, Travis Peak Formation Samples	41
Table 3-2	Petrographic Analyses of SFE No. 3 Core, Cotton Valley Group Samples	43
Table 3-3	Natural Fractures in SFE No. 3 Core	56
Table 3-4	Coring-Induced Fractures in SFE No. 3 Core	57
Table 3-5	Orientations of Open-Hole Stress Test Fractures Observed on the FMS and BHTV	66
Table 4-1	Zone Summary, Completed Interval	69
Table 4-2	Histogram Modes and Shift Required for Data Normalization	69
Table 4-3	Thin-Section Correlation Coefficients for Various Clay Indicators	71
Table 4-4	Results of Cased-Hole Stress Tests, SFE No. 3	77
Table 4-5	Summary of Routine Core Analysis Results, SFE No. 3	86
Table 4-6	Results of Sidewall Core Analyses, SFE No. 3	87
Table 4-7	Summary of SFE No. 3 Core Acoustic Velocities and Moduli Versus Water Saturation	89
Table 4-8	Basic Properties of Cores Used for Acoustic Measurements	92

Table 4-9	Tensile Strength by Splitting of Wafers Companion to Acoustic Property Samples	93
Table 4-10	Basic Properties of Relative Permeability Test Cores	96
Table 4-11	Basic Properties of Capillary Pressure Test Cores	99
Table 4-12	Summary of Basic Core Properties for Travis Peak Samples Used in Clay Dehydration Study	102
Table 4-13	Pore Size Distribution for Travis Peak Samples Used in Clay Dehydration Study	105
Table 5-1	SFE No. 3 Results of Open-Hole Stress Tests	108
Table 5-2	SFE No. 3 Results of Cased-Hole Stress Tests	108
Table 6-1	Mini-Frac No. 1 Pumping Schedule	125
Table 6-2	Major Events During Mini-Frac No. 1, SFE No. 3	127
Table 6-3	Base Gel Viscosity at Different Shear Rates for Mini-Frac No. 2, SFE No. 3	128
Table 6-4	Depths and Data Recording Inception Times at the SFE No. 3	138
Table 6-5	Comparison of Stress Input for Each Layer for the FRACPRO Analysis	146
Table 6-6	Viscous Properties of the Fracture Fluid	147
Table 6-7	Mini-Frac No. 1 Leakoff Parameters Used for the FRACPRO Analysis	148
Table 6-8	Reservoir Mechanical Properties Used for the FRACPRO Analysis	148
Table 6-9	Mini-Frac No. 1 Dimensions at the End of Pumping as Determined by FRACPRO Analysis	149
Table 6-10	Mini-Frac No. 2 and Main Frac Leakoff Parameters Used for the FRACPRO Analysis	153
Table 6-11	Mini-Frac No. 2 Dimensions at End of Pumping as Determined by FRACPRO Analysis	153
Table 7-1	Fracture Treatment Design and Actual Treatment Volumes for SFE No. 3	156

Table 7-2	Viscosity at 300 RPM of Batch-Mixed Fluid, SFE No. 3	157
Table 7-3	Viscosity at 300 RPM of Continuous Mix 40-lbm Fluid, SFE No. 3	157
Table 7-4	Main Fracture Perforation Erosion History	165
Table 7-5	Main Fracture Dimensions at End of Shut-In as Determined by FRACPRO Analysis	168
Table 8-1a	Results of Cinco Type-Curve Match of Post-Fracture PBU Data	173
Table 8-1b	Results of Ramey-Barker Type-Curve Match of Post- Fracture PBU Data	173
Table 8-1c	Combined Results of Analytical Analyses of Post-Fracture PBU Data	176
Table 8-2	Description of Models Used in SFE No. 3 History Matching	176
Table 8-3a	Parameters for 1-D, Radial, Single-Phase Model	179
Table 8-3b	Parameters for 2-D, Areal, Single-Phase Model	180
Table 8-3c	Parameters for 2-D, Areal, Single-Phase Model With Variable Fracture Conductivity	182
Table 8-3d	Parameters for 2-D, Single-Phase, Semi-Analytic Model	183
Table 8-3	Proof-of-Concept Logging at SFE No. 3 -- Well Status, Actual Logging Date, Responsible Company and Log Data Acquired	197

Executive Summary



INTRODUCTION

SFE No. 3 is the third well in a series of four Staged Field Experiments (SFE) being conducted by the Gas Research Institute (GRI) of Chicago, Illinois. SFE No. 3 was drilled as the Mobil Cargill Unit No. 15 in the Waskom Field, Harrison County, Texas. The well was spud on September 6, 1988, and was drilled to a total depth of 9,700 ft. Engineering and geologic data were measured and analyzed on the Travis Peak Formation and the Cotton Valley Formation. Both of these intervals are major gas-producing formations in East Texas.

A major objective of the GRI Staged Field Experiment program has been to develop technology using experiments conducted in field laboratories. SFE No. 3 provided a field laboratory site to test technology on in-situ stress profiling, fracture diagnostics, real-time fracture analysis, and post-fracture well performance analysis. The Cotton Valley Formation in SFE No. 3 provided an ideal laboratory for the verification of the technology developed by GRI during the Tight Gas Sands research project. This report documents the detailed information and results from GRI's research efforts on the Cotton Valley Formation in SFE No. 3.

OPEN-HOLE DATA ACQUISITION

An extensive open-hole data acquisition program was performed in SFE No. 3. Approximately 374 ft of core were cut in the Travis Peak, the Travis Peak-Cotton Valley transition zone and the lower Cotton Valley interval. Routine core analyses were performed on 320 plugs to measure values of water saturation, permeability, porosity and grain density. Special core analyses were run on 38 plugs. Values for dynamic mechanical properties, electrical properties,

relative permeability relationships and capillary pressure functions were all determined using Cotton Valley core samples. In general, excellent data were obtained. All available information indicated that the Cotton Valley Taylor interval was a typical low permeability gas reservoir that possessed ideal characteristics for conducting hydraulic fracturing experiments.

Open-hole logs were run on six different occasions as SFE No. 3 was drilled. Open-hole logging data were also obtained using measurement-while-drilling (MWD) systems. Several of the open-hole logging runs were made to study the effects of mud filtrate invasion on the readings from logging tools. A comprehensive logging suite was run at the conclusion of drilling to obtain data for calculating permeability-thickness (kh) profiles, porosity-thickness (ϕh) profiles, in-situ stress (σ_v) profiles and formation lithology.

From the combined log and core analysis, the total kh in the Cotton Valley Taylor sand was calculated to be 0.33 md-ft with an average porosity of 6 percent and an average water saturation of 41.3 percent. The bulk density log, the neutron log and the sonic log were all used to obtain estimates of porosity and in-situ stress. The logs were calibrated with in-situ stress test and core measurements. All equations used for these computations are included in this report.

One of the major results from the GRI research effort concerns the development of a methodology for completing and stimulating low permeability gas reservoirs. The normal method used by virtually all operators is to perforate a well based solely on the estimates of porosity and water saturation from the open-hole log analysis. Those data for the Taylor sand in SFE No. 3 are included in Figure E-1. The GRI contractor

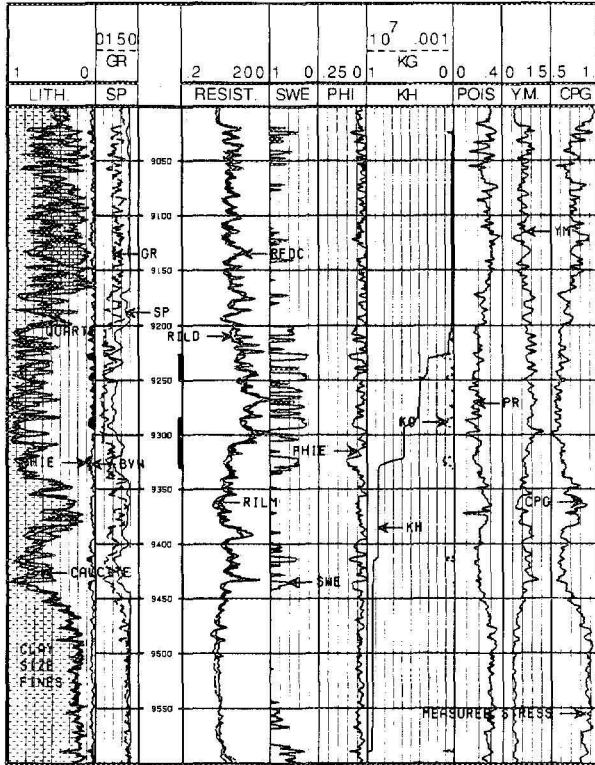


Figure E-1 Pre-Fracture Analysis Results for the Completion Interval, SFE No. 3

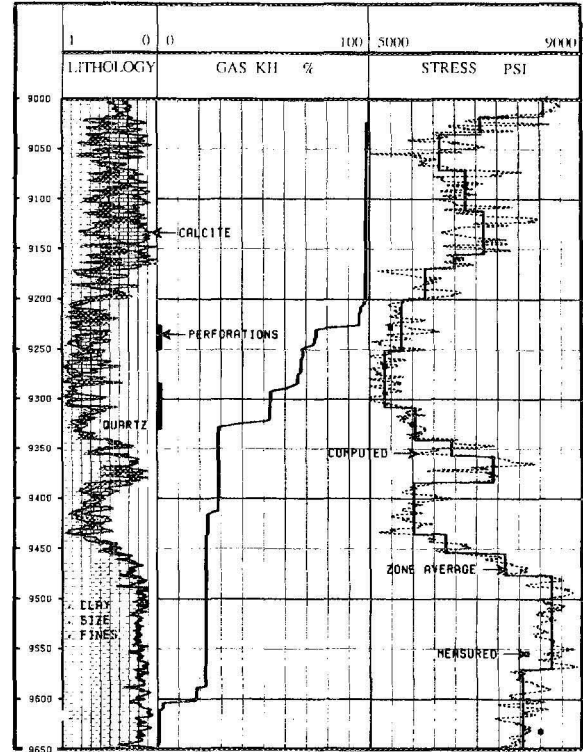


Figure E-2 Permeability-Thickness Profile and Stress Profile of the Completion Interval in SFE No. 3

team has determined that a better method of well completion is to consider three different profiles of data prior to determining where to place the perforations. The operator should look at the ϕh profile, the kh profile and the in-situ stress profile. Then, using both three-dimensional fracture propagation models and three-dimensional reservoir models, one can determine the optimum location for the perforations to connect the better, gas-productive intervals to the wellbore via a hydraulic fracture.

Details of the calculations of in-situ stress for SFE No. 3 are included in this report. Figures E-1 and E-2 illustrate the results from the log analyses where estimates of ϕh , kh and σ_x have been computed using the combined information from logs, cores and stress tests.

A mud logging system was used on SFE No. 3 from 5,700 ft to 9,700 ft (total depth). SFE No. 3 provided a test site for several new hardware and software systems being developed for mud logging programs. A new system was tested to obtain samples of cuttings continuously while drilling. Even though the system did not perform perfectly, the information obtained on the cuttings analysis were very informative.

A series of open-hole stress tests were run to obtain estimates of in-situ stress above and in the Taylor zone and to determine fracture azimuth using open-hole logging images. The Bureau of Economic Geology (BEG) used all of the log, core and stress test information to provide detailed geologic descriptions of the regional and local geologic setting for SFE No. 3. All of the de-

tailed sedimentological analyses of the cores have been included in this report. Of particular interest was the cored interval at the transition between the Travis Peak and Cotton Valley Formations.

The Bureau of Economic Geology demonstrated that diagenesis had a different effect on the Travis Peak Formation than on the Cotton Valley Taylor sand. The BEG has found that in the Travis Peak Formation, the presence of quartz overgrowths leads to extremely low formation permeabilities. If the Travis Peak sands were initially coated with a layer of clay, the precipitation of quartz overgrowth was stunted and permeability was maintained at a higher level. In contrast, the findings in the Cotton Valley Taylor sand were just the opposite. In the Cotton Valley Formation, the intervals with quartz cement maintained higher permeability. The zones with an abundance of clay were the lower permeability intervals. Detailed discussion of all the geologic findings is included in this report.

The BEG also studied the cores, the formation microscanner and the borehole televiewer data to estimate the preferred direction of fractures in the Cotton Valley Formation. On the basis of its findings, the preferred direction appears to be N80°E. A detailed discussion of the natural fractures and the structural setting in East Texas has been included in this report.

CASED-HOLE DATA ACQUISITION

After casing was set, a series of cased-hole logs was run to help estimate fracture height and to evaluate the cement bond for SFE No. 3. In addition, several cased-hole stress tests were run in the Bossier shale and in the Taylor sand. These tests were later used to calibrate the mechanical properties logs to obtain a detailed in-situ stress profile. The GRI research team has con-

cluded that several stress test measurements are normally required to properly calibrate the in-situ stress profile. Seldom can one use the data measured solely from open-hole logs and still obtain the correct stress profile. Detailed discussions of the in-situ stress profile and the steps needed to properly compute σ_x are included in this report.

PRE-FRACTURE WELL TESTS

After thoroughly analyzing the open-hole data, the Cotton Valley Taylor sand was perforated from 9,225 to 9,250 ft and 9,285 to 9,330 ft on January 24, 1989. After performing a perforation ballout treatment, the well produced 50 MCFD and 8 BWPD at 0 psi flowing tubing pressure (FTP). The well was produced for seven days, then shut in for a seven-day pressure buildup test. The analysis of the pressure buildup test resulted in the following estimates of formation properties:

Permeability-Thickness (kh), md-ft	0.378
Gas Permeability (k_g), md	0.01
Net Pay Thickness (h), ft	27
Skin (s)	+0.1
Extrapolated Reservoir Pressure (P*), psi	3,400

After the pressure buildup test, the first mini-fracture treatment was pumped on February 17, 1989. After the mini-fracture treatment, the well produced at 310 MCFD and 8 BWPD at a FTP of 150 psi. The well was produced for six days and then was shut in for another pressure buildup test on March 2, 1989. The analysis of the second pressure buildup test resulted in the following information:

Permeability-Thickness (kh), md-ft	0.88
Gas Permeability (k_g), md	0.022
Net Pay Thickness (h), ft	40

Skin (s) -3.2
 Extrapolated Reservoir Pressure (P*), psi 3,600

- 9,006 bbl of gel
- 1,168,900 lbm of 20/40 Ottawa mesh sand
- 8 lbm/gal maximum sand concentration

A comparison of the results from the two, pre-fracture pressure buildup tests led to the conclusion that additional pay was connected to the perforations as a result of the first mini-fracture treatment. SFE No. 3 was definitely more productive after the first mini-fracture treatment. In addition to an increased kh product, the data indicated the average reservoir pressure to be slightly higher after the mini-fracture treatment.

All of the important hydraulic fracture treatment data were monitored, measured and recorded during both the mini-fracture and the main fracture treatments. Before and during the treatments, extensive fracture fluid quality control operations were conducted by S. A. Holditch & Associates, Inc. The fluid viscosity data were supplied to RES for its real-time analysis of the hydraulic fracture treatment again using FRACPRO.

FRACTURE TREATMENT DATA ACQUISITION

The main purpose of Mini-Frac No. 1 was to allow Teledyne Geotech to gather data for estimating fracture height and fracture azimuth. On the basis of its analysis of data from Mini-Frac No. 1, Teledyne Geotech estimated the top of the fracture at ±9,125 ft and the bottom of the fracture at ±9,425 ft. The fracture azimuth was estimated to be N77°E.

The treatment was pumped down the casing-tubing annulus so that the bottomhole pressure could be measured continuously with a pressure gauge run inside the tubing. The main fracture treatment was pumped as designed. On the basis of the RES analysis of the treatment, the following dimensions were reported.

Resources Engineering Systems (RES) also analyzed the data from Mini-Frac No. 1 using FRACPRO, a 3-D fracture model developed by RES for the GRI Tight Gas Sands Program. Using that information, RES estimated the top of the fracture to be at about 9,144 ft and the bottom of the fracture to be at about 9,368 ft. The total leakoff coefficient (C_L) from Mini-Frac No. 1 was estimated to be 0.001 ft/ min.

Created Fracture Length, ft	1,751
Propped Fracture Length, ft	1,403
Created Fracture Height at Wellbore, ft	307
Propped Fracture Length at Wellbore, ft	296
Created Fracture Width at Wellbore, in.	0.72

A visual depiction of the hydraulic fracture dimensions in SFE No. 3 is given in Figure E-3.

Mini-Frac No. 2 was pumped immediately prior to the main fracture treatment on March 16, 1989. The data from Mini-Frac No. 2 was used to calibrate the fracture propagation model.

POST-FRACTURE PRODUCTIVITY ANALYSIS

The main fracture treatment consisted of

- 576 bbl of slickwater

After the hydraulic fracture treatment, the well was produced and detailed measurements of the gas flow rates, water flow rates, condensate flow rates and flowing tubing pressures were obtained and recorded. Experience gained through the GRI research effort has shown that exact mea-

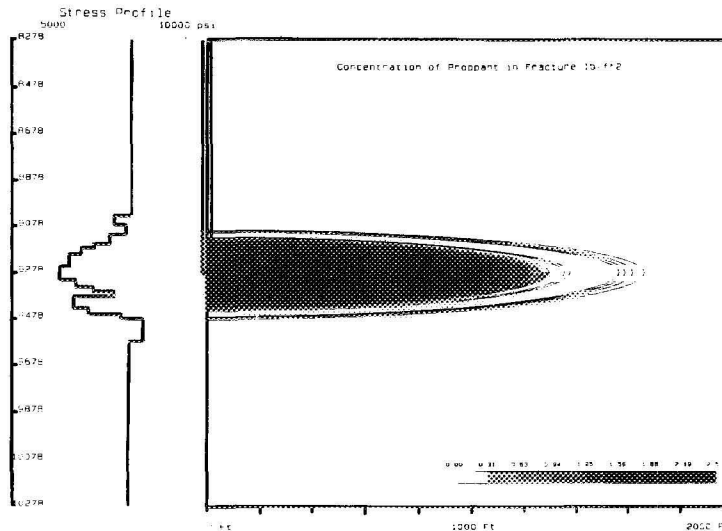


Figure E-3 Proppant Concentrate Profile at Treatment Shut-In Using Log-Derived Stresses

measurements of the producing characteristics immediately after a hydraulic fracture treatment are critical data for an engineer who is attempting to obtain accurate estimates of the propped and created fracture dimensions. The GRI research team has learned that multi-phase, multi-dimensional models are required to match all of the data during and after a hydraulic fracture treatment. Even though such an analysis can be expensive and time consuming, it is the only known method of determining the correct fracture dimensions, especially if a well is slow to clean up the fracturing fluids.

For this report, the final reservoir analysis was obtained using a three-phase, three-dimensional reservoir simulator called SABRE. Using SABRE, a history match was performed of the water injection data, the production data after the hydraulic fracture treatment and the pressure buildup data that were measured in SFE No. 3. Core and log analyses also provided critical input data into the model. The results from the analysis show clearly that only about the first 200 ft of the fracture had cleaned up at the time the pressure buildup test was run.

As such, the results of the analyses of the pressure buildup data using the single-phase models are not surprising. Those models estimated fracture lengths on the order of 200 ft (see Section 8.2).

The main parameters that were varied during the match were formation relative permeability, fracture half-length, and fracture conductivity. Details concerning the history match are included in this report; however, the analysis resulted in the following estimates of fracture and formation properties.

Created Fracture Length, ft	1,515
Propped Fracture Length, ft	1,100
Fracture Conductivity for First 600 ft, md-ft	1,880
Fracture Conductivity for Last 500 ft, md-ft	40
Formation Gas Permeability, md	0.04
Total Porosity, %	8.6
Net Pay Thickness, ft	40
Reservoir Pressure, psi	3,620
Drainage Area, acre	170

The results from the SABRE analysis of the post-fracture production and pressure build-

up test were very compatible with pre-fracture analyses and the analyses of the treatment reported by RES. Figure E-4 shows a schematic of the reservoir model used to perform the history match analysis.

The results illustrated by Figure E-4 represent the final match of production measured after using a chemical treatment to dissolve gel residue in the fracture. After the pressure buildup test, the well was loaded with water so that cased-hole logs could be run. The Halliburton product, OptiKleen, was used in the first 500 bbls of the kill fluid while logging was performed. During the five-day period, approximately 3,000 bbls of water were lost in the fracture. Most of this water went into the fracture and allowed the OptiKleen chemical to contact some of the gel residue left in the fracture. As a result, production has been increased.

Table E-1 is a summary of production tests from SFE No. 3.

Cumulative production as of July 1, 1990, was 156.1 MMCF of gas, 22,600 BW and

535 BC. Essentially all of the load water from the injection tests and fracture treatment has been recovered.

On the basis of an analysis of the post-fracture data, it has been estimated that SFE No. 3 will produce 1.14 BCF of gas over a 20-year period. The initial gas-in-place for SFE No. 3 was 2.13 BCF in a 160-acre drainage area. Therefore, a recovery efficiency of approximately 54 percent is predicted for SFE No. 3.

This report is a detailed accounting of the data collected and the analyses of those data by the GRI research team. As one would expect, however, not all the details of these analyses were included in this report. Moreover, additional research using these data sets will be conducted on an on-going basis. As a consequence, a bibliography of additional information has been included for use by interested parties. For more information, contact the Gas Research Institute, CER Corporation or S. A. Holditch & Associates, Inc.

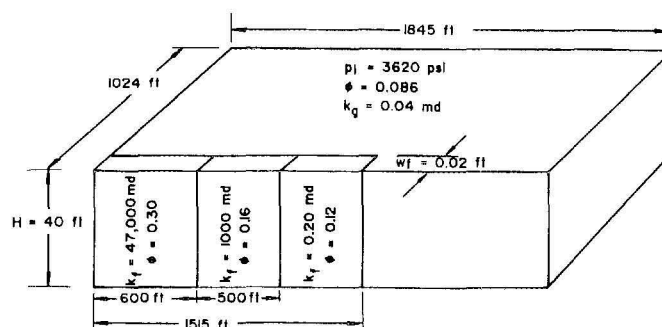


Figure E-4 Reservoir Model for Final History Match, SFE No. 3

Table E-1 Summary of SFE No. 3 Production Tests

Date	Gas Flow Rate, MCFD	Water Flow Rate, BWPD	Condensate Flow Rate, BCPD	Tubing Pressure, psig	Remarks
June 15, 1989	290	8	1.2	1,000	prior to PBU
Aug. 27, 1989	580	60	1.0	550	after cleanup treatment
Jan. 1, 1990	420	40	1.0	375	
July 1, 1990	350	24	1.0	230	20/64-inch choke

1.0 Introduction and Summary

1.1 CONCEPT OF STAGED FIELD EXPERIMENTS

Significant amounts of potentially recoverable natural gas exist in low-permeability sandstone formations located in sedimentary basins throughout the United States. Development of the tight gas resource has only occurred in those limited areas characterized by thick and fairly uniform formations, which, when hydraulically fractured, provide gas at production rates high enough for commercial exploitation. In more complex areas, the risks associated with drilling and stimulating are too high to allow full development of this resource without the use of advanced technology.

To permit lower cost exploitation of the full potential of the tight gas resource base, the Gas Research Institute has initiated an R&D program to do the following:

- 1) determine the relationship between geologic and engineering parameters;
- 2) further characterize tight gas reservoirs and improve resource estimates;
- 3) identify and evaluate potential new tight gas sands technologies;
- 4) identify parameters critical to formation evaluation and gas production;
- 5) understand more clearly the mechanisms of hydraulic fracture propagation and control;
- 6) diagnose fracture shape and down-hole conditions based on surface parameters; and
- 7) provide the capability to change fracture treatment designs in real time.

To integrate each of these goals, GRI-controlled Staged Field Experiments (SFEs) are being conducted to validate the effectiveness of technologies developed throughout the GRI Tight Gas Sands Program. In addition, SFEs are being conducted to determine the most effective combination of techniques for formation evaluation, hydraulic stimulation and completion to reduce the cost of producing gas from tight formations.

Research on SFE Nos. 1 and 2 focused on the Travis Peak Formation in East Texas. The results of this research have been previously documented (CER Corporation and Holditch & Associates, 1988; 1989; 1990). Verification of the technology's applicability to the Cotton Valley Formation in East Texas was the objective of the SFE No. 3 well. This document provides detailed information and results of GRI's research efforts in that formation.

As in the previous SFE wells, a group of GRI contractors was organized to conduct an integrated research program. The contractors who participated in conducting the research program on SFE No. 3 are shown in Table 1-1. Individuals from these organizations who performed the research and prepared the materials included in this report are also listed in this table. The individual reports were compiled, integrated and edited by GRI Tight Gas Sands Program management and CER Corporation.

1.2 SFE NO. 3 SITE SELECTION CRITERIA

When GRI originally planned the Staged Field Experiment Program, specific goals were outlined for each SFE well. The individual goals of each SFE were considered when choosing the location for the

Table 1-1 Contractors Involved in SFE No. 3 Research Programs

Organization	Project Responsibility	Contributing Authors	Report Section
Bureau of Economic Geology (BEG) -- The University of Texas at Austin	Assist in site selection process; design coring program; perform geological research and evaluations	Shirley P. Dutton Stephen E. Laubach Robert S. Tye Timothy N. Diggs	3.0
CER Corporation	Implement openhole data acquisition programs; provide project acministration; document project activities	Richard E. Peterson Eric R. Monson	1.0 2.0
Resources Engineering Systems	Recommend hydraulic fracture design; monitor fracture treatment parameters in real time; analyze and model hydraulic fracture treatments	Michael P. Cleary Chris Wright Phil Lewis	6.2 7.3
ResTech Houston	Design formation evaluation and data acquisition programs; evaluate log data and recommend completion intervals; determine stress profile from log data	William Howard Don Luffel	4.0
S.A. Holditch & Associates, Inc.	Perform drilling and completion engineering services; perform and analyze well tests; design and implement hydraulic fracture treatments; function as GRI's lead technical contractor	Stephen A. Holditch Bradley M. Robinson William S. Whitehead Brad C. Walters	5.0, 5.2 6.2, 7.1, 7.2 5.1, 8.2, 8.3 6.1, 8.1
Teledyne Geotech	Acquire and interpret borehole microseismic data for fracture dimensions and azimuth analysis	James E. Fix Kenneth D. Mahrer Jack G. Swanson	6.2.3 7.4 8.4

well. However, the selection of the Travis Peak as the initial "laboratory" in which to conduct the research dates back to studies conducted early in the project (Finley, 1984). The geologic and engineering studies planned for the first two SFE wells dictated that these wells be drilled where productive sandstones existed near the top and base of the Travis Peak Formation. The upper Travis Peak interval is the portion of the formation where historically a majority of the gas production has occurred. The lower Travis Peak is where a majority of the gas-in-place exists; however, the lower interval is not often completed by operators due to low permeability and difficulties in fracture stimulation. In addition, the potential for excessive water production also exists in the lower Travis Peak. Even though it was desirable to create a pure laboratory environment, it was also felt that realistic conditions should be maintained. For these reasons, the first two SFEs were drilled in the Waskom and North Appleby Fields of East Texas.

The research associated with SFE No. 3 represents a transitional period in the GRI Tight Sands project. Additional work was needed to understand the Travis Peak; however, because SFE No. 4 was to be completed in an entirely different basin and formation, there was an obvious need to begin technology transfer during SFE No. 3. Because a well-known tight gas formation existed below the Travis Peak (the Cotton Valley), it seemed logical to drill through the Travis Peak and complete SFE No. 3 in the Cotton Valley Formation. Thus, the objective of SFE No. 3 was not only to continue the work initiated on the Travis Peak, but also to begin evaluating the technologies, techniques and models developed by GRI in the Tight Sands project on the Cotton Valley Formation.

One of the problems with the Travis Peak is that it consists primarily of interbedded

siltstones, sandstones and sandy mudstones. No thick, pure shale intervals exist in the Travis Peak; therefore, adequate barriers to vertical fracture growth are not present. Consequently, all of the modeling and fracture measurements that were conducted in the Travis Peak indicated that circular-shaped fractures would be created. Even though the ability to analyze and model fracture treatments in the Travis Peak has progressed, it was obvious that only one dominant fracture geometry (circular) existed. To properly verify the fracturing models developed by GRI, additional geometries had to be analyzed. Treatments which created vertically-contained hydraulic fractures need to be analyzed.

The lower Cotton Valley (Taylor) sand offered the proper environment for this research to progress. In certain areas of East Texas, the Taylor sandstone is bounded by thick shales that are believed to be good barriers to vertical fracture growth. It was decided, therefore, to select a site for the SFE No. 3 where the Taylor sand could be used as the research laboratory. Other site-selection criteria included:

- The SFE well should offset existing production in the Cotton Valley Taylor sandstone to maximize the probability of penetrating a gas-productive pay interval.
- The Taylor sandstone in offsetting wells should have required a hydraulic fracture treatment to enhance gas production.
- Offsetting wells should also have Travis Peak gas production, in order to continue research objectives in the Travis Peak Formation.
- Total depth to the base of the Cotton Valley should be less than 10,000 ft.

After meeting with several operators, the Waskom Field of Harrison County, Texas, was selected as the most favorable site for SFE No. 3. The Waskom Field was attractive because GRI had previously participated in several cooperative research wells in the area, and SFE No. 1 was located there. As a result, the Tight Gas Sands Program contractors were familiar with the Travis Peak section in the Waskom Field. The regional and specific location of the SFE No. 3 well is shown in Figures 1-1 and 1-2, respectively. Well information applicable to SFE No. 3 is shown in Table 1-2.

1.3 PRINCIPAL ADVANCEMENTS RESULTING FROM SFE RESEARCH

Since the beginning of the project, SFE No. 3 was planned as a culmination point for the technologies developed early in the program. In 1984, the GRI cooperative well program and SFE program was initiated, and GRI pioneered significant developments in formation evaluation, fracture treatment monitoring, fracture treatment analysis and fracture diagnostics. SFE 3 was designed to demonstrate the usefulness of these technologies prior to moving the research program to a new basin.

1.3.1 In-Situ Stress Profiling

Because the effect of the in-situ stress profile on the fracture geometry is so important, significant research effort has been devoted to developing the procedures required to obtain accurate stress data. Due to cost, stress tests cannot be conducted in each individual layer within, above and below the formation of interest; therefore, a methodology was developed to correlate the results of stress test analyses with open-hole log data to compute a vertical stress profile. In SFE Nos. 1 and 2, most of the stress data were obtained in

cased hole, then a liner was set over the tested intervals to isolate the perforations. While sufficient for research purposes, this completion practice is not practical for routine operations. To improve the well completion and reduce the cost of obtaining stress data, a new approach was used on SFE No. 3. For this well, several open-hole tests were run above and below the Taylor sand. Then several cased-hole stress tests were run below and in the Taylor sand to obtain data needed to calibrate the logs.

The stress profile was used directly in formulating a completion strategy and in designing the hydraulic fracture treatment. For example, consideration was given to perforating the lower Taylor sand. However, based on the stress profile and the fracture geometry predicted by the model, it appeared that the hydraulic fracture, if initiated only in the upper Taylor sand, would grow through the thin shale interval below and into the lower Taylor sand. Therefore, to avoid potential problems with additional perforations below the main Taylor sand, the decision was made not to place perforations in the lower sand. The analysis of the hydraulic fracture treatment later indicated that the fracture did grow down into the lower Taylor sand.

1.3.2 Fracture Height Analysis

Production engineers commonly try to evaluate the created fracture height at the wellbore using conventional radioactivity and temperature logging tools. The literature contains several articles regarding the interpretation and validity of these production logs (Cooke, 1979; Dobkins, 1981; Bundy, 1982; Gadeken and others, 1989). The estimates of fracture height using these logs are usually inaccurate because the depth of investigation for these tools is only a few inches. If a fracture is more than 1 to 2 ft from the wellbore, a gamma ray or temperature log will not be able to detect it.

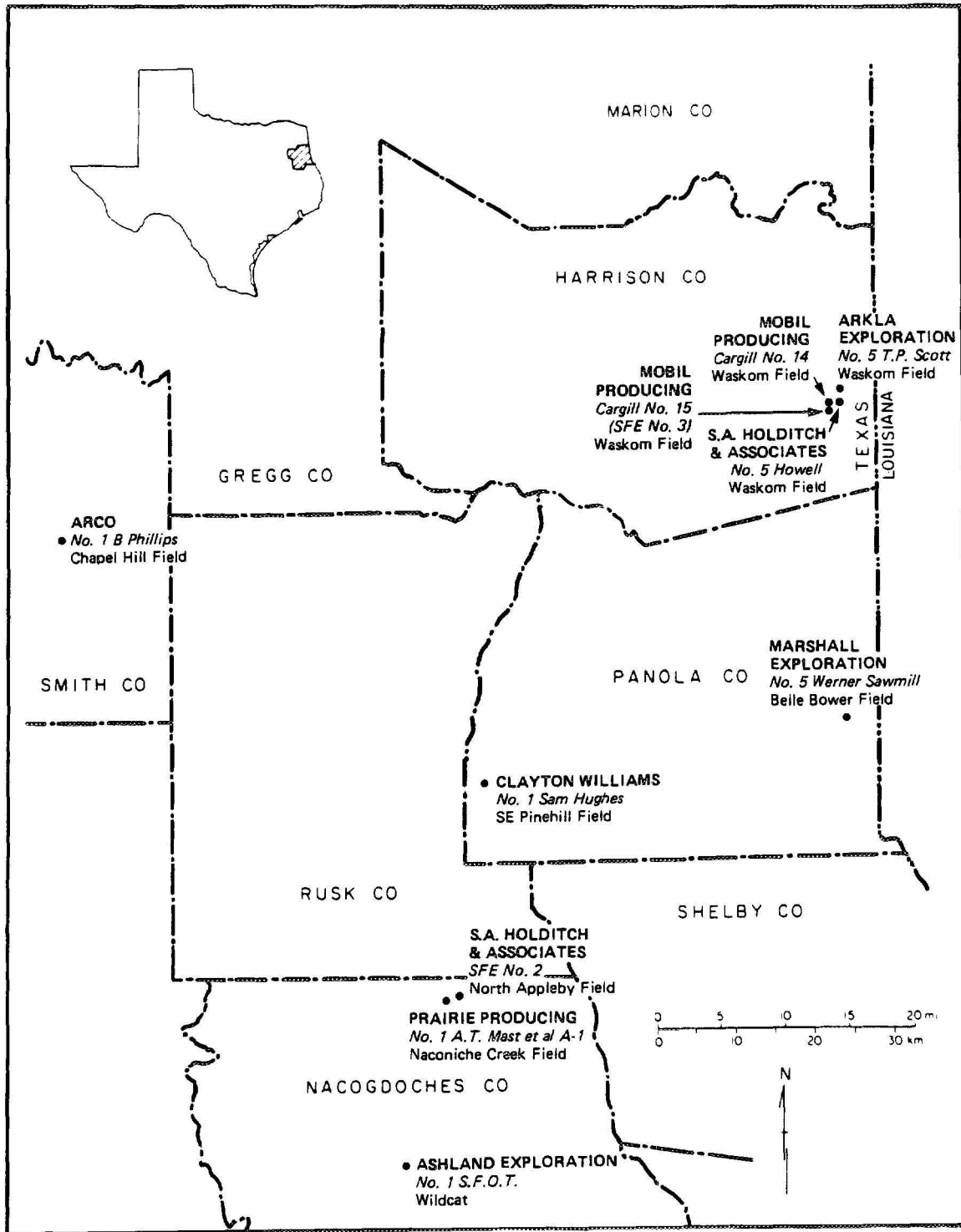


Figure 1-1 Regional Location of the SFE No. 3 Well

Table 1-2 SFE No. 3 Well Information

Permitted Well Name:	Cargill Unit No. 15
Completed Well Name:	Staged Field Experiment (SFE) No. 3
Lessee and SFE Partner:	Mobil Exploration and Production, USA
Well Operator:	S.A. Holditch & Associates, Inc.
API Well Number:	42-203-31726
Location:	Simpson Holloway A-295; 606 ft FNWL and 4,083 ft FNEL, Harrison County, Texas
Field:	Waskom
Elevations:	311.0 ft (Ground Elevation) 332.5 ft (KB Elevation and Depth Datum)

GRI has been conducting fracture diagnostics research since 1983. One promising concept developed by GRI to estimate fracture azimuth and height is to use a three-component geophone to gather data after a mini-fracture or hydraulic fracture treatment. Teledyne Geotech, the principal GRI contractor for this work, has developed a method that uses the geophones to measure the level of microseismic activity associated with the hydraulic fracture. The technique for determining fracture orientation was developed during SFE Nos. 1 and 2. The refinement of the H/Z ratio method for determining fracture height was demonstrated during SFE No. 3.

The fracture height determined using the Teledyne Geotech method was compared to the estimated values of fracture height as determined from conventional logging techniques. The RES fracture propagation simulator, FRACPRO, was also used to estimate a value for created fracture height. It appears that the Teledyne Geotech estimate of created fracture height in SFE No. 3 agreed very well with the fracture propagation modeling results. The conventional production logging techniques underestimated the created fracture height (which is usually the case) by a substantial amount.

GRI has developed a more accurate method to measure the created fracture height. This technology is vitally important when one is attempting to design an optimal fracture treatment or interpret results from a fracture treatment.

1.3.3 Hydraulic Fracture Analysis

A primary objective of the four Staged Field Experiments has been to provide a field laboratory for the development and verification of fracture analysis technology (three-dimensional fracture models and remote sensing equipment). At the conclusion of SFE No. 3, the goal was to have a system developed for analyzing the fracture in real time. Essentially, this goal was accomplished. GRI has a system that can be used in the field to determine fracture azimuth, fracture height and fracture length. A 3-dimensional fracture propagation model can be used to compute the shape and extent of the fracture in real time with data measured at the well site during the fracture treatment.

Resources Engineering Systems (RES) has developed a computer van, known as the Treatment Analysis Unit (TAU), that houses the hardware and software needed to

analyze a fracture treatment in real time. The GRI-funded TAU has been developed during the course of the Tight Sands program and has been the control center for fracture diagnostics during the SFE project.

The fracture treatment on SFE No. 3 was analyzed in real time by RES using FRACPRO. FRACPRO is a lumped 3-D model developed by RES for GRI. Using input data from the pre-fracture formation evaluation plus the data measured during the fracture treatment, RES successfully matched the bottomhole treating pressures recorded during the fracture treatment of SFE No. 3. Based upon this match, a prediction of fracture growth was generated as the treatment was being pumped. Even though an excellent match of the predicted vs. actual pressures was obtained, additional analysis is still being conducted with FRACPRO. Difficulties were encountered when modeling the mini-frac and main fracture treatment because fluids with different viscosities were distributed in the fracture. Because the initial version of FRACPRO averaged the viscosity distribution into a single value, matching the data from SFE No. 3 was complicated. As a result, radial weighting factors have now been added to FRACPRO to better simulate multiple fluid viscosities in the fracture.

Using its full 3-D numerical simulator (R3DH), RES has history matched the treatment data from SFE No. 3. In conjunction with R3DH, a finite element mesh was used to model the crack tip, thereby improving the calculation of fracture treating pressures.

1.3.4 Post-Fracture Performance Analysis

During the GRI Tight Gas Sands Program, experience has shown that conventional well test analysis techniques used on tight gas reservoirs will not usually provide accurate

estimates of permeability, fracture length, fracture conductivity and/or drainage area. Most simple analysis techniques assume that a single-phase fluid is being produced from a single, homogeneous formation. However, in most tight gas reservoirs, both gas and water are produced from multiple layers consisting of sandstones, siltstones and shales. As a result, the assumptions made to develop the conventional well analysis techniques are invalid and results obtained from conventional well analysis methods do not adequately describe the complex reservoir.

In the GRI Tight Gas Sands Program, S.A. Holditch & Associates, Inc. has used numerical reservoir simulators to analyze the post-fracture performance. The models are used to simulate both the production data and pressure buildup data. Production characteristics such as gas breakthrough time, fracture fluid cleanup, and gas/water ratio histories have all been identified as important parameters in determining reservoir and fracture properties. Analysis of post-fracture performance using numerical models is a time-consuming process; however, the numerical results are needed to understand previous treatments and to improve the design for future wells. GRI is funding research to develop a new generation of reservoir simulators that can run on personal computers with minimal data. These new PC models will allow the practicing engineer to analyze post-fracture data on a more routine basis.

The analysis of SFE No. 3 indicates that the results obtained from numerical modeling of the post-fracture performance provide more reliable estimates of reservoir and fracture properties than do conventional analysis techniques. The conventional techniques generally underestimated the values for fracture properties due to the fact that complete cleanup of fracturing fluids was not obtained. Therefore, the production and

pressure transient data were affected by the presence of this water. By using a two-phase, numerical simulator, these effects

were taken into account and the resulting analyses were more realistic and more reliable.

2.0 SFE No. 3 Data Acquisition Objectives and Results

Open- and cased-hole data acquisition programs on the SFE No. 3 well were designed by the team of GRI Tight Gas Sand Program contractors. The objectives of these programs, the data actually acquired and a discussion of the SFE No. 3 drilling and completion operations are provided in the following sections. A chronological summary of these operations is provided in Table 2-1.

2.1 OPEN-HOLE DATA ACQUISITION

2.1.1 Drilling Operations Summary

SFE No. 3 drilling operations occurred between September 6 and November 13, 1988, under the overall supervision of S.A. Holditch & Associates, Inc. Total depth of the well was 9,690 ft. The time vs. depth curve for the drilling operations is shown in Figure 2-1. An 8-3/4-in. hole was drilled through the Travis Peak and Cotton Valley Formations with 7-in. production casing ultimately set and cemented. Figure 2-2 illustrates a wellbore schematic showing details of the casing and cementing for the well.

2.1.2 Coring Objectives and Results

The overall SFE No. 3 coring objective was to recover 390 ft of 4-in. diameter core from the Travis Peak and Cotton Valley Formations. More specifically, this overall objective was subdivided into coring rationales for the following depth intervals in the SFE No. 3 well:

7,351 - 7,411 ft

This is a potentially productive interval in the lower Travis Peak with anomalously low resistivity sandstones that are of interest for formation evalua-

tion studies. Special core preservation techniques would be used to evaluate the effect of clay dehydration on measured core properties.

7,868 - 7,946 ft

This interval includes the contact of the Travis Peak with the Cotton Valley. Core from this interval would be used to refine geological interpretations of the Cotton Valley and Travis Peak stratigraphy.

9,017 - 9,047 ft

This is a shale interval overlying the Taylor sandstone which would provide important information on its hydraulic fracture barrier characteristics.

9,199 - 9,367 ft

Within this interval is the entire upper Taylor sandstone completion objective. It would provide the basis for extensive geological and petrophysical analysis.

9,449 - 9,509 ft

This interval includes the lower Taylor sandstone and the Bossier shale and would aid the evaluation of its fracture barrier and geological characteristics.

The core intervals were based on correlations, performed by the Texas Bureau of Economic Geology, to nearby reference wells: the Mobil Cargill Gas Unit Nos. 8 and 10 and the Mobil McLofflin Unit No. 3.

Coring operations implemented on SFE No. 3 resulted in a total recovery of 373.6 ft of 4-in. diameter core. Results of the individual coring runs are shown in Table 2-2. All but one core run used a 30-ft barrel

Table 2-1 Operations Summary, SFE No. 3, Harrison County, Texas

Drilling	
Spud Well	Sept. 6, 1988
Log Run No. 1	Sept. 8, 1988
Set Surface Casing (1,480 ft)	Sept. 9, 1988
Log Run No. 2	Sept. 21, 1988
Set Intermediate Casing (6,315 ft)	Sept. 22, 1988
Log Run No. 3	Sept. 30, 1988
Core Interval No. 1 (7,351 - 7,411 ft)	Sept. 30 - Oct. 1, 1988
O.H. Stress Test No. 1 (7,406 - 7,411 ft)	Oct. 2, 1988
Log Run No. 4	Oct. 5, 1988
Core Interval No. 2 (7,868 - 7,945 ft)	Oct. 6-7, 1988
O.H. Stress Test No. 2 (8,074 - 8,079 ft)	Oct. 9, 1988
Log Run No. 5	Oct. 15, 1988
O.H. Stress Test No. 3 (9,012 - 9,017 ft)	Oct. 16, 1988
Core Interval No. 3 (9,017 - 9,046 ft)	Oct. 17, 1988
O.H. Stress Test No. 4 (9,041 - 9,046 ft)	Oct. 18, 1988
Core Interval No. 4 (9,199 - 9,367 ft)	Oct. 20-26, 1988
Top of C.V. Taylor Sand - 9,200 ft	
O.H. Stress Test No. 5 (9,362 - 9,367 ft)	Oct. 26, 1988
Core Interval No. 5 (9,449 - 9,502 ft)	Oct. 28-29, 1988
O.H. Stress Test No. 6 (9,595 - 9,600 ft)	Oct. 31, 1988
Reach T.D. (9,700 ft)	Nov. 2, 1988
Open-Hole Logs	Nov. 2-11, 1988
Set Production Casing, Release Rig	Nov. 13, 1988
Completion	
Cased-Hole Logs	Nov. 29 - Dec. 5, 1988
C.H. Stress Tests (Bossier Shale)	Dec. 5-6, 1988
C.H. Stress Tests (Taylor Sand)	Dec. 13-15, 1988
Perforate Taylor Sand, 9,225 - 50 ft, 9,285 - 9,330 ft	Jan. 24, 1989
Production Testing	Jan. 27 - Feb. 3, 1989
Pressure Buildup Test	Feb. 3-10, 1989
Cased-Hole Logs	Feb. 11-12, 1989
Pre-Mini-Frac Surveys	Feb. 15-16, 1989
Mini-Frac Test, Logging	Feb. 17-24, 1989
Production Testing	Feb. 24 - Mar. 2, 1989
Pressure Buildup Test	Mar. 2-8, 1989
Injection Surveys	Mar. 11, 1989
Main Fracture Treatment	Mar. 16, 1989
Spectral GR Logging	Mar. 22, 1989
Production Testing	Mar. 23 - June 16, 1989
Pressure Buildup Test	June 16 - July 14, 1989
Kill Well, Run Logging Surveys	July 24-28, 1989
Production Testing	July 29, 1989 - Present

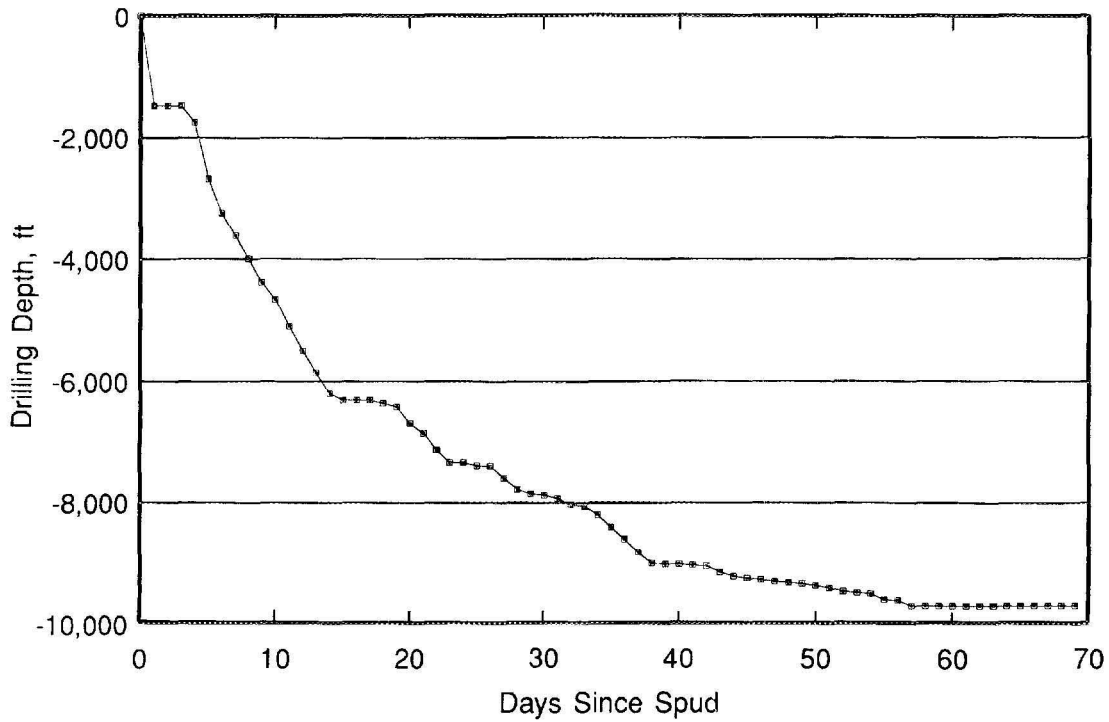


Figure 2-1 Time Versus Depth Drilling Curve for SFE No. 3

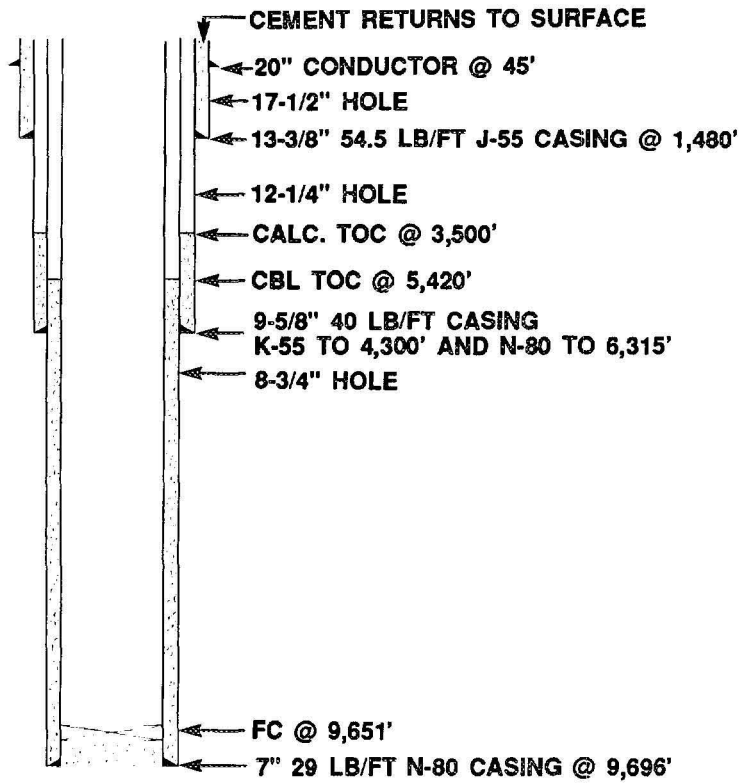


Figure 2-2 SFE No. 3 Wellbore Schematic Showing Casing and Cementing Record

Table 2-2 Results of SFE No. 3 Coring Operations

Core No.	Cored Interval, ft	Core Recovery, ft	Core Barrel Efficiency, %	Rate, ft/hr
1	7,351.0 - 7,381.0	28.7	96.0	3.6
2	7,381.0 - 7,411.0	30.0	100.0	3.8
3	7,868.0 - 7,888.6	20.6	68.7	2.9
4	7,888.6 - 7,916.7	23.9	93.7	5.6
5	7,916.7 - 7,949.7	26.6	96.7	4.0
6	9,017.8 - 9,046.8	25.7	96.7	2.6
7	9,199.0 - 9,229.4	30.0	100.0	1.8
8	9,229.4 - 9,259.6	30.2	100.0	2.8
9	9,259.6 - 9,283.0	23.3	78.0	1.4
10	9,283.0 - 9,313.3	28.3	100.0	1.7
11	9,313.3 - 9,321.3	7.4	27.3	1.5
12	9,321.3 - 9,340.0	18.9	63.0	1.8
13	9,340.0 - 9,367.9	27.9	100.0	1.8
14	9,449.0 - 9,469.0	19.1	33.0	1.9
15	9,469.0 - 9,482.0	13.0	43.0	2.3
16	9,482.0 - 9,502.0	20.0	66.0	2.0
Totals and Averages		373.6	78.9	2.6

(Core No. 14 used a 60-ft barrel). Core barrel efficiency, which is the ratio of the footage cut divided by the actual footage attempted on the particular run, averaged 78.9 percent (23.7 ft per 30-ft barrel). This relatively high percentage indicated that the coring assembly used (a 30-ft outer core barrel, 6-3/4-in. OD, stabilized at the top, middle and near the bit; and a 30-ft inner barrel, 4-in. ID, with brass stabilizer pads

brazed on at 10-ft intervals) improved core recovery when compared to using 60-ft, stabilized core barrels.

Processing and handling of all SFE No. 3 core was performed by CER using comprehensive techniques designed to provide a consistent, high-quality core product to subsequent analysts of the core. The core handling techniques used on SFE No. 3 are

fully described in CER Corporation and S.A. Holditch & Associates, Inc. (1990) but basically included an on-site trailer where core segments were reassembled; marked for depth and orientation; macroscopically described (lithology and fractures); preserved in oxygen-barrier sleeve material; and boxed prior to shipment to the Texas Bureau of Economic Geology (Austin) for slabbing and detailed geologic analysis.

2.1.3 Core Orientation Objectives and Results

To provide data primarily for the orientation of natural and induced fractures in Travis Peak and Cotton Valley core, three techniques were used: downhole surveys, paleomagnetic analysis and borehole imaging.

Only Core Interval No. 9 was oriented with a downhole electronic survey device. The tool operated from the beginning of Core No. 9 at 9,260 ft to a depth of 9,277 ft when a downhole power failure terminated data acquisition. Throughout the interval over which survey data were acquired, scribes on the core were either absent, or when visible, severely rotated about the core's circumference. Orientation data confirmed the rotation of the inner barrel. Due to the inner barrel rotation and the tool failure, consistent usable orientation information was not obtained with this technique.

Paleomagnetic core orientation data were acquired over intervals selected after the core was recovered and shipped to the Texas Bureau of Economic Geology. Using this technique, a total of 34.7 ft of core was oriented.

The main sources of orientation data were derived from wireline logging tools which included the Borehole Televiewers (BHTV) of Amoco, Mobil and Schlumberger-Doll Research and the Schlumberger Formation Microscanner (FMS). Fractures observed in

the core were correlated to the BHTV and FMS oriented images to determine true fracture strikes. Utilizing the two borehole imaging logs, 163 of the 204 (80 percent) observed core fractures were oriented. Further discussion of core fractures is presented in Section 3.3.

2.1.4 Geophysical Wireline Logging Objectives and Results

Log data quality control and supervision/coordination of open-hole logging operations on SFE No. 3 were the joint responsibility of GRI contractors ResTech Houston and CER Corporation. Tasks included coordination of the field operations and logistics, verification of tool calibrations and data quality, selection of logging speeds, presentation formats/scales and data distribution.

For the SFE No. 3 well, six open-hole logging runs were designed by the GRI contractor team. Implementation of the open-hole logging program, in general, would provide GRI contractors with the necessary data for the following:

- identification of zones with significant gas saturation, porosity and permeability; and
- development of a stress profile in intervals to be hydraulically fractured.

The individual run objectives, log data produced and observations recorded during each of the logging runs performed in the open hole on SFE No. 3 are described below.

2.1.4.1 Surface Logging Operations (Run No. 1)

Log Suite:
Dual Induction/Gamma Ray/
Spontaneous Potential

Depths Logged:
0 to 1,481 ft

The objective of the surface logging run was to acquire a complete record of the formation resistivity up to the conductor casing. The data acquired on this run are summarized in Appendix 1.

2.1.4.2 Intermediate Logging Operations (Run No. 2)

Log Suite:
Dual Induction Focused Log/GR/SP
Long Spaced Sonic/Caliper
Z-Density (Photoelectric Effect)
Formation Multitester/GR

Depths Logged:
1,470 to 6,311 ft

The objective of the intermediate logging run was to acquire a record of the resistivity and porosity characteristics of the formations to be isolated behind the intermediate casing string. In addition, formation pressure data were required in the upper Travis Peak sandstones to quantify the pressure depletion that may have resulted from nearby well production. The measurements acquired during this logging run are summarized in Appendix 1.

2.1.4.3 First TP/CV Logging Operation (Run No. 3)

Log Suite:
Dual Induction Focused Log/GR/SP
MicroLaterolog/Caliper/GR
MicroLaterolog/Caliper/GR
Proximity Log/Caliper
GR/MiniLog

Depths Logged:
6,310 to 7,354 ft

Logging Run No. 3 was the first of three intermediate logging operations whose major objective was to monitor the rate of invasion

of drilling fluid filtrate into the formation (i.e., time-lapsed resistivity logging). To attain this objective, mud weight would be maintained at an over-balanced 10.0 lbm/gal from the bottom of intermediate casing (6,310 ft) to the depth of this logging run (7,354 ft). A caliper survey of the wellbore was also planned to monitor the deterioration of the borehole as drilling operations continued. Log data acquired during Run No. 3 are summarized in Appendix 1.

2.1.4.4 Second TP/CV Logging Operation (Run No. 4)

Log Suite:
Dual Induction Focused Log/GR/SP
Dual Induction Focused Log/GR/SP
Z-Density (Photoelectric)/Caliper/GR
Proximity Log

Depths Logged:
6,310 to 7,868 ft

An objective of this run was to obtain the same types of resistivity measurements (for monitoring filtrate invasion) collected on the previous run. To acquire this invasion vs. elapsed time data, logging Run No. 4 would be performed 7 to 10 days after Run No. 3. Between Run Nos. 3 and 4, drilling fluid density would continue to be maintained at 10.0 lbm/gal. In addition, formation density data would be acquired on this run rather than risk the possibility of obtaining poor-quality data (due to borehole rugosity) on the final open-hole logging run. Caliper log data would also be acquired to continue monitoring wellbore enlargement. The log data actually collected on Run No. 4 are summarized in Appendix 1.

2.1.4.5 Third TP/CV Logging Operation (Run No. 5)

Log Suite:
Dual Induction Focused Log/GR/SP
Proximity Log/GR
Z-Density (Photoelectric)/GR/Caliper

Depths Logged:
6,310 to 9,018 ft

Log Run No. 5 was the final of three intermediate logging runs planned in the Travis Peak and Cotton Valley. In this run, resistivity data to quantify mud filtrate invasion and "insurance" density measurements (acquired prior to borehole deterioration) were emphasized. To exaggerate drilling fluid filtrate invasion, mud weight was increased from 10.0 lbm/gal to 10.7 lbm/gal at 8,079 ft; it was maintained at this level to the depth of this logging run (9,018 ft). The logging data collected on this run are summarized in Appendix 1.

2.1.4.6 Final Logging Operation (Run No. 6)

Log Suite:

Proximity Log/GR
Dual Induction Focused Log/GR/SP
Z-Density/Caliper/GR
Compensated Neutron
Long Spaced Sonic/Waveforms
(Amoco)
Borehole Televiwer (Amoco)
Digital Sonic/Waveforms
Electromagnetic Propagation Log
LithoDensity Log/Caliper
Neutron Log/GR
Formation Microscanner/GR
4-Arm Caliper
Modular Reservoir Testing Tool/GR
Digital Sonic Waveform
Tool/Waveforms
Borehole Televiwer
Stratigraphic High Resolution
Dipmeter/4-Arm Caliper Dipole
Sonic/GR
Geochemical Log/Natural GR
Rotary Sidewall Coring Tool
Borehole Televiwer (Mobil Research)
Shear Wave Sonic Log (Mobil
Research)
P-Wave Sonic Log (Mobil Research)
Stonely Wave Sonic Log (Mobil
Research)

High Resolution Induction
6-Arm Microsonic Dipmeter
Quadrapole Sonic Log - Large Source
Quadrapole Sonic Log - Small Source
Sonic Echo Log

Depths Logged:
4,550 to 9,690 ft

The objectives of the final logging operation, Run No. 6, were to acquire a comprehensive set of log data to assist in formation/reservoir evaluation, development of a completion strategy, and hydraulic fracture diagnostic research. Thus, the logging program was designed to accumulate data for the following interpretations:

- conventional log interpretation of matrix porosity, lithology components, water saturation and permeability;
- rock mechanical properties and formation pressures to develop a stress profile;
- identification and correlation of borehole images to core fractures for determination of orientations;
- quantification of the effects of filtrate invasion on the log interpretation results; and
- assessment of the drilling fluid system's ability to stabilize the borehole while exposed to the drilling fluid.

The logging data collected on this run are summarized in Appendix 1.

2.1.5 Downhole Measurements-While-Drilling

A Measurement-While-Drilling (MWD) data acquisition program was planned in the Travis Peak Formation. This interval was selected because drilling operations (and MWD data acquisition) would not be inter-

rupted by any coring operations. In addition, a wide range of formation characteristics would be encountered as drilling progressed from the upper to the middle Travis Peak. The specific objectives of the MWD program were to acquire the following:

- downhole mechanical drilling measurements (e.g., weight on bit, torque) as inputs for continuing research in relating rock strength to in-situ stress; and
- formation resistivity data immediately after penetration by the bit and prior to significant drilling fluid filtrate invasion. This data would then be incorporated into the time-lapsed wireline logging resistivity data set.

The MWD equipment fielded consisted of a specially-designed drill collar housing the transducers, downhole electronics and a data transmission telemetry system. At the surface, a unit received and recorded the data versus time and drill depth. In the drill string, the collar was placed directly above the bit.

The following sections document the data acquired in each of the MWD logging descents performed by Schlumberger-Anadril between September 24 and September 29, 1988.

2.1.5.1 MWD Descent No. 1

Descent No. 1 with the first MWD collar acquired Gamma Ray (GR), resistivity (short normal), surface rotary torque and weight on bit, rate of penetration, rotary speed, downhole bit torque and weight on bit and borehole azimuth and drift measurements over the interval 6,365 to 6,811 ft. A wiring failure in the collar caused erratic downhole bit torque and GR data, forcing a discontinuance of drilling operations to replace the MWD logging device.

2.1.5.2 MWD Descent No. 2

Upon exchanging the failed MWD collar for a functional one, Descent No. 2 commenced collecting data at 6,811 ft. Downhole bit torque and weight on bit and GR data were acquired to 6,966 ft while reliable short normal resistivity measurements ceased at 7,031 ft. A wiring failure in the collar was the source of the data loss at this depth. Since a replacement tool was not immediately available, drilling operations continued to the next scheduled wireline logging run depth at 7,348 ft. The functioning part of the MWD tool (surface rotary torque and weight on bit, rate of penetration, rotary speed and borehole azimuth and drift) acquired data to 7,348 ft.

Severe abrasive wear to the MWD collar during Descent No. 2 resulted in the loss of several external wiring cover plates on the MWD collar, allowing the destruction of the underlying wires. Further acquisition of data was discontinued after Descent No. 2 as a result of the harsh drilling environment and the unavailability of another MWD collar.

2.1.6 Surface Measurements-While-Drilling

2.1.6.1 Routine Mudlogging

Mudlogging and data logging services, performed by EXLOG, began at 5,700 ft and continued on a 24-hour basis until total depth was reached at 9,700 ft. Services included drill cuttings sample collection from the shale shaker tailings, sample description, continuous total mud gas and gas chromatograph. These data were recorded by a next-generation database software and computer hardware system. SFE No. 3 served as a beta test site for this new system. One feature of the advanced software is the computer-generated mud log included in CER Corporation and S.A. Holditch & Associates, Inc. (1990).

2.1.6.2 Drilling and Formation Data-logging

To support research directed at evaluating rock strength and its relationship to in situ stress, drilling and formation properties were measured and recorded at the surface. These data were merged with the downhole MWD data set. To acquire these data, a network of remote transducers, strategically placed on the drilling rig equipment, provided signals to the computer-based digital recording system housed in the mudlogging unit. Measurements acquired by these sensors are listed in Table 2-3.

2.1.6.3 Drill Cuttings Sampling

To develop equipment designed to automatically collect drill cuttings, Western Atlas Core Laboratories fielded prototype equipment at the SFE No. 3 site. The cuttings sampler was designed to provide a continuous automatic sampling of drill cuttings that would be more representative of the interval penetrated than that obtainable from cuttings collected at the shale shaker. The cuttings sampler accumulated drill cuttings in clear acrylic cylinders (3 in. in diameter

by 18 in. in length) which were periodically replaced. One cylinder would typically collect samples from 2 to 5 ft of drilled section.

Operation of the cuttings sampler on SFE No. 3 commenced at approximately 7,600 ft. Problems encountered with the internal plumbing and accelerated sample collection caused by the high solids content of the drilling fluid, dictated running the unit intermittently to 9,500 ft. Drill cuttings were collected over the intervals: 7,615 to 7,635 ft; 7,828 to 7,856 ft; 7,870 to 7,921 ft; 9,150 to 9,170.7 ft; 9,345 to 9,357 ft and 9,449 to 9,499 ft.

2.1.7 Open-Hole Stress Testing

The objectives of the open-hole tests were (1) to determine, in the open-hole environment, the average in-situ closure stress in specific lithologies of the Travis Peak and Cotton Valley Taylor sand and (2) to create open-hole fractures that could be imaged with the BHTV and FMS to obtain fracture azimuth. By developing the methodology needed to conduct and interpret an open-hole stress test procedures and interpretation, the technique might become more

Table 2-3 Data Measured by Surface Transducers During Drilling

Drilling Parameters	Rate of penetration Surface weight on bit Rotary speed Surface rotary torque (min, avg, max) Hook load Driller's depth
Mud Hydraulic Parameters	Standpipe pressure Pump flow rate Pump pressure
Formation Evaluation	Interpreted lithology Lagged total gas (min, avg, max) Chromatograph (C1 through nC4)

"routine" and more useful to operators. Because the fracture induced by the open-hole stress test can sometimes be over-cored, the characteristics of the fracture can be observed directly. Through orientation of the fracture found in the recovered core and by wireline tool images of the fracture in the borehole wall, fracture azimuth can also be measured.

In SFE Nos. 1 and 2, the in-situ stress profile was determined accurately by performing a large number of cased-hole stress tests. However, because many of these tests involved zones above the completion intervals, it was necessary to set a liner in each of the wells to isolate the stress test perforations. This added significantly to the cost of the operations. To eliminate the need for a liner to be set in SFE No. 3, the stresses in the zones above the Cotton

Valley completion interval were determined from open-hole stress tests only. Thus, the open-hole stress tests were concentrated in shales above the Taylor sandstone and in a lower Travis Peak sandstone.

Overall, six intervals were stress tested in the open hole. Table 2-4 summarizes the relevant information for these six intervals. For the open-hole tests, drilling mud was used for the injection fluid. The injection rates ranged from 5 to 20 gal/min. For each test, the well was drilled or cored to a specified depth. Then two DST packers were set approximately five feet above the bottom of the hole, with a perforated anchor pipe touching bottom. In the bottom packer, a shut-in nipple was run to allow downhole shut-in when the wireline pressure gauge was lowered through the drillpipe. The tested interval was between the bottom

Table 2-4 Summary of Open-Hole Stress Tests

Test No.	Interval, ft	Lithology	Objective
1	7,406 - 7,411	Mudstone/siltstone	Travis Peak shale
2	8,074 - 8,079	Shaly limestone	CV "B" limestone
3	9,013 - 9,018	Shaly limestone	Shaly fracture barrier 200 ft above upper Taylor sandstone
4	9,041 - 9,046	Shaly limestone	Shaly limestone fracture barrier above upper Taylor sandstone
5	9,363 - 9,368	Shale	Shale between upper and lower Taylor sandstone
6	9,595 - 9,600	Shale	Bossier shale

packer and the total depth of the borehole. Bottomhole pressures were measured using a downhole quartz pressure gauge with a surface readout and CER's High Speed Data Acquisition System. This specially modified surface and downhole equipment is capable of acquiring pressure data up to 85 samples per second. During each open-hole stress test, bottomhole pressure and temperature, injection rate, surface injection pressure and surface annulus pressure were monitored and recorded.

After conducting Stress Test No. 3, Core No. 6 was cut in an attempt to overcore the stress test-induced fracture. No stress test-induced fracture was observed in the core, indicating either the fracture did not propagate downward into rock cut by the core bit or the fracture was outside the area of rock cut by the core bit. Three stress tests, Nos. 1, 4 and 5, were performed immediately below Core Nos. 2, 6 and 13, respectively, so that core data could be acquired in rock immediately adjacent to the stress tested interval. The remaining two stress tests, Nos. 2 and 6, were not located near any core intervals.

The BHTV and FMS borehole imaging devices were logged over the six stress test intervals. Fractures, which were interpreted to be induced by the stress tests, were observed in three of the stress test intervals on the image logs.

2.2 CASED-HOLE DATA ACQUISITION

2.2.1 Cased-Hole Logging

An extensive cased-hole logging program was planned for the SFE No. 3 well primarily for the determination of fracture height following various hydraulic fracturing events (e.g., injection/ballout, mini-and main fracture treatments). In addition, the cased-hole logging would provide data to indicate the quality of cement bonding in potential completion

intervals. Specific objectives and data acquired in each of the cased-hole runs are summarized in the following sections.

2.2.1.1 Pre-Perforation Logging Operations (Run No. 7)

Log Suite:

- Tube Wave Reflection Log (Mobil Research)
- Cement Bond Log/Variable Density Log/GR
- Casing Collar Locator
- Cement Evaluation Log
- Borehole Gravimeter
- Continuous Microseismic Radiation Survey
- Anisotropic Shear Wave Log (Mobil Research)
- Long Spaced Acoustic Log (Mobil Research)
- Shear Wave Acoustic Log (Mobil Research)
- Temperature Log
- Quadrapole Sonic

Depths Logged:

250 to 9,650 ft

The objective of the pre-perforation logging operations (Run No. 7) was to acquire baseline cement bond quality, acoustical and microseismic radiation data before perforating the well. These data would be compared to equivalent data following various fracturing treatments to determine fracture height. In addition, borehole gravimeter density measurements were planned to determine if formation density anomalies existed. By comparing data from the standard, shallow-investigating, open-hole formation density tool with data from a deep-investigating, cased-hole borehole gravimeter, such anomalies could be identified. In addition, the gravimeter data would be used to derive the overburden pressure gradient. The log data obtained during this cased-hole run are outlined in Appendix 1.

2.2.1.2 Post-Perforation/Pre-Mini-Frac Treatment Logging Operations (Run No. 8)

Log Suite:

Tube Wave Reflection Log (Mobil Research)
Cement Evaluation Log/GR
Cement Bond Log/Variable Density
Casing Collar Locator
Continuous Microseismic Radiation Survey
Tracer Scan Log

Depths Logged:

8,800 to 9,639 ft

In Logging Run No. 8, the objective was to obtain acoustical, microseismic radiation and spectral gamma ray data to add to the database being accumulated for fracture height determinations. This run was to be conducted prior to Mini-Frac No. 1 but after having perforated the well. Between these two operations, multiple injections were performed (e.g., stress tests, injection/ballout treatment) which would have created hydraulic fractures. A summary of the Run No. 8 logging operations and data collected is shown in Appendix 1.

2.2.1.3 Mini-Fracture Treatment Logging Operations (Run No. 9)

Log Suite:

Continuous Microseismic Radiation Survey
Tube Wave Reflection Log (Mobil Research)
Cement Bond Log/Variable Density Log/GR/CCL
Cement Evaluation Log/GR/CCL
TracerScan Log

Depths Logged:

8,800 to 9,590 ft

Log Run No. 9 was designed to acquire acoustical, microseismic radiation and spectral gamma ray data for comparison to that obtained on the previous runs (Nos. 7 and 8) and to estimate the height of the fracture induced in the mini-frac treatment. A summary of the data actually acquired and logging operations implemented in Run No. 9 is shown in Appendix 1.

2.2.1.4 Post-Main Fracture Treatment Logging Operations (Run No. 10)

Log Suite:

Tracer Scan Log
Cement Bond Log/Variable Density Log/GR/CCL
Cement Evaluation Log/GR/CCL
Tube Wave Reflection Log - Small Source (Mobil Research)
Tube Wave Reflection Log - Large Source (Mobil Research)
Continuous Microseismic Radiation Survey
Quadrapole Sonic

Depths Logged:

8,700 to 9,516 ft

The objective of Log Run No. 10 was to acquire fracture height data following the main fracture treatment. Descent No. 1 was executed several days after the treatment. The remaining descents were not performed for several months due to flow back and pressure buildup testing operations. The log data acquired in Run No. 10 are summarized in Appendix 1.

2.2.2 In-Situ Stress Testing

Cased-hole stress tests were performed to determine the in-situ closure stresses in the Cotton Valley Taylor sandstone and the underlying Bossier shale interval. Open-hole stress tests were concentrated in the limey shale above the Taylor sand. With the data collected from the open-hole and

cased-hole stress tests, log-calculated stresses could be calibrated and an accurate stress profile could be developed for use in fracture treatment design and modeling.

The six cased-hole stress tests performed on SFE No. 3 included three tests in the Bossier shale below the Cotton Valley Taylor sandstone and three tests in the Taylor sand. The depth intervals of these tests are shown in Table 2-5. For the cased-hole tests, 10-lbm/gal brine water was used. As in the open-hole tests, injection rates varied from 5 to 20 gal/min. For each test, a one foot interval was perforated with two perforations. The intervals were isolated with straddle-type packers run on the tubing string. A downhole shut-in tool was used on each test. The three tests in the Bossier shale (CHST 1, 2 and 3) were performed December 5 and 6, 1988. Bottomhole pressure and temperature, injection rate, surface injection pressure, and surface casing pressure were monitored and recorded using the GRI Treatment Analysis Unit (TAU). Bottomhole pressure and temperature were measured using a Panex electronic gauge with surface readout. The three tests performed in the Taylor sand (CHST 4, 5 and 6) from December 13 to 15, 1988, were

monitored and recorded using CER's High Speed Data Acquisition System.

2.3 SUMMARY OF WELL TESTING AND COMPLETION OPERATIONS

2.3.1 Pre-Fracture Tests

To effectively design and implement the optimal fracture treatment for SFE No. 3, it was necessary to quantify reservoir properties. The important properties are formation permeability, average reservoir pressure, apparent skin and reservoir size. These properties are obtained from well tests. Well tests such as production tests (which accurately monitor gas, water and condensate flow rates) and pressure buildup tests (which accurately measure bottomhole pressures) are needed to characterize the formation. These data are then analyzed to obtain the desired reservoir properties which are, in turn, used in the fracture design models and reservoir simulators to optimize the stimulation recommendation.

Pre-fracture well tests on SFE No. 3 included two flow tests and two pressure buildup tests from the Taylor sandstone

Table 2-5 Summary of Cased-Hole Stress Tests

Test	Depth, ft	Objective
CHST1	9,630 - 9,631	Bossier shale
CHST2	9,600 - 9,601	Bossier shale
CHST3	9,554- 9,555	Bossier shale
CHST4	9,324 - 9325	Taylor sandstone
CHST5	9,266 - 9,267	Taylor sandstone
CHST6	9,227 - 9,228	Taylor sandstone

perforations (9,225 to 9,250 ft and 9,285 to 9,330 ft). The initial flow test was conducted after a perforation ballout treatment. The well was produced for seven days between January 27 and February 2, 1989. This flow period included two to three swab runs per day to be sure the well was not loading up. The average flow rate for the production period was 50 MCFD and 8 BWPD. The flowing wellhead pressure was essentially zero, while the flowing bottom-hole pressure was 507 psia. Production was through a 48/64-in. choke. After the initial production period, a seven-day pressure buildup test was performed and analyzed by S.A. Holditch & Associates, Inc. to obtain estimates of reservoir properties.

The analysis of this pressure buildup test led to the following values:

$$\begin{aligned} kh &= 0.378 \text{ md-ft} \\ k &= 0.014 \text{ md} \\ h &= 27 \text{ ft} \\ s &= +0.1 \\ P^* &= 3,400 \text{ psi} \end{aligned}$$

After the first pressure buildup test, a mini-frac was performed on February 17, 1989. During the mini-frac, Teledyne Geotech conducted geophone surveys to determine fracture orientation.

The well was then opened on February 24, 1989, for another flow test. SFE No. 3 was produced for six days at an average flow rate of 310 MCFD and 8 BWPD on a 24/64-in. choke. The flowing wellhead pressure was 150 psi, and the measured flowing bottomhole pressure was 727 psi. This production period was followed by a six-day pressure buildup test from March 2 to 8, 1989. The analyses of the two pre-fracture pressure buildup tests are discussed in detail in Section 6.1.

The analysis of the second pre-fracture pressure buildup test resulted in the following values:

$$\begin{aligned} kh &= 0.88 \text{ md-ft} \\ k &= 0.022 \text{ md} \\ h &= 40 \text{ ft} \\ s &= -3.0 \\ P^* &= 3,600 \text{ psi} \end{aligned}$$

Apparently, the mini-fracture treatment connected additional pay to the wellbore.

2.3.2 Fracture Treatments

A second mini-frac (No. 2) was pumped on March 16, immediately prior to the main fracture treatment. The main purpose of the second mini-frac was to provide data for use in calibrating the 3-D fracture models. A total of 1,281 bbl of 40-lbm/gal linear gel and 290 bbl of slick water (flush) were pumped at 50 bbl/min down the casing-tubing annulus at an average pressure of 3,450 psi. The instantaneous shut-in pressure (ISIP) was measured to be 2,450 psi. The main fracture treatment was performed on the Cotton Valley (Taylor) sandstone following the second mini-frac. The primary purpose of the treatment was to provide the opportunity to collect data for analysis by various fracture diagnostic contractors, so they could calculate and/or measure the dimensions of the hydraulic fracture. Therefore, the treatment volumes and operations were designed primarily for their benefit. Unlike past SFE wells, however, specific emphasis was also placed on optimizing gas recovery efficiency from this particular reservoir.

The main fracture treatment consisted of pumping 576 bbl of treated water as pre-pad followed by 9,006 bbl of 50-lbm/gal and 40-lbm/gal crosslink gel carrying 1,168,900 lbm of 20/40-mesh Ottawa sand. The maximum sand concentration achieved was 8 lbm/gal. The treatment was pumped at an injection rate of 50 bbl/min with an average treating pressure of 3,000 psi. The treatment was successfully pumped to completion. Additional details of the treatment can be found in Section 8.0.

Several operators (Mobil, Amoco, Texaco) and service companies (Halliburton, Dowell-Schlumberger) provided continuous support and valuable input to the treatment design. GRI wishes to acknowledge the support and effort put forth by these companies. Although the final treatment was influenced by many of their recommendations, in general it was designed using the methodology developed in the GRI research program (specifically, on previous co-op wells in the Travis Peak).

2.3.3 Post-Fracture Tests and Production History

To determine the effectiveness of the hydraulic fracture treatment in SFE No. 3, post-fracture well tests were conducted. The post-fracture tests consisted of a long-term production test and an extended pressure buildup test. Flow rates (including gas, water, and condensate) were measured from the beginning of the post-fracture flow-back. Surface and bottomhole pressures were also measured during both the flow period and the shut-in period. The objectives of these tests were to supply the necessary data for reservoir simulation history matching so that the reservoir and fracture properties could be evaluated and then compared to the results of the fracture design models and the fracture diagnostic techniques used on this well.

To initiate testing after the fracture treatment, the well was flowed back to induce fracture closure. A total of 48 bbl of water was produced in 1-1/2 hours (average flow-back rate of 0.5 bbl/min) through a 4/64-in. choke. The well was then shut in until 7 a.m. on the following day, March 17, 1989, when it was opened to a frac tank on a 6/64-in. choke. SFE No. 3 produced only water for about four days, and on March 20, the well was killed with a 10-lbm/gal brine so that the wellbore could be cleaned out to the PBTD. A packer was then run into

the well, and a post-fracture gamma ray log was run. On March 23, the well was swabbed and began flowing to a tank on a 20/64-in. choke. It was later changed to a 10/64-in. choke. On the morning of March 25, after about 40 hours of flow, the well began making gas. At 8 a.m. on March 26 the gas rate had increased to 260 MCFD on a 12/64-in. choke with a flowing tubing pressure (FTP) of 1,335 psig. The water flow rate was 335 BPD.

The gas flow rate continued to increase during the flow test. On April 11, bottom-hole pressure gauges were run into the well, and an absolute open flow (AOF) test was run for the Texas Railroad Commission. Maximum flow rate during this test was 583 MCFD on a 14/64-in. choke with a FTP of 1,060 psig. At the conclusion of the AOF test, the well was put back on a 12/64-in. choke. On April 21, SFE No. 3 was shut in for six hours while the sales line was connected. All further testing was into the gas sales line.

Flow testing was continued for a period of about six weeks. Gas flow rate increased to 580 MCFD on May 8, through an 18/64-in. choke with a water rate of 105 BPD and a condensate rate of 4.6 BPD. Gas production then began declining slowly until June 15 when SFE No. 3 was shut in for a pressure buildup test. At shut-in, the well was producing 290 MCFD, 8 BWPD and 1.2 BCPD through an 18/64-in. choke with a FTP of 1,000 psig.

After about two hours of shut-in, the lubricator began leaking and the well was opened to the sales line again. It was produced for an additional 32 hours and was shut in again for the pressure buildup test at 7 p.m. on June 16, 1989. At shut-in, the flow rates had stabilized to approximately the same rates as before the initial two-hour shut-in period. Flowing bottomhole pressure at shut-in was 1,856 psia. A total of 659 hours of

pressure buildup data were acquired. When the buildup test was ended at 8 a.m. on July 14, 1989, the bottomhole pressure was 2,716 psia and surface pressure was 2,200 psig.

After the pressure buildup survey, SFE No. 3 was again opened to the sales line. Flow rate initially increased to a maximum of 610 MCFD on a 9/64-in. choke with a FTP of 1,450 psig, but it soon began to decline. On July 24, the well was shut in and killed using fluid that contained Halliburton Opti-Kleen chemicals. The tubing and packer

were then pulled so that additional post-fracture logging tools could be run. Logging was completed by July 28 and the well was returned to production after swabbing and flowing approximately 80 percent of the load fluid. At this point, a compressor was also installed. Maximum flow rate since that time has been 580 MCFD, 60 BWPD and 1 BCPD on an 18/64-in. choke with a FTP of 550 psig. As of January 1, 1990, the well was making 420 MCFD and 40 BWPD on an 18/64-in. choke with a FTP of 375 psig. Cumulative production was 99.4 MMCF of gas, 14,175 bbl of load water (out of 16,500 bbl of total load) and 360 bbl of condensate.

3.0 Geological Analysis of the Travis Peak Formation and Cotton Valley Sandstone

Geologic studies based on SFE No. 3 core, logs and well tests were performed by the University of Texas at Austin, Bureau of Economic Geology (BEG). Sedimentological studies, presented in Section 3.2, include (1) regional and local stratigraphic analyses and (2) detailed studies of the diagenesis and physical properties of Travis Peak and Cotton Valley reservoir rocks and surrounding fracture barriers. In Section 3.3, the structural studies focus on natural and artificially-created fractures and on the state of stress in East Texas. The following sections provide detailed geological analyses in each of the above areas.

3.1 GEOLOGIC SETTING

3.1.1 Regional Structural Setting of the East Texas Basin

SFE No. 3 is located in Waskom Field, Harrison County, East Texas, in the northern Gulf of Mexico Basin. The structural setting of the study area and its surroundings is depicted in Figure 3-1a. The northern Gulf of Mexico structural province is characterized by gentle bedding dips, open periclinal folds, normal faults and various structures caused by diapiric movement of salt. The Sabine Arch is a large, basement-cored, low-amplitude anticline that marks the eastern side of the East Texas Basin. SFE No. 3 is located on the northwest flank of the Sabine Arch, an area which is highlighted in Figure 3-1a by the shaded rectangle. Figure 3-1b illustrates this area in greater detail. It shows the positions of SFE No. 1 (Waskom Field), SFE No. 2 (North Appleby Field), SFE No. 3 (Waskom Field) and several GRI Tight Gas Sands Program cooperative wells.

Current stresses in the Travis Peak and Cotton Valley primarily reflect loading by overlying sedimentary rocks and mild gulfward extension. The orientation of the greatest principal stress is vertical, and the least principal stress is typically oriented normal to regional fault trends (see Figure 3-1a). Three factors suggest that the modern least horizontal stress in the study area trends generally north-northwest: (1) recent movement on east-northeast-trending normal faults near the Elkhart-Mount Enterprise fault zone (Collins and others, 1980), (2) hydraulic-fracture stress tests (Holditch and others, 1987), and (3) borehole-breakout trends (Baumgardner and Laubach, 1987).

3.1.2 Local Structural Setting of Waskom Field

As seen in Figure 3-2, Waskom Field is located on a gentle structural dome. The Cotton Valley and Travis Peak produce primarily from structural traps associated with the Sabine Arch and with numerous salt structures (Kosters and others, 1989). The Waskom structure exists in a region of northwesterly dipping beds, and the top of the Travis Peak occurs at approximately 6,000 ft below sea level. The top of the Cotton Valley occurs at approximately 8,000 ft below sea level. Saucier and Finley (1984) and Saucier and others (1985) postulated that the Waskom structure is a salt-cored, low-amplitude anticline that developed syndepositionally as a consequence of unequal loading of the underlying salt during Travis Peak progradation from the northwest. At least one well over the Waskom structure, the Arkla Waskom-Smackover No. 1, penetrated salt at a depth of 11,341 ft.

30

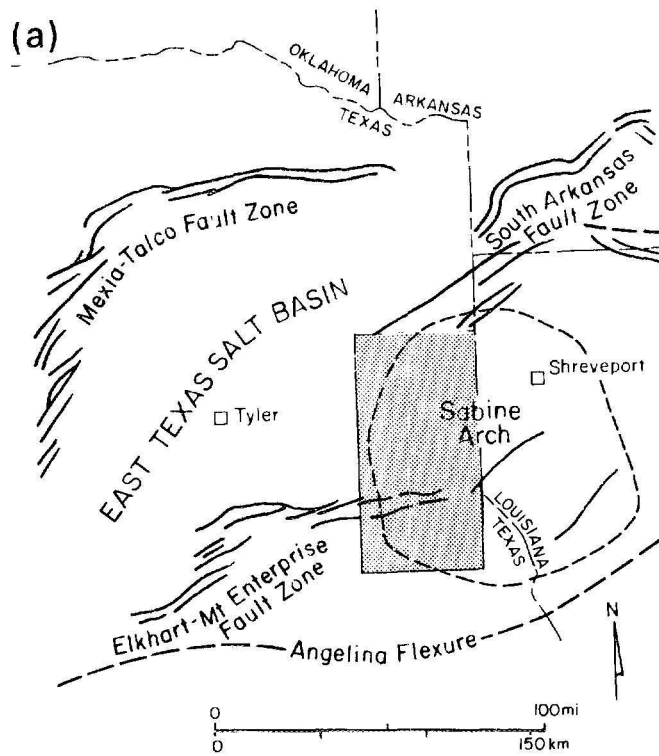


Figure 3-1a Structural Setting of the Study Area in the Northern Gulf of Mexico Basin

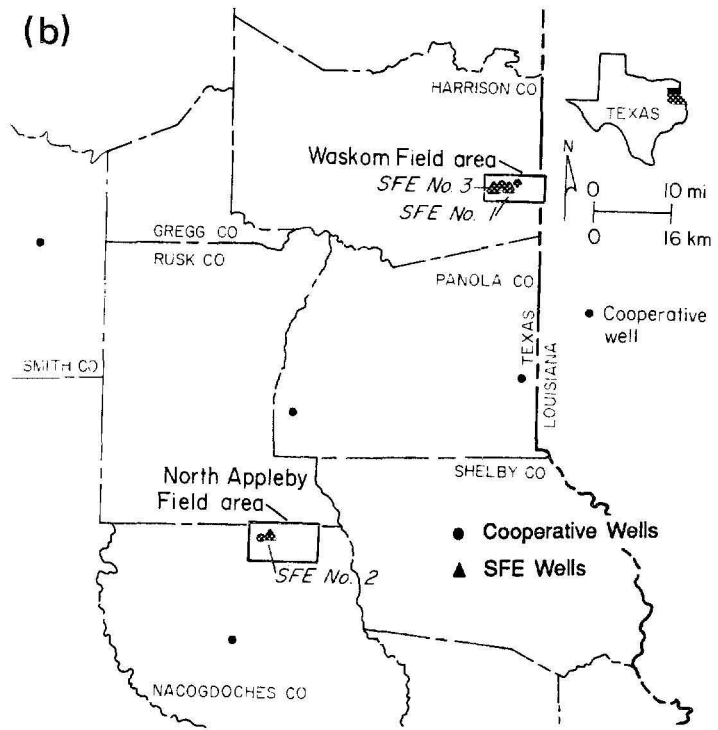


Figure 3-1b Location of Gas Research Institute Research Wells in East Texas

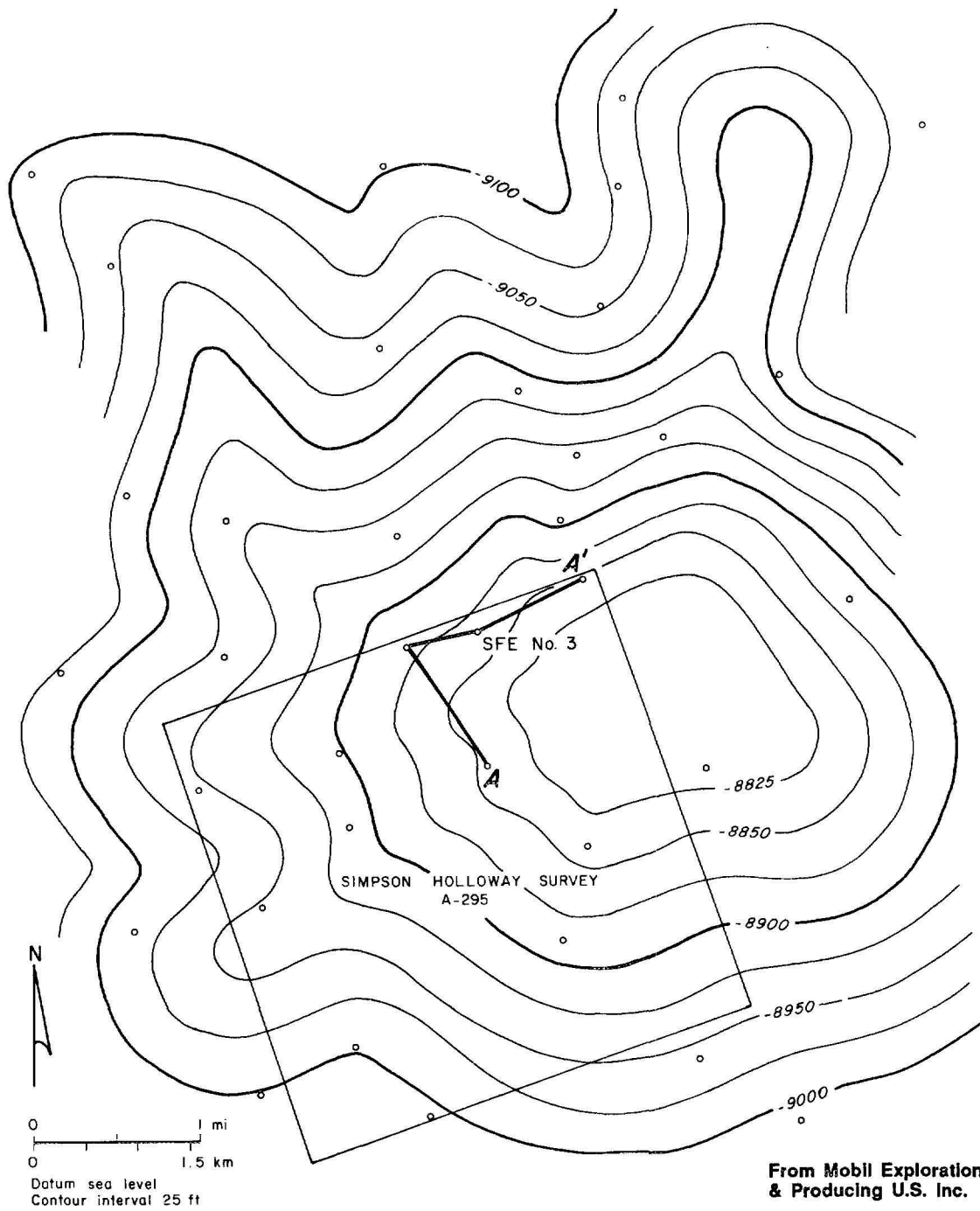


Figure 3-2 Structure Map of the Top of the Lower Cotton Valley Taylor Sandstone, Waskom Field

3.1.3 Regional Stratigraphy and Depositional Systems of the Travis Peak Formation and Cotton Valley Group

Sandstones of the Jurassic Cotton Valley Group and Lower Cretaceous Travis Peak Formation represent the first major progradation of terrigenous clastics into East Texas after the opening of the Gulf of Mexico in the Jurassic (Seni and Jackson, 1983). From bottom to top, the Cotton Valley Group consists of the Bossier shale, the Cotton Valley sandstone (also called the Schuler Formation), and in some places, the Knowles limestone. A thin, transgressive-marine deposit, the Knowles limestone overlies the Cotton Valley sandstone in the distal parts of the East Texas Basin, but pinches out updip (to the northwest). Where the Knowles limestone is absent, the Travis Peak-Cotton Valley contact is considered to be unconformable (Tye, 1989). The end of Travis Peak deposition was also marked by marine transgression; the top of the Travis Peak is picked at the base of the limestones of the overlying Sligo Formation.

Depositional history of Cotton Valley sandstones has been summarized by Thomas and Mann (1966) and by Wescott (1983). In Louisiana and Mississippi, Cotton Valley sandstones probably were deposited in a strike-fed, strandplain-barrier bar depositional system with most of the sediment being derived from the ancestral Mississippi River. Cotton Valley sandstones on the Sabine Arch generally are interpreted as barrier-island deposits (Wescott, 1983) that may have had a different sediment source than the Mississippi River. Cotton Valley sandstones in the East Texas Basin are interpreted by Wescott (1983) as having been supplied by fluvial-deltaic systems with source areas in the Ouachita Mountains to the north and west. Sedimentation rates appear to have been fairly continuous, resulting in a relatively continuous progradational sandstone-shale sequence (Wescott, 1983).

The main Cotton Valley reservoir on the Sabine Arch in East Texas is the Taylor sandstone, which occurs at the base of the Cotton Valley interval, directly above the Bossier shale (Presley and Reed, 1984). Along the northern part of the Sabine Arch, the Taylor interval consists of one or more upward-coarsening reservoir sandstones. The Taylor pinches out to the south in central Panola and Rusk Counties (Presley and Reed, 1984).

The Travis Peak Formation in East Texas was probably a major fluvial-deltaic system that prograded from the northwest (Bushaw, 1968; Saucier and others, 1985; Tye, 1989). It has been divided into two main depositional systems: a middle fluvial system and a paralic system that gradationally underlays and overlays the fluvial deposits. The 1,600-ft-thick, sandstone-rich fluvial interval is interpreted as a braided- to meandering-stream system containing stacked sandstones that individually range from 10 to 50 ft thick (Dutton, 1987; Tye, 1989). In the study area, the upper paralic system ranges from 150 to 600 ft thick. The lower paralic deposits are less than 100 to 300 ft thick. The paralic system, which contains thinner sandstones and a higher percentage of mudstone beds, was deposited in a range of environments, including coastal-plain, marsh, estuary, bay, and tidal-flat (Finley and others, 1985; Dutton, 1987; Tye, 1989).

3.1.4 Local Stratigraphic Setting of Waskom Field

In its entirety, the Travis Peak section in Waskom Field is approximately 2,000 ft thick, and the Cotton Valley sandstone and Knowles limestone together are about 1,500 ft thick. The top of the Travis Peak Formation in SFE No. 3 is at 5,908 ft below kelly bushing (KB), or 5,576 ft below sea level (-5,576 ft SL). The top of the Cotton Valley (Knowles limestone) is at 7,943 ft KB (-7,611 ft SL). The Taylor sandstone interval occurs from 9,200 to 9,356 ft KB (-8,868

to -9,024 ft SL). The top of the Bossier shale is at 9,435 ft KB (-9,103 ft SL).

3.2 SEDIMENTOLOGICAL ANALYSES - SUMMARY AND CONCLUSIONS

The availability of core and log data from the SFE No. 3 well permitted BEG to perform detailed stratigraphic and petrologic studies of the Travis Peak Formation, Cotton Valley sandstone and Bossier shale. An understanding of tight sandstone reservoirs, from a regional to a microscopic perspective, was attained from these analyses and integrated into other Tight Gas Sands Program research areas.

Subsurface data from SFE No. 3 indicate that environments of deposition of the cored intervals range from fluvial (lower Travis Peak) to marginal marine (base of Travis Peak and lower Cotton Valley) and marine (Bossier). Sandstones and mudstones deposited in the lower Travis Peak represent deposition in meandering fluvial channels and laterally adjacent floodplain environments. Interbedded sandstones and mudstones at the base of the Travis Peak are indicative of sediments deposited in paralic environments, including bays or estuaries. These nearshore-marine environments developed during the earliest stages of Travis Peak deposition, following deposition of the Cotton Valley Knowles limestone.

Fossiliferous mudstones in the lower Cotton Valley (above the Taylor sandstone) are interpreted as being deposited in oyster bioherms that developed in low-energy marine bays. Sandstones and mudstones in the Taylor interval were deposited in a marine-shoreline setting. In an upward direction, the environments represented include the following: (1) shoreface, (2) microtidal barrier island, (3) lagoon and washover, (4) microtidal barrier island, (5) tidal inlet, and (6)

marsh-lagoon. This vertical sequence was formed by an initial shoreline regression, a subsequent transgression, and later relative sea level stillstand as indicated by the stacking of barrier and tidal-inlet deposits. Shales from the upper Bossier were deposited in a low-energy shelf environment below normal wave base.

Sandstone geometry, continuity and internal heterogeneity influence reservoir performance and well-to-well communication. Small-scale bedforms, biogenic structures, clay drapes and scour surfaces create fluid-flow barriers and segment reservoirs. Sandstones with the best reservoir potential in the lower Travis Peak are fluvial channels oriented parallel to depositional dip. Reservoir quality decreases in channel margins (levees), in tops (abandoned channel deposits), and in interchannel areas where siltstones and mudstones accumulated.

The best reservoir sandstones in the Cotton Valley are barrier-island deposits oriented parallel to depositional strike and tidal-inlet sandstones oriented perpendicular to depositional strike. Reservoir quality decreases vertically in lagoon and washover deposits above barrier-island sandstones and in abandoned-inlet deposits above tidal-inlet sandstones. Marsh and lagoon mudstone deposits cap the Taylor sandstone and form a seal for hydrocarbons.

Petrographic analysis of SFE No. 3 core provided detailed reservoir descriptions that aided in the development of the completion strategy. Thin-section point-count data supplied accurate information on mineral composition, which was used to calibrate geophysical log responses. Petrographic data also indicated zones of potential fluid sensitivity. For example, locally abundant ankerite cement in the Travis Peak and Cotton Valley could form a damaging iron-hydroxide gel if it were treated with acid.

Finally, the petrographic data indicated important differences between Travis Peak and Cotton Valley reservoir sandstones. Whereas Travis Peak sandstones are cemented primarily by quartz, calcite is the most extensive cement in many Cotton Valley sandstones. The calcite-cemented zones have the lowest permeability within the Taylor sandstone, unlike the quartz-cemented sandstones which exhibit higher porosity and permeability.

Important differences also exist in the composition of the finer-grained deposits interbedded with the sandstones. Mudstones interbedded with Travis Peak sandstones contain significant volumes of sand- and silt-sized grains, in addition to clay-sized particles. Mudstones in the Cotton Valley have a much higher percentage of clay-sized grains, particularly in the Bossier shale. Mudstones in the lower Cotton Valley sandstone interval contain abundant oyster fragments in a clay matrix. Because of the finer grain size, mudstones in the Cotton Valley are more likely to be effective fracture barriers than are mudstones in the Travis Peak.

3.2.1 Stratigraphy of Travis Peak and Cotton Valley, Waskom Field

Figures 3-3 and 3-4 show the SP and resistivity (RILD) logs from SFE No. 3 in the cored intervals of the Travis Peak Formation, Cotton Valley sandstone and Bossier shale. The perforated intervals in the Cotton Valley Taylor sandstone are shown in Figure 3-4. Travis Peak core was recovered from 7,351.0 to 7,409.8 ft (Cores 1 and 2, labeled Zone 1) and from 7,868.0 to 7,943.3 ft (Cores 3 to 5, labeled Zone 2). The Travis Peak core samples are from 1,443 to 2,035 ft below the top of the formation. Cotton Valley core was recovered from 9,017.8 to 9,043.5 ft (Core 6, labeled Zone 3) and 9,199.0 to 9,367.9 ft (Cores 7 to 13, labeled Zone 4). These Cotton Valley core

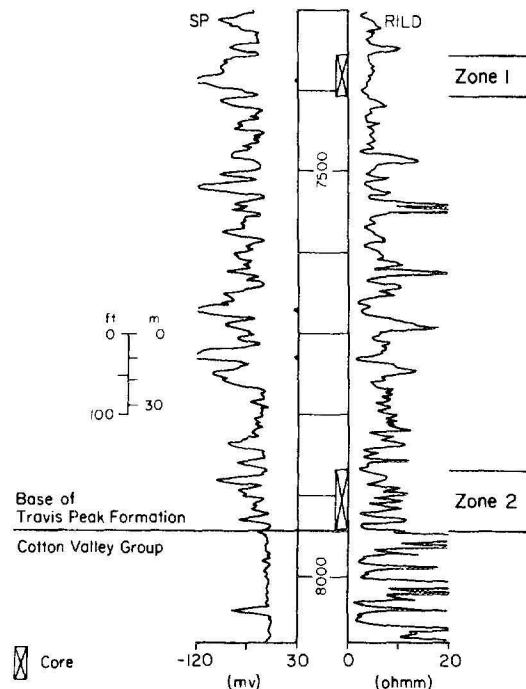


Figure 3-3 Gamma Ray and Resistivity Logs of Lower Travis Peak, SFE No. 3

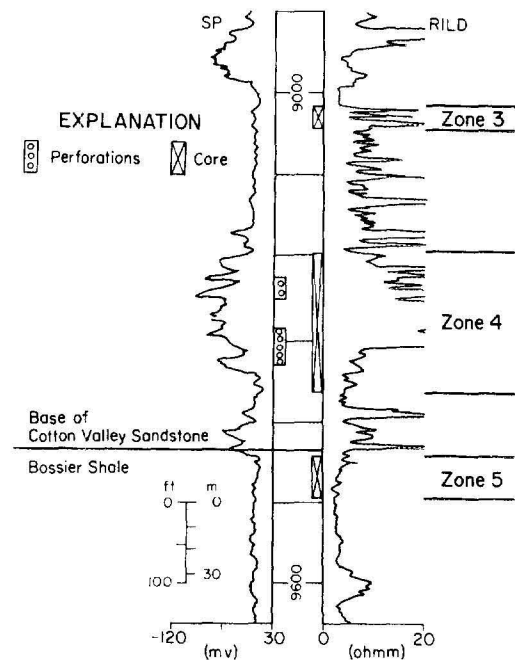


Figure 3-4 Gamma Ray and Resistivity Logs of Lower Cotton Valley Sandstone and Upper Bossier Shale, SFE No. 3

samples are from 1,075 to 1,425 ft below the top of the Cotton Valley Group. Bossier shale core was recovered from 9,449.0 to 9,500.0 ft (Cores 14 to 16, labeled Zone 5).

Shown in Figure 3-5, the cross section of the lower Cotton Valley sandstone interval, including the Taylor, is based on data from SFE No. 3 and adjacent wells. Figure 3-2 traces the path (A to A') on a structure map of the top of the Taylor sandstone. In Waskom Field, the Taylor sandstone consists of an upper sandstone that is up to 100 ft thick and a lower sandstone up to 25 ft thick. The division between upper and lower Taylor sandstones in SFE No. 3 occurs at a depth of 9,360 ft. Both the upper and lower Taylor sandstones are elongated, trending northeast-southwest across Waskom Field, as illustrated by net sandstone isoliths shown in Figures 3-6 and 3-7.

3.2.2 Macroscopic Core Descriptions and Interpreted Depositional Environments

Macroscopic sedimentary characteristics of 16 cores representing five stratigraphic intervals from SFE No. 3 were logged using standard sedimentologic techniques. A hand lens and binocular microscope were used to provide a better visual estimate of the range in sediment grain sizes present. The vertical scale at which the cores were logged is 1 in. = 5 ft (Tye and others, 1989). The following primary characteristics are noted on the logging form: rock type, sedimentary structures (primary and biogenic), sediment grain size, and texture (sorting). Also included in the descriptions are secondary attributes such as induration, color, relative occurrence of carbonate cement, bedding contacts (scoured, sharp, gradational, broken, etc.), and accessories (bitumen, organic material, diagenetic nodules).

To simplify the following discussion of the cored zones, each stratigraphic interval is

described separately in descending order of occurrence. Lithologic and sedimentary descriptions are given for the lithofacies that comprise each stratigraphic interval, and the vertical lithofacies arrangement is discussed. For clarity, the label assigned to each facies also identifies the zone in which it occurs. An example is Facies 1.4. This label signifies the fourth type of facies in Zone 1. Next appears an interpretation of the depositional environments represented by the cores. These interpretations are based solely on data obtained from the SFE No. 3 well and are somewhat general. The environments of deposition range from fluvial (Zone 1, Travis Peak) to marginal marine (Zone 2, Travis Peak and Zones 3 and 4, Cotton Valley), and marine (Zone 5, Bossier).

3.2.2.1 Travis Peak Formation

Seven lithofacies are present in the upper cored interval of the Travis Peak Formation (see Zone 1, Figure 3-3). They are, in order of decreasing abundance, (1) rippled to planar-laminated sandstone; (2) planar crossbedded sandstone; (3) burrowed to rippled, muddy sandstone; (4) planar-laminated to burrowed sandstone; (5) burrowed sandy mudstone; (6) sandstone and clay-clast conglomerate; (7) burrowed to laminated mudstone. These categories will be referred to as Facies 1.1 - 1.7, respectively.

The gamma-ray log signature of Zone 1 (Figure 3-3) signifies the presence of two stacked sandstones: a basal, 17-ft-thick, sharp-based and sharp-topped sandstone with a blocky-appearing log pattern and an upper, 42-ft-thick sandstone with a bell-shaped log pattern. Approximately 10 ft of mudstone and muddy sandstone separate the sandstones. Only the upper 6 ft of the basal sandstone was cored, and it consists of Facies 1.1 and 1.4. Four feet of rippled sandstone (Facies 1.1) grade upward into laminated and burrowed sandstone (Facies

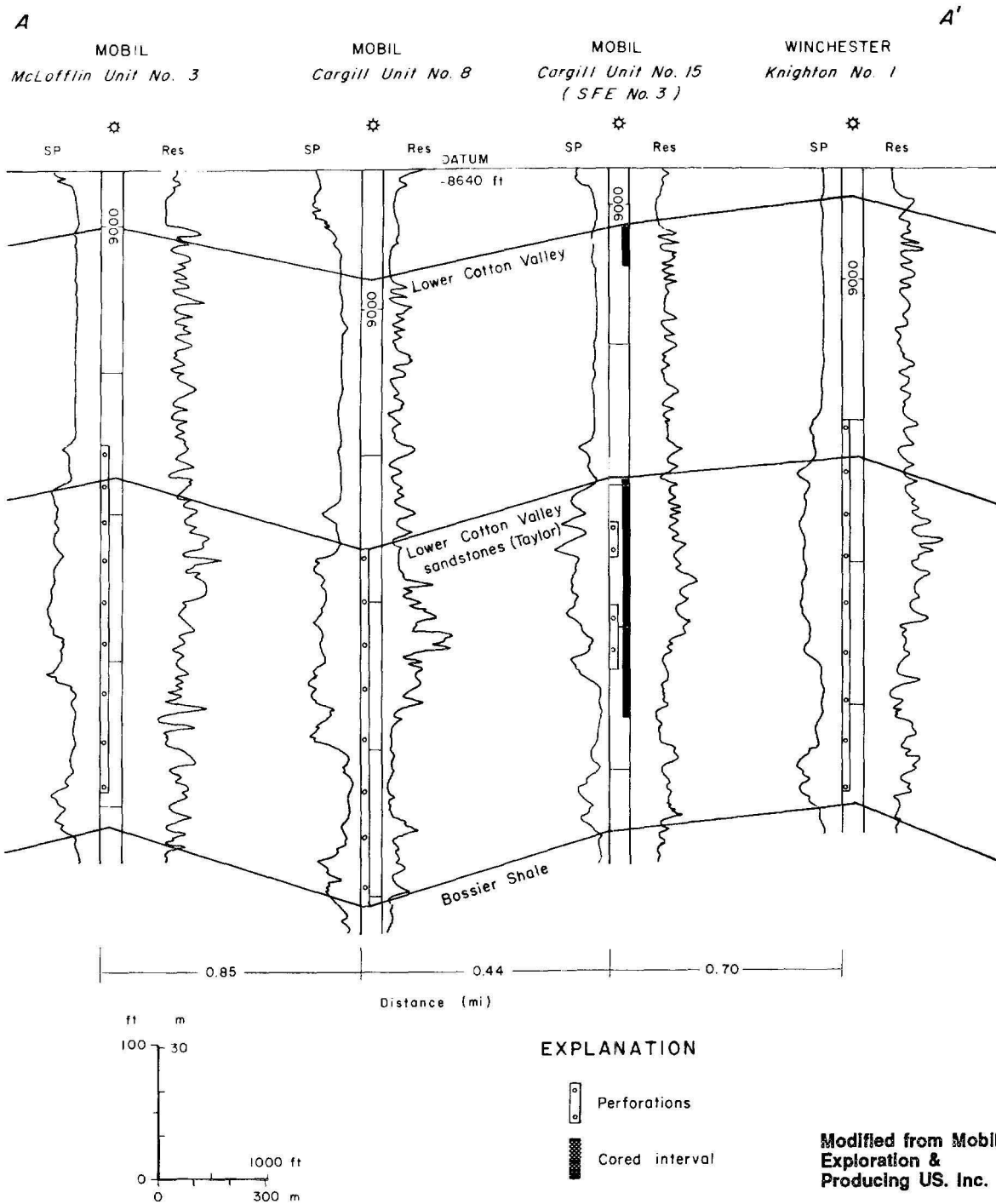


Figure 3-5 Cross Section of Lower Cotton Valley Taylor Sandstone Interval in the Area Around the SFE No. 3

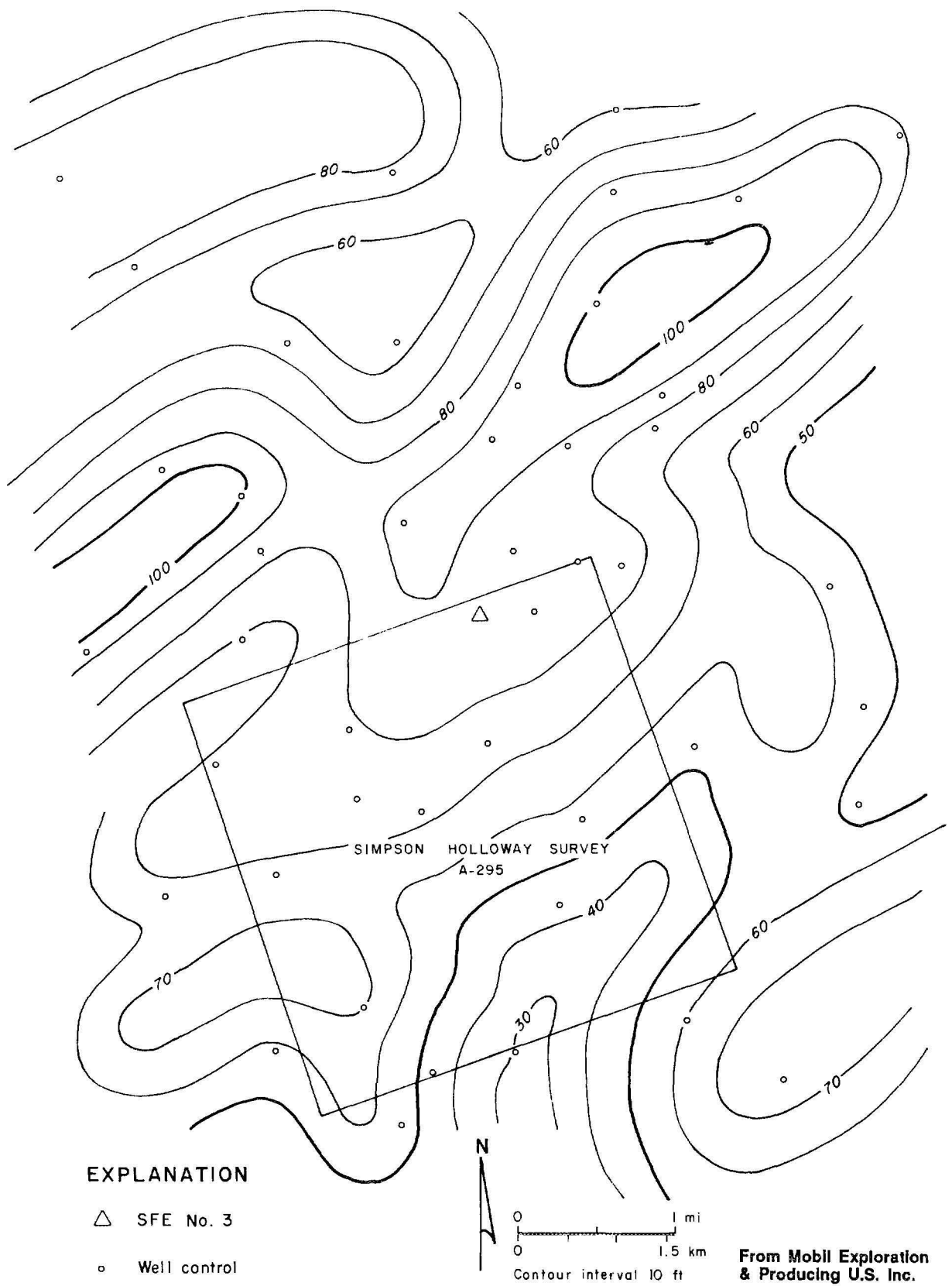


Figure 3-6 Net Sandstone Isolith Map of Upper Taylor Sandstone, Waskom Field

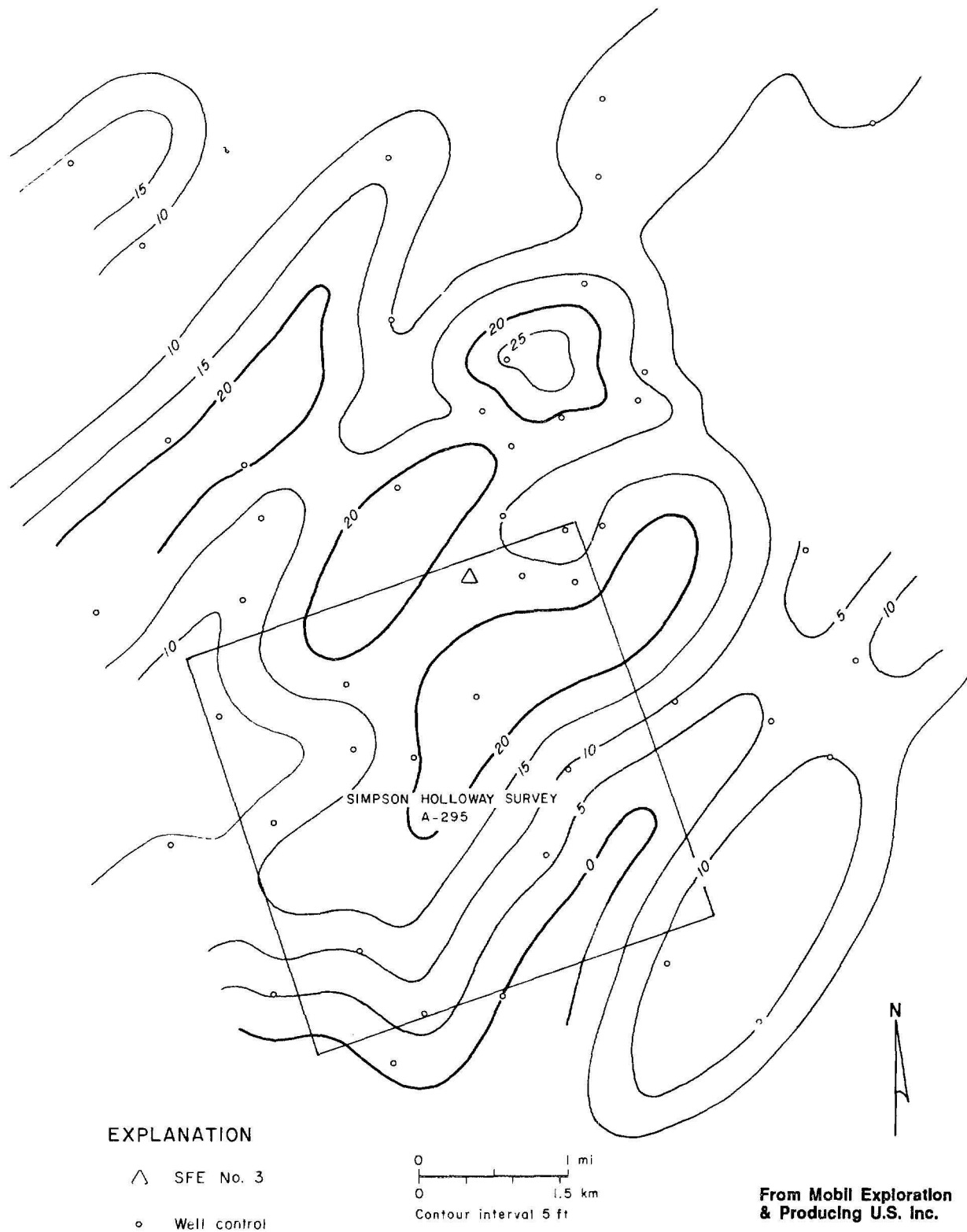


Figure 3-7 Net Sandstone Isolith Map of Lower Taylor Sandstone, Waskom Field

1.4) that is in turn overlain by 4 ft of laminated mudstone (Facies 1.5). Within the muddy interval between the sandstones overlying Facies 1.5 is an upward-coarsening, rippled and burrowed sandstone (Facies 1.3) that is 5 ft thick. Facies 1.2 abruptly overlies Facies 1.3, forming the basal portion of the second sandstone. Planar cross-bedded sandstone of Facies 1.2 grades upward into a thick sequence (33.5 ft) of Facies 1.1 rippled sandstone. Three minor scoured contacts represent the only significant sedimentary breaks in Facies 1.1. At the top of the cored interval, Facies 1.1 is separated from Facies 1.6 by a scoured contact, and Facies 1.6 is capped by laminated mudstone of Facies 1.7.

Sandstones and mudstones found in Zone 1 represent deposition in fluvial channels and laterally adjacent floodplain environments. Facies 1.1 and 1.2 in the lower and upper sandstones were deposited by current flow through fluvial channels. The dominance of ripple-laminated sandstone and the "upward-fining" log and lithologic character imply deposition in a meandering-fluvial system. The basal crossbedded sandstone (Facies 1.2) probably was formed by the migration of sand waves or transverse bars along the channel bottom. The planar and trough-ripple lamination, parallel lamination and rare root traces in Facies 1.1 are indicative of deposition in upper channel reaches (point bar) and levee environments.

Mudstones and muddy sandstones separating the two sandstones are indicative of abandoned-channel (Facies 1.4, 1.6 and 1.7), lacustrine (Facies 1.5), and overbank (Facies 1.3) deposits. The finer-grained sediments in Facies 1.6 and 1.7 that cap the channel deposits accumulated in response to the abandonment of the channels. The lacustrine deposits may represent a small pond or ox-bow lake, or they may have accumulated in an extensive floodplain lake. The muddy sandstone overlying the

lacustrine deposits was probably formed by flood-induced processes that resulted in deposition of a prograding crevasse splay or lacustrine delta.

The best potential reservoir sandstones in the lower Travis Peak are fluvial channels oriented parallel to depositional dip. Highest permeability in the lower Travis Peak in SFE No. 3 occurs from 7,384 to 7,398 ft (log depth) in planar crossbedded, medium- to fine-grained sandstone. Reservoir quality decreases at channel margins (levees) and tops (abandoned channel deposits), as well as in interchannel areas where siltstones and mudstones accumulated.

3.2.2.2 Travis Peak-Cotton Valley Transition

Four lithofacies occur within the 71.1-ft-thick Travis Peak-Cotton Valley transition interval in Zone 2, shown in Figure 3-3. In order of decreasing abundance, they are (1) rippled, silty sandstone; (2) burrowed, fossiliferous, silty sandstone; (3) fossiliferous, sandy mudstone; and (4) sandy mudstone. These facies will be referred to as Facies 2.1 - 2.4, respectively.

The gamma-ray log signature for Zone 2, in the Travis Peak-Cotton Valley transition, reveals four sandstones with sharp bases and tops that range from 9 to 17 ft thick, as shown in Figure 3-3. Thin (2 to 5 ft) shaly interbeds separate the sandstones and thus impart a serrate character to the gamma-ray log. The shallier sections of Zone 2 are comprised of Facies 2.3 and 2.4. These facies are present at the base of the cored interval and between the sandstones. Facies 2.1 forms the basal portion of the sandstone beds, and it can abruptly overlie Facies 2.3 or 2.4. In most instances, Facies 2.1 is gradationally overlain by Facies 2.2. Facies 2.2 forms the upper portion of the sandstone beds, and it generally fines upward into Facies 2.4.

These interbedded sandstones and mudstones are indicative of sediments deposited in paralic environments that developed during early stages of Travis Peak deposition (Tye, 1989). Fossil content and sedimentary attributes of the finer-grained facies (Facies 2.3 and 2.4) imply deposition in a semi-protected bay. The preservation of articulated and unabraded mollusk shells, the predominance of grazing burrows, and the presence of wave-formed ripple laminations indicate low-energy, marginal-marine to marine deposition. Faunal diversity in the mudstones and sandstones is low which suggests that fluvial systems may have emptied into this area. Such systems would produce brackish to marine conditions, indicating that the bay was actually an estuary. A well-developed, 3-ft-thick, oyster bioherm is present between 7,901.7 and 7,905.0 ft. The presence of mudstone matrix in the bioherm and the scarcity of wave- or current-formed structures in the mudstones implies deposition in a protected environment.

Sandstone beds abruptly overlie the bay mudstones and fine upward. Ripple cross-laminated sandstone at the base grades upward into burrowed and wavy-bedded sandstone. These sediments were deposited by relatively high-energy processes (wave, tidal current, storm) that formed thin shoals within the bay. An upward increase in burrowing activity in the shoal sandstones and the presence of root traces at the top of shoal sandstones indicate a progressive decrease in depositional energy and subaerial exposure of the shoal top. A thin marsh deposit and a storm-emplaced, fossiliferous, silty sandstone (7,874.0 to 7,876.0 ft) cap the uppermost sandstone in the cored interval. The stacked bay-shoal sequences imply that consistent depositional processes operated within a slowly subsiding basin. Perhaps because of progradation during early Travis Peak deposition, shoal sandstones are thicker and somewhat better sorted at the top of the cored interval.

3.2.2.3 Cotton Valley Sandstone

Two lithofacies occur in Zone 3, the mudstone above the Taylor sandstone, as shown in Figure 3-4. Facies 3.1 is a fossiliferous sandy mudstone, and Facies 3.2 is a fossiliferous silty mudstone. The gamma-ray log shows that this 26-ft-thick interval is relatively shaly, but there are three slightly sandier beds within it. The Facies 3.1 sediments that comprise these coarser beds generally contain less than 10 percent very fine-grained sandstone. Although Facies 3.1 and 3.2 are both mudstones, the gamma-ray log is responding to the large increase in shell material and slight increase in sandstone in Facies 3.1. Occurrences of Facies 3.2 are thin and intercalated with Facies 3.1 beds.

Facies 3.1 and 3.2 mudstones were deposited in a semi-protected or low-energy bay. Faunal evidence and sparse, wave-formed, physical sedimentary structures indicate that oyster bioherms grew in a low-energy marine bay. Facies 3.1 represents deposits associated with the bioherms, whereas Facies 3.2, which is finer grained, consists of bay deposits that apparently accumulated after the death of the bioherm. Bioherm demise probably occurred because of a change in hydrographic conditions (sea level, waves, tides) in the bay. Other environmental possibilities include estuary, lagoon or marine shelf (within storm wavebase); a more precise explanation requires additional data.

The following four lithofacies comprise Zone 4, shown in Figure 3-4: (1) well-sorted, fine-grained sandstone; (2) pebbly fine-grained sandstone; (3) burrowed sandy mudstone; and (4) fossiliferous silty mudstone. The gamma-ray log through the Taylor interval of the Cotton Valley depicts a basal, 22-ft-thick, upward-coarsening sandstone that overlies a 40-ft-thick shale. Facies 4.1 occupies the top 14 ft of this lowermost sandstone. Below this sandstone are alternating beds of Facies 4.1 sandstone and Facies

4.3 mudstone. The only occurrence of Facies 4.4 is in this lower shale zone, just below the upward-coarsening sandstone.

A 10-ft-thick mudstone that consists of alternating beds (2 to 5 ft thick) of Facies 4.1 and Facies 4.3 separates the basal sandstone from an overlying 120-ft-thick sandstone. Facies 4.1 sandstone (approximately 25 ft thick) occupies the basal portion of the upper Taylor sandstone, and it imparts an inverse-bell (upward-coarsening) shape to the log. This Facies 4.1 interval is erosionally overlain by stacked sequences of Facies 4.2 sandstone. The thickness of Facies 4.2 sandstones decreases upward, and near the top, thin beds of Facies 4.1 sandstone and Facies 4.3 mudstone divide the Facies 4.2 region. The gamma-ray log represents the Facies 4.2 deposits as bell-shaped intervals (upward-fining) with thin shaly tops. The uppermost portion of the cored interval contains approximately 16 ft of Facies 4.1 sandstone capped by 0.5 ft of Facies 4.2 and 3.0 ft of Facies 4.3.

Lithologic and sedimentologic characteristics of core from the lower Cotton Valley (Zone 4) imply that the sediments were deposited in a marine-shoreline setting. In an upward direction, the environments represented are (1) shoreface, (2) microtidal barrier island, (3) lagoon and washover, (4) microtidal barrier island, (5) tidal inlet, and (6) marsh-lagoon. The vertical sequence was formed by an initial shoreline regression, a subsequent transgression, and later, relative sea level stillstand as indicated by the stacking of barrier and tidal-inlet deposits.

The basal sandstone was deposited by a regressive barrier island that prograded over a low-energy shoreface. Continued shoreline progradation resulted in deposition of back-barrier sediments (lagoon and washover, Facies 4.1 and 4.3) over the first barrier island. Marine transgression is indicated by the Facies 4.3 deposits at 9,315 ft and the presence of overlying barrier-island de-

posits. Progradation of a second barrier island was initiated because of a decrease in the rate of sea-level rise or an increase in sedimentation rate, or both. The barrier islands were probably similar to the microtidal barrier islands that line the coast of North Carolina and the U.S. Gulf Coast. Physical sedimentary structures indicate wave processes were important in reworking the sandstones, but tidal influences were minimal by comparison.

Tidal inlets eroded and reworked the second barrier-island deposit. Inlet migration and shoreline subsidence resulted in the incorporation of stacked, tidal-inlet sequences in the uppermost portion of the Taylor sandstone. Interbedded with the tidal-inlet deposits are beds of Facies 4.1 sandstone that may represent abandoned-inlet deposits. These deposits account for the upward-fining log character and emphasize the ephemeral nature of the tidal-inlet channels. Marsh and lagoon deposits cap the cored portion of the Taylor sandstone.

The best reservoir sandstones in the Cotton Valley are barrier-island deposits that are oriented parallel to depositional strike and tidal-inlet sandstones oriented perpendicular to depositional strike. Highest permeability in barrier-island sandstones occurs in well-sorted, fine-grained sandstone with low-angle planar crossbeds; gently inclined to horizontally oriented parallel laminae; and current and wave ripple laminations. Examples of this facies occur at 9,284 to 9,294 ft and 9,320 to 9,330 ft as shown in Figure 3-4.

Other permeable zones occur at the base of tidal-inlet channels, for example from 9,225 to 9,231 ft and from 9,243 to 9,250 ft, as shown in Figure 3-4. These tidal-channel sandstones are (1) well-sorted, fine-grained sandstones with sedimentary structures similar to the barrier-island deposits and (2) pebbly, fine-grained sandstones with erosional lower contacts and abundant pebble-sized chert clasts at the base. Planar-

ripple cross lamination is the prevailing physical structure. Reservoir quality decreases vertically in lagoon and washover deposits above barrier-island sandstones and in abandoned-inlet deposits above tidal-inlet sandstones. Marsh and lagoon mudstone deposits cap the Taylor sandstone and form a seal for hydrocarbons.

3.2.2.4 Bossier Shale

Two lithofacies occur in Zone 5, in the Bossier shale: (1) fossiliferous, silty mudstone and (2) fossiliferous, sandy mudstone. The gamma-ray log through this portion of the Bossier shale has a spiky appearance indicating that the sand content increases upward, as shown in Figure 3-4. The spiky log character is a response to bedded shell material and increased sandstone content of Facies 5.2. Facies 5.1 comprises the basal 30 ft of this cored interval; the upper 30 ft consists of interbedded Facies 5.1 and Facies 5.2 deposits. Facies 5.2 becomes more abundant upward.

The mudstones in this cored interval were deposited in a low-energy shelf environment. Rare ripple laminations and normally graded shell beds indicate that although this environment was below the normal wave base, storm processes affected sedimentation. Association with a prograding shoreline (Taylor sandstone) is implied by the upward increase in sand (Facies 5.2).

3.2.3 Petrographic Description

Thin-sections of 48 samples from SFE No. 3 were examined using standard petrographic techniques to evaluate the mineralogy of detrital and authigenic phases, the porosity, and the grain size. Eighteen thin-sections are from the Travis Peak Formation; 24 samples are from the lower Cotton Valley Taylor sandstone; 3 samples are from undifferentiated Cotton Valley above the Taylor

sandstone; and 3 samples are from the Bossier shale. Each thin-section was stained for plagioclase and orthoclase feldspars (Amaranth and sodium cobaltinitrite, respectively) and for carbonate phases (alizarin red S and potassium ferricyanide).

3.2.3.1 Grain Size

Grain size of clastic and bioclastic particles (primarily oyster fragments) in these thin-sections was estimated visually. Grain size estimates of each thin-section, listed in Tables 3-1 and 3-2, pertain to terrigenous clastic framework grains only. Detrital clay matrix and bioclasts are not included in grain size estimates.

Fifteen of 18 samples from the Travis Peak Formation are fine- to very fine-grained sandstone (0.06 to 0.25 mm), whereas the remaining 3 samples are medium sandstone (0.25 to 0.50 mm). Sandstones from the Cotton Valley exhibit a wider range in grain size, primarily because of the presence of granule- to pebble-sized fossil fragments. Bioclasts observed in thin-section reach a maximum size of about 1 cm (long dimension), but whole oyster shells up to about 4 cm across are present in some intervals of the core. Twenty of 24 samples from the Taylor sandstone are fine- to very fine-grained sandstone, and the remaining samples are medium sandstone. Framework grains in the samples from undifferentiated Cotton Valley above the Taylor sandstone are coarse silt and very fine sand. With a content of 25.5 to 29.0 percent clay-sized fines, these samples are classified as mudstone, which contains a mixture of clay-, silt- and sand-sized grains. Framework grains in three samples from the Bossier shale are medium to coarse silt. The volume of clay-sized fines varies from 55.5 to 81.0 percent, so these samples are classified as mudstones and claystones, in the textural classification of Folk (1974).

Table 3-1 Petrographic Analyses of SFE No. 3 Core, Travis Peak Formation Samples

Depth, ft	<u>Framework Grains</u>							<u>Matrix</u>	
	Quartz	Plagioclase	Orthoclase	MRF	Chert	Clay Clasts	Mica	Other	Clay-Sized Fines
7354.5	49.0	3.5	2.0	2.5	0	3.0	0.5 ¹	0	14.0
7357.4	54.0	5.0	1.5	2.0	0.5	0	0	0	0
7370.1	64.0	2.0	0	1.5	0	0.5	0	0	0
7383.7	69.0	1.0	0	0.5	1.0	0	0	0	0
7386.0	63.5	0.5	0	0	1.0	0	0	0.5 ²	0
7386.1	68.0	0	0	2.0	0	0.5	0	0	0
7392.2	62.5	1.0	0.5	0.5	1.0	0	0	0	0
7399.5	38.0	1.0	1.0	0	0	0	0	0.5 ³	58.5
7407.9	66.0	1.5	0.5	1.0	0	0.5	0	0.5 ⁴	1.5
7876.7	66.5	2.5	0	1.5	0	0	0	0	0
7881.5	67.5	3.5	0	0	0	1.5	0	0	0
7883.5	62.0	10.0	0.5	0	0	1.0	0	0	0.5
7895.7 ⁵	28.0	0	0	0	0	0	0	0	0
7897.4	63.5	0.5	0.5	0	0	0.5	0	0	0
7917.8	64.0	4.0	0	0.5	0	0	0	0	2.0
7925.7	13.5	0	0	0	0	0	0	0	9.5
7930.8	65.5	3.0	0	0.5	0.5	1.5	0	0	0
7943.2	26.5	0	0	0	0	0	0	0	2.5

¹Muscovite ²Sandstone fragment ³Tourmaline ⁴Plutonic rock fragment

⁵Two rock types present in sample: ankerite-cemented sandstone and sparsely sandy limestone

Continued

Table 3-1, Continued

Depth, ft	<u>Cements</u>							<u>Porosity</u>		<u>Grain Size,</u>
	Quartz	Dolomite	Ankerite	Illite	Chlorite	Kaolinite	Other	Primary	Secondary	mm
7354.5	11.5	3.5	9.0	0	0	0	0	1.5	0	0.105
7357.4	19.5	0	0	7.0	1.0	0	1.5 ¹	4.5	3.5	0.113
7370.1	18.5	0	0	0	1.0	1.0	0.5 ¹	8.0	3.0	0.165
7383.7	14.5	0	0	4.0	0	1.5	0	7.0	1.5	0.218
7386.0	21.5	0	0	0	0.5	0.5	0	10.0	2.0	0.338
7386.1	14.0	0	0	1.0	1.5	0.5	0	9.0	3.0	0.300
7392.2	17.5	0	0	0.5	0.5	1.0	0	12.5	2.5	0.263
7399.5	1.0	0	0	0	0	0	0	0	0	0.060
7407.9	19.5	0	0	2.0	0	0.5	0.5 ¹	3.5	2.5	0.173
7876.7	17.5	0	0	1.0	0.5	0.5	0	6.0	4.0	0.128
7881.5	10.0	2.5	3.0	0	0	0.5	0	9.0	2.5	0.102
7883.5	16.0	0	2.0	0	1.0	0	0	4.5	2.5	0.098
7895.7	1.0	0	67.5 ⁵	2.0	0	0	1.5 ²	0	0	0.165
7897.4	19.5	0	10.5	0	0.5	0	1.5 ^{2,3}	2.0	1.0	0.135
7917.8	13.0	0	16.0	0.5	0	0	0	0	0	0.068
7925.7	0	2.5	72.5 ⁵	0	0	0	2.0 ^{2,4}	0	0	0.060
7930.8	15.5	1.0	2.0	0	4.0	0	0.5 ²	4.0	2.0	0.113
7943.2	2.0	0	66.0 ⁵	0	0	0	3.0 ²	0	0	0.105

¹Anhydrite²Pyrite³Reservoir Bitumen⁴Calcite⁵Includes replaced grains

Table 3-2 Petrographic Analyses of SFE No. 3 Core, Cotton Valley Group Samples

Depth, ft	<u>Cements</u>							<u>Porosity</u>		<u>Grain Size,</u> mm
	Quartz	Ankerite ¹	Fe-Calcite ²	Illite	Chlorite	Pyrite	Other	Primary	Secondary	
9022.5	0	21.0	7.0	0	0	0.5	0	0	0	0.075
9028.4	0	1.0	34.5	0	0	3.0	0	0	0	0.056
9034.5	0	35.0	0	0	0	1.5	0	0	0	0.053
9207.5	14.0	6.0	0	5.0	0	0	0	1.0	1.0	0.113
9210.5	12.5	1.5	0	5.0	0	0	0	0	1.0	0.135
9210.6	9.0	0	0	0	0	1.5	0	3.5	2.5	0.135
9213.4	0	8.0	61.5	0	0	0	0	0	8.0 ³	0.263 ⁴
9218.4	13.5	9.5	0	0	0.5	0.5	0	0	1.0	0.180
9232.0	14.5	0.5	0	3.0	0.5	0	0	1.0	0.5	0.128
9240.9	11.5	3.0	0	0	0.5	2.0	1	0	0.5	0.128
9249.5	15.5	5.5	0	5.0	0.5	0	0	2.5	0.5	0.158
9252.5	13.5	2.0	0	0	3.0	1.0	0	2.5	1.0	0.113
9260.6	7.0	3.0	0	0	0.5	2.0	0	0.5	0	0.165
9270.0	8.0	0	39.0	1.0	0	0	0	0	0	0.261
9275.6	22.0	2.5	0.5	0	0	0	0	1.5	0	0.165
9280.6	4.5	5.0	0	0	0	0.5	0.5 ⁵	0.5	0	0.135
9281.1	2.5	0	34.5	0	0	0.5	1.0 ⁵	0	0	0.105
9295.0	21.0	0.5	0	4.5	0	0	0	3.0	1.0	0.135
9295.2	15.0	0	0	0	1.0	0	0	3.5	2.0	0.135
9310.5	0.5	0	38.0	0	0	0	0	0	0	0.195
9322.9	1.0	2.5	0	0	0	5.0	0	1.0	1.5	0.075
9326.0	8.5	1.0	0.0	0	0	0	0	1.5	1.5	0.083
9329.0	14.5	0.5	0.0	5.5	3.5	0	0	1.0	0.5	0.090
9333.2	19.0	1.0	0	0	0	0	0	0	0	0.105
9341.3	1.5	0	12.5	0	0	3.0	0	0	0	0.060
9358.5	7.0	0	26.5	0	0.5	0	0	0	0	0.098
9364.0	0	2.0	0	0	0	7.0	0	0	0	0.060
9457.7	0	2.5	0.5	0	0.5	3.0	0	0	0	0.034
9475.0	0	2.5	0	0	0	5.5	0	0	0	0.038
9496.0	0.5	3.0	0	0	0	3.5	0	0	0	0.034

¹Includes dolomite

²Includes calcite

³After fossil dissolution

⁴Clastic fraction only

fossils average 2.5 mm

⁵Albite

Continued

Table 3-2, Continued

Depth, ft	Framework Grains							Matrix	
	Quartz	Plagioclase	Orthoclase	MRF	Chert	Clay Clasts	Mica	Other	Clay-Sized Fines
9022.5	18.5	0	0	0	0.5	0	0	23.5 ¹	29.0
9028.4	12.0	0	0	0	0	0	0	24.0 ¹	25.5
9034.5	19.0	0.5	0	0	0	0	0	15.0 ¹	29.0
9207.5	57.5	9.5	1.5	1.0	0	1.0	0	0	2.5
9210.5	60.5	9.0	4.5	2.0	0	1.5	0	0	2.5
9210.6	61.5	8.0	8.5	2.5	0	1.5	0	0	1.5
9213.4	13.4	0	0	0.5	0	0	0	8.0 ¹	0.5
9218.4	59.0	4.5	2.0	0	0	0.5	0	0.5 ¹	8.5
9232.0	59.5	8.0	5.0	3.5	0	1.5	0.5 ⁴	1.0 ²	0.5
9240.9	59.0	4.0	1.5	1.0	0	0	0	0.5 ³	16.0
9249.5	59.0	4.5	2.0	0.5	0.5	0	0	3.0 ¹	1.0
9252.5	54.5	7.0	2.0	5.5	0	2.5	1.0 ⁵	0	4.5
9260.6	63.0	2.5	0.5	0.5	0	0	0	0.5 ¹	20.9
9270.0	45.0	0.5	0.5	0.5	0	1.0	0	2.0 ¹	2.5
9275.6	61.0	4.5	3.0	3.0	0	0	0	1.0 ¹	1.0
9280.6	63.0	4.5	2.0	0.5	0	0	1.5 ⁵	0	17.5
9281.1	49.0	9.0	2.0	0.5	0.5	0.5	0	0	0
9295.0	59.5	5.0	3.5	1.5	0	0	0	0	0
9295.2	66.0	7.0	1.0	1.0	0	1.5	0	0	2.0
9310.5	56.5	2.5	1.0	0	0	0.5	0	1.0 ¹	0
9322.9	52.0	4.5	0	1.5	0	0	0.5 ⁴	0	30.5
9326.0	52.5	9.0	2.0	3.0	0	3.0	0	0	14.0
9329.0	55.0	13.5	0	2.0	0	1.0	0	0	3.0
9333.2	64.5	4.0	2.0	1.5	0	0.5	0	0	7.0
9341.3	46.5	6.0	0	0	0	3.0	1.0 ^{4,5}	0	26.5
9358.5	54.5	4.0	0.5	4.0	0.5	0.5	1.0 ⁴	0.5 ⁶	0
9364.0	17.0	5.5	0.5	0.5	0	0	0.5 ⁴	0	66.5
9457.7	35.0	2.0	0.5	0	0	0.5	0	0	55.5
9475.0	11.5	0	0	0	0	0	0	0.5 ¹	80.0
9496.0	11.0	0	0	0	0	0	0	1.0 ¹	81.0

¹Fossil Fragments²Tourmaline³Zircon⁴Muscovite⁵Biotite⁶Volcanic rock fragment

3.2.3.2 Mineral Composition and Porosity

Travis Peak Formation

Sandstones from the Travis Peak Formation in SFE No. 3 are mineralogically mature and have the same narrow range of framework grain compositions as other Travis Peak sandstones (Dutton, 1987). Eleven of 18 samples are quartzarenites (or possibly diagenetic quartzarenites produced as detrital feldspar grains dissolved with increasing burial depth), whereas the remaining seven samples are subarkoses (Tables 3-1 and 3-2). For the most part, the suite of Travis Peak samples chosen for study are clean sandstones. Only seven of the samples examined contain detrital clay matrix.

Detrital quartz comprises 85.5 to 100.0 percent of essential framework constituents (quartz, feldspar, rock fragments) in these sandstones (Tables 3-1 and 3-2). Total feldspar content, which ranges from 0.0 to 10.5 percent, is dominated by plagioclase. Plagioclase in all thin-sections did not accept Amaranth stain, suggesting that it was converted to diagenetic albite during burial diagenesis. Orthoclase is present in 7 of 18 thin-sections and has a maximum value of 2.0 percent. Rock fragments, in every case chert or low-rank metamorphic rock fragments, are volumetrically insignificant, making up between 0.0 and 4.0 percent of the essential framework grain fraction.

Authigenic cements and replacive minerals constitute between 1.0 and 32.0 percent of the rock volume in 15 of 18 thin-sections (Table 3-1). The remaining three sections are from the Travis Peak-Cotton Valley transition zone. In these samples, authigenic phases (primarily ankerite) constitute from 71.0 to 76.5 percent of the whole rock volume. Authigenic quartz, kaolinite, illite, chlorite, dolomite, pyrite, anhydrite and reservoir bitumen are other pore-filling substances present in Travis Peak samples from SFE No. 3.

Quartz cement is the most abundant authigenic phase in most samples, making up as much as 21.5 percent of the whole rock volume. Quartz cement averages 16.7 percent in the 13 sandstones that are not dominated by ankerite or detrital clay matrix. This average is significantly less than the average volume of 23.5 percent quartz cement observed in Travis Peak sandstones from the Holditch SFE No. 2 (Laubach and others, 1989). It is, however, close to the overall average for quartz cement in clean Travis Peak sandstones in East Texas (Dutton, 1987).

Illite, chlorite and kaolinite are common authigenic clays occurring in primary and secondary pores in Travis Peak sandstones. Whereas only one of 13 samples from SFE No. 2 contains kaolinite (Dutton and others, 1987), 7 of 18 samples from SFE No. 3 contain at least 0.5 percent kaolinite. Authigenic clays are volumetrically more important in Travis Peak sandstones that are free of carbonate phases (Table 3-1). Although the total volume of authigenic clays in SFE No. 3 samples does not exceed 8 percent (it is more commonly less than 2 percent), the net effect of these clays is to further clog pore throats already narrowed by quartz overgrowths.

Ankerite and dolomite occur as pore-filling cements and replacive minerals (commonly after feldspars) in many Travis Peak sandstones. Ankerite is the most common mineral in samples containing carbonate cement. Dolomite is present in only 4 of 18 samples and has a maximum volume of only 3.5 percent of the whole rock volume. Ankerite occurs in volumes of up to 72.5 percent in samples in which it has extensively replaced framework grains and fossil fragments. In Travis Peak sandstones from SFE No. 3, other authigenic phases are present only as accessory minerals. They probably have little effect on overall reservoir quality.

Primary intergranular pores, secondary pores produced by the dissolution of feldspar grains, and microporosity within detrital and authigenic clays contribute to total porosity in the sandstones examined. Total porosity, the sum of primary and secondary porosity, varies from 0.0 to 15.0 percent in the 18 thin-sections examined. Values reported in Table 3-1 for total thin-section porosity are commonly lower than porosity measured by porosimeter because of the presence of microporosity within clays. Microporosity cannot be quantified petrographically. Excluding samples containing more than 70 percent total cement and replacive minerals (which have no visible porosity), total thin-section porosity in Travis Peak sandstones in SFE No. 3 averages 8.0 percent.

Influence of Fibrous Illite on Permeability

An experiment carried out in conjunction with ResTech and Core Labs was conducted on Travis Peak samples from SFE No. 3 to determine if extraction and air drying of plugs damages the morphology of fibrous illite in pore systems and consequently alters measured permeability. Previous studies have shown that when fibrous illite is present in core samples, the method of sample preparation can alter fundamental petrophysical properties, including permeability (de Waal and others, 1988; Pallatt and others, 1984).

In tight gas sandstones, the permeability measurement of interest is that of gas under reservoir stress at connate water saturation. This value is generally interpreted from log response, which is calibrated by core permeability measurements. Gas permeability is measured on dry core at in-situ stress and then corrected for the slippage effect to convert to absolute, dry-core permeability (Luffel and others, 1989). Absolute dry-core gas permeability must then be adjusted to a brine permeability (at 100 percent water saturation); in low-permeability sandstones,

brine permeability commonly is lower than absolute, dry-core gas permeability (D. Luffel, Personal Communication, 1990). Relative permeability to gas is then measured to determine the effect of variable water saturation.

If even minor amounts of fibrous illite are present in the sample, then the method of sample preparation can significantly alter air and brine permeability, as well as the relationship between them. This alteration is attributed to the change in morphology that illite undergoes during air drying. As a gas-liquid interface passes through the pore, its surface tension is sufficient to collapse the delicate fibers and matt them against the pore walls. Critical-point drying and freeze drying are the two techniques that dry the sample without the presence of a gas-liquid interface and preserve the pore-bridging arrangement of the illite fibers. Gas permeabilities of air-dried samples are higher than those measured on samples that have been critical-point dried (de Waal and others, 1988).

In this experiment, ten pairs of plugs were collected from the Travis Peak fluvial-channel sandstone at 7,382.5 to 7,390.5 ft. End trims from each plug were saved for Scanning Electron Microscope (SEM) observation. Each SEM sample was divided into three parts. One part was air dried at room temperature. A second part was flash frozen in liquid nitrogen and then placed in a vacuum flask and dried for 48 hours under vacuum (freeze dried). The third part underwent Dean-Stark extraction, methanol leaching, and then vacuum oven drying at 230°F (extraction dried).

The morphology of illite in its unaltered state was determined by SEM analysis of the freeze-dried samples. Illite commonly coats feldspar grains; it also occurs in secondary pores generated by feldspar dissolution. Although it coats detrital quartz grains as

well, illite appears to nucleate on impurities on the grains rather than on the quartz itself. Illite does not grow on quartz overgrowths, and conversely, quartz overgrowths are unable to form on grains that have been coated by illite.

Two types of illite morphology occur. The first has the appearance of short blades, approximately 5 μm in height and 10 μm in width, that line the walls of pores. The ends of these sheets taper to fibers that extend another 3 to 5 μm into pores. The second morphology consists of illite fibers that project across pore spaces (pore-bridging illite). These fibers are 10 to 30 μm long and 0.1 μm thick with variable width. It is likely that they began as smaller fibers like those associated with the bladed illite. Their pore-bridging configuration is probably due to a more advanced growth stage. Examples of illite in freeze-dried samples are shown in Figure 3-8:

- Figure 3-8a is of the sample from 7,389.9 ft, showing fibrous illite that has replaced a feldspar grain. Scale bar is 100 μm .
- Figure 3-8b illustrates the lack of illite in pores between quartz overgrowths in the sample from 7,388.8 ft. Scale bar is 100 μm .
- Figure 3-8c is a close-up view of Figure 3-8b, showing fibrous illite coating a detrital quartz grain. Scale bar is 10 μm .
- Figure 3-8d illustrates the bladed-illite morphology in the sample from 7,388.2 ft. Scale bar is 10 μm .

Air drying and extraction drying both caused the fibrous illite to collapse and matt against pore walls. In some cases, the collapse of fibers was so complete that it was difficult to determine that fibrous illite had been

present. Only by high magnification of the pore walls could the matted fibers be detected. The shorter, bladed illite also showed evidence of damage and collapse, but in general, it was better preserved than the fibrous illite. Comparisons of freeze-dried versus extraction-dried or air-dried samples are shown in Figure 3-9:

- Figure 3-9a illustrates delicate illite fibers from the freeze-dried part of the sample from 7,388.8 ft. Scale bar is 10 μm .
- Figure 3-9b shows collapsed illite fibers from the extraction-dried part of the sample from 7,388.8 ft. Scale bar is 10 μm .
- Figure 3-9c is a view of illite fibers in the freeze-dried part of the sample from 7,382.7 ft. Scale bar is 10 μm .
- Figure 3-9d shows matting and collapse of illite fibers in the air-dried part of the sample from 7,382.7 ft. Scale bar is 10 μm .

The effect of the changed illite morphology on petrophysical properties is discussed in detail in Section 4.2.3. In general, it resulted in a 2.6X increase in permeability to air compared to permeability to brine measured on preserved core. Brine permeabilities of cleaned and extracted cores were an average of 1.5X higher than brine permeabilities measured on the same plugs before cleaning and extraction.

Cotton Valley Sandstone

Although sandstones from the Cotton Valley are also classified as subarkoses or quartzarenites, they exhibit considerably more variation in framework grain composition than overlying Travis Peak sandstones, as shown in Table 3-2. Cotton Valley samples from SFE No. 3 are more feldspathic, more

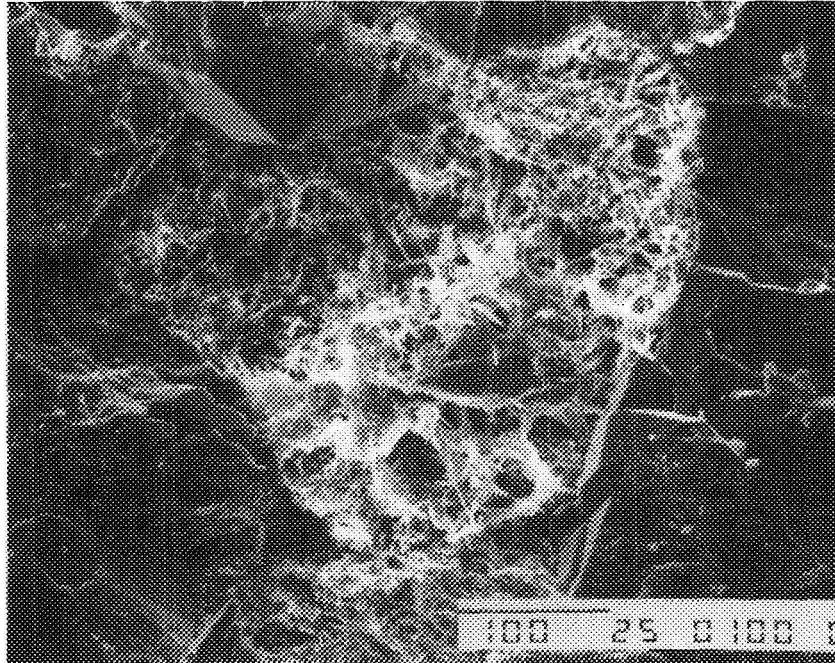


Figure 3-8a Freeze-Dried Sample in Which Fibrous Illite Has Replaced Feldspar Grain, SFE No. 3

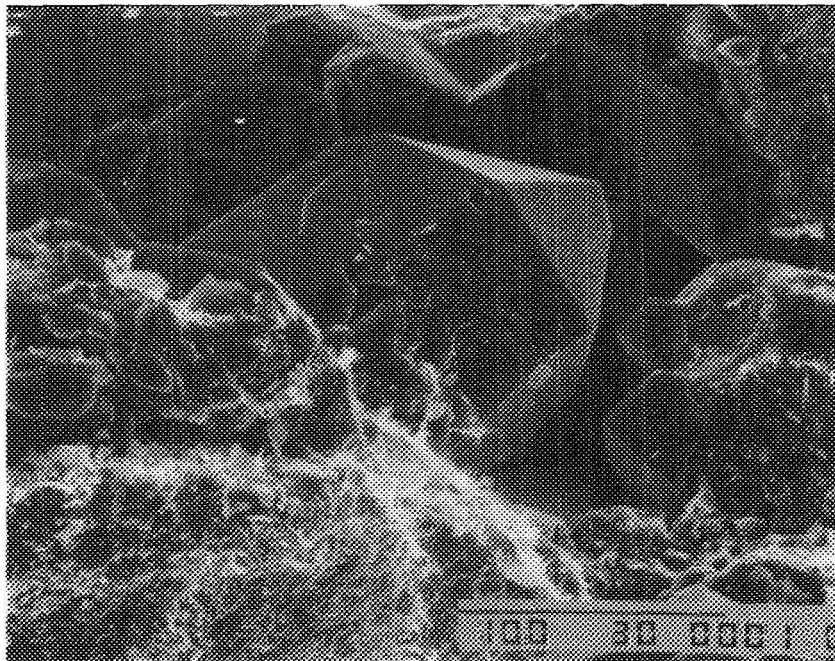


Figure 3-8b Freeze-Dried Sample Which Lacks Significant Illite Growth, SFE No. 3

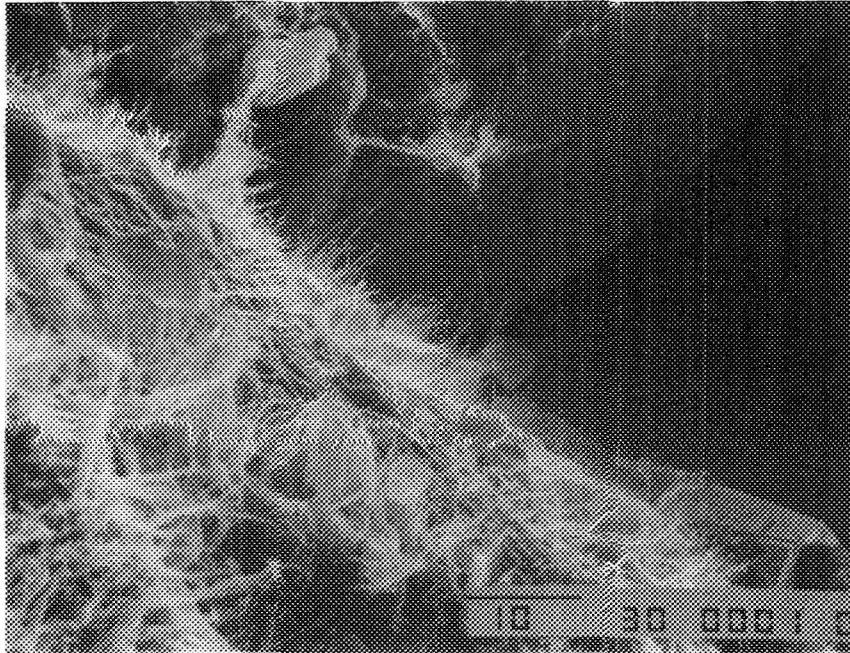


Figure 3-8c Freeze-Dried Sample With Fibrous Illite Coating Quartz Grain, SFE No. 3

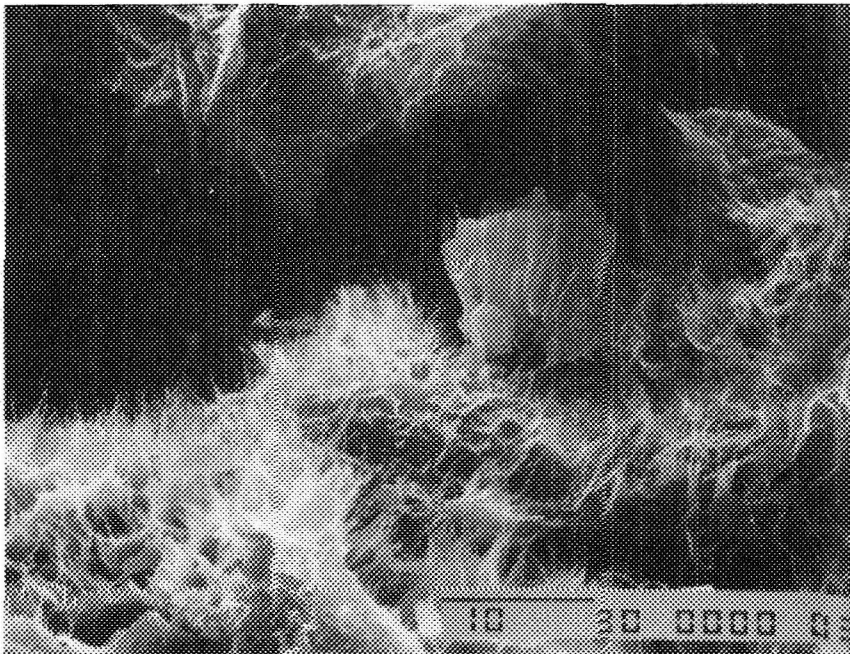


Figure 3-8d Freeze-Dried Sample With Bladed Illite Morphology, SFE No. 3

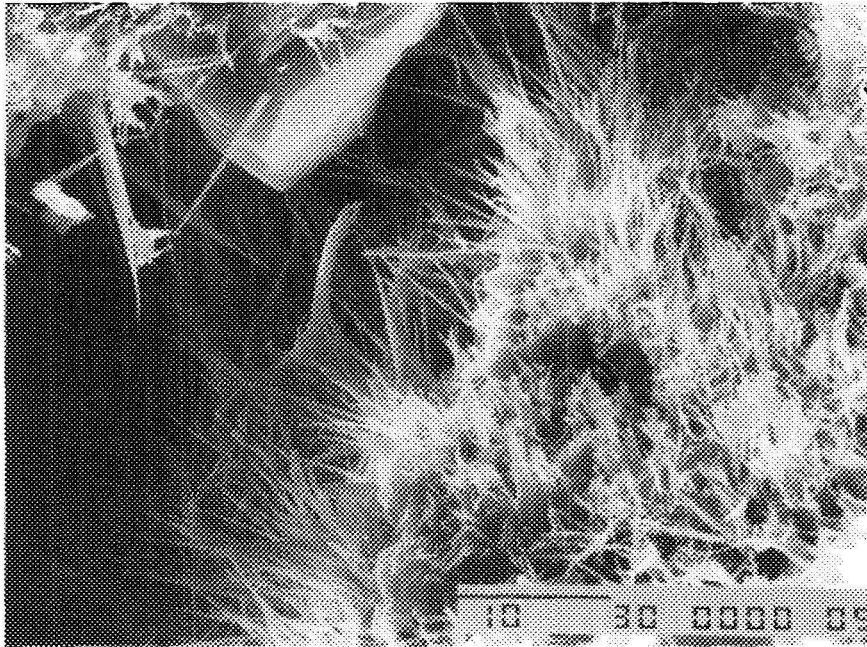


Figure 3-9a Delicate Illite Fibers in Freeze-Dried Sample from 7,388.8 ft, SFE No. 3

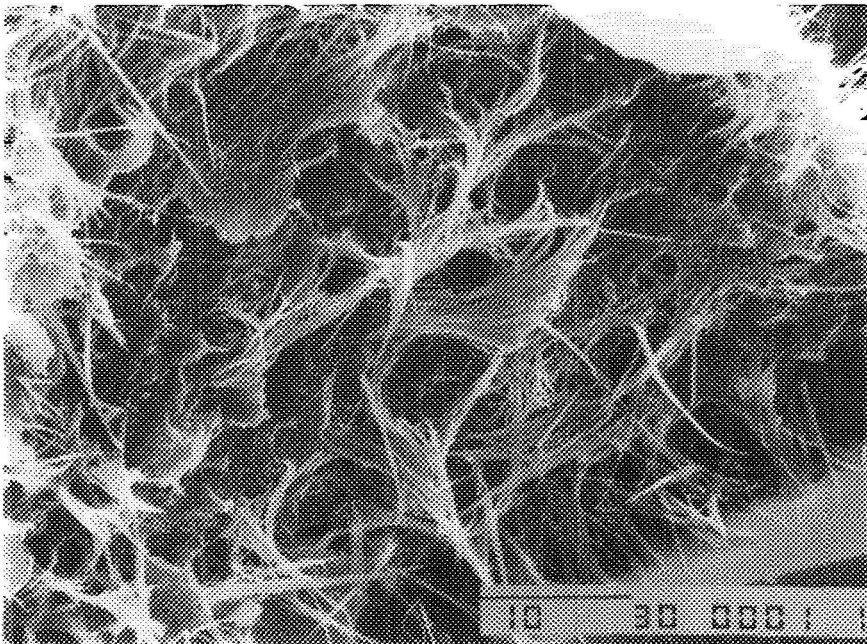


Figure 3-9b Collapsed Illite Fibers in Extraction-Dried Part of Sample from 7,388.8 ft, SFE No. 3

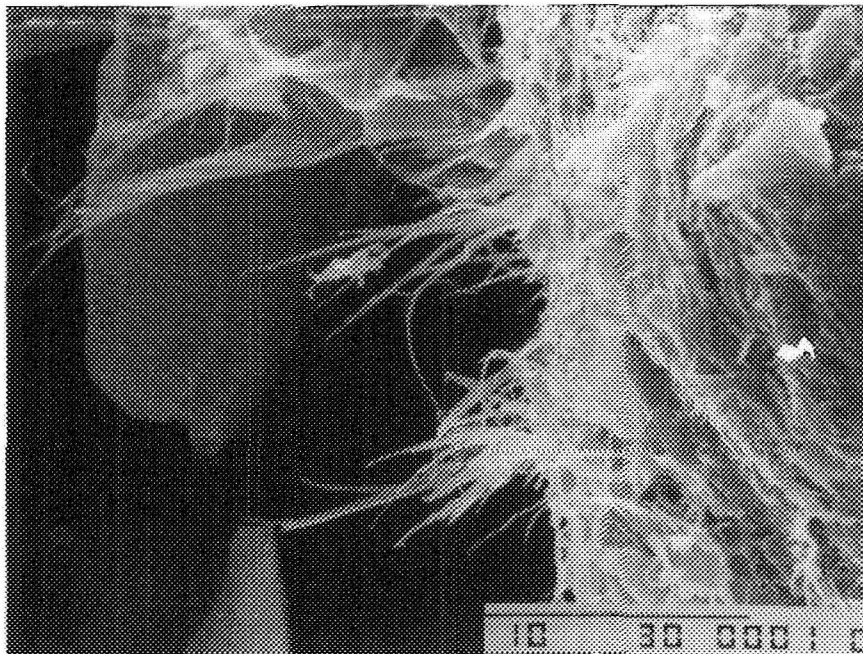


Figure 3-9c Illite Fibers in Freeze-Dried Part of Sample from 7,382.7 ft, SFE No. 3

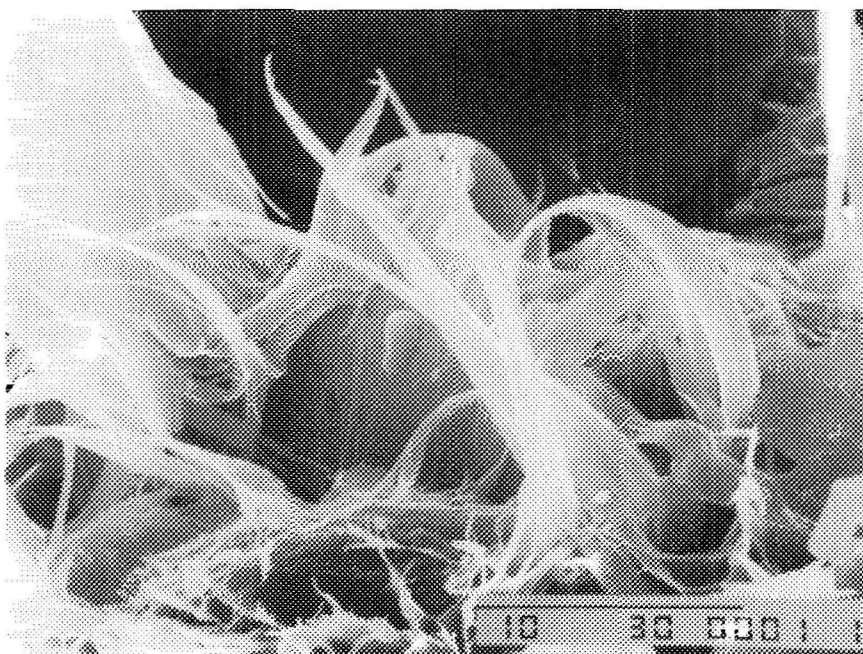


Figure 3-9d Matted and Collapsed Illite Fibers in Air-Dried Part of Sample From 7,382.7 ft, SFE No. 3

lithic, and more matrix-rich than are Travis Peak samples. The prevalence of feldspar is rather surprising because deeper burial should result in more extensive feldspar dissolution and in progressive enrichment of the framework fraction of detrital quartz. It is possible that abundant detrital clay matrix may have inhibited fluid flow through the Cotton Valley sandstones, thus decreasing rates of feldspar dissolution. Only 3 of 27 Cotton Valley thin-sections are matrix-free. The remaining samples contain as much as 66.5 percent detrital clay matrix. Much of the matrix observed in the sandstone samples may have been mixed into the sand-rich horizons during bioturbation.

Most of the Cotton Valley samples are subarkoses. Detrital quartz comprises from 76.4 to 100.0 percent of essential framework constituents. Total feldspar content ranges from 0.0 to 16.5 percent whole rock volume, or up to 20.5 percent of essential framework grains. As in the Travis Peak, the feldspar fraction in the Cotton Valley is dominated by plagioclase, but orthoclase makes up a high proportion of total feldspar content in a few samples. The sample from 9,210.6 ft contains 8.5 percent orthoclase, or slightly more orthoclase than plagioclase (Table 3-2). As observed in the Travis Peak samples, plagioclase did not accept Amaranth stain; it has apparently been converted to diagenetic albite. Rock fragments, commonly of low-rank metamorphic origin, constitute between 0.0 and 8.0 percent of the essential framework fraction. Because fossil fragments are interpreted to be of intrabasinal (allochemical) origin, they were not included in calculations of framework-grain ratios.

In addition to having framework-grain compositions that are distinct from Travis Peak samples, Cotton Valley sandstones from SFE No. 3 also have a different suite of authigenic phases. Authigenic quartz and ferroan calcite are the most common diagenetic minerals. They are accompanied by

ankerite, iron-free calcite, dolomite, pyrite, chlorite and albite.

Quartz cement is the most abundant authigenic phase in most samples, including the one shown in Figure 3-10. However, in the Cotton Valley more than the Travis Peak, other pore-filling phases are locally of greater importance than the quartz. Carbonate cement (calcite, ferroan calcite and ankerite) is the most abundant authigenic mineral in eight samples. Quartz cement attains a maximum volume of 22.0 percent of the whole rock volume in the sample from 9,275.6 ft (Table 3-2), but it averages only 14.1 percent in samples having quartz as the dominant authigenic phase. While the lower volume of quartz cement is at least partly a function of the greater matrix content, early carbonate cements are significant in that they inhibited quartz precipitation. This effect, however, appears to have greater importance in the Cotton Valley than in the Travis Peak.

Averaging about 30 percent of whole rock volume, ferroan calcite is the dominant authigenic phase in several samples -- for instance, the one seen in Figure 3-11. Ferroan calcite reaches a maximum volume of 39.0 percent in the sample from 9,270.0 ft, where it is the dominant pore-filling phase. Based on the color of stained samples, there appears to be a gradation between iron-rich and iron-free calcite in Cotton Valley sandstones. Ferroan and non-ferroan calcite pre-date quartz cement, resulting in strong local inhibition of quartz precipitation.

Samples that have been extensively cemented by calcite and ferroan calcite have the lowest porosity and permeability in the Taylor sandstone. In contrast, sandstones that are dominantly quartz-cemented have retained better reservoir quality. Thus, the zones with the best permeability in the perforated intervals in the Taylor sandstone occur where there is little or no calcite or

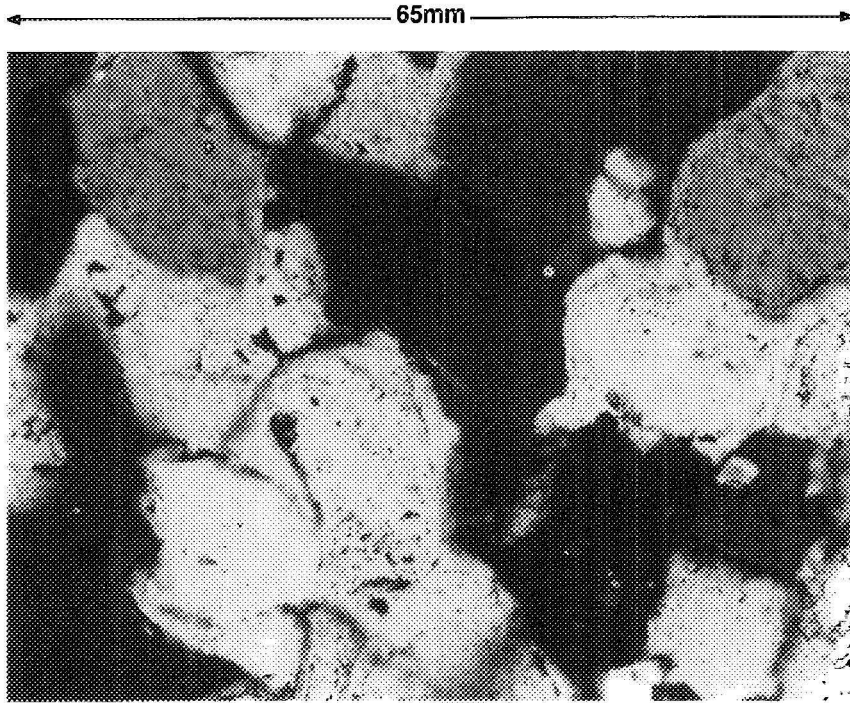


Figure 3-10 Photomicrograph of Quartz-Cemented Sandstone from 9,275.6 ft (Taylor Sandstone)

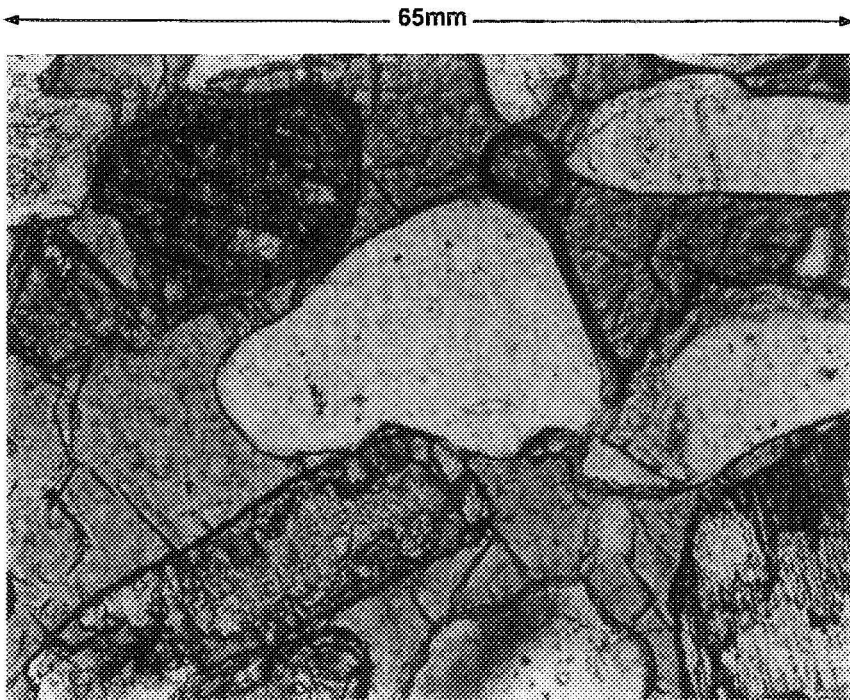


Figure 3-11 Ferroan-Calcite Cement Filling Primary Pores and Intragranular Secondary Porosity (Taylor Sandstone)

ferroan calcite cement, as will be shown on the Pre-Fracture Analysis log (Figure 4-7).

Cotton Valley sandstones from SFE No. 3 contain much smaller volumes of authigenic clays than do Travis Peak sandstones (Table 3-2). Pyrite, present in many Cotton Valley samples, reaches a maximum volume of 7 percent of the whole rock volume in the sample from 9,364.0 ft.

Clearly, the diagenetic histories of Cotton Valley and Travis Peak sandstones are quite different. Because of the importance of carbonate phases, reservoir quality of Cotton Valley sandstones cannot be directly equated with quartz cement content, as is commonly the case in Travis Peak sandstones. In addition, the greater amount of iron-bearing carbonate phases in the Cotton Valley may result in completion problems. For example, if carbonate-cemented horizons are treated with acid, an iron-hydroxide gel will form.

Total porosity in Cotton Valley sandstones is the sum of primary porosity, secondary porosity developed during feldspar dissolution, and microporosity within detrital and authigenic clays. Another form of secondary porosity was developed locally where fossil fragments (probably originally aragonite) dissolved. This dissolution produced pores visible to the unaided eye, creating secondary porosity as great as 8 percent (9,213.4 ft). Some secondary pores were subsequently filled with a late generation of ferroan calcite cement or with ankerite (Figure 3-11). In general, samples from the Cotton Valley have considerably higher porosimeter porosity than thin-section porosity because of the relative abundance of detrital clay matrix and, therefore, microporosity.

Total thin-section porosity in samples from SFE No. 3 is consistently lower in Cotton Valley sandstones than Travis Peak sandstones, in part because of the relatively high

matrix content. Ten Cotton Valley samples contain no visible macroporosity, although five of them contain abundant detrital clay matrix (25.5 to 66.5 percent) and thus should have considerable microporosity. The other samples that lack visible porosity contain abundant pore-filling quartz, ferroan calcite and ankerite cements. They have low porosimeter porosity and permeability.

3.3 STRUCTURAL GEOLOGY ANALYSIS OF SFE NO. 3 DATA - OBJECTIVES AND CONCLUSIONS

Objectives of structural studies included characterization of fractures, evaluation of fracture-imaging logs, and determination of stress directions in the Cotton Valley sandstone.

Core and log data show that fractures are common in the lower Cotton Valley Taylor sandstone. They are vertical extension fractures that are open or partly open in subsurface, but they differ from fractures in the Travis Peak by having calcite as the principal mineral fill. Even where they appear filled with calcite, microporosity and large, interconnected macropores exist within the fractures. Such fractures need to be considered in hydraulic fracture treatment design and reservoir evaluation.

Fracture detection with Formation Microscanner and borehole televiewer logs was successful, but the distinction between natural and drilling-induced fractures using these data remains difficult. The strike of drilling-induced fractures in core and borehole breakouts, as detected with borehole televiewer logs, was used to determine stress directions. Moreover, it was used to predict an east-northeast (80°) strike of hydraulic fractures created in the vicinity of SFE No. 3.

Finally, potential Cotton Valley fracture barrier rocks (mudstone and shale) contrast

sharply with Travis Peak silty mudstones. They lack the drilling-induced fractures which were quite extensive in the Travis Peak, providing qualitative evidence that Cotton Valley and Travis Peak barrier rocks behave differently.

3.3.1 Analysis of Natural Fractures

Fracture analysis distinguished natural from drilling-induced fractures and established the opening mode, distribution, attitude, strike, length in core, width, shape and mineral fill of the natural fractures. Results of the analysis are tabulated in Tables 3-3 and 3-4. Fracture orientation was determined by paleomagnetic core-orientation techniques for selected intervals. Another orientation method was correlation of fractures in core to oriented fracture images on wellbore-imaging borehole televiwer (BHTV) or on Formation Microscanner (FMS) logs (E.R. Monson, Written Communication, 1989). Each of these orientation techniques were discussed in Section 2.1.3.

The strike of drilling-induced fractures may indicate the horizontal stress directions near SFE No. 3. These fractures are described in the following section. Preliminary descriptions of fractures were made by researchers from the BEG and CER. Further study of fractures using binocular, petrographic and scanning electron microscopes was carried out at the BEG.

3.3.1.1 Physical Characteristics and Abundance of Natural Fractures

Vertical natural extension fractures and fracture zones are present in core from the Taylor sandstone (Cotton Valley sandstone) and from sandstones in the lower Travis Peak. Figure 3-12 is a photograph of natural extension fractures in core from 9,246 to 9,241 ft (data listed in Table 3-3). Few natural fractures occur in intervening shale,

and no fractures were found in the underlying Bossier shale. Travis Peak sandstone core has 15 fractures or fracture zones, and the Taylor sandstone has 32 fractures or fracture zones. Fracture zones are defined in this study as closely-spaced, coplanar parallel or en echelon fractures. As indicated by Figure 3-13, fractures in sandstone are uniformly distributed throughout the Taylor sandstone interval, without any apparent systematic variation with depth of abundance or length in core.

Fractures in the Taylor sandstone are filled or partly filled with calcite and quartz, calcite being the predominant fracture-filling mineral. Fracture-filling quartz is not as widespread as it is in the Travis Peak Formation; it is present in only a portion of the Cotton Valley fractures. Quartz precipitated in fractures before calcite. The calcite occurs as massive white crystals that variably fill fractures. The volume of fracture porosity filled by calcite varies considerably, in one example ranging from <10 percent to 100 percent within a single fracture (Figure 3-12).

Fractures in the Taylor sandstone are extension fractures that have opened by movement normal to fracture walls. In cross section, Taylor sandstone fractures are lens-shaped (elliptical). Commonly, fractures have simple, gradually tapering terminations. Fracture dips are generally subvertical ($>85^\circ$ and commonly $>89^\circ$), but considerable fracture curvature is evident in individual fractures (Figure 3-12), resulting in opposed dip directions for different parts of a single fracture. Fractures in the Taylor sandstone are tall and narrow with height/width ratios of 3,000 to 6,000. Short, wide, vug-like fractures, common in some deep Travis Peak core (e.g., the lower zone of SFE No. 2; Laubach and others, 1989), were not observed in Cotton Valley core from SFE No. 3. Fractures and interconnected fracture zones range in height from a few inches to

Table 3-3 Natural Fractures in SFE No. 3 Core

Fracture ID Core/ Frac No.	Top Depth, ft	Bottom Depth, ft	Length, ft	Midpoint, ft	Width, mm	Minera- logy	Strike	Dip
1, N2	-7355.9	-7356.7	0.8	-7356.3	0.05	q?		84
1, N3	-7557.8	-7557.9	0.1	-7557.9	0.05	q?		88
1, N5	-7360.5	-7361.6	1.1	-7361.1	0.05			89
1, N6	-7361.4	-7361.8	0.4	-7361.6		q		90
1, N7	-7362.7	-7364.0	1.3	-7363.4	0.05	q		88
1, N10	-7369.7	-7371.1	1.4	-7370.4		q		86
2, N2	-7385.6	-7386.5	0.9	-7386.1		q		85
2, N9	-7408.1	-7408.6	0.5	-7408.4	0.15	q		89
3, N4	-7875.2	-7875.5	0.3	-7875.4	0.05			
3, N6	-7878.4	-7879.0	0.6	-7878.7	0.10			87
3, N7	-7878.4	-7879.8	1.4	-7879.1	0.15			90
3, N10	-7881.1	-7881.5	0.4	-7881.3	0.05			89
3, N12	-7887.0	-7888.8	1.8	-7887.9	0.10	q?		89
5, N3	-7928.8	-7929.2	0.4	-7929.0		q?,c?		89
5, N4	-7929.8	-7930.2	0.4	-7930.0	0.05	q?,c?		90
5, N6	-7931.4	-7933.0	1.6	-7932.2		c?		86
8, N7	-9237.9	-9238.2	0.3	-9238.1	0.05	q,c?		89
8, N12	-9246.3	-9246.7	0.4	-9246.5	0.64	c		89
8, N14	-9248.7	-9249.7	1.0	-9249.2	0.05	q,c		87
8, N15	-9249.4	-9251.0	1.6	-9250.2	0.50	q,c		88
8, N16	-9251.0	-9251.1	0.1	-9251.1	0.50	q,c		
9, N1	-9259.6	-9260.1	0.5	-9259.9	0.05	q		90
9, N2	-9259.6	-9260.1	0.5	-9259.9	0.05			90
9, N7	-9265.0	-9266.1	1.1	-9265.6	0.05	q,c		89
9, N10	-9272.5	-9273.0	0.5	-9272.8		q,c		85
9, N11	-9273.7	-9274.2	0.5	-9274.0	0.05			89
9, N13	-9275.2	-9276.3	1.1	-9275.8	0.05	c?		88
9, N14	-9276.6	-9277.0	0.4	-9276.8	0.05	q,c?		85
9, N16	-9279.0	-9280.0	1.0	-9279.5	0.05	q?,c?		88
9, N18	-9282.5	-9283.1	0.6	-9282.8				87
10, N3	-9286.8	-9288.0	1.2	-9287.4	0.05		77.1	86
10, N6	-9288.4	-9289.1	0.7	-9288.8	0.05	q?	74.1	82
10, N12	-9291.0	-9291.8	0.8	-9291.4		q	83.1	90
10, N18	-9303.1	-9304.6	1.5	-9303.9	0.33	q		87
10, N19	-9305.8	-9309.9	4.1	-9307.9				89
10, N20	-9306.0	-9306.4	0.4	-9306.2	1.10	q?,c		89
10, N21	-9310.9	-9311.2	0.3	-9311.1		q?,c		87
11, N2	-9313.0	-9313.2	0.2	-9313.1		c?		89
11, N5	-9316.8	-9317.3	0.5	-9317.1		c?		88
11, N8	-9317.4	-9318.1	0.7	-9317.8	0.05			89

Table 3-3, Continued

Fracture ID Core/ Frac No.	Top Depth, ft	Bottom Depth, ft	Length, ft	Midpoint, ft	Width, mm	Minera- logy	Strike	Dip
11, N9	-9317.7	-9318.1	0.4	-9317.9	0.05	c?		88
11, N12	-9319.6	-9320.4	0.8	-9320.0		c		88
12, N1	-9321.1	-9322.2	1.1	-9321.7	0.05			87
12, N5	-9325.8	-9326.2	0.4	-9326.0	0.05			87
12, N16	-9336.0	-9336.5	0.5	-9336.3	0.05			86
12, N18	-9337.1	-9338.8	1.7	-9338.0	0.15			85
13, N5	-9341.6	-9341.8	0.2	-9341.7		c		78
13, N6	-9342.7	-9344.2	1.5	-9343.5	0.05			89
13, N7	-9342.8	-9344.1	1.3	-9343.5	0.05			89
13, N15	-9356.3	-9356.9	0.6	-9356.6		c		90

q = quartz
c = calcite

Table 3-4 Coring-Induced Fractures in SFE No. 3 Core

ID Core/ Frac No.	Top Depth, ft	Bottom Depth, ft	Length, ft	Width, mm	Strike	Dip
1, C4	-7359.9	-7360.0	0.1			45
1, C8	-7367.0	-7367.3	0.3			80
1, C9	-7368.5	-7368.9	0.4			86
1, C11	-7374.6	-7374.9	0.3			85
1, C12	-7376.0	-7376.5	0.5			82
1, C13	-7376.8	-7377.0	0.2			79
2, C1	-7381.5	-7382.0	0.5			86
2, C3	-7391.9	-7392.0	0.1			78
2, C5	-7405.2	-7405.4	0.2			78
2, C6	-7405.4	-7405.6	0.2			58
2, C7	-7407.0	-7407.1	0.1			83
2, C8	-7407.2	-7407.7	0.5			89
3, C1	-7869.1	-7870.1	1.0			90
3, C2	-7874.2	-7874.9	0.7			83
3, C3	-7874.2	-7874.2	0.0			75
3, C5	-7876.2	-7876.9	0.7			90
3, C6	-7878.4	-7879.0	0.6			87
3, C7	-7878.5	-7879.9	1.3			90
3, C8	-7879.4	-7879.8	0.4			78

Table 3-4, Continued

ID Core/ Frac No.	Top Depth, ft	Bottom Depth, ft	Length, ft	Width, mm	Strike	Dip
3, C9	-7880.4	-7881.1	0.7			81
3, C11	-7884.0	-7884.6	0.6			86
4, C1	-7889.5	-7889.8	0.3			75
4, C2	-7890.3	-7890.4	0.1			87
4, C3	-7890.7	-7890.9	0.2			88
4, C4	-7891.2	-7891.3	0.1			88
4, C5	-7895.0	-7896.5	1.5			84
4, C6	-7897.6	-7898.0	0.4			80
4, C7	-7900.3	-7900.7	0.4			80
4, C8	-7905.3	-7908.4	3.1			89
4, C9	-7911.0	-7911.6	0.6			83
5, C1	-7916.7	-7917.1	0.4			88
5, C2	-7928.5	-7929.1	0.6			69
5, C5	-7930.5	-7930.8	0.3			85
5, C8	-7942.4	-7943.3	0.9			86
6, C1	-9030.7	-9030.9	0.2			42
6, C2	-9032.0	-9033.0	1.0			90
6, C3	-9043.2	-9043.3	0.1			68
7, C1	-9203.8	-9204.1	0.3			76
7, C2	-9204.7	-9204.9	0.2	0.10		73
7, C3	-9205.2	-9205.3	0.1			76
7, C4	-9205.2	-9205.3	0.1			89
7, C5	-9207.3	-9208.3	1.0	0.03		81
7, C6	-9207.3	-9207.6	0.3	0.03		81
7, C7	-9209.2	-9209.4	0.2	0.03		81
7, C8	-9210.0	-9211.2	1.2			54
7, C9	-9211.0	-9211.1	0.1	0.05		5
7, C10	-9211.8	-9211.9	0.1			6
7, C11	-9211.8	-9212.0	0.2	0.03		83
7, C12	-9212.0	-9214.4	2.4			85
7, C13	-9214.8	-9215.2	0.4			84
7, C14	-9214.9	-9215.2	0.3	0.05		83
7, C15	-9216.0	-9216.2	0.2			66
7, C16	-9216.2	-9216.5	0.3			89
7, C17	-9216.8	-9217.7	0.9	0.05		89
7, C18	-9217.7	-9218.0	0.3			79
7, C19	-9218.6	-9218.8	0.2	0.03		83
7, C20	-9222.3	-9222.4	0.1			68
7, C21	-9224.0	-9225.3	1.3			86
7, C22	-9225.3	-9225.4	0.1	0.03		66

Table 3-4, Continued

ID Core/ Frac No.	Top Depth, ft	Bottom Depth, ft	Length, ft	Width, mm	Strike	Dip
7, C23	-9226.4	-9227.7	1.3			85
8, C1	-9229.7	-9229.8	0.1			75
8, C2	-9230.0	-9230.1	0.1			75
8, C3	-9230.3	-9230.4	0.1		65.4	74
8, C4	-9234.0	-9234.6	0.6		72.4	84
8, C5	-9236.5	-9237.0	0.5			90
8, C6	-9237.4	-9237.7	0.3			78
8, C8	-9238.3	-9238.6	0.3			62
8, C9	-9239.0	-9239.1	0.1			75
8, C10	-9243.0	-9243.2	0.2			71
8, C11	-9245.0	-9245.4	0.4			80
8, C13	-9246.4	-9246.7	0.3			82
8, C14	-9248.7	-9249.7	1.0			87
8, C17	-9251.3	-9251.5	0.2			78
8, C18	-9251.9	-9253.4	1.5			89
8, C19	-9254.4	-9255.7	1.3			78
8, C20	-9255.5	-9255.7	0.2			71
8, C21	-9256.1	-9256.3	0.2			76
8, C22	-9257.4	-9257.8	0.4			85
8, C23	-9259.0	-9259.4	0.4	0.03		63
9, C3	-9261.0	-9262.4	1.4			89
9, C4	-9262.9	-9263.0	0.1			71
9, C5	-9263.4	-9264.0	0.6			86
9, C6	-9264.0	-9264.1	0.1	0.03		68
9, C8	-9267.1	-9267.5	0.4		67.6	78
9, C9	-9267.3	-9267.6	0.3	0.03	70.5	86
9, C12	-9274.0	-9274.1	0.1	0.03		69
9, C17	-9280.1	-9280.2	0.1			79
10, C1	-9283.5	-9284.2	0.7			81
10, C2	-9286.8	-9287.0	0.2	0.03		73
10, C3	-9287.2	-9288.0	0.8			86
10, C4	-9287.8	-9288.6	0.8	0.03	76.6	85
10, C5	-9288.4	-9289.0	0.6		77.6	83
10, C7	-9289.3	-9289.7	0.4	0.03	84.6	79
10, C8	-9289.5	-9289.7	0.2	0.03	82.6	73
10, C9	-9290.1	-9290.7	0.6	0.03	86.1	89
10, C10	-9290.4	-9290.7	0.3	0.03	92.1	77*
10, C11	-9291.0	-9291.3	0.3	0.03	85.6	82
10, C12	-9291.0	-9291.8	0.8			
10, C13	-9292.4	-9294.0	1.6	0.03	76.6	60
10, C14	-9295.0	-9297.6	2.6	0.03	76.4	90

Table 3-4, Continued

ID Core/ Frac No.	Top Depth, ft	Bottom Depth, ft	Length, ft	Width, mm	Strike	Dip
10, C15	-9297.6	-9298.1	0.5	0.03	76.1	67
10, C16	-9298.7	-9299.3	0.6		82.1	85
10, C17	-9301.5	-9302.2	0.7		86.6	70
11, C1	-9313.0	-9313.2	0.2			90
11, C3	-9315.1	-9315.3	0.2			67
11, C4	-9316.0	-9316.5	0.5	0.03		81
11, C6	-9316.9	-9317.0	0.1	0.03		63
11, C7	-9317.2	-9317.4	0.2			71
11, C10	-9319.6	-9319.9	0.3			83
11, C11	-9319.6	-9319.9	0.3			87
12, C2	-9321.1	-9322.2	1.1			65
12, C3	-9324.9	-9325.1	0.2			72
12, C4	-9325.4	-9326.2	0.8			89
12, C6	-9326.6	-9326.7	0.1	0.03		72
12, C7	-9327.2	-9327.5	0.3			88
12, C8	-9328.3	-9328.4	0.1			59
12, C9	-9328.6	-9328.7	0.1	0.03		61
12, C10	-9330.0	-9330.4	0.4		78.6	78
12, C11	-9331.1	-9331.2	0.1	0.05	68.6	72
12, C12	-9332.5	-9332.7	0.2	0.03	74.9	76
12, C13	-9333.0	-9334.1	1.1		67.4	85
12, C14	-9334.6	-9335.1	0.5		74.4	85
12, C15	-9335.4	-9335.7	0.3		69.9	87
12, C17	-9336.3	-9336.9	0.6	0.05	72.4	79
13, C2	-9340.1	-9340.4	0.3	0.03		79
13, C3	-9340.4	-9341.0	0.6			85
13, C4	-9340.5	-9341.1	0.6			82
13, C8	-9348.6	-9348.8	0.2	0.03		64
13, C9	-9348.7	-9348.9	0.2	0.03		62
13, C10	-9348.9	-9349.0	0.1	0.03		61
13, C11	-9349.0	-9349.1	0.1	0.03		44
13, C12	-9349.2	-9349.3	0.1	0.03		54
13, C13	-9349.2	-9349.3	0.1	0.03		49
13, C14	-9354.0	-9354.3	0.3	0.03		61
13, C16	-9358.5	-9358.7	0.2	0.03		64
13, C17	-9358.7	-9358.8	0.1	0.03		67
13, C18	-9359.0	-9359.1	0.1	0.03		73
13, C19	-9359.0	-9359.1	0.1	0.03		76
13, C20	-9359.2	-9359.4	0.2	0.03		46
13, C21	-9359.5	-9359.6	0.1	0.03		49
13, C22	-9359.8	-9360.0	0.2	0.03		48

Table 3-4, Continued

ID Core/ Frac No.	Top Depth, ft	Bottom Depth, ft	Length, ft	Width, mm	Strike	Dip
13, C23	-9360.2	-9360.4	0.2	0.03		54
14, C1	-9449.0	-9449.2	0.2			83
14, C2	-9450.3	-9450.5	0.2	0.03		57
14, C3	-9453.3	-9453.9	0.6	0.03		80
14, C4	-9458.0	-9458.6	0.6			81
14, C5	-9458.8	-9459.5	0.7			89
14, C6	-9460.0	-9460.3	0.3			85
14, C7	-9466.6	-9466.8	0.2			31
15, C1	-9469.0	-9469.2	0.2			53
15, C2	-9470.5	-9470.7	0.2			46
15, C3	-9479.2	-9479.4	0.2			45

*Strike of 20 petal fractures (-9290.4 to -9290.7)

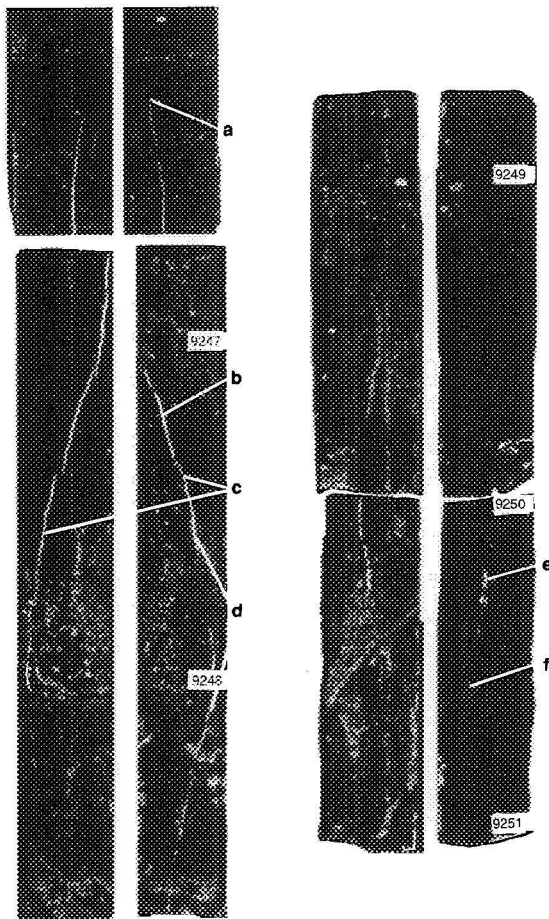


Figure 3-12 Photograph of Natural Extension Fractures in the Taylor Sandstone at a Depth of 9,246 to 9,251 ft

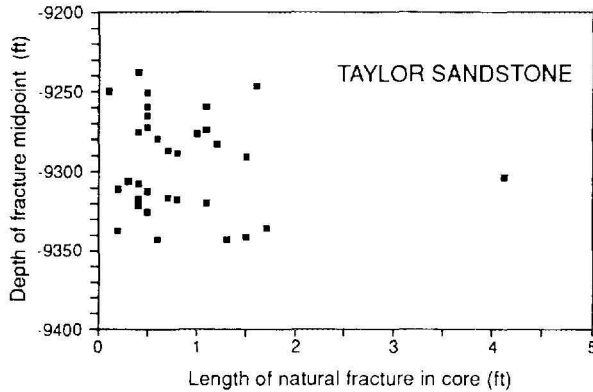


Figure 3-13a Vertical Fracture Length (Height) of Natural Fractures in Travis Peak and Cotton Valley Core Plotted Against Depth, SFE No. 3

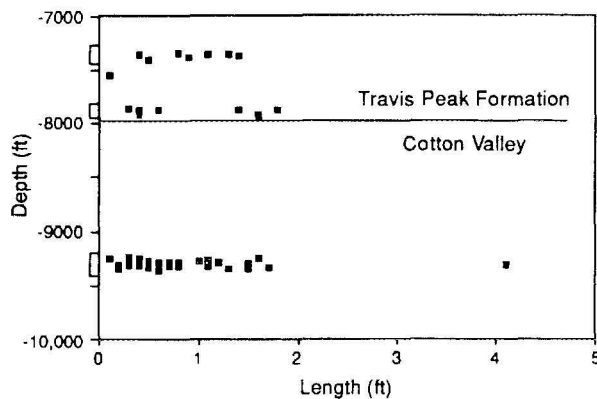


Figure 3-13b Vertical Fracture Length (Height) of Natural Fractures in Taylor Sandstone Plotted Against Depth, SFE No. 3

over four feet (Figure 3-13). Most individual fractures are less than two feet tall, but these fractures are arranged in more continuous vertical networks than fractures in the lower zone of SFE No. 2. Vertical interconnection of fractures within the Taylor sandstone is also suggested by fracture traces, seen in Figure 3-14, that were imaged with BHTV and FMS.

3.3.1.2 Natural Fracture Strike

Natural extension fractures strike east-north-east in SFE No. 3 (Table 3-3). The azimuth of 30 natural fractures in the upper Taylor sandstone (Zone 4) was determined by correlating fractures in core with BHTV and FMS images. Fracture strike ranges from 005° to 175°, with a vector mean strike of 082°. Three natural fractures in the Taylor sandstone that were oriented by paleomagnetic methods have strikes of 077°, 074° and 083° (Table 3-3), in agreement with BHTV and FMS observations. These results are also in agreement with fractures strikes in the Travis Peak in Waskom Field (Dutton and others, 1988).

3.3.1.3 Considerations for Reservoir Development

Observations of SFE No. 3 core indicate that natural fractures are abundant in the cored interval of the Taylor sandstone. Some of the fractures are open in the subsurface. Tall fractures in the Taylor sandstone may indicate fractures that are more extensive (longer) in plan view. Such fractures are more likely to be interconnected laterally, and therefore, are more likely to enhance reservoir permeability. On the other hand, many fractures in the Taylor sandstone are partly or completely filled with calcite, potentially reducing their effectiveness as conduits for fluids. However, even fractures that macroscopically appear filled have considerable microporosity that locally is interconnected within the fracture. Widespread calcite in natural fractures should be taken into account in engineering operations in Taylor sandstone to avoid damage to the natural fracture system.

Evidence from drilling-induced fracture strike, borehole breakout orientation, and previous hydraulic fracture treatments in Waskom Field indicates that natural fractures are subparallel to the maximum horizontal stress

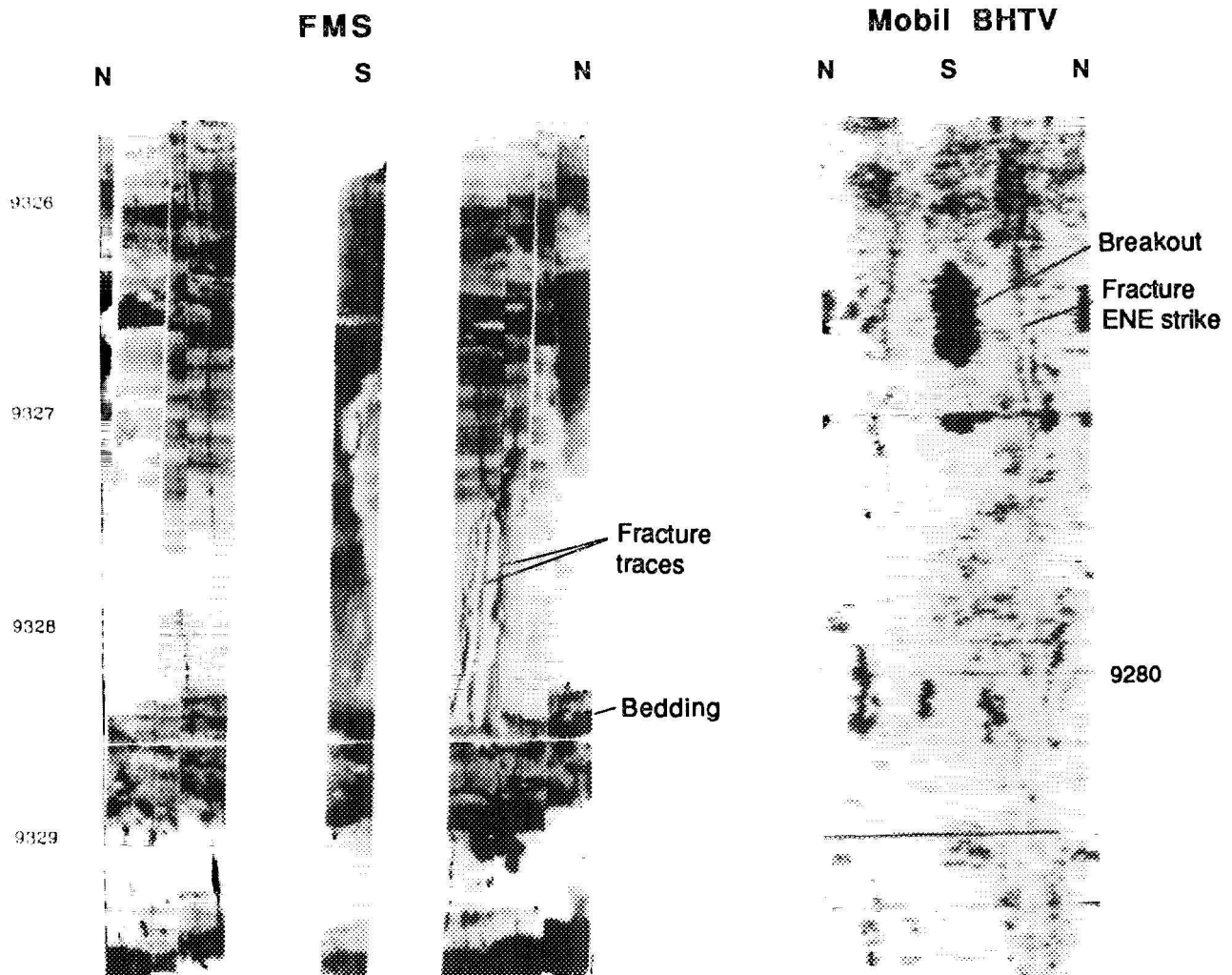


Figure 3-14 Examples of BHTV and FMS Logs Imaging Fractures in the Taylor Sandstone

direction in this area (Dutton and others, 1988). Thus, hydraulic fractures will tend to propagate subparallel to natural fractures, and natural fractures may be opened during fracture treatment.

3.3.2 Drilling-Induced Fractures and Direction of S_{Hmax}

Drilling-induced fractures were distinguished from natural fractures based on criteria described by Kulander and others (1979).

These criteria include (1) location of fracture origins near or within core, (2) characteristic fracture shapes, and (3) absence of mineralization. Fracture surface structures (plume structure and arrest lines) and fracture shape were used to identify fracture origins.

A total of 156 drilling-induced fractures were identified in SFE No. 3 core (Table 3-4). Fracture dips are generally steep ($>70^\circ$). As Figure 3-15 illustrates, heights of drilling-induced fractures range from a few inches

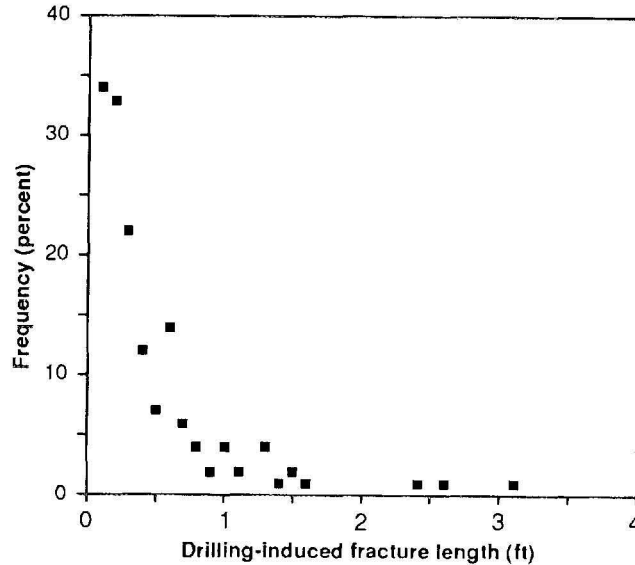


Figure 3-15 Lengths of Drilling-Induced Fractures in SFE No. 3 Core

to over three feet, with most fractures less than one foot tall. Widths of induced fractures were measured where the core had not separated completely along the fracture. These widths are probably not representative of subsurface induced-fracture widths.

In the upper Taylor sandstone, 32 petal and 44 petal-centerline fractures were oriented by using distinctive features visible on BHTV or FMS logs and core. In addition, 23 drilling-induced fractures were independently oriented by paleomagnetic techniques (Van Alstine, 1988). The means of fractures in six intervals oriented by paleomagnetic methods range from 067° to 081°, as shown by Figure 3-16. The overall mean strike is 072°. The vector mean strike of 76 drilling-induced fractures in the upper Taylor sandstone oriented by reference to borehole-imaging logs is 078°.

Previous work in the Travis Peak Formation suggests that drilling-induced petal and petal-centerline fractures strike parallel to maximum horizontal stress (S_{Hmax}), and that they can therefore be used to predict the propagation direction of hydraulic fractures

(Laubach and Monson, 1988). Drilling-induced fractures in the Taylor sandstone indicate east-northeast propagation of the hydraulic fracture. A mean strike of 078° is indicated by fractures oriented by reference to BHTV and FMS images. A mean strike of 072° is indicated by the average strike of fractures in core oriented by paleomagnetic methods. The difference between these means is not significant in view of the uncertainties in tool orientation. These results are consistent with determinations of horizontal stress directions from analysis of borehole breakouts, which indicate east-northeast maximum horizontal stress.

The distribution of drilling-induced petal and petal-centerline fractures in the Cotton Valley differs from that of the Travis Peak Formation. In the Travis Peak, petal and petal-centerline fractures are present in equal numbers in both sandstone and intervening silty mudstone and muddy siltstone. Many of the longest petal-centerline fractures are in muddy rock types. The number of drilling-induced fractures per foot of Taylor sandstone core is greater than in typical Travis Peak sandstone, but in the Bossier

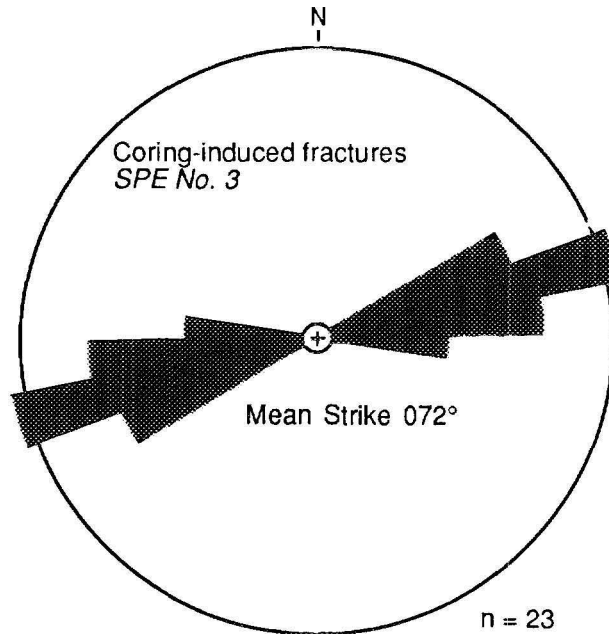


Figure 3-16 Drilling-Induced Fracture Strike in SFE No. 3 Core

shale and in shales within the lower Cotton Valley in SFE No. 3, petal-centerline fractures are virtually absent. These differences may indicate that compared to silty mudstone in the Travis Peak, mudstone and shale (potential fracture-barrier rock) in the Cotton Valley Group in SFE No. 3 are less readily fractured, at least by drilling operations. Contrasts in mineralogy, which occurred during early burial, probably account for the greater apparent resistance to fracturing in the Cotton Valley and Bossier shales.

3.3.3 Open-Hole Stress Test Fractures and Direction of S_{Hmax}

As discussed Section 2.1.7, six open-hole stress tests (OHST) were performed in the intervals shown in Table 2-4. One attempt was made to over-core the induced fracture; however, this attempt did not successfully result in recovery of an OHST fracture.

The BHTV and FMS borehole-imaging devices were logged over the OHST intervals.

Fractures, interpreted to have been hydraulically induced during the stress test, were observed in three of the stress test intervals. Table 3-5 lists the stress test intervals, observed fracture intervals and interpreted azimuths. The average azimuth of 086° is again consistent with other determinations of horizontal stress direction which indicate east-northeast maximum horizontal stress.

3.4 APPLICATION OF GEOLOGICAL ANALYSES TO THE SFE NO. 3 COMPLETION STRATEGY

At Waskom Field, data from core and logs from SFE No. 3 and adjacent wells have established a foundation upon which predictions about reservoir origin, degree and type of diagenesis, and occurrence of natural fractures can be made. Stratigraphic analysis of core from SFE No. 3 indicates that the upper perforated interval in the Cotton Valley Taylor sandstone is producing from two tidal-inlet channels that are separated

*Table 3-5 Orientation of Open-Hole Stress Test Fractures
Observed on the FMS and BHTV*

Stress Test No.	Stress Test Interval, ft	Log Interval, ft	True Azimuth, degree
1	7,406 - 7,411	7,411 - 7,417	88°
4	9,041 - 9,047	9,044 - 9,046	86°
5	9,362 - 9,367	9,355 - 9,365	84°

by foreshore deposits. The lower perforated interval is producing from two, microtidal barrier-island, sandstone deposits that are separated by lagoon and washover deposits. Thin-section point counts supplied data on mineral composition that was used to calibrate geophysical log responses. Petrographic data indicate that calcite is the most extensive cement in many Cotton Valley sandstones. The calcite-cemented zones have the lowest permeability within the Taylor sandstone, whereas quartz-cemented sandstones have retained higher porosity and permeability. Thus, the best permeability in the perforated intervals occurs in sandstones that contain little or no calcite ce-

ment, as will be shown on the Pre-Fracture Analysis log in Figure 4-7.

Knowledge of the characteristics and distribution of natural fractures permitted these structures to be taken into account in fracture treatment design (described in Section 7.1). Experiments to monitor and test methods of documenting hydraulic fracture propagation (described in Sections 6.2.3, 8.4 and 8.5) were designed using stress directions inferred from core data. In addition, awareness of natural fractures in Cotton Valley reservoir rocks can be used to refine engineering reservoir evaluation (see Sections 8.2 and 8.3).

4.0 Well Log and Core Analyses in the Cotton Valley Formation

Petrophysical modeling was conducted by ResTech Houston using well logs and core analyses acquired in the SFE No. 3 well. The purpose of this modeling was to perform the following functions:

- Test the applicability of methods developed in the Travis Peak data set to a different geological horizon (Cotton Valley).
- Evaluate the data to interpret lithology, porosity, water saturation, permeability and rock mechanical properties using the Travis Peak methodology.
- Develop an accurate closure stress profile using log-derived and in-situ stress data.
- Acquire core-derived measurements of reservoir flow properties for use in engineering studies and in advanced techniques of reservoir modeling.
- Identify the Cotton Valley intervals that have potential for gas production.

The following section of this report describes the techniques of analysis and compares the results to those from core analyses.

4.1 RESULTS OF WELL LOG ANALYSES AND SELECTION OF COMPLETION INTERVALS

The gross interval from 9,198.0 to 9,345.5 ft was selectively completed between 9,225 and 9,250 ft and between 9,285 and 9,330 ft in the Cotton Valley Taylor sand. The results of the petrophysical analysis across

the Taylor interval are displayed in Figure 4-1. Results of select types of core analyses are also shown on the figure. Table 4-1 displays average values for porosity, water saturation and permeability. Two different sets of values are shown: gross interval and gas sand. The values for "gross interval" are the averages for the entire Taylor section including all the various lithologies. The values listed for "gas sand" are calculated based on 2 percent porosity and 70 percent water saturation cut-offs. These cut-offs were used to establish the amount of gas-saturated sand within the completed interval only, an amount which may not represent the net gas pay.

The petrophysical analyses for this well used the same methodology developed in the Travis Peak Formation. As shown on Figure 4-1, the close agreement between log analyses and core analyses indicates that the methodology developed in the Travis Peak may be successfully applied to the Cotton Valley. This agreement is also confirmed by well test analyses discussed in the section pertaining to log-derived permeability (Section 4.1.1.6) of this report.

4.1.1 Log Analysis Methodology and Petrophysical Modeling

Methodologies associated with petrophysical formation evaluation in the Travis Peak have previously been reported (Howard and Hunt, 1986; and Luffel and Others, 1989). The drilling of SFE No. 3 provided an excellent opportunity to test the applicability of these technologies in a geologic horizon underlying the Travis Peak, yet still in the same basin. In SFE No. 3, approximately 245 ft of core was acquired from the Cotton Valley to assist in the verification of log analysis re-

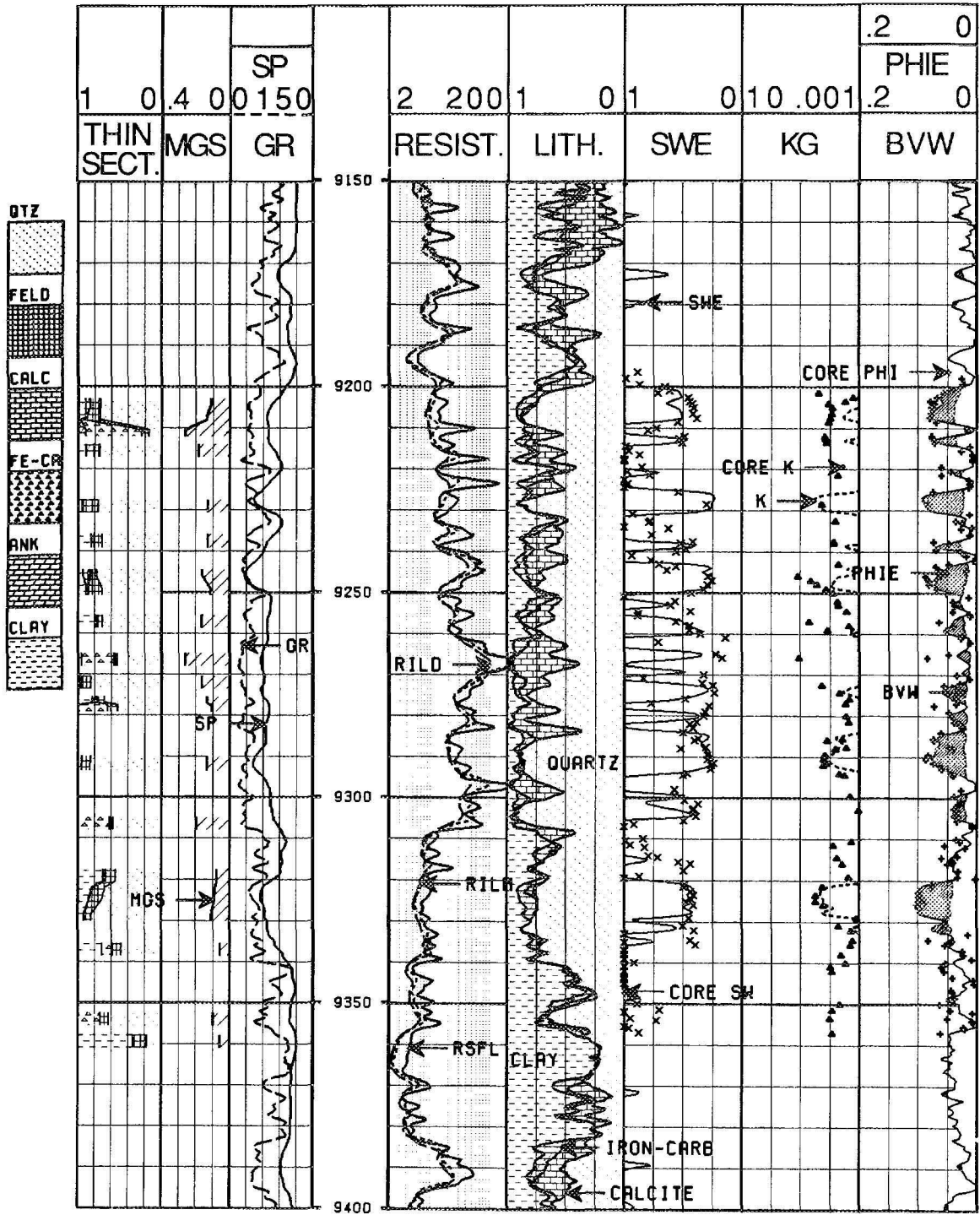


Figure 4-1 Presentation of the Log Results Over the Completed Interval in SFE No. 3 Displayed With Core Analysis

Table 4-1 Zone Summary, Completed Interval

Parameter	Gross Interval	Gas Sand
Thickness, ft	147.5	68.0
Average Porosity	0.039	0.060
Average Water Saturation	0.569	0.413
Permeability-Thickness, md	0.34	0.33

sults. The following sections of this report describe the methodologies used to develop log interpretations and compares these log-derived results to those from core analyses.

4.1.1.1 Log Data Normalization

Mobil Exploration and Production, U.S. provided data from five offset wells to aid in log analysis parameter selection and to provide a calibration data set for use in the SFE No. 3. All of these offset wells were drilled in the Waskom Field into or through the Cotton Valley Formation. To check for errors, a base histogram of the wells was established for each appropriate logging curve. When the SFE No. 3 was logged, the resulting

histograms were compared with the corresponding calibration data sets, and the appropriate re-calibrations were made.

Miscalibration of logging tools has been well documented in the past (Kukul and Others, 1983; and Conolly, 1974). Indeed, Res-Tech's previous experience in the Travis Peak indicates that about 50 percent of the porosity logs commonly require some type of normalization. Table 4-2 lists the field-wide values for neutron, density and sonic logs. Also listed are logging service company (Western-Atlas and Schlumberger) histogram modes for the three logging values in SFE No. 3.

Table 4-2 Histogram Modes and Shift Required for Data Normalization

Data Set	Δt	Shift Required	ρ_b	Shift Required	ϕ_N	Shift Required
Field wide	60	0.0	2.60	0.00	0.11	0.0
WA run	60	0.0	2.62	-0.02	0.11	0.0
SWS run	none	-	2.60	0.00	0.11	0.0

4.1.1.2 Borehole Effects on Density and Sonic Data

Most wellbores drilled through tight gas sands have frequently-occurring, stress-induced borehole breakouts. Where these breakouts occur, the density and sonic log data may be invalid due to poor density-tool pad contact or due to longer sonic-tool transit times caused by the breakout.

These invalid readings were compensated for in the data processing. If one of these values appeared to be invalid, the corresponding depth interval was flagged. The porosity of a flagged interval was then determined from the density data alone. However, if the density data was invalid, porosity was calculated with an algorithm using the sonic data:

$$\phi_e = \phi_s - V_{sh}\phi_{sh} \quad \text{Eq. 4-1}$$

where

- ϕ_e = effective porosity
- ϕ_s = porosity derived from the sonic log
- V_{sh} = shale volume
- ϕ_{sh} = shale correction factor

Frequently, both sonic and density log data were invalid. When this situation occurred, a maximum porosity was assigned to the sands; this value was then adjusted according to the shaliness of the sand.

4.1.1.3 Lithology Determination

Based on petrographic analyses, framework grains in the Cotton Valley consist primarily of quartz with a smaller fraction of feldspars that are plagioclase dominated (letter report to GRI by BEG, 1989). Authigenic quartz and ferroan calcite are the most common diagenetic minerals, and they are accompanied by ankerite, iron-rich calcite, dolom-

ite, pyrite, chlorite and albite. In comparison to Travis Peak sandstones, Cotton Valley sandstones in SFE No. 3 contain much smaller volumes of authigenic clays. Cotton Valley rock samples in SFE No. 3 are free of authigenic illite and kaolinite, although small amounts of chlorite may be observed. Detrital matrix is probably illite or mixed-layer illite-smectite, except where the matrix has been partially converted to chlorite.

Because of the amount of iron-rich carbonates in the Cotton Valley, estimations of various lithology percentages from well logs are difficult. X-ray diffraction and thin-section analyses provided the basis for log-calculated lithology. The semi-quantitative nature of X-ray diffraction analyses makes the fully quantitative thin-section analyses the more desirable measurement. A drawback to thin-section analysis is its inability to distinguish the mineralogy of clay-sized fines. Experience has shown that grouping the clay-sized fines together as a calibration point for various log-derived clay indicators provides a useful log estimation of clay volume. This volume estimate can then be used to correct porosity log responses for clay effect. Of all the rock constituents present in the Cotton Valley, clay had the most dramatic effect on well log response.

After a calibrated clay volume was determined, volumes of other minerals were calculated with several simultaneous equations that used the Schlumberger Geochemical Log (GLT) data to provide the base values. The responses of iron, calcium and silica from geochemical log data were sufficient to solve for the remaining lithology values once the clay volume was established.

Figure 4-2 is a graph of clay volume from thin-section analysis versus log-derived clay volume. Several clay indicators were plotted against the thin-section data to determine those with the highest correlation coefficient. Table 4-3 shows the clay indicators and their respective correlation coefficients.

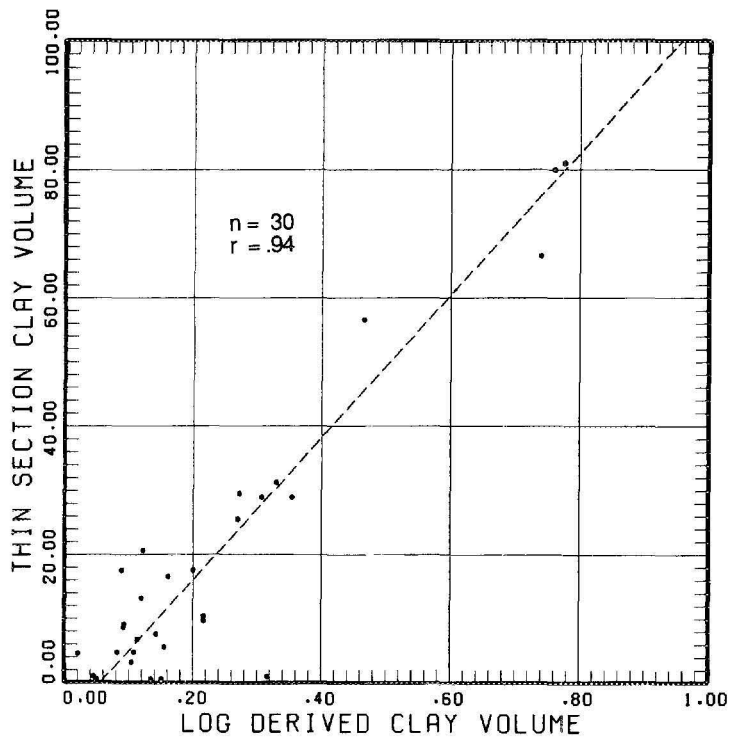


Figure 4-2 Comparison of Log-Derived Clay Volume and Thin-Section Clay Volume

Table 4-3 Thin-Section Correlation Coefficients for Various Clay Indicators

Clay Indicators	Thin-Section Analyses Correlation Coefficient
Gamma Ray	0.92551
Apparent Grain Density	0.85469
Aluminum Yield	0.90242
Final V_{clay}	0.93236

Response equations were written from these relationships, and the minimum value of the three was used in the analyses for volume of clay. The remaining mineral volume was broken into three components: quartz, calcite and iron carbonate. Iron calcite, ankerite

and dolomite were all grouped into one category because of the subtlety of the differences in their respective log responses. Moreover, because of similar difficulties distinguishing feldspars from quartz using log analyses, the volume of feldspars was not determined. Figure 4-3 presents the results of the lithology calculations along with the thin-section analyses results.

4.1.1.4 Porosity Determination

Two methods have been recommended for determining porosity in the Travis Peak Formation (Howard and Hunt, 1986). The first method uses the results from the lithology determination to calculate a grain density (Patchett and Coalson, 1982) and the electromagnetic propagation tool data (Kenyan and Baker, 1984) to determine fluid density. After these values are obtained, the bulk density log is used to directly derive porosity (Alger and Others, 1963). Use

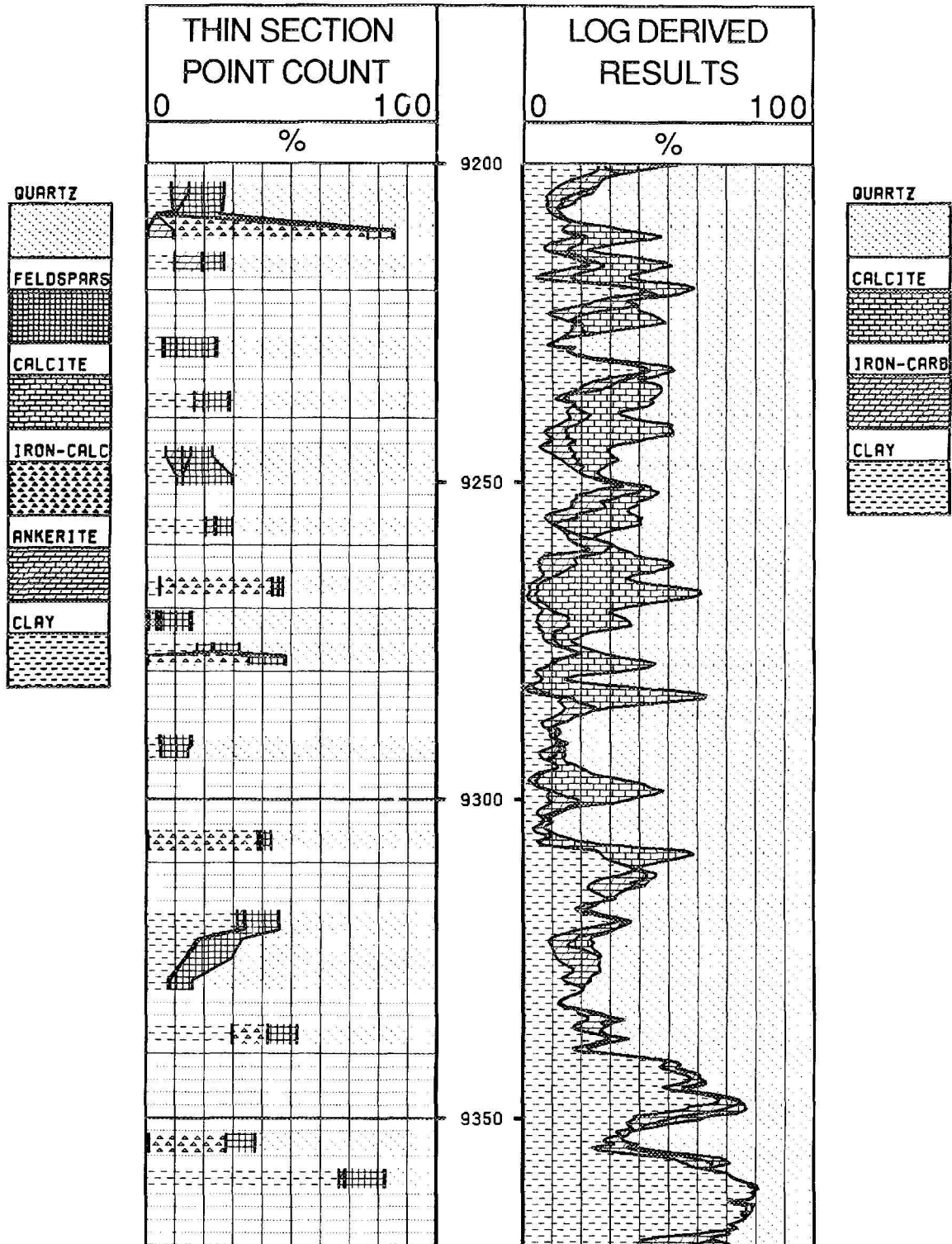


Figure 4-3 Comparison of Log-Derived Lithology and Thin-Sections

of this technique requires extreme accuracy in the lithology determination as well as high-quality, electromagnetic propagation log data. Unfortunately, in most of the wells in the Travis Peak or Cotton Valley, hole rugosity is a severe problem which negatively affects each of these.

The second method used to evaluate the SFE No. 3 well employs a shale-corrected crossplot of the neutron and density log data. In small quantities, the effects of the heavy minerals have opposite (and almost equal) effects on the shale-corrected neutron and density values. The effect of gas is similar in that both log values are affected in opposite ways. For this technique, equations for porosity can be written as follows:

$$\phi_{De} = \phi_D - V_{sh}\phi_{Dsh} \quad \text{Eq. 4-2}$$

and

$$\phi_{Ne} = \phi_N - V_{sh}\phi_{Nsh} \quad \text{Eq. 4-3}$$

where

ϕ_{De} = effective porosity from density log

ϕ_D = porosity derived from the density log

ϕ_{Dsh} = shale correction factor for density log

ϕ_{Ne} = effective porosity from neutron log

ϕ_N = porosity derived from the neutron log

ϕ_{Nsh} = shale correction factor for neutron log

Once the two effective porosities are derived, the calculation of porosity (ϕ) can be treated in two ways. For cases in which $\phi_{Ne} > \phi_{De}$ (i.e., when heavy minerals are present),

$$\phi = \frac{\phi_{Ne} + \phi_{De}}{2} \quad \text{Eq. 4-4}$$

For cases in which $\phi_{Ne} < \phi_{De}$ (i.e., when gas is present),

$$\phi = \frac{\phi_{Ne} + 4\phi_{De}}{5} \quad \text{Eq. 4-5}$$

Density and neutron porosity are weighted in Equation 4-5 to reflect the effect of gas on both measurements. Figure 4-4 displays the results of this analysis on the SFE No.

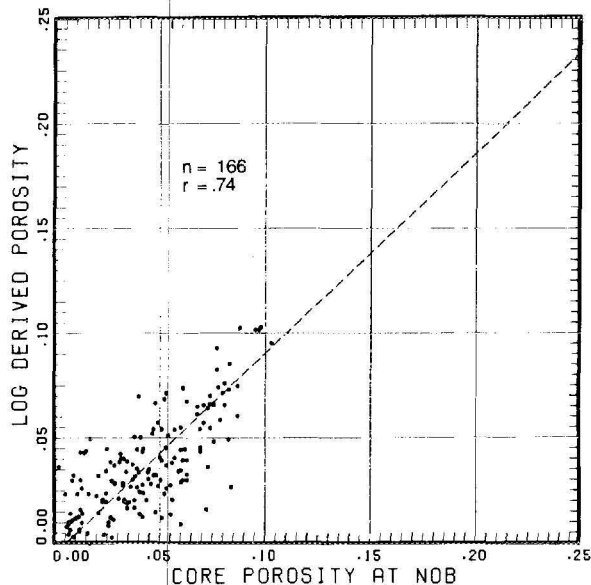


Figure 4-4 Comparison of Log-Derived Porosity and Core Porosity Measured at Net Overburden Pressure

3 well. As can be seen, significant scatter occurs in the lower porosity region. This scatter is common when porosity is not uniform throughout the sands and when the vertical resolution of the logging tools is different from the sampling frequency of the core analysis.

4.1.1.5 Water Saturation

The dual water model (Clavier and Others, 1984) was used for water saturation determination in SFE No. 3. The dual water

model assumes that the water associated with the shales is bound to the shale matrix and is of a different salinity than the water associated with the sands. Required input to the dual water model includes free water resistivity, "m" (cementation factor), and "n" (saturation exponent). A value of 0.048 ohm m at 75°F was chosen for free water resistivity based on measurements on Cotton Valley water samples in the area. The values of "m" and "n" were taken from composite plots of the electrical properties of seven core samples from the Cotton Valley. These values were 2.07 for "m" and 1.50 for "n". Figure 4-5 presents the resulting, calculated water saturations and the water saturations from core analyses corrected to in-situ conditions.

4.1.1.6 Permeability

Permeability was estimated by comparing core properties to log porosities. Core permeabilities and porosities were measured routinely on dry cores under net overburden pressures. The permeabilities obtained were permeabilities to helium corrected for Klinkenberg effect. To correct these values to in-situ conditions, two algorithms were applied. One converts the Klinkenberg gas permeabilities to permeabilities of the cores saturated with brine. The other uses variations in water saturation to calculate effective permeability to gas. Section 4.2.2.2, Relative Permeability Behavior, discusses how these relations were derived for the SFE No. 3.

The equation relating Klinkenberg-corrected gas permeability (k_{∞}) to porosity measured at net overburden stress is

$$k_{\infty} = 178.89 \phi^{3.50} \quad \text{Eq. 4-6}$$

To convert this permeability to a brine permeability (k_b) requires a correction using the equation

$$k_b = 0.9531 k_{\infty}^{1.19} \quad \text{Eq. 4-7}$$

Finally, to correct this brine permeability to a net permeability to gas requires an equation similar in form to that developed by Corey (1954), which allows for the variances of water saturation. The equation is

$$k_g = k_b \left[\frac{0.97 - S_w}{0.97 - S_{iw}} \right]^{3.22} \quad \text{Eq. 4-8}$$

where

$$\begin{aligned} k_g &= \text{gas permeability} \\ S_w &= \text{water saturation} \\ S_{iw} &= \text{irreducible water saturation} \end{aligned}$$

Table 4-1 summarized average property values for the completed interval. Log-calculated kh was 0.33 md-ft, which agrees quite well with the pre-frac well test analysis results of 0.38 md-ft (see Section 6.1). The permeability results are plotted along with S_w in Figure 4-5. The pre-fracture flow rate was 50 MCFD, confirming the low permeabilities calculated by log analysis.

4.1.2 Interpretation Techniques and Application of Acoustic Well Log Data to Calculations of Rock Mechanical Properties and In-Situ Stress

4.1.2.1 Introduction

In-situ stress has been widely accepted as the most important control factor for the vertical growth of hydraulic fractures (Nolte and Smith, 1979). The ability to determine stress profiles and, therefore, to predict the vertical growth of hydraulic fractures, is an essential part of a successful stimulation treatment in tight gas reservoirs. Depending on the rock stress in and adjacent to a treatment zone, vertical height growth may become excessive as fracture pressure increases. The consequence, in many cases, may be poor well performance because the desired propped length was not achieved or because the fracture extended into a water-

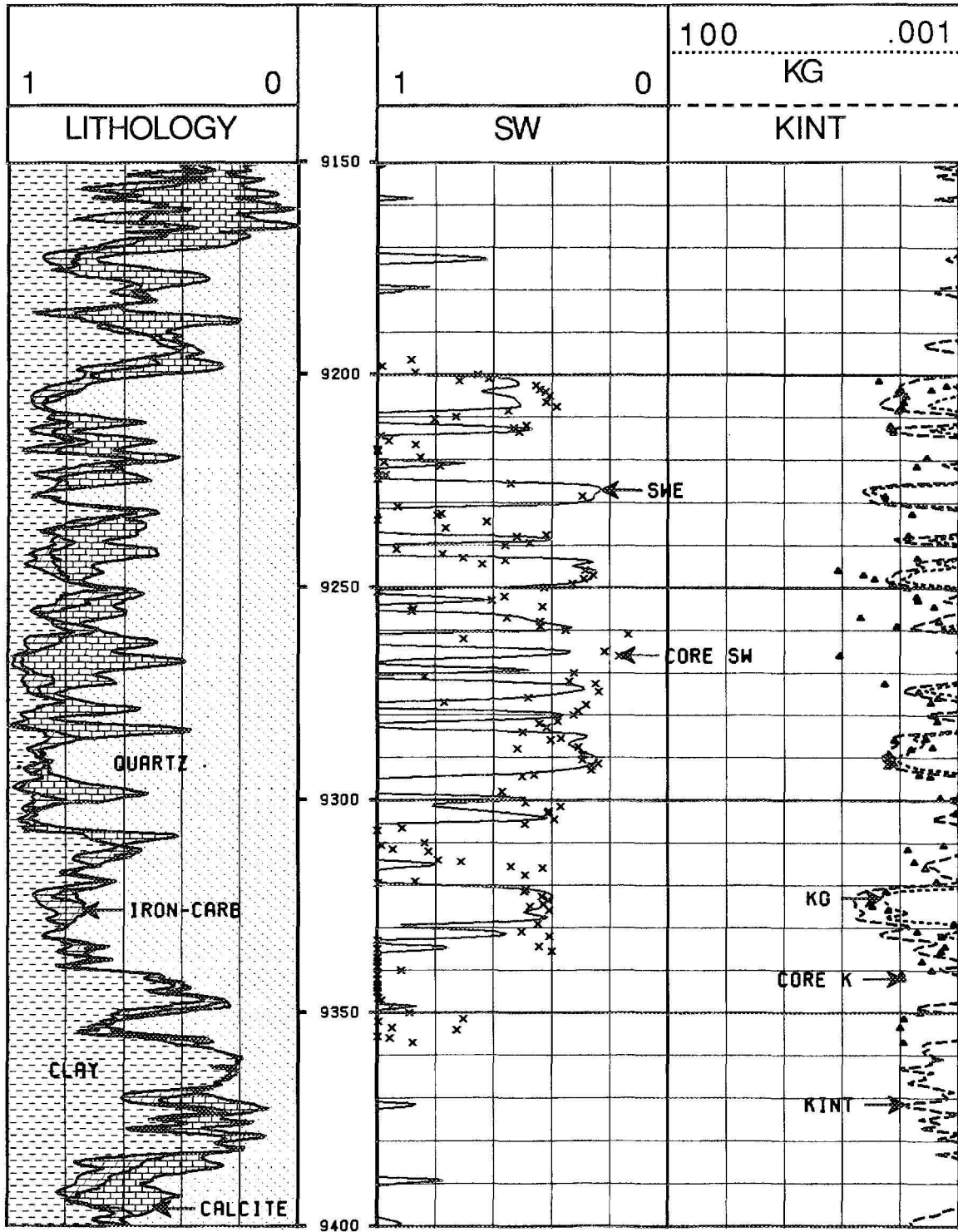


Figure 4-5 Comparison of Log-Derived Permeability and Water Saturation to Core Data

producing interval (Whitehead and Others, 1987). Thus, understanding the most probable growth pattern is critical to the successful design and implementation of hydraulic fracture treatments.

There are published techniques for computing in-situ stress profiles from log responses and from core analyses (Tixier and Others, 1973). These techniques relate either dynamic or static elastic parameters to in-situ stresses. Techniques using log-derived results must be verified and calibrated with in-situ stress measurements from micro-injection tests. This step ensures that the log is properly calibrated even when some other stress is present that has not been accounted for in the model. The following sections describe the data and analysis methods needed for calculation of in-situ stress profiles from logs.

4.1.2.2 Basis for Calculating Log-Derived Stress

Log-based methods for calculating closure stress use the shear and compressional velocities (V_s and V_p) along with density (ρ_b) in some modified form of Hooke's law:

$$\epsilon_x = \frac{1}{E}(S_x - S_p) - \frac{\nu}{E}(S_y - S_p) - \frac{\nu}{E}(S_z - S_p) \quad \text{Eq. 4-9}$$

where ϵ_x is the elastic strain in the x direction; E is Young's modulus; S_x , S_y , S_z are the stresses (actually stress gradients, but will be referred to as stresses in the remainder of this section) in the x, y, z directions; S_p is the stress gradient produced by the internal pore pressure; and ν is Poisson's ratio. Note that when ϵ_x is assumed to be zero and $S_x = S_y = S_h$ (closure stress) and $S_z = S_v$ (overburden stress), Equation 4-9 reduces to the classical equation,

$$S_h = \frac{\nu}{1 - \nu} (S_v - S_p) + S_p \quad \text{Eq. 4-10}$$

When the formation pressure is normal and is near original conditions, S_p is equated to pore pressure gradient (see Equation 4-17). When a production depletion transient has occurred, a non-linear relationship of the pore pressure gradient is used for S_p (see Equation 4-18).

Equation 4-10 has been used to compute closure stress in the Travis Peak Formation. However, some adjustments were necessary before Equation 4-10 could be applied successfully in the Taylor section of the Cotton Valley Formation.

One disadvantage associated with using log data in calculations of in-situ stress is that only the elastic component of stress can be estimated. Other factors, such as ductility of the formation, residuals of tectonic stresses, and thermal and subsidence history of the basin, cannot be included in this analysis because the theory only relates the horizontal stress component to the vertical component through Poisson's ratio. Fortunately, in many cases such as SFE No. 3, which is located in a passive basin, all these non-elastic variables can be lumped together into a single variable. In the Taylor sand interval of the Cotton Valley Formation, this variable has been designated as the empirical factor called "X". To calibrate the log-computed stresses using actual measured values, the following equation was used:

$$S_h = \frac{\nu}{1 - \nu} (S_v - S_p) + S_p + X \quad \text{Eq. 4-11}$$

where

- S_h = minimum horizontal stress gradient
- S_v = vertical (overburden) stress gradient
- S_p = stress gradient produced by pore pressure

- v = Poisson's ratio
- X = empirical stress factor

Measured stress values from the cased-hole stress tests are found in Table 4-4.

Previously, S_v was determined to be 1.03 psi/ft and S_p was found to be 0.5 psi/ft. Using these values in Equation 4-10 yielded stresses that were too low in the Bossier shale and too high in the Taylor sand (further discussion will be provided in Section 5.2.1). Therefore, the X factor needs to be large and positive in shale and conversely, negative in the gas sands.

Fortunately, the neutron data provided the needed correlation. Neutron porosity values are much larger than true porosity in Bossier shale, and, conversely, the neutron porosity is much lower than true porosity in gas sands. In the case of SFE No. 3, the X factor is related to the neutron response as follows:

$$X = 0.794 \phi_{nls} - 0.075 \quad \text{Eq. 4-12}$$

where ϕ_{nls} is the neutron porosity in limestone units as recorded.

Figure 4-6 is a crossplot of the stress gradients computed with Equations 4-11 and 4-12 versus the measured stress gradients (see Section 5.2). The correlation coefficient (r)

for these test data is 0.99. The agreement between the calculated and the measured stress gradient values is excellent.

Two possible explanations are offered as to why the neutron log seems to work so well for determining the X factor. First, the sonic log (used to evaluate Poisson's ratio) and the neutron log are both influenced by the gas saturation of the formation. In sandstones, the gas has approximately an equal

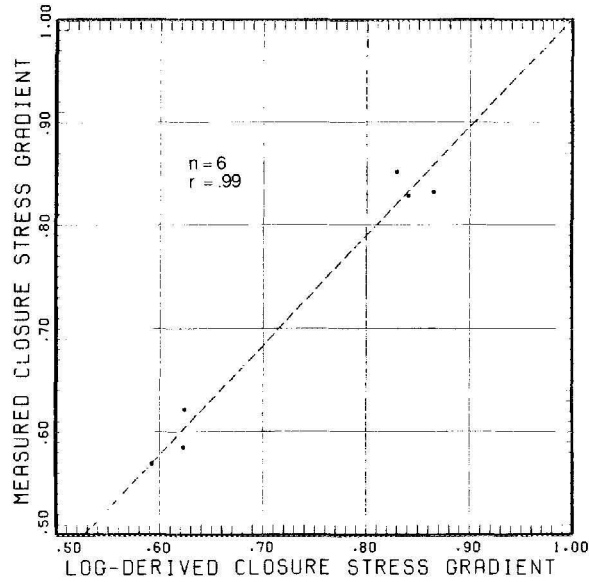


Figure 4-6 Computed Closure Stress Gradient Versus Measured Closure Stress Gradient in the Cotton Valley Formation of SFE No. 3

Table 4-4 Results of Cased-Hole Stress Tests, SFE No. 3

Depth, ft	Lithology	Fracture Closure, psi	Stress Gradient, psi/ft
9,227.0 - 9,229.0	Sandstone	5,400.0	0.585
9,266.0 - 9,268.0	Sandstone	5,275.0	0.569
9,324.0 - 9,326.0	Shaly Sand	5,800.0	0.622
9,554.0 - 9,556.0	Shale	7,950.0	0.832
9,600.0 - 9,602.0	Shale	7,950.0	0.828
9,630.0 - 9,632.0	Shale	8,200.0	0.851

but opposite effect on the responses of the two respective logs. As such, using the neutron log to calculate the X factor in gas-saturated sandstones tends to compensate for the gas effects introduced by using the sonic log to calculate Poisson's ratio. Second, in shale, the horizontal stress is sometimes larger than that calculated from the Poisson ratio equations. In these cases, there is probably a non-elastic component of stress present. The inference here is that this non-elastic component of stress is related to the amount of water present in the shales, which is a function of the neutron porosity of the shale. Thus, if one shale has a higher indicated neutron porosity than another, the shale with the highest porosity contains more water. The shale that contains more water will have a larger horizontal-to-vertical stress gradient ratio.

4.1.2.3 Determination of Poisson's Ratio

For the purposes of this analysis, Poisson's ratio is defined as the ratio of the transverse expansion to the longitudinal stress when a body is compressed. The Poisson's ratio of rocks may be determined from static loading tests or from acoustic (dynamic) measurements. The static loading tests tend to yield a wide range of values. The scatter may be due, at least in part, to damage of the sample from the opening and closing of microcracks. The dynamic (acoustic log) loading produces very small oscillations because the load variations are too small to make the microcracks open and close. The elastic parameters used in the remainder of this discussion, namely either Poisson's ratio or Young's Modulus, are the values determined by the dynamic, acoustic log measurements, which have tended to give more consistent results.

Poisson's ratio (ν) is related to the ratio (R) of compressional velocity (V_p) to shear velocity (V_s) using the following expressions:

$$R = \frac{V_p}{V_s} \quad \text{Eq. 4-13}$$

$$\nu = \frac{1}{2} \left[\frac{R^2 - 2}{R^2 - 1} \right] \quad \text{Eq. 4-14}$$

The velocities are extracted by computer processing the full-waveform, acoustic log data. Since these extracted velocities do vary with gas saturation, the calculated value for Poisson's ratio will also vary with gas saturation. However, no consistent and satisfactory means have been found to correct the acoustic logs for gas effects. As such, the log velocity values are used as processed, i.e., at in-situ gas saturation to calculate Poisson's ratio.

4.1.2.4 Poroelasticity

The classical approach for computing closure stress (S_h) is Equation 4-10 which relates S_h to Poisson's ratio, the overburden stress (S_v), and the stress gradient resulting from the internal pore pressure (S_p) (Hubbert and Willis, 1957). In this approach, S_p is assumed to be linearly related to the pressure gradient (p_g) by either one of the following equations of poroelasticity:

$$S_p = (1 - \beta) P_g \quad \text{Eq. 4-15}$$

$$S_p = (1 - \beta - \phi) P_g \quad \text{Eq. 4-16}$$

The term β is the biot constant, which is the ratio of compressibility of the solid rock (such as quartz) to the compressibility of the drained porous rock (such as sandstone). Porosity is denoted by ϕ and P_g is formation pressure gradient.

The disadvantage to using Equations 4-15 or 4-16 is that β cannot be determined from log analysis. It must be determined from

special core analysis. In addition, the linear relationship of S_p to P_g is often criticized because in the limit when $P_g = 0$, the computed closure stress using Equation 4-10 is too low. Attempts to use the actual measured β values in the Travis Peak study have not yielded acceptable results. In fact, using any value for β that is greater than zero reduced the correlation coefficient between measured stresses and computed stresses. When the formation pressure is from 0.6 times normal to normal, the following relationship is recommended:

$$S_p = P_g \quad \text{Eq. 4-17}$$

If a production depletion transient has occurred, such as when formation pressure is drawn down to less than 0.6 times normal, the S_p term used in Equation 4-16 must be somewhat larger than P_g if computed stresses are to fit measured stresses. (Note that this condition is equivalent to setting β to a negative value in Equations 4-15 or 4-16.) Therefore, if pressure is less than 0.6 times normal pressure, use of the hyperbolic relationship between S_p and P_g , described in Equation 4-18, is recommended.

$$S_p = a_0(a_1 P_g^2 + 1)^{1/2} - a_2 \quad \text{Eq. 4-18}$$

where the coefficients a_0 , a_1 and a_2 for the Travis Peak Formation are 1.15, 2.80 and 1.00, respectively.

4.1.2.5 Calculation of Formation Pressure

The largest component of Equation 4-10 is the formation pressure term. In fact, in normally-pressured zones, the formation pressure term contributes well over one half of the closure stress. Formation pressure must be known or closely estimated for any calculations of closure stress to be accurate enough for use in fracture design and engineered completions. In the more permeable

zones, pressure can be found from wireline testing, but permeable zones are scarce in tight gas sand intervals.

Formation pressure was determined in 21 of 46 Repeat Formation Tester (RFT) sets on SFE No. 1 (generally high permeability). However, on SFE No. 2 where very low permeability zones were encountered, only one successful RFT pressure was recorded in 57 attempts. Numerous attempts failed to yield a single valid pressure record in the Cotton Valley interval of SFE No. 3. Formation pressure remains a critical unknown for computing stresses in individual rock layers.

Performing a pre-fracture pressure buildup analysis to determine pressure is time consuming and, realistically, is not likely to be implemented in each layer of a multi-layered interval. Even if such buildup testing were performed in the interval to be fractured, the formation pressure in the boundary layers is still needed to compute a stress profile. Developing efficient methods of measuring formation pressure remains a major challenge to computing stress profiles in layered reservoirs.

4.1.2.6 Closure Stress Calculations

Closure stresses were computed on SFE No. 3 using Equations 4-11, 4-12 and 4-17. These computed stresses have proven to be reliable indicators of fracture growth not only in the Travis Peak Formation, but also in the Cotton Valley Formation. The results of these computations as well as the moduli computations are presented on Figure 4-7. The closure stress gradient is labeled CPG, the Poisson's ratio is labeled POIS, and Young's modulus is labeled Y.M. The importance of a closure stress profile in a comprehensive completion design will be described more fully in Section 5.2.

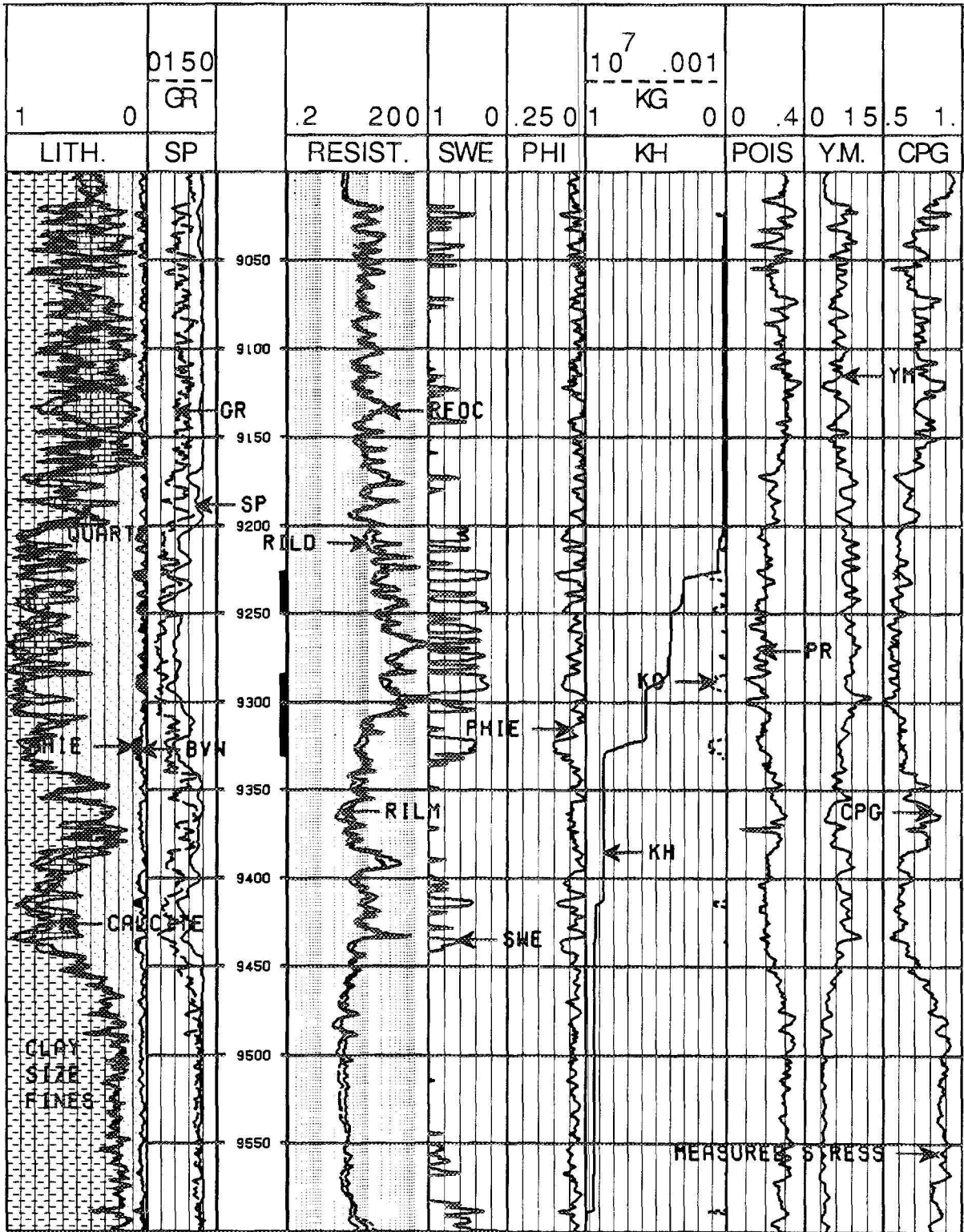


Figure 4-7 Pre-Fracture Analysis Results for the Completion Interval, SFE No. 3

4.1.2.7 Determination of Elastic Properties with Acoustic Logs

Elastic moduli are determined from acoustic data with the Equations 4-19 through 4-23.

$$\nu = \frac{1}{2} \frac{\left[\frac{V_p}{V_s} \right]^2 - 2}{\left[\frac{V_p}{V_s} \right]^2 - 1} \quad \text{Eq. 4-19}$$

where the ν is Poisson's ratio, and V_p and V_s are compressional and shear velocities.

$$G = c \rho_b V_s^2 \quad \text{Eq. 4-20}$$

where G is shear modulus, ρ_b is bulk density, and c is a units constant.

$$E = 2G (1 + \nu) \quad \text{Eq. 4-21}$$

where E is Young's modulus.

$$K_b = \frac{GE}{9G - 3E} \quad \text{Eq. 4-22}$$

where K_b is bulk modulus.

$$c_b = \frac{1}{K_b} \quad \text{Eq. 4-23}$$

where c_b is bulk compressibility.

Young's modulus determination from acoustic logs is a severe test of the acoustic log accuracy. Using the derivative of Equation 4-21, a 1 percent error in ρ_b , V_p and V_s results in a 3.2 percent error in Young's modulus calculations. A small error translates into a much larger error because the modulus equation contains the product of ρ_b and a squared velocity term. Even so, this percentage error is acceptable if the acoustic log data are truly accurate within 1 percent. Experience to date is that the full-

waveform, acoustic log acquisition and processing is not nearly this accurate. Additional information on this subject is provided in the "Full Wave Acoustic Logging (FWAL) Forum" section of Res Tech's final report to GRI (1988).

4.1.2.8 Summary

In-situ stress and moduli profiles accurate enough for use in hydraulic fracture design can be determined from integrated log analysis provided a few injection-type stress tests are available and formation pressures are known. To calibrate the stress profile, two to four in-situ stress tests are needed if formation pressure is known; six to eight in-situ stress tests are needed if formation pressure is not known. Once calibrated, these stress profiles are not only useful for fracture design, but are also useful for selection of perforation intervals.

Technical challenges in the area of stress profiling include:

- improving the formation pressure determination in very tight rocks, including mudstones;
- improving the techniques of analyzing acoustic log responses to minimize the negative impact of insufficient precision in recorded velocities, regardless of the tool or the service company;
- gaining a better understanding of the elastic strain term of Hooke's law (see Equation 4-9); and
- developing an alternative method or methods for determining stress (such as may be found in rock strengths derived from a drilling model) to verify, enhance or replace the acoustic log responses.

4.2 RESULTS AND APPLICATION OF CORE ANALYSIS

Core analyses provide a valuable link to log analyses in building reliable petrophysical models for formation evaluation, especially in geologic formations such as the Cotton Valley in East Texas where this type of integration has not been done extensively. In the SFE No. 3, a major purpose of the coring and core analysis program was to test the applicability of formation evaluation methods developed in the Travis Peak on the Cotton Valley Formation.

The core from SFE No. 3 was studied primarily for application in geological analyses, formation evaluation, in-situ stress prediction, and hydraulic fracture design and analysis. This section addresses the core analyses aimed at formation evaluation. These analyses can be broken further into two categories:

- routine core analyses (porosity, water saturation, permeability and grain density) that are performed on one sample each foot; and
- special core analyses (mechanical, electrical, relative permeability, and capillary pressure properties) that are much more difficult to conduct and, hence, are performed on only 10 to 15 core samples.

In addition to the tests described above, a special study was performed using Travis Peak core samples from SFE No. 3 to determine the effects of clay dehydration on core analyses. Most of the data previously collected on the Travis Peak in the Tight Gas Sands Program involved use of extracted, resaturated cores. This special study in SFE No. 3 was performed to determine to what extent these previous results are satisfactory, to determine what corrections might be needed, and to provide

guidelines on future core analyses in other geologic formations.

4.2.1 Routine Core Analysis Measurements

Routine core analyses were performed on 320 core samples taken from 374 ft of recovered conventional core to measure porosity, water saturation, permeability and grain density. In addition, these same measurements were made on 21 rotary sidewall cores taken after the well reached total depth (6 in the Travis Peak and 15 in the Cotton Valley). In the conventionally-cored section, 59 ft of core was recovered from the Travis Peak, 71 ft from the Travis Peak/Cotton Valley transition, 192 ft from the Cotton Valley, and 52 ft from the Bossier. Results of these routine conventional and sidewall core tests were reported by Western Atlas International (WAI) Core Lab (1989a, 1989b). The results appear in Appendix 2.

4.2.1.1 Introduction

Routine core analyses performed were similar to those done on SFE No. 1 and No. 2 (CER Corporation and S.A. Holditch & Associates, Inc., 1988 and 1989). However, in SFE No. 3, no tritium tag was used in the drilling mud, since previous experience has shown that drilling-mud filtrate invasion into the cores in the Travis Peak is not a major factor. Cores were described, preserved in an oxygen-barrier sleeve (ProtecCore) at the wellsite, then transported to the BEG core repository in Austin. The cores were removed from their protective sleeves and fitted together. A natural gamma ray scan was made for correlation with the downhole well logs, and the cores were slabbed 1/3 to 2/3 using water as a cutting fluid. The 2/3 core pieces (butts) were re-preserved and transported to WAI Core Lab Houston for plugging and routine core analyses.

Overall, a total of 318 core samples were taken at 1-ft intervals from the 370 ft of recovered core. Most of these samples were core plugs 1.5 in. in diameter, although in a few cases, those in which shales were involved, core pieces were used. The routine tests performed were as follows:

- As-Received Saturation
 - Water saturation (S_w)
 - Oil saturation (S_o) in the sidewall cores only
- Porosity
 - Porosity of the dry, conventional cores with measurable gas permeability at both 800 psi and net overburden (NOB) stress
 - Porosity, measured at ambient conditions, of the dry shale cores (or pieces), the conventional core plugs with visible fractures, and the sidewall cores
- Permeability
 - Measured helium permeability of the sidewall cores at 200 psi stress
 - Measured helium permeability and Klinkenberg-corrected helium permeability of the dry, conventional, non-fractured cores at 800 psi and NOB stress
- Grain Density
 - Measured grain density on the dry cores at ambient conditions

The as-received fluid saturations were measured in the following manner. In the case of the conventional core plugs, since no oil content was expected and since no tritium mud tag was used, the water content was determined by measuring weight loss after drying the plugs in an oven at 230°F. This method is more reliable than Dean Stark extraction when no oil is present. In the

case of the sidewall cores, Dean Stark extraction with boiling toluene was used followed by oven drying.

Porosity of the dry shale plugs, the sandstone plugs containing fractures, and the sidewall cores was measured at ambient conditions only. For these plugs, grain volume was measured in a cell using helium, and bulk volume was measured by immersion in mercury. For the other core plugs, porosity was measured at both 800 psi and NOB sleeve pressure. In these cases, pore volume was measured directly in the core which was confined in a sleeve while grain volume was measured at ambient conditions in a cell. For core plugs with < 0.001 md at NOB stress, no porosity was measured at NOB.

Permeability of the sidewall cores was measured using helium at 200 psi sleeve pressure in a low pressure core holder. For the conventional core plugs, permeability was measured with helium at 800 psi and NOB stress using the WAI Core Lab, CMS-300, automated measuring system. These measurements provide Klinkenberg factor, turbulence factor and Klinkenberg-corrected gas permeability (k_{∞}). The value k_{∞} is more representative of gas permeability at reservoir pore pressure. Permeabilities of core plugs with fractures (usually coring induced) were not measured since they are not representative of true matrix permeabilities. Of the 318 conventional core samples taken for analysis, 122 core plugs either contained fractures or were otherwise unsuitable for permeability testing. For the 196 core plugs with permeability measured at 800 psi sleeve pressure, 166 showed permeability > 0.001 md at NOB pressure. Value of NOB pressure was assumed to be 0.52 times depth.

4.2.1.2 Results of Routine Core Analysis

Detailed results of the routine plug and sidewall core analyses have been documented

(WAI Core Lab, 1989a and 1989b). Histograms of all the permeabilities (k_{∞}) and porosities measured at 800 psi sleeve pressure are shown, along with other statistics, in Figures 4-8 and 4-9 for the Cotton Valley section. For the same Cotton Valley section, Figure 4-10 provides a histogram of the grain densities, and Table 4-5 summarizes the core data that was collected. Results of the entire analysis of the 21 sidewall cores are shown in Table 4-6.

As can be seen on the graphical and tabular summaries, permeabilities (k_{∞}) measured at 800 psi on the cores are low in all the Cotton Valley samples. In fact, at NOB stress, only two non-fractured core plugs showed k_{∞} greater than 0.1 md, and only one core plug showed porosity greater than 10 percent.

4.2.2 Special Core Analysis Measurements

Special core analyses were performed on 38 core plugs from 18 separate depths (4 in the Travis Peak, 10 in the Cotton Valley and 4 in the Bossier shale) from the conventionally cored intervals of SFE No. 3. These special tests included measurement of permeability and porosity, dynamic mechanical properties, electrical properties, relative permeability behavior, and capillary pressure properties. These results have been previously reported (WAI Core Lab, 1989c).

4.2.2.1 Introduction

On February 10, 1989, representatives of BEG, SAH, WAI Core Lab and ResTech met at BEG in Austin and selected core depth locations from which core plugs were to be taken for special core analyses. These analyses were performed by WAI Core Lab in Dallas on 38 core plugs from 18 depth locations. The special tests can be grouped into four categories:

- Dynamic Mechanical Properties - 14 core plugs, 1-in. diameter
 - Basic properties (helium porosity and grain density)
 - Acoustic compressional and shear velocity and calculated dynamic elastic moduli at three or four levels of water saturation and at in-situ stress
 - Tensile strength of wafers from the end of the same 14 plugs, measured by loading until failure
- Electrical Properties - 8 core plugs, 1.5-in. diameter
 - Basic properties (helium porosity, brine porosity, helium permeability, grain density)
 - Formation resistivity factor at NOB stress
 - Resistivity at different water saturations at NOB stress
 - Cation exchange capacity (CEC) from end trims
- Relative Permeability Behavior - 8 core plugs, 1.5-in. diameter
 - Basic properties (helium porosity, brine porosity, helium permeability, grain density)
 - Brine permeability at NOB stress
 - Gas and water relative permeability during unsteady state gas injection, at NOB stress
- Capillary Pressure Properties - 8 core plugs, 1-in. diameter
 - Basic properties (helium porosity, brine porosity, helium permeability, grain density)
 - Air-brine capillary pressure using high speed centrifuge

For measurement of mechanical properties, 14 core samples representing a variety of

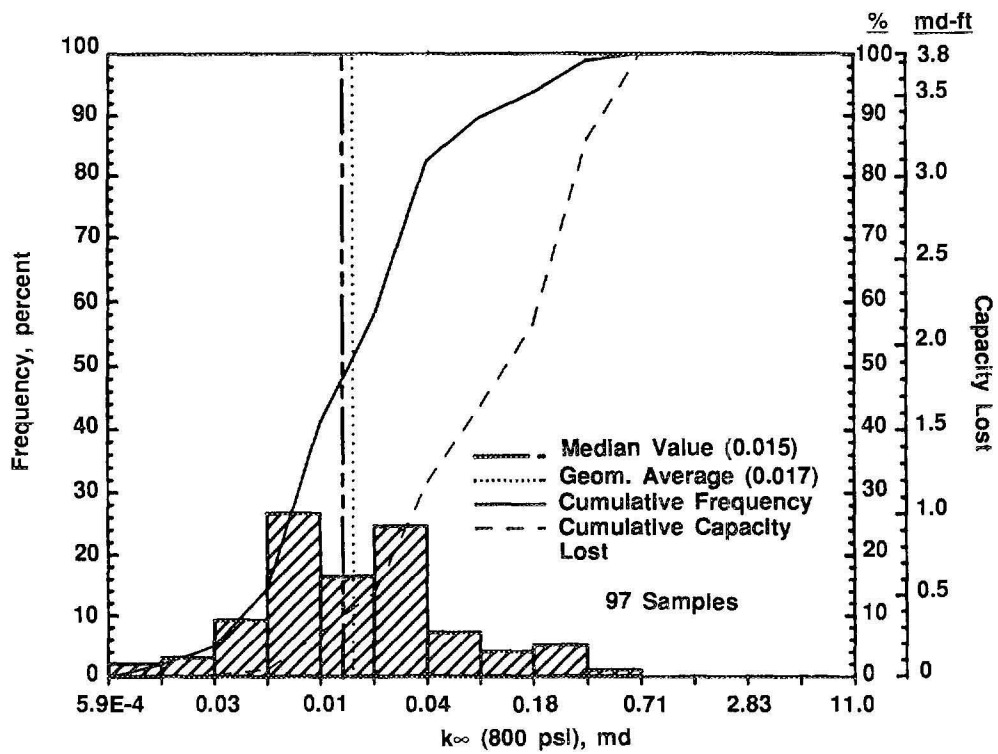


Figure 4-8 Frequency Percent of Klinkenberg-Corrected Gas Permeability at 800 psi Stress Measured from Routine Core Analysis in the Cotton Valley, SFE No. 3

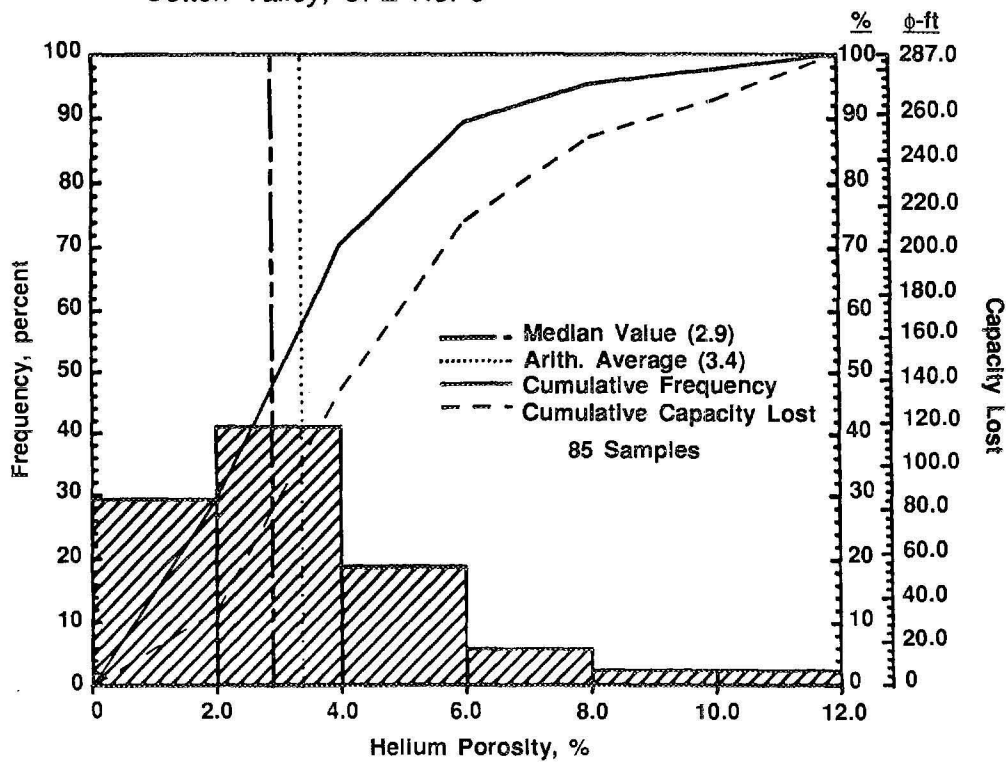


Figure 4-9 Frequency Percent of Porosities Measured from Routine Core Analysis in the Cotton Valley, SFE No. 3

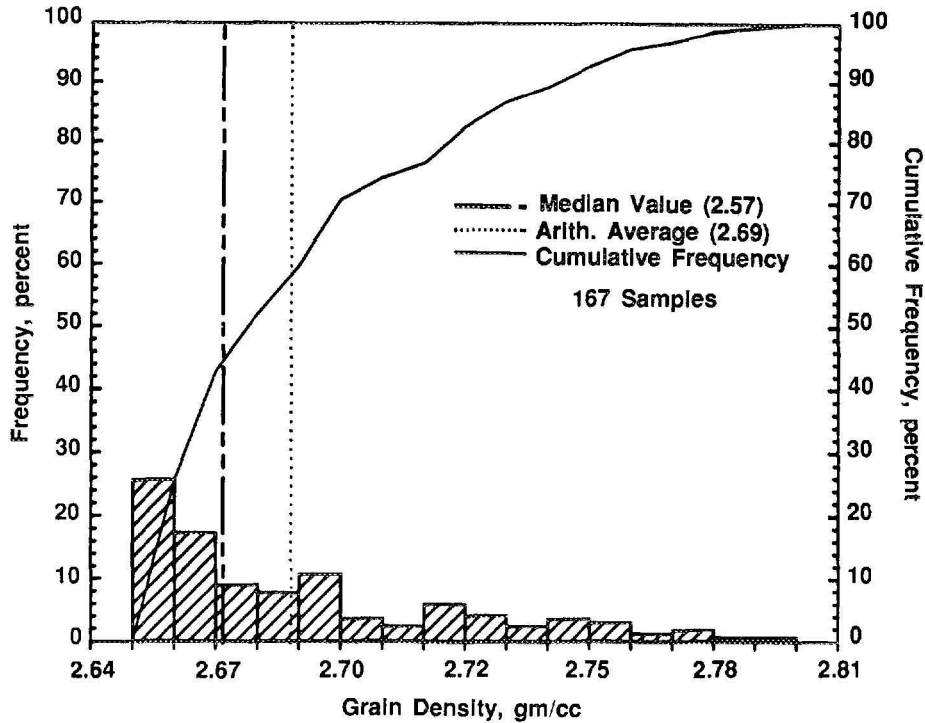


Figure 4-10 Frequency Percent of Grain Density Measured from Routine Core Analysis in the Cotton Valley, SFE No. 3

Table 4-5 Summary of Routine Core Analysis Results, SFE No. 3

<u>ZONE AND CUTOFF DATA</u>		<u>CHARACTERISTICS REMAINING AFTER CUTOFFS</u>			
ZONE:		ZONE:		PERMEABILITY:	
Identification	Cotton Valley	Number of Samples	167	Flow Capacity	3.7 md-ft
Top Depth	9017.8 ft.	Thickness Represented	167.0 ft.	Arithmetic Average	0.039 md
Bottom Depth	9367.9 ft.			Geometric Average	0.017 md
Number of Samples	181			Harmonic Average	0.009 md
		POROSITY:		Minimum	0.001 md
DATA TYPE:		Storage Capacity	287.0 Ø -ft.	Maximum	0.523 md
Porosity	(HELIUM)	Arithmetic Average	3.4%	Median	0.015 md
Permeability	K _∞ (800 psi)	Minimum	0.9%		
		Maximum	10.5%	Standard Dev. (Geom)	K · 10 ⁻⁴ ± 0.520 md
		Median	2.9%		
CUTOFFS:		Standard Deviation	±2.1%	HETEROGENEITY	
Porosity (Minimum)	0.0%			(Permeability):	
Porosity (Maximum)	100.0%	GRAIN DENSITY:		Dykstra-Parsons Var.	0.622
Permeability (Minimum)	0.0000 md	Arithmetic Average	2.69 gm/cc	Lorenz Coefficient	0.407
Permeability (Maximum)	1000. md	Minimum	2.65 gm/cc		
Water Saturation (Maximum)	100%	Maximum	2.80 gm/cc	AVERAGE SATURATIONS	
Oil Saturation (Minimum)	0.0%	Median	2.67 gm/cc	(Pore Volume):	
Grain Density (Minimum)	2.50 gm/cc	Standard Deviation	±0.04 gm/cc	Oil	0.0%
Grain Density (Maximum)	3.00 gm/cc			Water	60.5%
Lithology Excluded	NONE				

Table 4-6 Results of Sidewall Core Analyses, SFE No. 3

Sample Number	Depth, ft	Horizontal Permeability (200 psi), md	Porosity (Helium), %	SATURATION (Pore Volume)		Grain Density, gm/cc	Description
				Oil, %	Water, %		
TRAVIS PEAK							
1	6504.0	6.60	13.1	0.0	87.8	2.65	Sst wh f vf gr hd no flu
2	6468.0	1.90	12.1	0.0	89.7	2.66	Sst wh f vf gr hd no flu
3	7104.0	1.30	9.2	0.0	89.3	2.65	Sst wh f m gr hd slily calc no flu
4	7390.0	51.0	11.3	0.0	88.1	2.64	Sst wh f m gr hd slily calc no flu
5	7505.0	5.30	15.7	0.0	87.1	2.65	Sst wh f vf gr hd calc no flu
6	7732.0	230.	13.5	0.7	87.2	2.65	Sst wh m f gr fri mott dull yel flu
COTTON VALLEY							
7	8211.0	*	8.7	0.0	94.2	2.65	Sst gry f gr hd no flu
8	8352.0	0.17	11.0	15.5	64.5	2.65	Sst gry f gr fri slily calc spotty bri yel flu
9	8359.0	0.01	5.7	17.3	43.2	2.65	Sst wh f gr hd slily calc evn bri yel flu
10	8511.0	0.02	8.3	8.9	33.7	2.66	Sst gry f vf gr evn dull yel flu
11	8787.0	*	7.2	0.0	88.9	2.64	Sst gry f vf gr hd no flu
12	8801.0	*	9.4	0.0	80.6	2.65	Sst wh f gr hd v slily calc no flu
13	8957.0	0.03	10.5	0.0	85.0	2.66	Sst gry vf f gr v hd v slily calc no flu
14	9060.0	*	5.5	0.0	85.5	2.70	Sst gry vf gr v hd shly slily calc no flu
15	9207.0		1.5	0.0	85.4	2.68	Sst gry vf gr v hd v calc shy lam no flu
16	9227.0	0.02	9.2	0.0	49.1	2.66	Sst gry vf gr v hd v slily calc no flu
17	9289.0	0.03	9.2	0.0	90.5	2.65	Sst gry vf gr v hd v slily calc no flu
18	9324.0	0.01	11.5	0.0	68.3	2.66	Sst gry vf gr v hd v slily calc no flu
19	9390.0		5.3	0.0	67.6	2.69	Sst gry vf gr v hd slily calc shy lam no flu
20	9414.0	0.07	9.2	0.0	85.1	2.67	Sst gry vf gr v hd slily calc no flu
21	9600.0	*	6.1	0.0	91.3	2.72	Sh blk pily hd no flu

* Unsuitable for analysis

lithologies from the Travis Peak, the Cotton Valley and the Bossier shale were selected. Acoustic compressional and shear velocities were measured on all plugs at as-received water saturations (S_w) and at NOB stress (0.5 psi/ft). The plugs were then centrifuged to about half of their S_w and allowed to equilibrate before the acoustic velocities were measured at NOB. Subsequently, the plugs were dried at 145°F and 60 percent relative humidity for one week, and acoustic velocities were remeasured at NOB. At this point, the porosities and grain densities of the plugs were also measured. The plugs were then fully saturated with brine and acoustic velocities remeasured at NOB. Afterwards, wafers (1-in. diameter x 0.5-in. length) cut from each plug were tested for tensile strength. Each sample was placed into a hydraulic load frame where a force was applied across the sample's diameter. The force required to split the wafer was measured, and with this information, the tensile strength at failure was calculated.

Electrical properties were measured on eight 1.5-in.-diameter, sandstone plugs (one Travis Peak, seven Cotton Valley). The fresh, preserved plugs were saturated with 150,000 ppm NaCl brine and 10 pore volumes brine were injected. Resistivity was measured on each plug at 25°C and NOB stress (0.52 psi/ft) in a two-electrode system at 1 kHz. Then the plugs were partially desaturated by centrifuge, equilibrated and weighed, and resistivity was remeasured at NOB. This process was repeated at a total of four to six intermediate values of S_w . Next, the plugs were cleaned and leached of salt, and basic properties were measured. On companion end trims from each plug, CEC was measured by wet chemistry on crushed samples.

Relative permeability tests were performed on eight 1.5-in.-diameter plugs which were cut from the same long plug as the samples used for electrical measurements. The

fresh, preserved plugs were saturated with 150,000 ppm NaCl brine and 10 pore volumes brine were injected. Permeability to brine was then measured at NOB stress. Next, with the core at NOB stress, humidified gas was injected at constant pressure to displace the brine until a produced gas-water permeability ratio of 30 was reached. Gas and water permeabilities were calculated from produced gas and water measured as a function of time. Afterwards, the core plugs were cleaned and extracted of salt, and gas permeabilities and porosities were measured on the dry plugs.

The same eight plugs were used to determine the capillary pressure properties, although an adjustment in size was required. The original plans called for the capillary pressure tests to be run immediately following the relative permeability tests using the porous plate method. However, the permeability was too low for the porous plate method, so the high-speed centrifuge was used instead. While the former needed a core 1.5 in. in diameter, the latter required a diameter of 1 in. Therefore, after the relative permeability tests were completed, the cores were extracted and dried, the basic properties were measured, and then the plugs were trimmed down to 1-in. diameter. Permeabilities and porosities were measured on the 1-in.-diameter, dry cores. The extracted cores were then saturated with 150,000 ppm NaCl brine and capillary pressure determined in the centrifuge up to 1,000 psi.

4.2.2.2 Results of Special Core Analysis

Mechanical Properties

The results of the acoustic measurements of compressional (V_p) and shear (V_s) velocities and the those of the rock moduli calculations are shown in Table 4-7. These results indicate an increase in compressional velocity of about 15 percent when going

Table 4-7 Summary of SFE No. 3 Core Acoustic Velocities and Moduli Versus Water Saturation

Sample Depth, ft	Net Stress Pnet, psi	Sw, %	Vp, (ft/s)	Vs, (ft/s)	Poisson's Ratio	Shear Modulus, psi * 10 ⁶	Bulk Modulus, psi * 10 ⁶	Young's Modulus, psi * 10 ⁶
7354.5	3688	0.0	14020	9680	0.04442	3.0860	2.3582	6.4461
		9.5	14650	9680	0.11300	3.0800	2.9500	6.8600
		57.6	15345	9740	0.16264	3.1915	3.6663	7.4210
		100.0	14780	9140	0.19107	2.8593	3.6747	6.8113
7386.0	3688	0.0	15060	10420	0.04101	3.3688	2.5468	7.0139
		57.6	15630	10420	0.10000	3.4869	3.1963	7.6711
		100.0	15930	10230	0.14947	3.4548	3.7764	7.9424
7399.5	3688	0.0	14865	9760	0.12066	3.3101	3.2596	7.4190
		42.9	15560	9650	0.18800	3.2700	4.1500	7.7700
		71.3	14865	9270	0.18184	3.0214	3.7411	7.1416
		100.0	14865	8340	0.24501	2.6529	4.3177	6.6058
9022.5	4543	0.0	14140	9060	0.15149	2.9340	3.2313	6.7569
		23.5	14640	9060	0.18977	2.9398	3.3821	6.9954
		70.7	15040	9530	0.16400	3.2700	3.7900	7.9620
		100.0	16080	8960	0.27466	2.9117	5.4901	7.4228
9034.5	4543	0.0	14660	9660	0.11653	3.3817	3.3821	7.5515
		35.0	15061	9328	0.18890	3.1648	4.0315	7.5253
		58.4	15340	9275	0.21200	3.1400	4.4000	7.6100
		100.0	17280	9540	0.28051	3.3462	6.5073	8.5697
9200.5	4543	0.0	14140	8830	0.18065	2.7724	3.4165	6.5464
		32.9	14940	9457	0.16547	3.1939	3.7091	7.4449
		61.3	14810	9034	0.20300	2.9200	3.9500	7.0300
		100.0	17000	9290	0.28706	3.0567	6.1586	7.8683

Table 4-7, Continued

Sample Depth, ft	Net Stress Pnet, psi	Sw, %	Vp, ft/s	Vs, ft/s	Poisson's Ratio	Shear Modulus, psi * 10 ⁶	Bulk Modulus, psi * 10 ⁶	Young's Modulus, psi * 10 ⁶
9232.2	4655	0.0	13630	9430	0.04091	2.9454	2.2261	6.1318
		10.8	13400	9372	0.02100	2.9200	2.0800	5.9700
		52.9	15440	9830	0.15972	3.2531	3.6957	7.5453
		100.0	15740	9595	0.20452	3.3088	4.4960	7.9710
9249.2	4655	0.0	15420	9510	0.19303	3.1681	4.1042	7.5592
		38.1	17850	9685	0.29130	3.3030	6.8114	8.5301
		100.0	18260	9511	0.31375	3.0853	7.2545	8.1067
9295.0	4655	0.0	14500	10450	-0.04063	3.6119	2.1365	6.9303
		55.7	15780	10590	0.09039	3.7685	3.3448	8.2183
		100.0	16100	10125	0.17280	3.5033	4.1856	8.2173
9329.0	4655	0.0	13390	9220	0.04907	2.7015	2.0949	5.6681
		7.4	13630	9110	0.09600	2.6500	2.3900	5.8100
		56.2	14390	9220	0.15179	2.7765	3.0613	6.3958
		100.0	14810	9110	0.19524	2.7816	3.6364	6.6493
9364.0	4724	0.0	10620	7850	-0.10282	2.1369	1.0601	3.8343
		39.4	10830	7780	-0.03299	2.1145	1.2788	4.0895
		77.6	12100	7930	0.12300	2.6500	2.3900	5.8100
		100.0	12940	7230	0.27280	1.8632	3.4794	4.7430
9460.0	4724	0.0	12440	9160	-0.09190	2.9010	1.7836	5.2687
		26.3	12820	9110	-0.00940	2.8824	1.8686	5.7109
		59.8	12920	8820	0.06400	2.7200	2.2100	5.7800
		100.0	14880	8680	0.24211	2.6658	4.2798	6.6224

Table 4-7, Continued

Sample Depth, ft	Net Stress Pnet, psi	Sw, %	Vp, ft/s	Vs, ft/s	Poisson's Ratio	Shear Modulus, psi * 10 ⁶	Bulk Modulus, psi * 10 ⁶	Young's Modulus, psi * 10 ⁶
9496.0	4724	0.0	10290	7500	-0.06618	1.9987	1.0988	3.7328
		35.3	11650	7190	0.19209	1.8856	2.3947	4.4241
		57.5	12710	7310	0.25300	1.9300	3.2600	4.8300
		100.0	12370	6370	0.32731	1.4327	3.6708	3.8033
9475.0	4724	0.0	10710	7760	-0.05177	2.1169	1.2127	4.0147
		51.8	11450	7790	0.06817	2.1524	1.7747	4.5983
		95.3	12980	7690	0.22900	2.1200	3.2100	5.2100
		100.0	13070	7060	0.29373	1.7970	3.7568	4.6496

from dry to fully saturated core plugs. Shear velocity showed little or no dependence on saturation. The basic properties of these plugs are shown in Table 4-8. Results of tensile strength at splitting failure for the companion wafers are shown in Table 4-9.

Electrical Properties

In the Cotton Valley, the seven preserved core plugs tested for electrical properties have stressed helium porosities ranging from 6.9 to 11.9 percent and stressed Klinkenberg permeabilities of 0.005 to 0.089 md. A graph of formation resistivity factor versus helium porosity, both measured at NOB stress, is shown in Figure 4-11 for the Cot-

ton Valley plugs. The average cementation exponent (m) is 2.07 (for a = 1.00) based on a best-fit line. This value agrees closely with previous results obtained in the Travis Peak Formation in the Tight Gas Sands Program. In addition, measurements of CEC made on end trims from each core range from 0.57 to 1.41 meq/100 gm of rock. These values, which reflect only moderate amounts of clay, can be used in the Waxman-Smiths method of log analysis for calculating water saturation.

On these same seven preserved Cotton Valley core plugs, electrical resistivity was measured at NOB stress for various decreasing water saturations. The combined results of these measurements are pre-

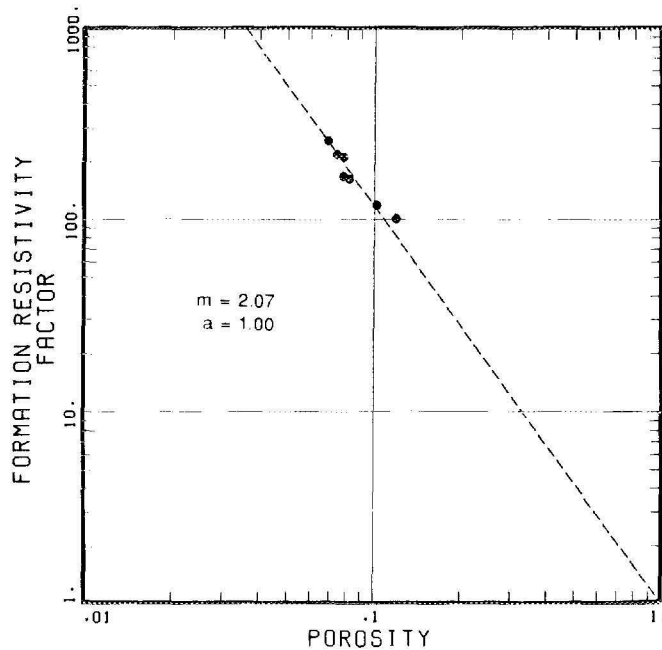
Table 4-8 Basic Properties of Cores Used for Acoustic Measurements

Sample Depth	Porosity, %	Grain Density, g/cc	Formation	Lithological Description
7,359.5	8.55	2.68	Travis Peak	Sst, vf, gr, v slty, slily calc
7,386.0	12.53	2.64	Travis Peak	Sst, f gr, w/srt
7,399.5	4.18	2.69	Travis Peak	Slst, hem
9,022.5	2.57	2.72	Cotton Valley	Ls, foss, sh
9,034.5	2.22	2.76	Cotton Valley	Ls, foss, sh
9,200.5	3.23	2.73	Cotton Valley	Ls, foss
9,232.2	7.01	2.65	Cotton Valley	Sst, vf gr, slty calc
9,249.2	3.54	2.70	Cotton Valley	Sst, fg, slty, pbl calc
9,295.0	6.62	2.63	Cotton Valley	Sst, vf gr, slty, slily calc
9,329.0	10.64	2.64	Cotton Valley	Sst, vf gr, slty, slily calc
9,364.0	5.45	2.70	Cotton Valley	Sh, calc
9,460.0	4.59	2.69	Bossier	Slst, calc
9,475.0	3.68	2.72	Bossier	Sh, calc
9,496.0	3.63	2.75	Bossier	Sh, calc

Table 4-9 Tensile Strength by Splitting of Wafers Companion to Acoustic Property Samples

Depth, ft	Length, in.	Diameter, in.	Tensile Strength, psi
7,354.5	0.485	0.986	2,431
7,386.0	0.571	0.981	1,684
7,399.5	0.541	0.957	2,065
9,022.5	0.537	0.967	1,877
9,034.5	0.511	0.983	1,630
9,200.5	0.534	0.966	1,769
9,232.0	0.503	0.984	2,349
9,249.2	0.458	0.972	1,204
9,295.0	0.517	0.976	2,242
9,329.0	0.557	0.967	2,274
9,364.0	0.521	0.958	2,392
9,460.0	0.512	0.962	2,170
9,475.0	0.468	0.953	2,536
9,496.0	0.514	0.953	1,926

Figure 4-11 Formation Resistivity Factor Versus Porosity Measured at NOB Stress for Cotton Valley, SFE No. 3



sented in Figure 4-12, with resistivity index plotted versus water saturation. From this plot, the average value of the saturation exponent (n) -- slope of the best-fit line -- is found to be 1.50. This is substantially less than the average value of 1.91 found in extracted cores from the Travis Peak in eight Tight Gas Sands Program wells prior to SFE No. 2. Note that in extracted cores from SFE No. 2, "n" in the Travis Peak was 1.39. Reasons for this rather wide swing in "n" are not clear; it requires further study.

Relative Permeability Behavior

As discussed earlier, gas/water permeability behavior was determined on eight preserved core plugs from SFE No. 3. Seven of these plugs were from the Cotton Valley Formation. A typical set of relative permeability curves is shown in Figure 4-13 for the Cotton Valley core plug at 9,295 ft, which has a k_{∞} to gas of 0.013 md and a brine k of 0.0058 md. The brine permeability is the base for the relative permeabilities shown. Basic properties of the Cotton Valley core plugs used in the relative permeability tests are shown in Table 4-10.

To apply these relative permeability data to log interpretation so that effective gas permeability at reservoir conditions may be predicted, three steps were required. The methodology is similar to that reported previously in a final GRI contract report (ResTech, 1988).

First, a correlation of Klinkenberg-corrected gas permeability (k_{∞}) to porosity at NOB stress was required. This correlation is shown for the Cotton Valley cores in SFE No. 3 in Figure 4-14. The best-fit RMA (reduced major axis) line for these data describes the equation

$$k_{\infty} = 178.89 \phi^{3.50} \quad \text{Eq. 4-6}$$

where k_{∞} is in md and ϕ is a fraction.

Next, a linkage of absolute brine permeability to Klinkenberg gas permeability (k_b to k_{∞}) was needed. This correlation is shown in Figure 4-15 for the seven Cotton Valley cores used for relative permeability tests. The best-fit RMA line is

$$k_b = 0.9531 k_{\infty}^{1.19} \quad \text{Eq. 4-7}$$

Note that this equation is really appropriate solely for $k_{\infty} < 1.0$.

Last, to convert k_b to effective gas (k_g) and effective water (k_w) permeabilities, two correlations were needed that relate effective permeabilities to water saturation. For the effective gas permeabilities, the correlation shown in Figure 4-16 represents the best RMA line for six of the Cotton Valley cores used for relative permeability tests (one core at 9,249.2 ft with anomalous results was omitted). The equation for this best-fit line is

$$k_g = k_b \left[\frac{0.97 - S_w}{0.97 - S_{iw}} \right]^{3.22} \quad \text{Eq. 4-8}$$

For the effective water permeabilities, the correlation shown in Figure 4-17 represents the best RMA line for the same six Cotton Valley cores. The equation for this best-fit line is

$$k_w = k_b \left[\frac{S_w - S_{iw}}{1 - S_{iw}} \right]^{3.65} \quad \text{Eq. 4-24}$$

In both these relative permeability correlations, S_{iw} (irreducible water saturation) was assigned a value of 0.30 to 0.35 depending on the core involved. These correlations (Equations 4-6, 4-7, 4-8 and 4-24) were then applied to log-calculated ϕ and S_w to derive effective gas and water permeability foot-by-foot, as well as permeability-thickness product within intervals of interest to predict well productivity. This methodology was described in Section 4.1.1.6.

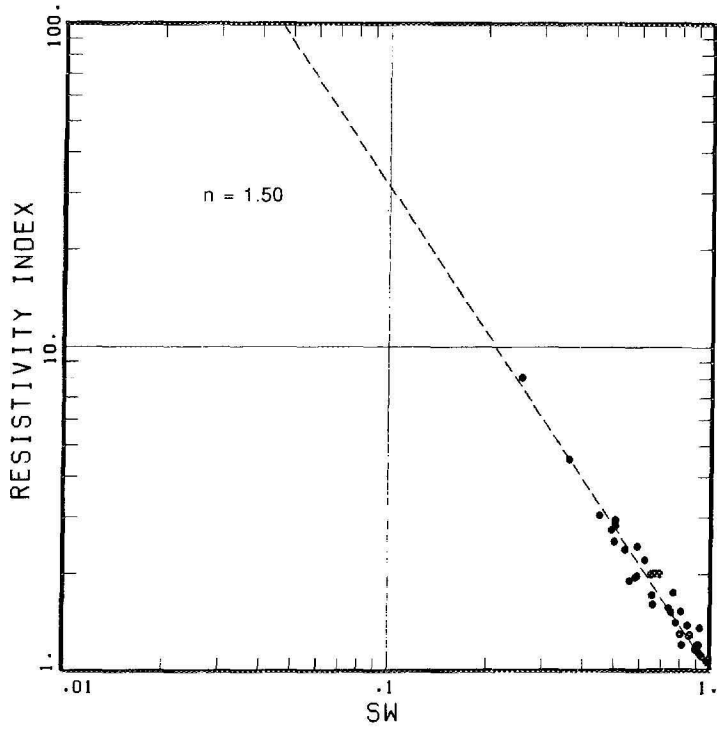


Figure 4-12 Resistivity Index Versus Water Saturation Measured at NOB Stress for Cotton Valley, SFE No. 3

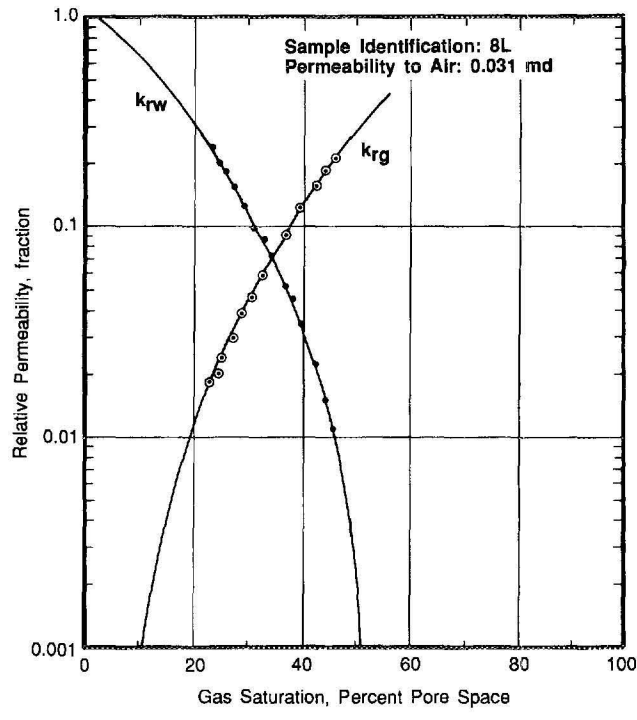


Figure 4-13 Typical Set of Gas and Water Relative Permeability Curves for Cotton Valley Sandstone, Sample Depth 9,295.0 ft

Table 4-10 Basic Properties of Relative Permeability Test Cores

Sample Depth	Stress Porosity, %	Stress Gas Permeability (k_{∞}), md	Preserved Core Stress Brine Permeability (k_{∞}), md
9,207.5	7.9	0.003	0.0011
9,210.0	7.8	0.004	0.0013
9,232.2	8.1	0.009	0.0032
9,249.2	7.8	0.090	0.0590
9,295.0	7.1	0.013	0.0058
9,326.0	11.9	0.019	0.0075
9,329.0	9.6	0.013	0.0054

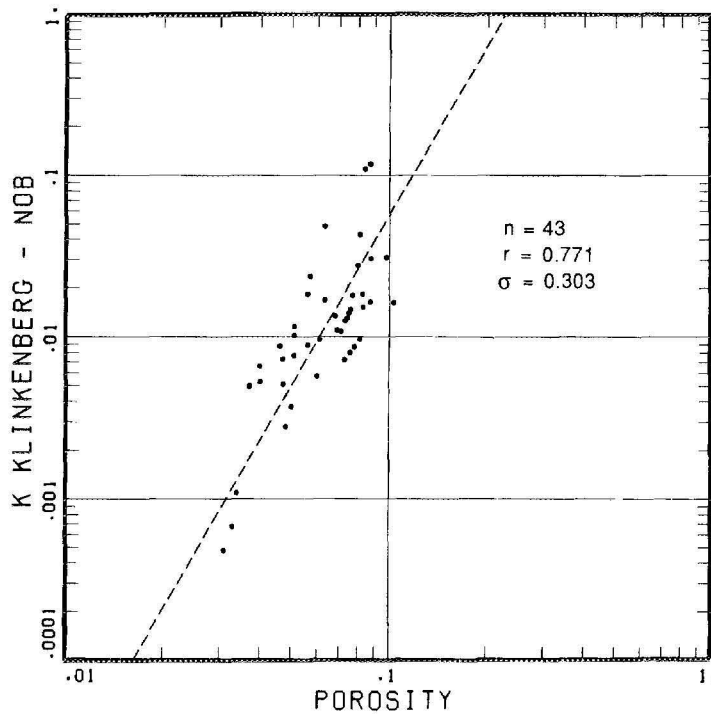


Figure 4-14 Klinkenberg-Corrected Gas Permeability Versus Porosity Measured at NOB Stress for Cotton Valley, SFE No. 3

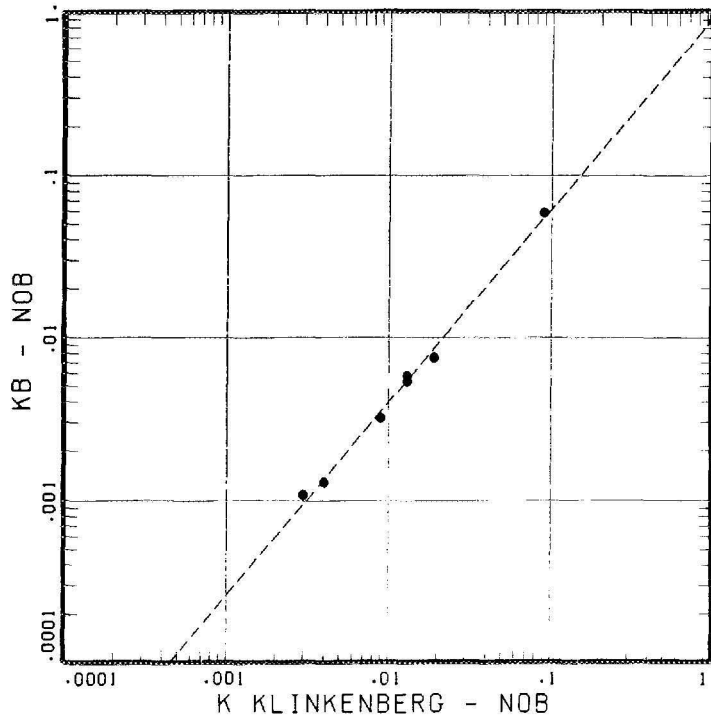


Figure 4-15 *Brine Permeability Versus Klinkenberg-Corrected Gas Permeability at NOB Stress for Cotton Valley, SFE No. 3*

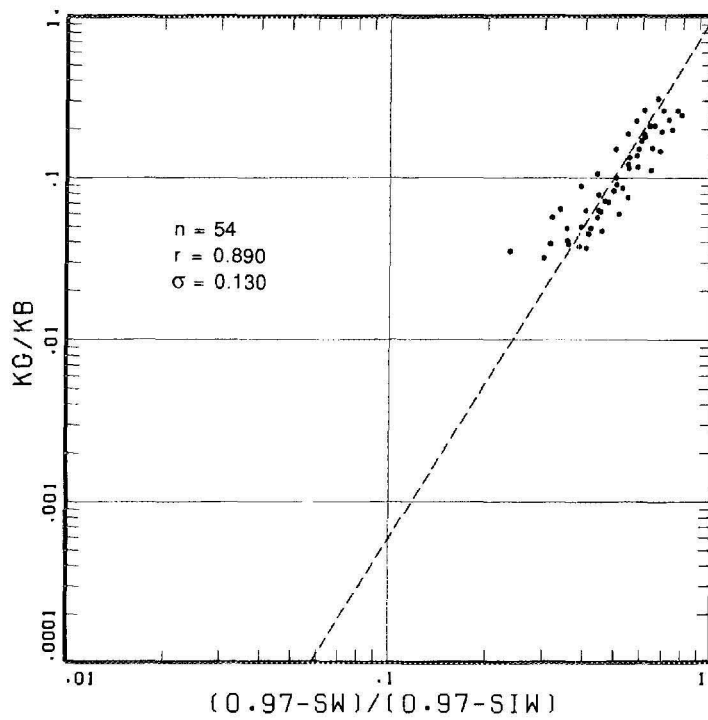


Figure 4-16 *Gas Relative Permeability With Normalized Gas Saturations for Cotton Valley, SFE No. 3*

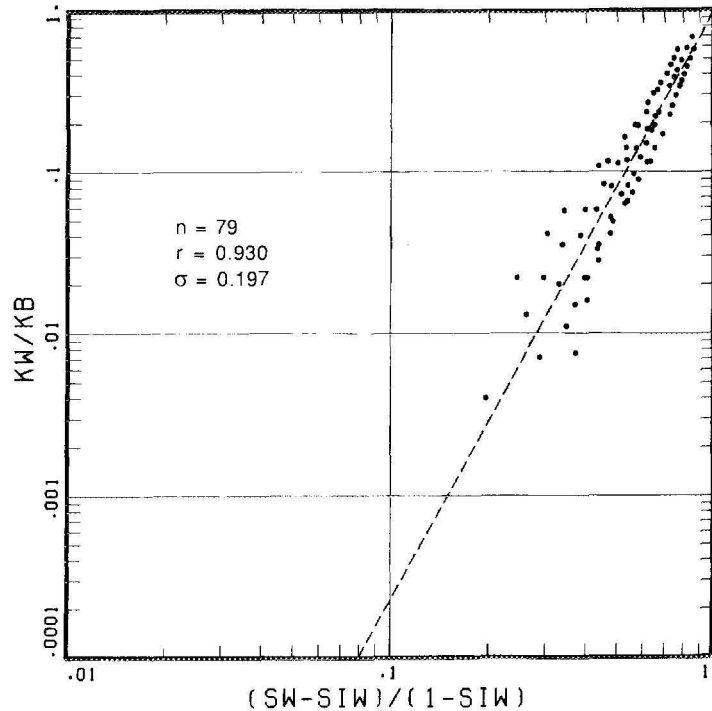


Figure 4-17 Water Relative Permeability Correlated with Normalized Water Saturation for Cotton Valley, SFE No. 3

Capillary Pressure Properties

Capillary pressure was measured on the same eight core plugs used for relative permeability tests. Between the two types of tests, the plugs were extracted and trimmed to 1 in. diameter. These trimmed plugs have slightly different properties. Basic properties for the seven Cotton Valley core plugs are shown in Table 4-11. A typical capillary pressure curve is shown in Figure 4-18 for the plug at 9,295 ft.

4.2.3 Effects of Clay Dehydration on Core Analysis

Special tests were conducted on cores from ten depths in the Travis Peak in the SFE No. 3 to examine the effects of extraction and drying on flow, capillary and electrical properties. Brine permeability, relative permeability, capillary pressure and electrical

measurements were made both before and after extraction and drying. In addition, SEM photos of companion core end trims were prepared from freeze-dried, air-dried and toluene extracted/dried samples. Results of the study show that fibrous illites present collapse upon drying but partially rebound upon resaturation with brine. The only reservoir properties significantly affected are the effective permeability to water and capillary pressure behavior at intermediate water saturations. Properties not significantly affected include effective gas permeability and electrical resistivity as a function of water saturation. Detailed results of this study were presented by WAI Core Lab (1989d).

4.2.3.1 Introduction

In most of the core analyses performed for the Tight Gas Sands Program, normal pro-

Table 4-11 Basic Properties of Capillary Pressure Test Cores

Sample Depth, ft	Ambient Porosity, %	Ambient Air Permeability, md
9,207.5	7.9	0.030
9,210.0	8.5	0.051
9,232.2	9.0	0.094
9,249.2	8.2	0.190
9,295.0	8.8	0.065
9,326.0	12.5	0.097
9,329.0	12.0	0.081

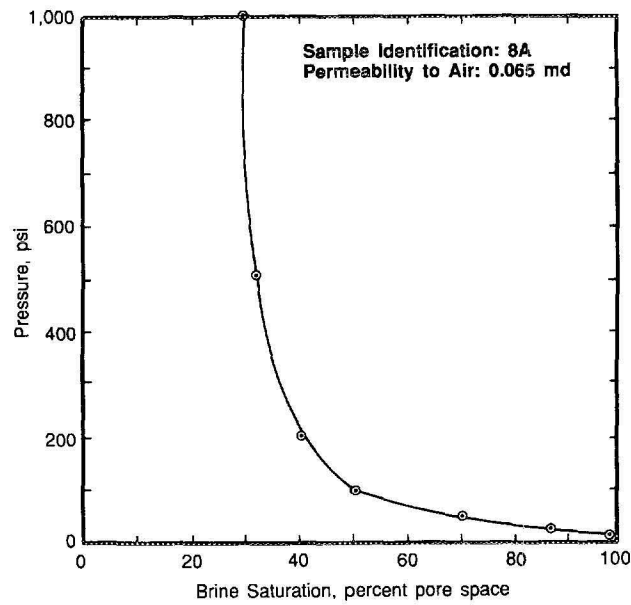


Figure 4-18 Typical Air-Brine Capillary Pressure Behavior for Cotton Valley Sandstone, Sample Depth 9,295.0 ft

cedure was to extract and dry the core samples prior to measuring reservoir rock properties such as flow, capillary and electrical properties. The procedure was favored because the rocks were regarded as strongly water-wet for the gas-water system present in the reservoir. However, recent work by Tye, Laubach and Herrington (1989) shows that fibrous illites present in the Travis Peak of East Texas are sensitive to the extraction and drying process. Previous work by Pallet and Others (1984) demonstrated that for rocks containing fibrous illites, extraction and drying collapsed the clay structure and caused the dry core gas permeability to increase several-fold over the brine permeability. Later, de Waal and Others (1988) showed that upon resaturation with brine, the fibrous illites largely rebound so that resaturated brine permeability is nearly equal to original brine permeability.

There is no work reported on the effect of extraction, drying and resaturation on important reservoir properties such as gas/water effective permeability, capillary pressure and electrical properties. For the Tight Gas Sands Program, it is important to determine the magnitude of these effects to ascertain if any adjustments are needed in using the database generated previously for the Travis Peak. In addition, guidelines for future core analyses depend in part upon this information.

To address these concerns, a special study was conducted on Travis Peak core from the interval 7,380 to 7,390 ft in the SFE No. 3, a sandstone zone with good porosity and permeability. Preserved, full-diameter core from this interval was taken to WAI Core Lab (Dallas). A total of 40, horizontal, 1.5-in.-diameter plugs were drilled at 10 separate depths. At each depth, a long plug was drilled across the diameter of the whole core; then two short plugs were drilled at the identical depth by rotating the core 90°. The long plug was cut in two

unequal sections. The short section was labeled A, while the long section was labeled B. Three wafers were taken for petrographic analysis. The two short plugs taken at 90° were labeled C and D. Each C plug was saturated with 150,000 ppm NaCl brine and flushed with 10 pore volumes of brine, after which brine permeability measured at 3,700 psi NOB stress. These 10 plugs were then extracted with toluene and methanol, and dried at 230°F. Permeability and porosity were then measured at NOB stress using helium. The plugs were resaturated with brine and permeability re-measured at NOB stress.

Five sample depths were selected, and the B samples were tested as follows.

- Relative Permeability (Preserved State). Each preserved plug was saturated with 150,000 ppm NaCl brine and flushed with 10 pore volumes of brine. Then brine permeability was measured at 3,700 psi NOB stress. Afterwards, humidified gas was injected at constant pressure to displace the brine until a gas-water permeability ratio greater than 30 was reached. Volumes of produced gas and water were recorded with time. From these data as well as water saturations, gas and water relative permeability were derived.
- Capillary Pressure (Preserved State). Each of the plugs were resaturated. Brine and air-brine capillary pressure behavior were measured in a porous plate cell at several pressures from 1 to 35 psi.
- Relative Permeability (Restored). Following the capillary pressure tests, the same plugs were extracted and dried, and porosities and gas permeabilities were measured. The cores were then resaturated with brine,

permeability remeasured at NOB stress, and gas-water relative permeability remeasured.

- **Capillary Pressure (Restored).** These same plugs were resaturated with brine and air-brine capillary was pressure remeasured.

The A plugs from the same five depths as above were used for measurement of electrical properties. Each preserved plug was saturated and flushed with several pore volumes of 150,000 ppm NaCl brine. Resistivity was measured at room temperature and 3,700 psi NOB stress using a two-electrode cell at 1 kHz. The plugs were then desaturated to various lower water saturations using a porous plate cell, the resistivity being measured at NOB stress at each step. Subsequently, the cores were extracted and dried, and porosities and gas permeabilities were measured. The cores were resaturated and the above procedures and measurements were repeated. To provide complete electrical properties, CEC measurements were also made on end trims from each of the five core plugs.

For petrographic study, preserved core end trims from each of the ten depths were examined by BEG using the SEM. To determine the effect of extraction and drying on the clay morphology, different core specimens were prepared four different ways. First, preserved pieces were flash frozen in liquid nitrogen and vacuum dried while frozen. This process sublimates the ice crystals with little or no alteration of the original fibrous illite structure. Second, companion core pieces were air-dried at room temperature. Third, companion core pieces were extracted with boiling toluene, leached with methanol, and then oven dried at 230°F. Fourth, companion end trims were taken from the five cores tested by WAI Core Lab after they had undergone flow testing, extraction, resaturation, flow testing and

resaturation. These samples were prepared for SEM study by flash freezing and vacuum drying to determine how much rebound the clays exhibit by resaturation.

4.2.3.2 Results of Study

Permeability

For the effect of extraction and drying on brine permeability, a comparison is shown for the 10 plug set (short plugs designated C) in Table 4-12. Helium porosity at 3,700 psi NOB stress is included as well. Note that in each case, k_w extracted > k_w preserved, and on average, the increase is a factor of 1.5. This result is about what was expected. Further note that air permeability (k_a) also measured at 3,700 psi NOB stress, is higher than either preserved or extracted k_w . On average $k_a = 2.6(k_w)$ preserved or $k_a = 1.5(k_w)$ extracted. Thus, when proceeding from preserved-core to dried-core to resaturated-core conditions, the clays change from the original fibrous state to a matted state, and then upon resaturation to a partially rebounded fibrous state. SEM photos shown in Figures 3-9a and 3-9b illustrate this effect, which was also discussed in Section 3.2.3.2, Influence of Fibrous Illite on Permeability.

These permeability changes are useful in showing the effect of core handling on the clay structure. However, to determine the influence on properties needed for reservoir engineering application, one must consider the specific effects on relative permeability, capillary pressure and electrical properties.

Relative Permeability

Typical behavior of the gas and water effective permeability is shown in Figure 4-19 for the core plug from 7,387.8 ft. This sample is representative of the relative permeability data acquired from all five core plugs taken at 7,387.8 ft. Note that the effective gas

Table 4-12 Summary of Basic Core Properties for Travis Peak Samples Used in Clay Dehydration Study

Sample Depth, ID, ft	Stress Porosity, %	Stress Brine Permeability, md		Stress Air Permeability, md
		Preserved	Restored	
7,382.5C	10.8	15	21	45
7,383.3C	11.6	11	16	30
7,383.7C	11.0	11	15	32
7,384.0C	12.1	18	27	59
7,384.7C	12.9	68	100	127
7,387.8C	11.5	14	25	37
7,388.2C	11.4	9	15	24
7,388.8C	11.2	12	19	30
7,389.9C	11.1	14	22	32
7,390.5C	11.4	18	24	41

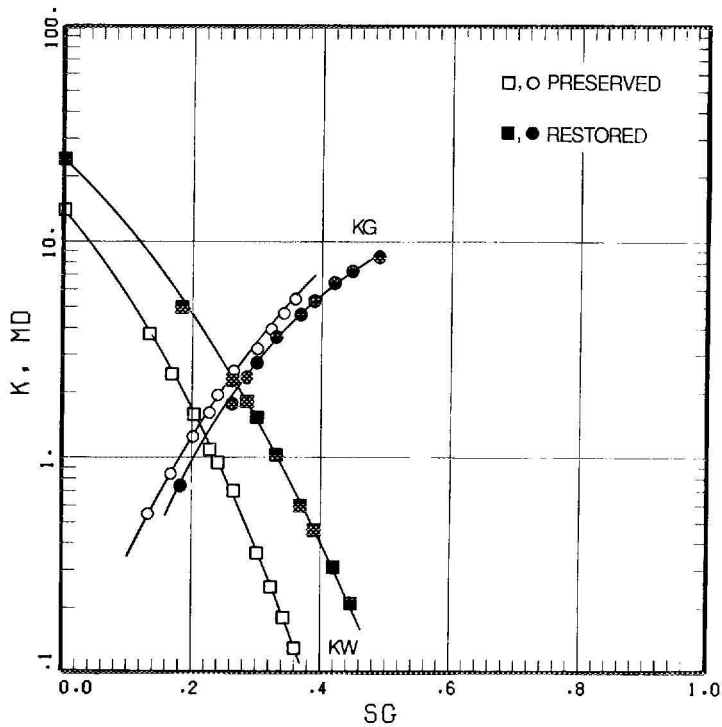


Figure 4-19 Comparison of Effective Permeability to Gas and Water of Preserved Versus Extracted/Restored Core at 7,387.8 ft at Various Gas Saturations

permeability as a function of S_w is about the same for either the preserved or the restored state. However, effective permeability to water is 3 to 5 times higher for the restored state in the intermediate range of S_w ; at $S_w = 100$ percent, restored brine permeability is 1.7 times the preserved state.

This general behavior was found in all five cores. Evidently, the clay structure partially rebounds upon full brine resaturation. However, as S_w is lowered, the residual alteration or matting of the clay fibers appears more pronounced in the smaller pore throats. These effects are magnified on effective water permeability at intermediate levels of S_w .

Capillary Pressure

Typical behavior of the air-brine capillary pressure (P_c) properties is shown in Figure 4-20 for the same core plug from 7,387.8 ft. There is little or no difference between preserved cores and extracted/restored cores for $P_c < 2$ psi. For higher values of P_c , the restored state shows lower P_c values at any S_w , which corresponds to larger pore throats. The P_c data in Figure 4-20 can be translated into pore throat distribution as a function of percent of pore space. Table 4-13 provides this information for all five cores, both preserved and restored, for pore throat sizes of 0 to 4 μm , 4 to 10 μm , and > 10 μm . After extraction and resaturation, on average about 6 to 7 percent of the pore space has enlarged throat radii that have increased from a size of 0 to 4 μm up to 4 to 10 μm . These observations are in harmony with the relative permeability effects just discussed.

Electrical Properties

The electrical properties of the cores can be characterized in two ways. First, the resistivity of the brine saturated cores can be compared. This is best accomplished by comparing the cementation exponent (m) in

the Archie relation of formation resistivity factor (F) to porosity (ϕ).

$$F = \phi^{-m} \quad \text{Eq. 4-25}$$

For the preserved cores, a best-fit correlation of F to ϕ yields $m = 2.01$. After extraction and resaturation, $m = 1.96$. This change is probably not significant.

Second, the resistivity of each core as a function of S_w can be compared before and after extraction. Typical results, shown in Figure 4-21 for the core plug at 7,383.3 ft, indicate that there is no significant difference in resistivity. This outcome is not surprising since electrical properties are not affected as much as permeability properties by changes in pore throat sizes. For completeness, note that resistivity as a function of S_w can be expressed through the relation

$$S_w = \left[\frac{R_O}{R_T} \right]^{1/n} \quad \text{Eq. 4-26}$$

where

- n = saturation exponent
- R_O = resistivity at $S_w = 100$ percent
- R_T = resistivity at each S_w

For the five preserved cores, composite $n = 1.57$ while for the restored cores, composite $n = 1.74$; the difference between these is not regarded as significant. The composite $n = 1.65$ for all data.

Summary

This study shows that in the Travis Peak, fibrous illites collapse upon core extraction but partially rebound upon resaturation with brine. The only reservoir properties significantly affected are the effective permeability to water and capillary pressure behavior at intermediate water saturations. In gas reservoirs where fibrous illites are present, the

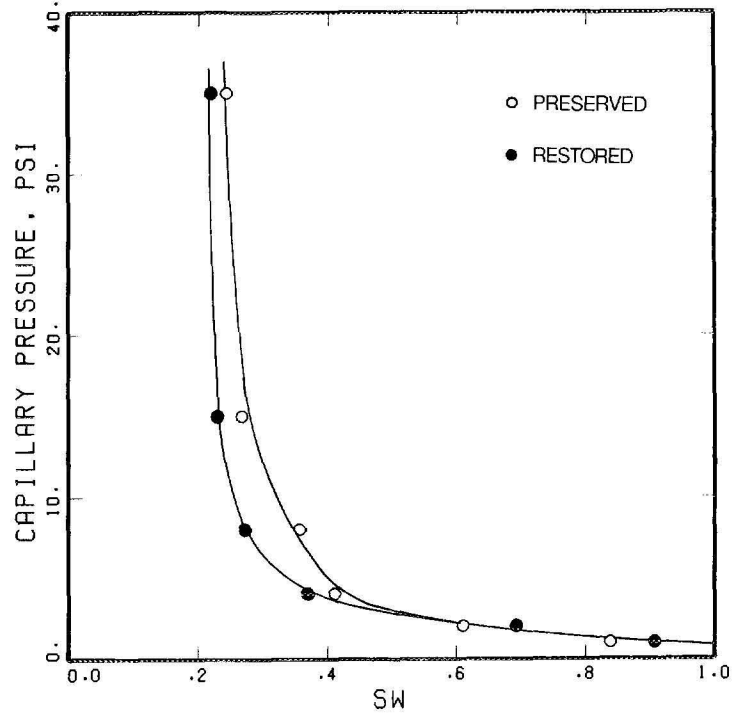


Figure 4-20 Comparison of Capillary Pressure Behavior of Core Sample at 7,387.7 ft, Preserved Versus Extracted/Restored

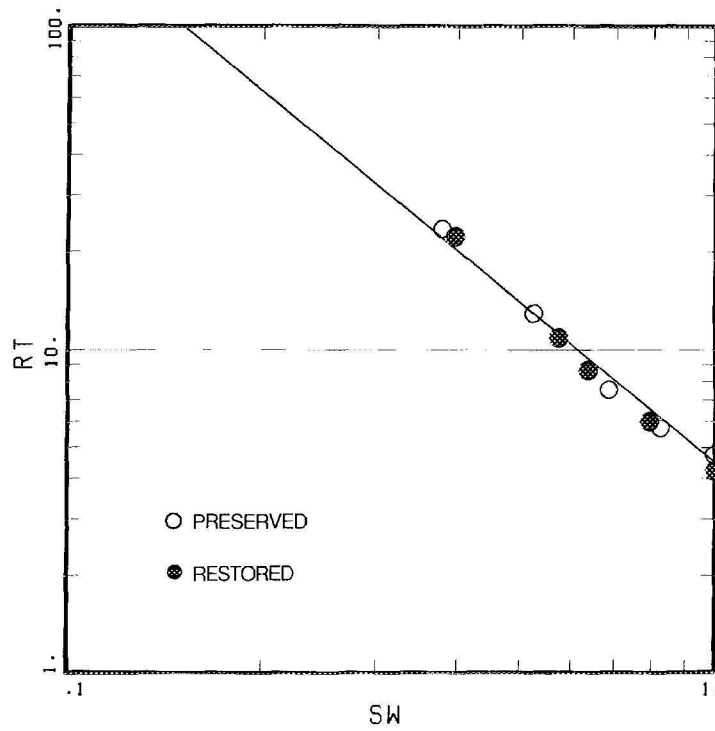


Figure 4-21 Comparison of Electrical Resistivity of Core Sample at 7383.3 ft, Preserved Versus Extracted/Restored

Table 4-13 Pore Size Distribution for Travis Peak Samples Used in Clay Dehydration Study

Sample Depth, ID, ft	Test State	Percent Pore Space for Pore Throat Radius and Air-Brine Capillary Pressure		
		0 - 4 μm > 5 psi	4 - 10 μm 5 - 2 psi	> 10 μm < 2 psi
7,383.3B	Preserved	49.5	19.5	31.0
	Restored	46.0	26.0	28.0
	Δ	+3.5	-6.5	+3.0
7,383.7B	Preserved	44.5	14.0	41.5
	Restored	39.0	25.5	35.5
	Δ	+5.5	-11.5	+6.0
7,384.7B	Preserved	33.0	11.0	56.0
	Restored	26.5	12.5	61.0
	Δ	+6.5	-1.5	-5.0
7,387.8B	Preserved	39.5	18.0	42.5
	Restored	32.0	28.5	39.5
	Δ	+7.5	-10.5	+3.0
7,388.2B	Preserved	40.5	27.0	32.5
	Restored	33.0	33.5	33.5
	Δ	+7.5	-6.5	-1.0
Average	Δ	+6.1	-7.3	+1.2

flow, capillary and electrical properties should be measured on preserved cores unless mixed wettability is a factor.

Most of the data previously collected on the Travis Peak in the Tight Gas Sands Program involved use of extracted, resaturated cores. In general, the data can be used

with confidence except for effective water permeabilities that were measured at intermediate values of S_w . These permeabilities may be too high. Consequently, using these older core data to predict productivity of well completions could, in turn, lead to the prediction of erroneously high water cuts in zones with transition water saturations.

5.0 In-Situ Stress Testing and Stress Profiling

5.1 IN-SITU STRESS TESTING

5.1.1 Introduction

Of major concern to the design and modeling of hydraulic fracture treatments is the ability to correctly predict the vertical height growth of the fracture. If the hydraulic fracture grows significantly more in the vertical direction than anticipated in the original design, then fracture width and length will be less than designed. Essentially, the relative stress contrast between rock layers governs the vertical height growth. The fracture is more likely to be contained if the in-situ stress in the target interval is small compared to the in-situ stress in the potential barrier rocks. By physically performing tests to determine the stress contrast between layers, one can more accurately design an optimal fracture treatment to obtain the desired dimensions.

On SFE No. 3, in-situ stress tests were performed in both an open-hole and cased-hole environment in the lower Cotton Valley Formation. In these stress tests, very small fluid volumes (typically less than 100 gal) were pumped at low injection rates (less than 10 gal/min) to break down the isolated interval. The falloff or flowback stages were then monitored until fracture closure pressures were obtained. A downhole shut-in tool was used during both the open-hole or the cased-hole stress tests to minimize the effects of wellbore storage.

5.1.2 Open-Hole Stress Tests

Table 5-1 presents the results of the six open-hole stress tests performed on SFE No. 3. As can be seen from the error range listed for each test, the quantitative analyses generally were not very definitive. The most definitive test appears to be the

one conducted at 7,406 to 7,411 ft in the Travis Peak sandstone.

In the open-hole environment, more definitive results were obtained in the sandstones as opposed to the shales because it is very difficult to get a packer to seal in a shale. When poor sealing occurs, it is often unclear which zone is actually being tested since fracturing occurs in the lowest stress interval exposed to the pressure increase. As such, the low stresses that were measured in the shales were probably measurements of the in-situ stress in a nearby sandstone.

5.1.3 Cased-Hole Stress Tests

Table 5-2 summarizes the results of the six cased-hole stress tests performed on SFE No. 3. In general, these tests were easier to perform and less complicated to analyze than the open-hole stress tests. Relatively good packer seats in the cased hole allowed for better control of the point of injection. For the same reason, the confidence level of the cased-hole stress tests is much higher than that of the open-hole tests.

There were three cased-hole stress tests performed in the Cotton Valley Taylor sand and three tests in the Bossier shale, which lies directly below the Taylor sand. Each test included multiple pump-in/falloff and pump-in/flowback tests. Typically, the injection rates were 5 to 10 gal/min with a total volume for each injection period of 25 to 50 gal. A bottomhole shut-in tool was used for the falloff periods; however, wellbore storage still affected the pressure falloff to some degree, as expected.

To determine the extent of wellbore storage effects, a log-log graph of the change in pressure after shut-in versus shut-in time

Table 5-1 SFE No. 3 Results of Open-Hole Stress Tests

Test No.	Depth, ft	Lithology	Fracture Closure Pressure, psi	Error Range, psi	In-Situ Stress Gradient, psi/ft	Possible Range of Stress Gradient, psi/ft
OHST1	7,406 - 7,411	Sandstone	4,750	-50, +150	0.64	0.63 - 0.66
OHST2	8,074 - 8,079	Limestone	5,600	±300	0.69	0.66 - 0.73
OHST3	9,013 - 9,018	Shale	6,000	±400	0.67	0.62 - 0.71
OHST4	9,041 - 9,046	Limestone	6,300	-400, +300	0.70	0.65 - 0.73
OHST5	9,363 - 9,368	Shale	6,200	-300, +200	0.66	0.63 - 0.68
OHST6	9,595 - 9,600	Shale	6,500	±500	0.68	0.63 - 0.73

Table 5-2 SFE No. 3 Results of Cased-Hole Stress Tests

Test No.	Depth, ft	Lithology	Fracture Closure Pressure, psi	Error Range, psi	In-Situ Stress Gradient, psi/ft	Possible Range of Stress Gradient, psi/ft	$\frac{\nu}{1 - \nu}$
CHST1	9,630 - 9,631	Shale	8,200	±100	0.85	0.84 - 0.86	0.380
CHST2	9,600 - 9,601	Shale	7,950	±100	0.83	0.82 - 0.84	0.430
CHST3	9,554 - 9,555	Shale	7,950	±100	0.83	0.82 - 0.84	0.340
CHST4	9,324 - 9,325	Sandstone	5,800	±250	0.62	0.60 - 0.64	0.205
CHST5	9,266 - 9,267	Sandstone	5,275	±75	0.57	0.56 - 0.58	0.300
CHST6	9,227 - 9,228	Sandstone	5,400	±100	0.59	0.58 - 0.60	0.210

was constructed for each test. On such a graph, wellbore storage is characterized by a unit slope. One example, Figure 5-1, shows data gathered from the cased-hole stress test performed at 9,630 to 9,631 ft in the Bossier shale.

The presence of a one-half unit slope on the log-log graph usually corresponds to a straight line on a square-root-of-time graph. This correlation assumes that for as long as the fracture remains open, the pressure decline after shut-in represents the linear flow regime caused by treatment fluid leaking into the formation. Therefore, a plot of the falloff pressure versus the square-root-of-time should yield a straight line.

Figure 5-2, which again displays the data from the test at 9,630 to 9,631 ft, exhibits the behavior described above. When the fracture closed, the graph of pressure change versus the square-root-of-time began to deviate from a straight line. The point at which the falloff pressure first deviated from the linear-flow straight line indicates fracture closure. The fracture closure pressure, also called the in-situ stress, should be repeatable using multiple tests in the same interval as long as back stress is negligible. Indeed, this was the case for each of the six cased-hole stress tests.

5.2 VERTICAL STRESS PROFILING THROUGH THE INTEGRATION OF LOG-DERIVED ROCK MECHANICAL PROPERTIES AND IN-SITU STRESS TESTS

5.2.1 Introduction

The performance of a well with a hydraulic fracture is controlled by the nature of the reservoir, the fracture and the well. To enhance the reservoir's productivity, the engineer must optimize the design and execution of well completions and fracture

treatments. This optimization depends in part on the ability to accurately predict the effects of various treatment and completion scenarios.

All predictions, especially those generated with simulators, require information about the reservoir. Most tight gas formations consist of several different layers of rock, each of which vary in composition, porosity, water saturation, permeability and areal extent, among other things. The vertical distribution of permeability has a particularly significant effect on the computation of flow rate versus time.

The hydraulic fracture that connects the rock layers to the wellbore must be characterized as well. To determine the three-dimensional shape of a hydraulic fracture, detailed information is needed concerning the mechanical properties of all layers that will be connected by the fracture. Values of Young's modulus, Poisson's ratio, fracture toughness and in-situ stress are required as input data for a hydraulic fracture simulator. Of primary importance to the calculation of fracture shape and extent is the in-situ stress profile.

For most well completions, the operator perforates based upon the porosity and water saturation calculated by a petrophysical engineer. Afterwards, the production engineer designs a fracture treatment for the interval perforated. However, research from the Tight Gas Sands Program, particularly the SFE wells, indicates that perforation placement should be based upon more than just the porosity and water saturation calculations; one should also consider the in-situ stress profile.

Besides the petrophysical information, the completion engineer also must consider the porosity-thickness (ϕh) profile, the permeability-thickness (kh) profile, and the in-situ stress profile. By using these profiles in

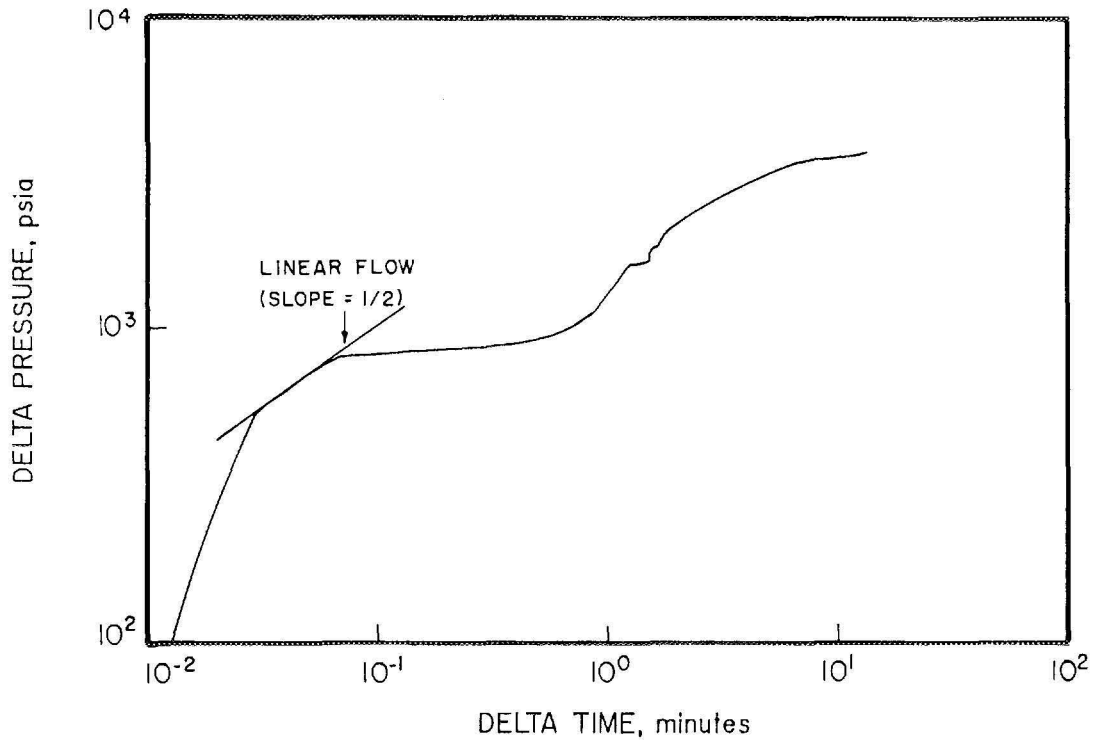


Figure 5-1 Log-Log Plot of Cased-Hole Stress Test No. 1

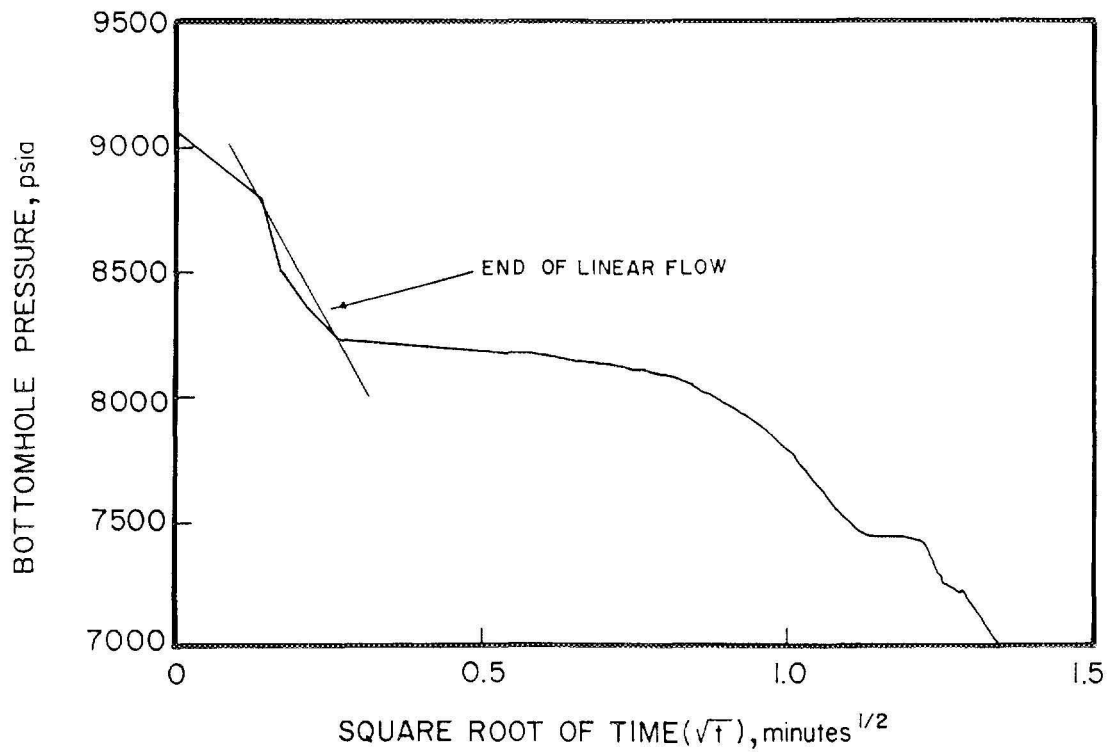


Figure 5-2 Linear Flow Analysis of Cased-Hole Stress Test No. 1

conjunction with 3-D hydraulic fracture models and 3-D reservoir flow models, one can choose the optimum perforation interval and fracture treatment. The data in the ϕh and kh profiles indicate conductive portions of the pay zone that, when connected to the wellbore, will provide adequate flow rates and ultimate recoveries. The in-situ stress profile can be used to determine which of those zones is most likely to have a contained fracture treatment, i.e., which one is most likely to have a good connection.

There are two methods for obtaining values of in-situ stress in a specific rock layer. One method, described in Section 5.1, is to perform an in-situ stress test which measures stress directly. The second method is to calculate values of Poisson's ratio with acoustic log data. Using Poisson's ratio along with an estimate of the overburden stress and the reservoir pressure, the in-situ stress can be calculated based upon the properties of a poroelastic material. This technique is described in Section 4.1.2.

There is potential error associated with calculating in-situ stress from log data (using poroelastic equations) because only the elastic component of stress can be estimated. Other factors such as tectonic stresses, thermal history of a formation, and subsidence history of a basin cannot be included in this analysis. The theory only relates the horizontal stress component to the vertical component through Poisson's ratio; other effects are neglected.

Because of cost and operational considerations, stress profiles are not normally generated from in-situ tests alone, but rather from a combination of the two methods. By performing a discrete number of stress tests in specific types of lithology, log-derived stress values can be correlated with measured values to give a reliable estimate of stress in each layer. The resulting stress profile can then be empirically calibrated to

account for the forces not attributable to elastic behavior.

5.2.2 Review of SFE No. 1 and SFE No. 2 Results

GRI and the Tight Gas Sands contractors have made substantial progress in both developing and applying the concepts of permeability (kh) and stress (σ_c) profiling to decisions concerning well completion and stimulation. In 1986, when SFE No. 1 was completed, the technology for developing these profiles on a routine basis was in its formative stages. During SFE No. 2 (1987 to 1988), this technology progressed rapidly. For all subsequent wells evaluated in the Tight Gas Sands Program, the use of kh profiles and stress profiles has been and will be standard operating procedure, as well as a continuing part of the research effort.

SFE No. 1 marked the development of the first detailed, in-situ stress profile of the Tight Gas Sands Program. The profile was generated by correlating in-situ stress test measurements with values of Poisson's ratio computed from digital sonic logs. The following equations were derived to create the stress profile:

$$\sigma_c = (1 - P'_g) \left[\frac{v}{1 - v} \right] + P'_g \quad \text{Eq. 5-1}$$

and

$$P'_g = 1.15 (2.8 P^2 + 1)^{1/2} - 1 \quad \text{Eq. 5-2}$$

where

- P_g = formation pressure gradient, psi/ft
- P'_g = effective formation pressure gradient, psi/ft
- σ_c = in-situ stress gradient, psi/ft
- v = Poisson's ratio

The in-situ stress profile computed from Equations 5-1 and 5-2 was presented in a

report detailing the results of SFE No. 1 (CER Corporation and S.A. Holditch & Associates, Inc., 1988). Although the profile did not play a major role in the making of decisions about how SFE No. 1 should be perforated and treated, it was used after-the-fact to evaluate the hydraulic fracture treatment.

For SFE No. 2, a different equation was used to correlate measured closure stress values from in-situ stress tests:

$$S_h = \left[\frac{\nu}{1 - \nu} \right] (S_v - S_p) + S_p \quad \text{Eq. 5-3}$$

where

S_h = minimum horizontal stress gradient, psi/ft

S_v = vertical (overburden) stress gradient, psi/ft

S_p = stress gradient produced by pore pressure, psi/ft (see Equation 4-17)

ν = Poisson's ratio

This equation was discussed in greater detail in Section 4.1.2.2 where it was referred to as Equation 4-10.

Figure 5-3 shows the relationship of Poisson's ratio function and measured closure stress in SFE No. 2 (CER Corporation and S.A. Holditch & Associates, Inc., 1989). These data suggest that the difference between measured closure stress and the value of $\nu/(1-\nu)$ as calculated from logs can be explained by the variation in pore pressure between different layers of reservoir rock.

Several important technological advances were made during the SFE No. 2 project. For the first time, both a detailed kh profile

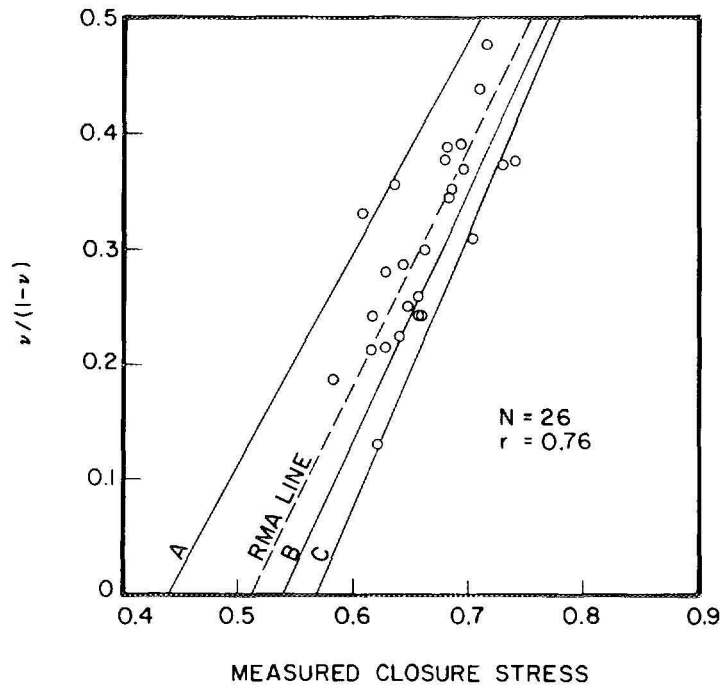


Figure 5-3 Measured Closure Stress Versus Poisson's Ratio Function for SFE No. 2

and a detailed stress profile were computed on a foot-by-foot basis using calibrated log data. These profiles were presented in a report giving the results of SFE No. 2 (GER Corporation and S.A. Holditch & Associates, 1989). Although they were used extensively in the post-fracture analysis of the lower Travis Peak, they were not used to plan the completion of the lower zone.

It is in the upper Travis Peak of SFE No. 2 that, for the first time in the Tight Gas Sands Program, the in-situ stress and kh profiles played a significant role in determining the best strategy for completing and stimulating a well. Also, after the well was hydraulically fractured, the stress profile was again used to analyze the treatment data.

5.2.3 Permeability and Stress Profiles for SFE No. 3

5.2.3.1 Calibration With Open-Hole Stress Tests

After SFE No. 3 was logged and open-hole stress tests were conducted, ResTech generated a preliminary in-situ stress profile using sonic log and open-hole stress data. Figure 5-4 illustrates the preliminary profile for the lower 1,000 ft in SFE No. 3.

Although this profile represents the best estimate of stress using the open-hole test data for calibration, it was not used in the design or analyses of the fracture treatment for SFE No. 3. Later comparison with the cased-hole data indicated that these open-hole data are not an accurate reflection of in-situ conditions.

The open-hole stress test data suggest that in SFE No. 3, very little difference in horizontal stress exists as a function of

lithology. As seen in Table 5-1, the average in-situ stress gradient was 0.64 psi/ft in the sandstone, 0.70 psi/ft in the limestone and 0.67 psi/ft in the shale. In contrast, the cased-hole data, listed in Table 5-2, revealed substantial differences in the measured stress in each rock layer. The open-hole data were deemed invalid because the fracture created during the test grew around the open-hole packer and actually broke down lower stress zones near the zone being tested.

5.2.3.2 Calibration With Cased-Hole Stress Tests

After casing was set in SFE No. 3, six cased-hole in-situ stress tests were conducted to improve estimates of stress in the Bossier shale (between 9,500 and 9,650 ft) and the Cotton Valley Taylor zone (between 9,200 and 9,450 ft). Within the Cotton Valley Taylor zone, stress tests were performed in the upper part of the sand, a shaly member below the upper sand and the lower part of the Taylor sandstone. Results for the cased-hole stress tests are presented in Table 5-2.

Once the cased-hole test data were analyzed, it was apparent that the original log-derived values of stress, the open-hole test values and cased-hole test values did not correlate very well. Figure 5-5 is a graph of the ratio $v/(1-v)$ vs. measured in-situ stress from the cased-hole tests. The solid line represents Equation 5-3 with $X = 0$, $S_v = 1.03$, and $S_p = 0.50$. In general, stresses are lower in the sandstones (Nos. 4 to 6) and higher in the shales (Nos. 1 to 3) than classical equations indicate.

A comparison of the initial stress profile using an elastic model and the measured stress from the cased-hole stress tests is

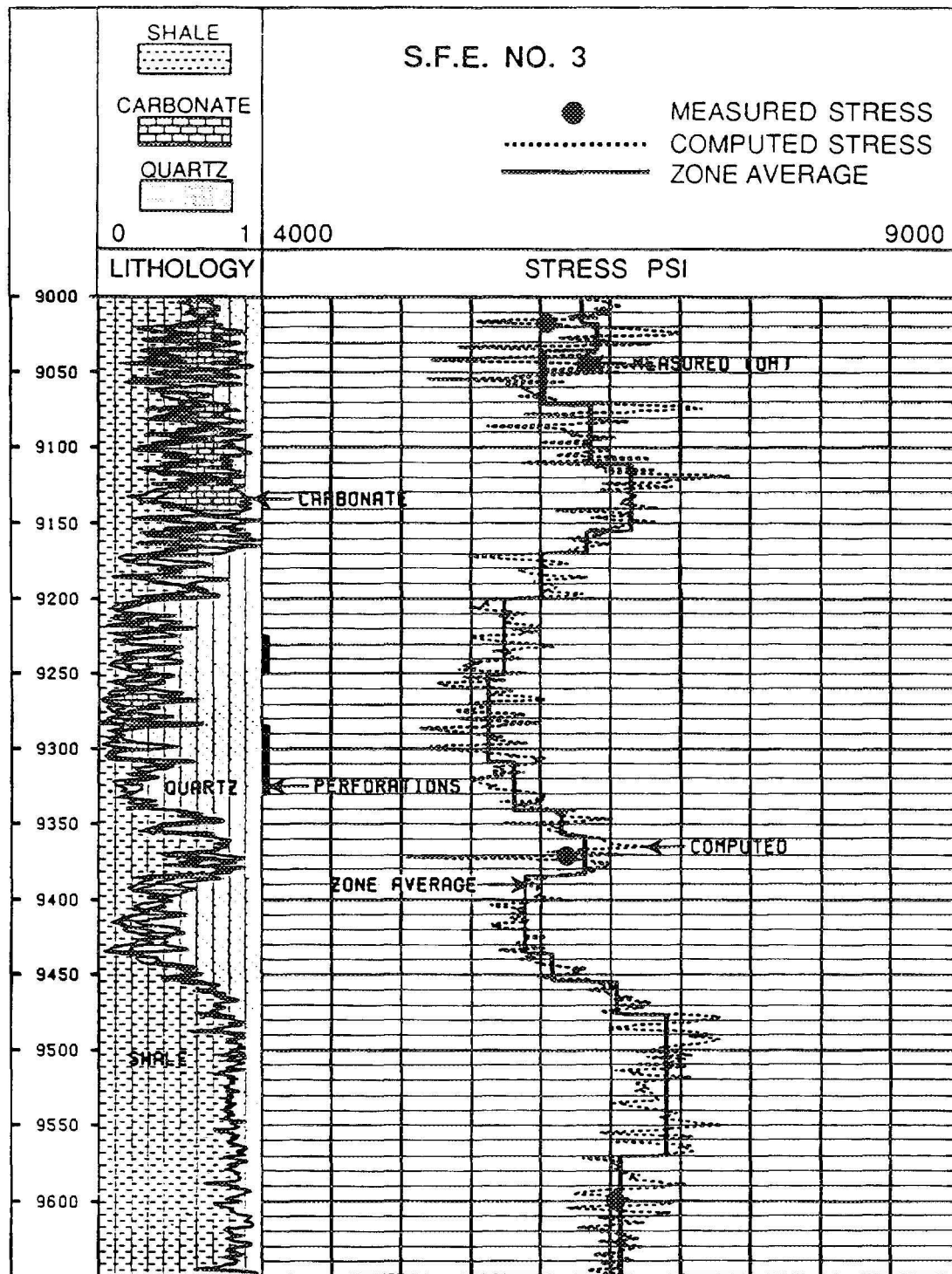


Figure 5-4 Preliminary Stress Profile Calibrated With Open-Hole Test Data From SFE No. 3

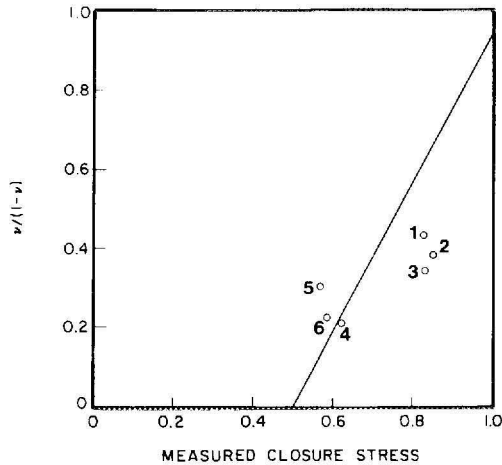


Figure 5-5 Measured Closure Stress (Cased-Hole) Versus Poisson's Ratio Function

presented in Figure 5-6. The implications are similar to those of Figure 5-5. For the sandstones which have lower stresses, the computed curve appears somewhat reasonable, albeit a little high. However, for the higher stress shales, it is significantly lower than the measured values suggesting the presence of a non-elastic component of stress.

When the cased-hole test results revealed that the open-hole data were not accurate, a new correlating parameter was developed resulting in the following equation:

$$S_h = \left[\frac{\nu}{1 - \nu} \right] (S_v - S_p) + S_p + X \quad \text{Eq. 5-4}$$

where X is an empirical stress factor. Equation 5-4 was also referred to in Section 4.1.2.2 as Equation 4-11.

The empirical factor X was obtained from a graph of delta stress vs. neutron porosity for all layers of rock where stress was measured. This factor was used to compensate for changes in stress due to changes in lithology, porosity and water saturation. It

substantially changed the log-calculated stresses and properly correlated them with the results from cased-hole tests. Figure 5-7 presents the final correlation between calculated in-situ stress using Equation 5-4 and the cased-hole stress test results. The resulting stress profile is provided in Figure 5-8. Figure 5-8 also includes kh percentages. A mechanical properties profile generated for SFE No. 3 is included in Figure 5-9.

This new, more accurate stress profile was used successfully to assist in designing the SFE No. 3 completion, in performing real-time analyses of the fracture treatment, and in performing post-fracture analyses of both the production and fracture treatment data. It is important to recognize that empirical correlation of measured stresses and log data such as that described for SFE No. 3 will be required for most situations.

5.2.4 Summary of In-Situ Stress Profiling

During the Staged Field Experiment program, the GRI research team has demonstrated that in-situ stress profiles and kh profiles can be routinely generated from properly calibrated log data. This technology provides accurate results which, among other things, can be used to design and implement a completion and stimulation strategy for a tight gas sand well.

Simple elastic theory and log data should not be used to generate stress profiles. For accurate profiles, the log data must be calibrated with pressure buildup tests and in-situ stress tests. With proper petrophysical analyses and field measurements, logs can be used to generate reliable values of kh, in-situ stress and modulus. The resulting vertical profiles are essential to successfully completing and stimulating in a tight gas sand reservoir.

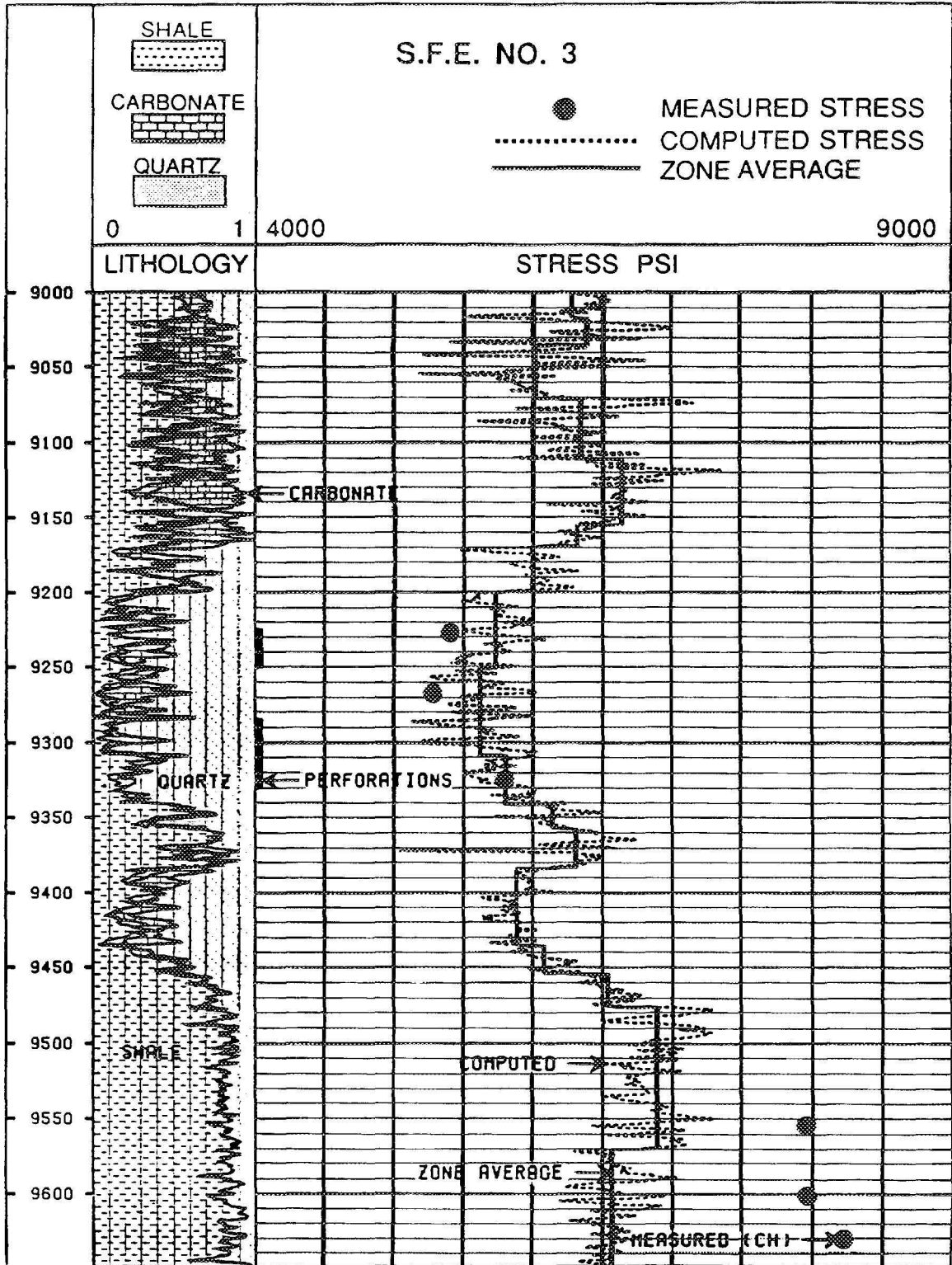


Figure 5-6 Comparison of Measured Stress With Stress Profile Generated Using Elastic Model

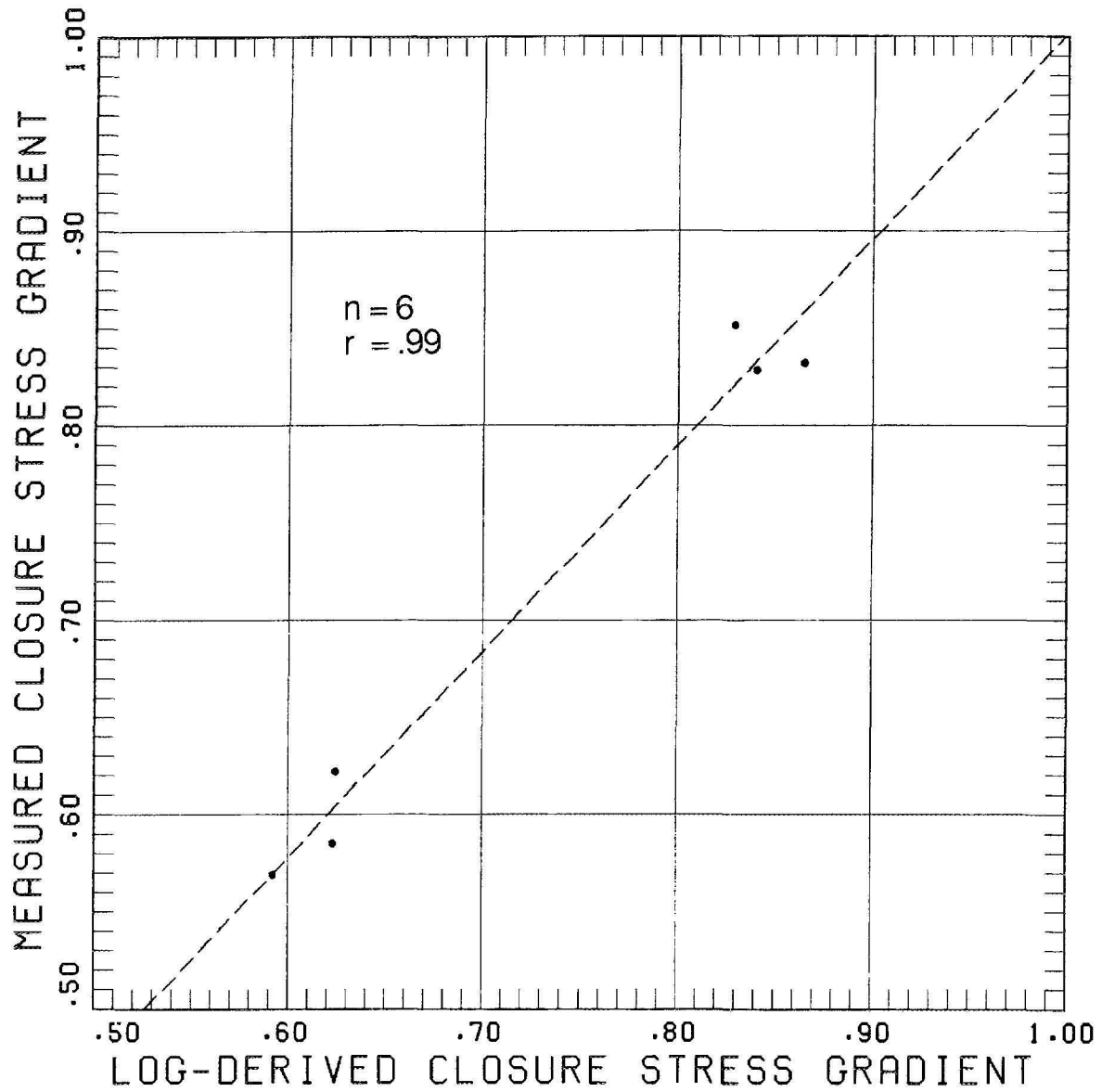


Figure 5-7 Final Correlation Between Log-Derived Closure Stress Gradient and Measured Closure Stress Gradient

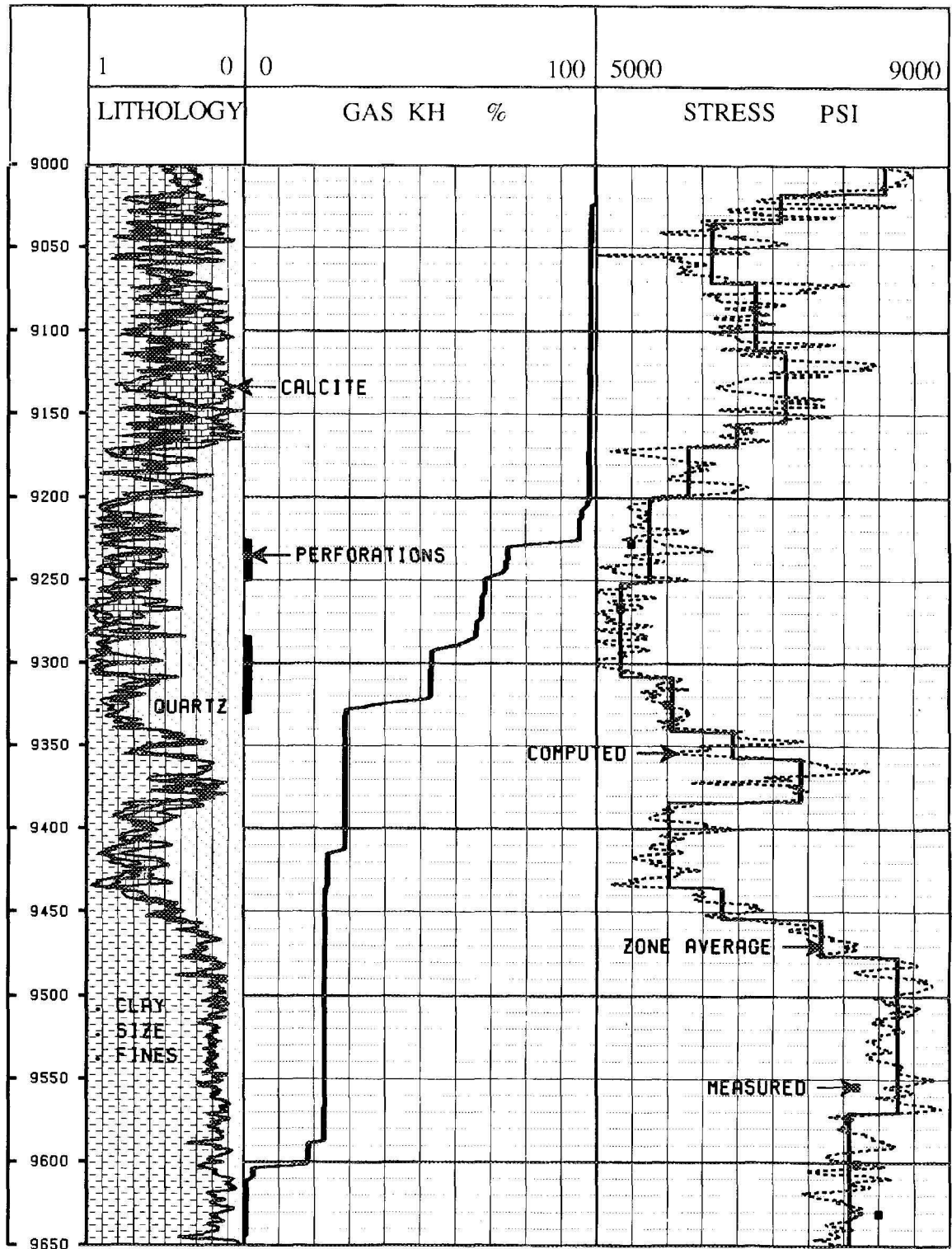


Figure 5-8 Permeability-Thickness Profile and Stress Profile of the Completion Interval in SFE No. 3

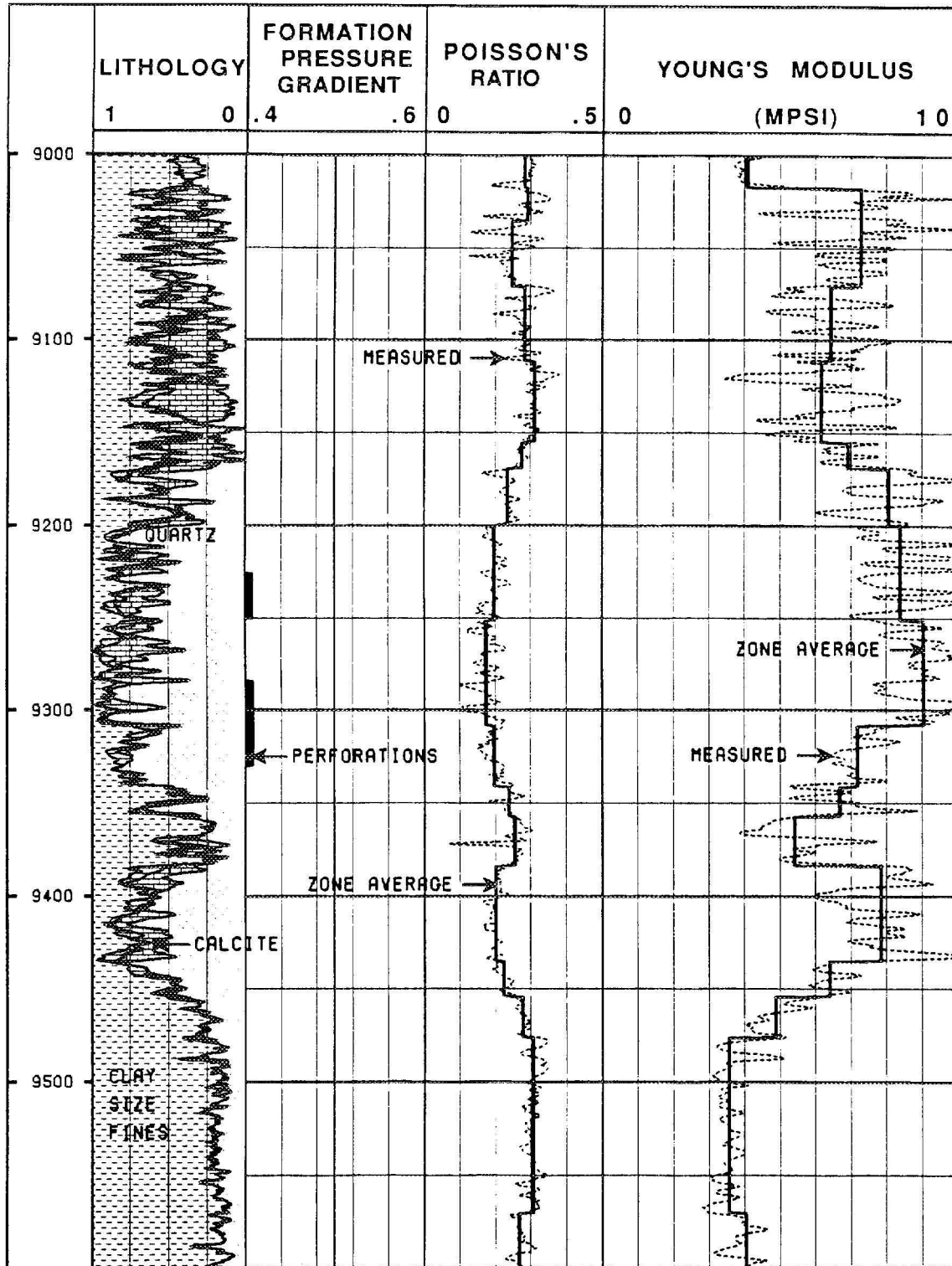


Figure 5-9 Computed Values for Poisson's Ratio and Young's Modulus for the Completion Interval in SFE No. 3

6.0 Analyses and Interpretations of Pre-Fracture Data

6.1 PRODUCTION AND PRESSURE BUILDUP TESTS

On January 24, 1989, SFE No. 3 was perforated in the Cotton Valley Taylor sand over two intervals: 9,225 to 9,250 ft and 9,285 to 9,330 ft. The well was then produced for seven days through a three-phase portable separator to obtain accurate measurements of gas, condensate and water flow rates. A 48/64-in. choke was used. Two to three swab runs were made daily to ensure that there was no liquid loading in the wellbore. The average flow rates were 50 MCFD and 8 BWPD. Although the flowing wellhead pressure was too small to measure, the flowing bottomhole pressure at the end of the flow period was measured at 507 psia.

After producing for seven days, SFE No. 3 was shut in on February 3, 1989, for a seven-day pressure buildup test. Bottomhole pressures were recorded with an electronic memory gauge run on slick line. After the shut-in period, the acquired bottomhole pressure data were analyzed to estimate formation properties.

In performing conventional analyses of pressure transient tests, bottomhole pressures and shut-in times must be adjusted to account for changing gas properties. The gas viscosity, Z-factor and gas compressibility are all pressure dependent; they change as pressure changes. Because the simplified equations used in pressure transient analyses were derived with the assumption that these values were constant (i.e., for slightly compressible liquids), the equations cannot be used to analyze gas wells. However, by using adjusted pressures and adjusted times (Lee, 1982), one can use the standard equations.

Figures 6-1 and 6-2 are the Horner and type-curve plots of the pressure buildup data. Based on the type-curve match, it appears the correct Horner semi-log straight line necessary for analysis was reached. Using ResTech's Pre-Fracture Analysis Log, a net pay of 27 ft was calculated for the perforated interval. Formation permeability to gas was 0.014 md with an apparent skin of +0.1. Extrapolation of the Horner semi-log straight line to infinite shut-in (Horner time = 1) yielded an extrapolated pressure (P^*) of 3,400 psi. Because of the limited production from the reservoir, the average reservoir pressure was assumed to be about 3,400 psi as well. The type-curve analysis confirmed the Horner analysis.

After the initial pressure buildup test, a mini-frac was performed, followed by additional cased-hole logging. The well was then produced for six days. From February 24 to March 2, 1989, flow rates were monitored prior to the start of the next pressure buildup test. The final flow rates before shut-in were 310 MCFD and 8 BWPD. Flow was through a 24/64-in. choke with a flowing wellhead pressure of 150 psig and a flowing bottomhole pressure of 727 psig. The six-day pressure buildup test that followed was of sufficient length to obtain reservoir properties from conventional Horner semi-log and type-curve analyses.

Figures 6-3 and 6-4 are the Horner plot and type-curve plot, respectively. Because of the much higher flow rates observed from this test versus the original flow test (50 MCFD), additional net gas sand appeared to be in communication with the wellbore. This is reasonable since not all of the Taylor sand was perforated initially. Most likely, the fracture created during the mini-frac opened up new pay that had not been pre-



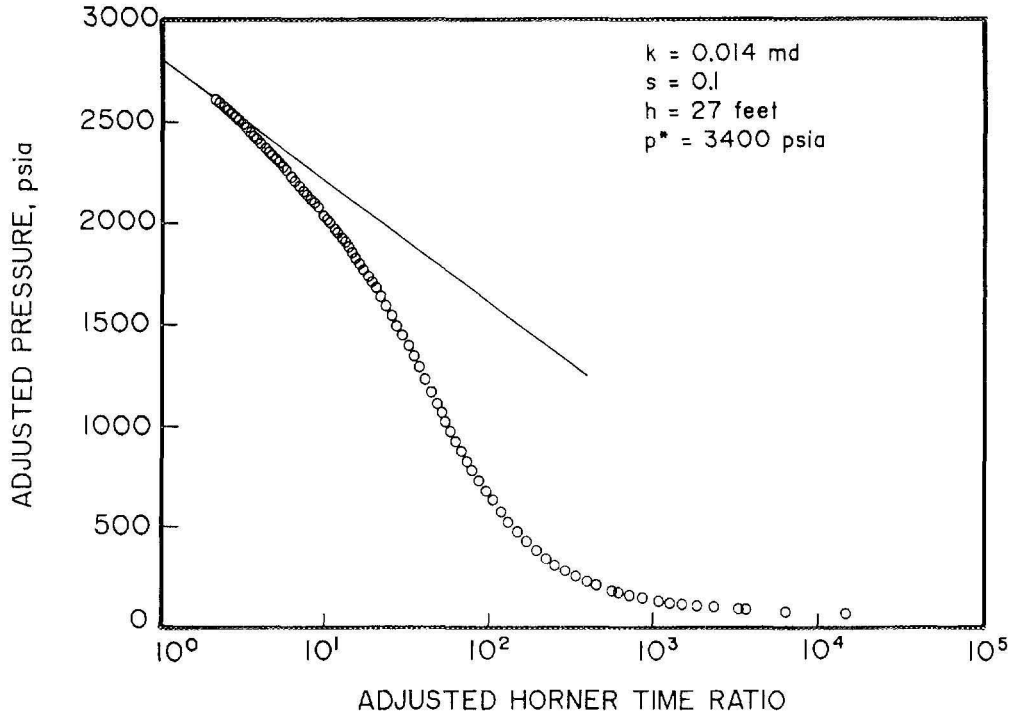


Figure 6-1 Horner Analysis of the Pressure Buildup Test Conducted Before Mini-Frac No. 1

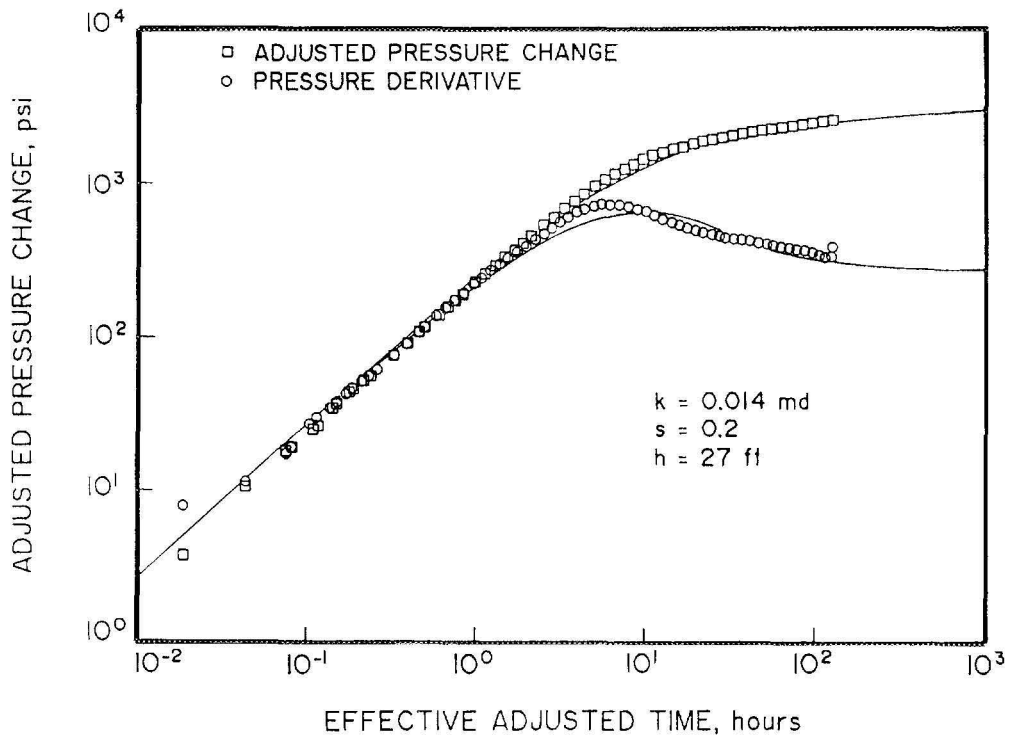


Figure 6-2 Type Curve Analysis of the Pressure Buildup Test Conducted Before Mini-Frac No. 1

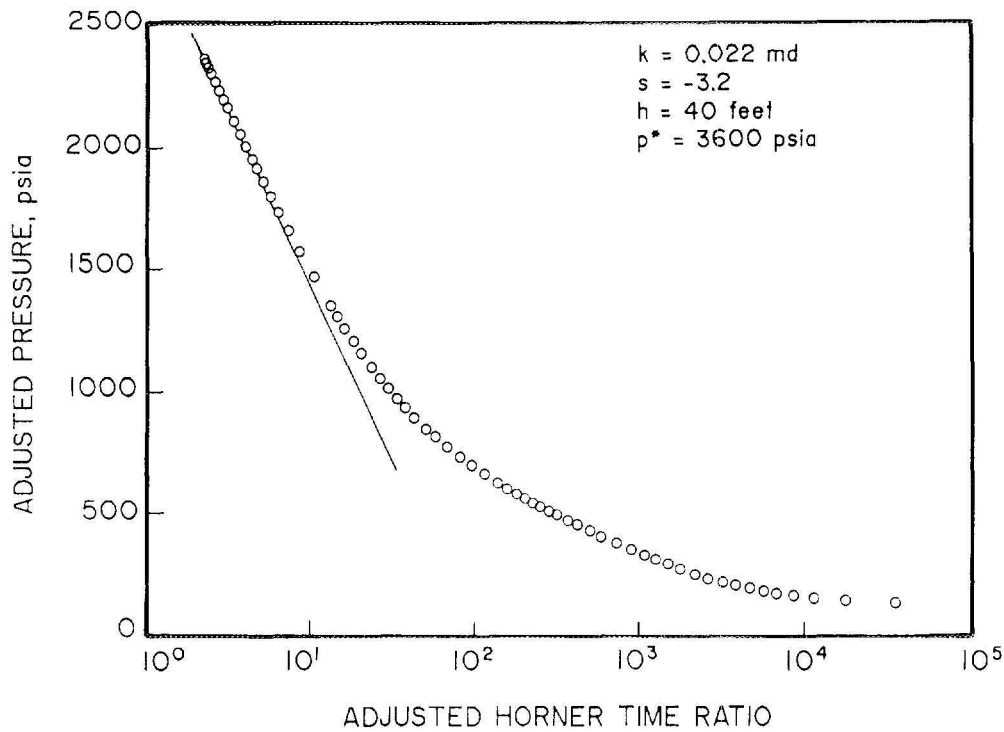


Figure 6-3 Horner Analysis of the Pressure Buildup Test Conducted After Mini-Frac No. 1

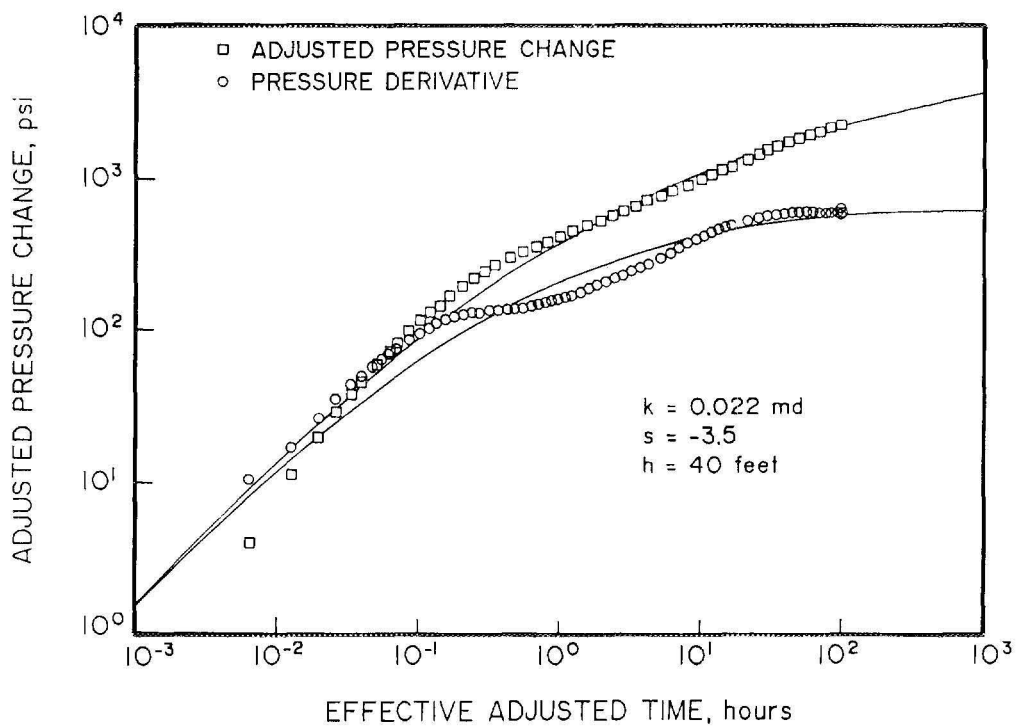


Figure 6-4 Type Curve Analysis of the Pressure Buildup Test Conducted After Mini-Frac No. 1

viously exposed. Therefore, a net gas pay of 40 ft was used in the interpretation of this buildup test.

The calculated formation permeability to gas was 0.022 md with an apparent skin of -3.2. This negative skin reflects the stimulation from the mini-frac. Extrapolation of the Horner semi-log straight line to infinite shut-in yielded a P_i (and an average reservoir pressure) of 3,600 psi. This value is 200 psi higher than that obtained from the initial buildup test, which also indicates additional communication with new net gas pay. The results of the type-curve analysis agreed well with those of the Horner analysis.

6.2 EXECUTION AND ANALYSIS OF MINI-FRAC TREATMENTS

6.2.1 Mini-Frac No. 1

6.2.1.1 Objectives and Design

As with mini-fracs in previous SFE wells, Mini-Frac No. 1 provided a setting in which to perform fracture diagnostic experiments. The ultimate goal of these experiments was to develop improved methods for determining the orientation and height of hydraulic fractures.

Teledyne Geotech was the primary diagnostics contractor for Mini-Frac No. 1, which was performed on February 17, 1989. With a three-component geophone and orientation gyroscope on a wireline, microseismic activity associated with the fracturing operation was recorded. Previous mini-fracs performed for diagnostic purposes utilized low friction, low viscosity water as the injection fluid; however, for SFE No. 3, it was decided to evaluate the effects of thicker fluids on the microseismic activity. Consequently, both linear and crosslinked gel systems were used during this treatment. Table 6-1 presents the pumping schedule.

As can be seen, the design proposed different volumes of gel in order to create a progressively larger fracture during each pump stage. Also, two different injection rates were planned so that the effects of injection rate on downhole treating pressure (as well as viscosity) could be evaluated.

After each pump stage, Teledyne Geotech planned to acquire seismic data with a triaxial geophone stationed at various points in the well. To simplify the data analysis, the mini-frac stages were designed to create fracture lengths that were not multiples of each other. Shut-in times between stages were designed to be of sufficient length to allow complete fracture closure.

After the mini-frac treatment was completed, the acoustic and radiation logging tools were run (Run No. 9) from February 17 to 24, 1989. These data acquired are described in Appendix 1.

Mini-Frac No. 1, in conjunction with Mini-Frac No. 2 and the main fracture, provided an excellent opportunity to test the basic components of the fracture model developed by Resources Engineering Systems (RES) for GRI. By going from the highly complex conditions of the Travis Peak Formation (SFE Nos. 1 and 2) to the relatively simple environment of the Cotton Valley Formation (SFE No. 3), researchers hoped to isolate the basic differences between the FRACPRO system and other models in the industry. In addition, they hoped to establish FRACPRO's ability to make accurate and unique predictions (e.g., for fracture dimension and associated pressures) by collecting data from various tests (e.g., with different fluids, volumes and pump rates).

6.2.1.2 Treatment Monitoring and Quality Control

During Mini-Frac No. 1, the GRI Treatment Analysis Unit (TAU) operated by RES was

Table 6-1 Mini-Frac No. 1 Pumping Schedule

Stage	Gel Type	Fluid Volume, bbl		Injection Rate, bbl/min	
		Design	Actual	Design	Actual
1	40-lbm linear	150	128	20	19.0
2	40-lbm linear	300	298	40	38.4
3	S.D., monitor falloff, run surveys				
4	40-lbm linear	600	547	40	41.3
5	40-lbm linear	300	349	20	22.8
6	S.D., monitor falloff, run surveys				
7	40-lbm x-link	450	308	20	18.9
8	slickwater	342	312	40	35.6
9	S.D., monitor falloff, run surveys				

Total 40-lbm gel: design = 1,800 bbl and actual = 1,630 bbl

on location to monitor the following parameters: casing pressure, bottomhole pressure, base gel viscosity, fluid temperature and pH, pump rate and cross-linker injection rate. These parameters were recorded by instruments placed at various points within the fracturing equipment.

To monitor more specific fluid properties, S.A. Holditch & Associates, Inc. (SAH) used the GRI Rheology Van. A complete water analysis was performed, including tests for total chlorides, iron content, bacteria cultures, pH, phosphates and temperature. Once all of the gel was mixed in each tank, the base gel viscosity at three different

shear rates was measured using a Fann 35 viscometer. The fluid that was to be cross-linked was tested in the Rheology Van for crosslinked viscosity using the Fann Model 50 viscometers. These viscometers can subject the fluid to downhole temperature and shear rate. All of the fluids planned for use during the mini-frac tested satisfactorily.

Because the treatment was pumped down casing to allow for the seismic traverses by Teledyne Geotech, a pressure gauge with surface readout could not be run into the well. As a result, a battery-powered electronic pressure gauge with downhole memory was used to record bottomhole treating

pressures. This gauge was retrieved after the treatment and subsequent analysis of the pressures was performed. These bottomhole pressures are illustrated in Figure 6-5 which also denotes, by number, the major events during the treatment. These events are explained in Table 6-2. Figure 6-6 presents all of the data streams measured.

6.2.2 Mini-Frac No. 2

6.2.2.1 Objectives and Design

The objective of the second mini-frac treatment was to gather additional data to calibrate the 3-D fracture models and to estimate values of fluid loss coefficient. As a result, some of the analysis of Mini-Frac No. 2 is coupled with the main-frac analysis in Section 7.0.

Mini-Frac No. 2 was pumped just prior to the actual fracture treatment on March 16, 1989. The fluid consisted of a linear (non-crosslinked) 40 lbm CMHPG (carboxymethyl-hydroxypropyl guar). A total of 1,281 bbl of gel were pumped down the casing-tubing annulus and flushed to the perforations with 290 bbl of slick water (total volume = 1,571 bbl). The tubing provided a "dead string" pressure measurement.

The leakoff coefficient expected during the main frac treatment was estimated by allowing the pressure to fall off. Additionally, the pressures measured during the mini-frac were used to calibrate the 3-D fracture model since the fluid properties were relatively constant.

6.2.2.2 Treatment Monitoring and Quality Control

During the mini-frac treatment, the GRI Rheology Van and the Treatment Analysis Unit (TAU) were on location to monitor various treating properties. The Rheology Van

was operated by SAH. The TAU, with its fracture monitoring trailer, was operated by RES personnel.

In addition to measurement of fluid properties, SAH personnel were responsible for conducting a total inventory of all materials and fluids both before and after the treatment. An analysis of each water tank was performed which included total chlorides, iron content, bacteria cultures, pH, phosphates and temperature. Once the base gel for the mini-frac was totally mixed, the base gel viscosity was measured for each tank to insure proper gel loading. A Fann 35 viscometer was used to take the measurements at four different shear rates. These data for the base gel used during Mini-Frac No. 2 are given in Table 6-3.

After the base gel viscosity measurements, the actual viscosities of the linear gel at downhole temperature were measured for each tank using Fann model 50 viscometers. These tests helped to ensure the proper mixing of the gel and provide viscosity data for input into the FRACPRO model.

RES monitored and recorded all other pertinent treating variables with the TAU. Following is a list of all the data monitored for Mini-Frac No. 2 (as well as the main frac): casing, tubing and bottomhole pressures; fluid and bottomhole temperatures; base gel viscosity; proppant concentration; slurry pH and clean pH; and slurry, LGC, diesel and cross linker flow rates. Further details including tables and figures are provided in Section 7.2.2.

The mini-frac treatment was pumped as designed with few problems. However, the Panex pressure gauge did start malfunctioning during the treatment, as shown in Figure 6-7. The apparent dead string specific gravity by comparison to bottomhole pressures was 0.949. This low value was the

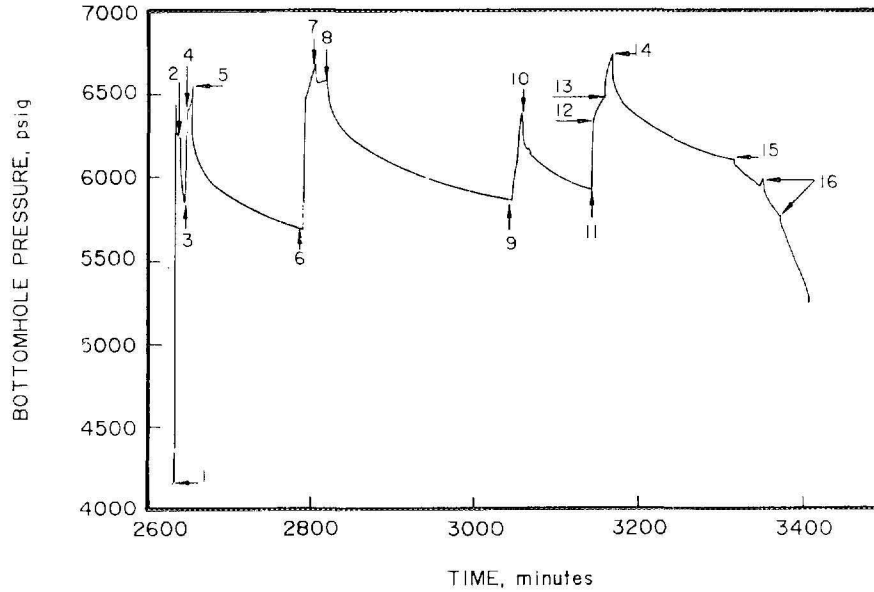


Figure 6-5 Bottomhole Pressure History During Mini-Frac No. 1

Table 6-2 Major Events During Mini-Frac No. 1, SFE No. 3

Number	Event
1	Start pumping 40-lbm gel
2	S.D. to fix leak
3	Resume pumping at 20 bbl/min
4	Increase rate to 40 bbl/min
5	S.D. for falloff
6	Start pumping gel at 40 bbl/min
7	Decrease rate to 20 bbl/min
8	S.D. for falloff
9	Start pumping x-link gel
10	S.D. -- lost prime
11	Resume pumping
12	X-link gel on perms
13	Increase injection rate to 40 bbl/min
14	Finished treatment -- S.D.
15	Open well for flowback
16	Change choke

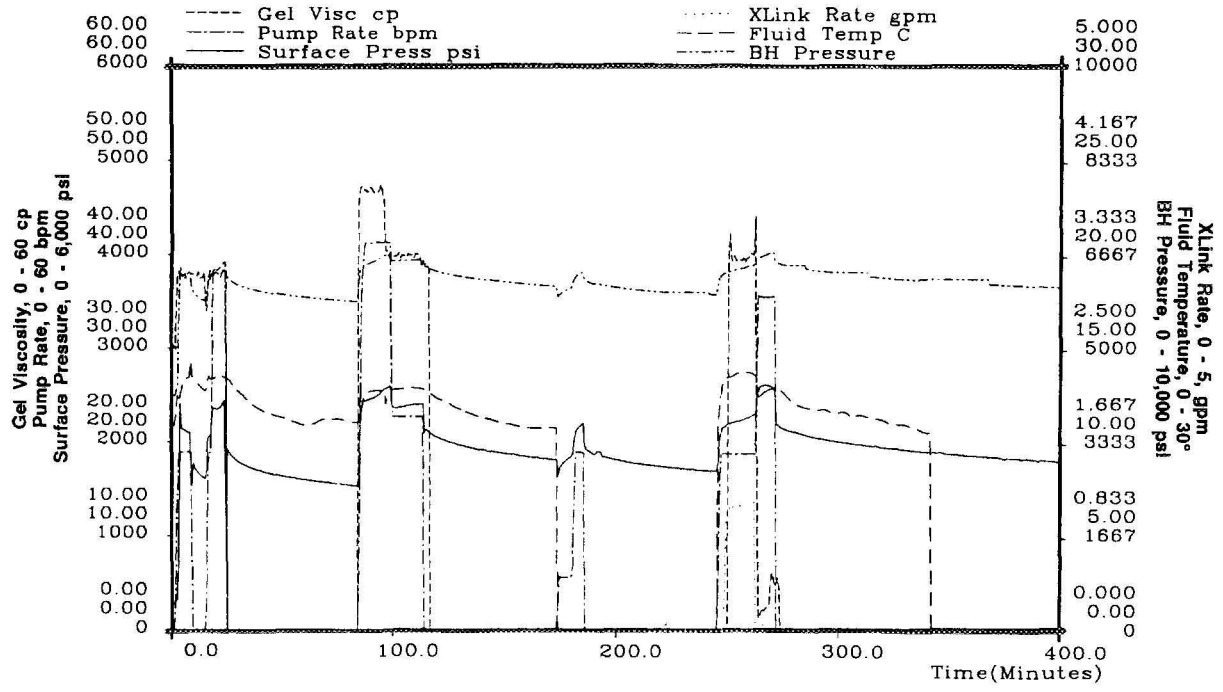


Figure 6-6 Treatment Data History During Mini-Frac No. 1

Table 6-3 Base Gel Viscosity at Different Shear Rates for Mini-Frac No. 2, SFE No. 3

Tank No.	Fluid Type	Viscosity at Various Shear Rates, cp			
		100 rpm	200 rpm	300 rpm	600 rpm
2	40 lbm	22.0	30.0	37.0	50.0
3	40 lbm	24.0	32.0	32.0	50.0
4	40 lbm	21.0	30.0	35.0	50.0

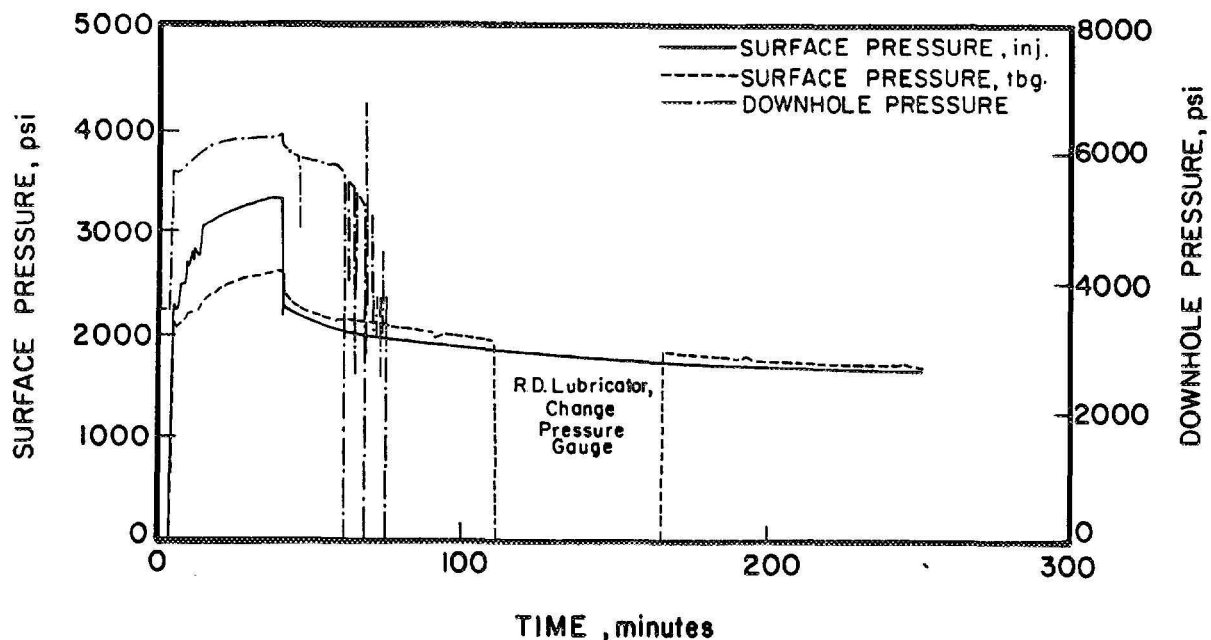


Figure 6-7 Pressures Measured During Mini-Frac No. 2, SFE No. 3

result of either a malfunctioning bottomhole gauge or the presence of gas in the dead string. Since the Panex bottomhole pressure gauge was transmitting data intermittently, it was replaced after Mini-Frac No. 2 and the tubing was circulated. No problems were experienced during the main fracture treatment.

6.2.3 Microseismic Analysis of Mini-Frac No. 1: Azimuth and Height

Teledyne Geotech's research in the Tight Gas Sands Program has focused on identifying, developing and evaluating commercially feasible methods for reliable estimation of the dimensions and orientation of hydraulic fractures in tight natural gas reservoirs. Passive microseismic signals are the source of the information on the fracture geometry.

One objective of Mini-Frac No. 1 was to provide the opportunity for collecting an additional data suite of passive microseismic

information to be used for estimating fracture azimuth and height. In addition to the Mini-Frac No. 1 data set, microseismic data had been previously acquired following the injection/ballout treatment and prior to any perforations being placed in the casing. This entire data set provided the basis for fracture azimuth and fracture height analyses before conducting the main hydraulic fracture treatment. The results and analyses of these fracture orientation and fracture height surveys are included in the following sections.

6.2.3.1 Fracture Orientation Results and Analyses

CMR During Mini-Frac No. 1 Shut-In Stages

In implementing Mini-Frac No. 1, three sets of pumping stages were performed (see Table 6-1) to provide variable data for deter-

mining fracture height and length dimensions. Prior to pumping, a three-component seismic sonde and an orientation gyroscope were lowered to the maximum depth possible in the wellbore and clamped in place during the pumping. Prior to initiating the mini-frac, vertical traverses of the borehole were made with the oriented geophone. Continuous microseismic radiation (CMR) activity in the well was recorded for 4 to 8 minutes at each of 12 depths during shut-in Stages 3 and 9 and at each of 22 depths during shut-in Stage 6. Many low-frequency signals, with dominant frequencies of 10-20 Hz, were observed at 9,000 ft and 9,100 ft during Stages 3 and 9. For these depths above the fracture, this type of event began to occur approximately one hour into Stage 3 and about one hour and four minutes into Stage 9. The mean occurrence rate of these low-frequency signals recorded at the two depths above the fracture was one per minute. In addition, one low-frequency signal was observed at 9,590 ft during Stage 6. A large number of similar signals occurred during the flowback after the treatment was completed. Examples of these signals are shown in Figure 6-8. Orientations of the particle motion of these signals were determined by application of the SMART processor to the first half-cycle of each signal. The SMART algorithm yields a best linear fit, in a least-squares sense, of the observed particle motion over a specified time window and frequency band.

For best results, the SMART processor is applied to the first half-cycle of a signal, and the frequency band accepted is centered on the dominant frequency of the signal. The low-frequency signals were recorded at 9,000 ft, 9,100 ft and 9,590 ft during shut-in stages of Mini-Frac No. 1. Resulting particle motion orientations, after rotating the observational axes to a north-east coordinate system, are shown in Figure 6-9.

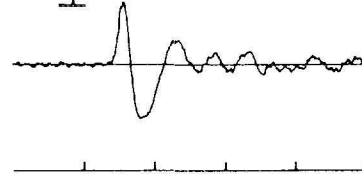
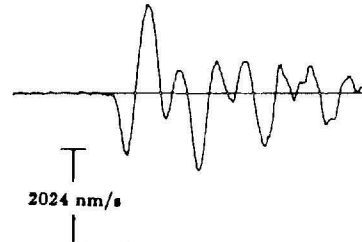
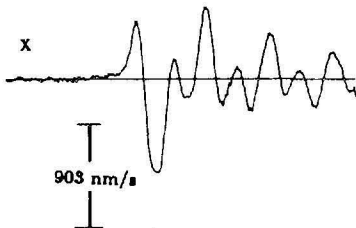
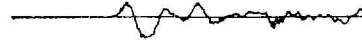
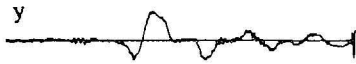
Particle motion orientations for three of the signal sets -- those recorded at 9,100 ft during Stage 3, at 9,000 ft during Stage 9, and at 9,590 ft during Stage 6 -- are consistent with a fracture orientation azimuth of 77° relative to North. Particle motions for signals recorded at 9,100 ft during Stage 9 are oriented perpendicular to this direction, while signals recorded at 9,000 ft during Stage 3 are oriented 30° from the perpendicular direction. The differences in particle motion orientation observed for the five sets of low-frequency signals are not understood at this time.

Low Frequency Signals During Flowback

After all the pumping had been completed, the well was flowed back to provide seismic signals during fracture closure. This was the first time that passive microseismic data had been recorded during a flowback following a hydraulic fracture. While performing this flowback survey, a new class of low-frequency microseismic signals was observed. This class of signals was not observed in either of the two previous SFE wells and were infrequently observed during the 18 commercial and cooperative surveys performed over the last 4 years. The number of events of a given amplitude can be estimated from the statistical distribution of amplitudes. The frequency content of these signals is between 5 and 50 Hz. The polarization of the initial part of these signals is oriented along the fracture. Additional research is expected to yield estimates of the fracture geometry and dimensions that can be provided at a reduced cost over the present microseismic fracture diagnostic surveys. The dimensions implied by these low-frequency signals are on the order of hundreds of feet rather than the tens of feet implied from the more common high-frequency signals.

D 0:0:0.00
SFE351-9000-43.DAT
CTS/IN: 0.339E+04
SEC/IN: 0.100

D 0:0:0.00
SFE351-9100-28.DAT
CTS/IN: 0.760E+04
SEC/IN: 0.100



D 0:0:0.00
SFE353-9000-01.FLD
CTS/IN: 0.111E+04
SEC/IN: 0.100

80 HZ LD PASS

D 0:0:0.00
SFE353-9100-09.FLD
CTS/IN: 0.409E+04
SEC/IN: 0.100

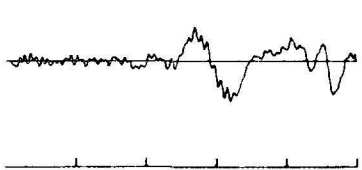
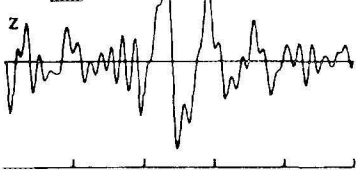
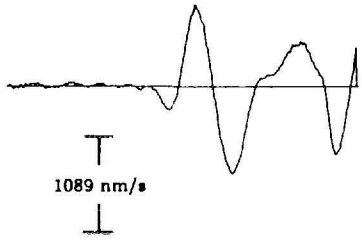
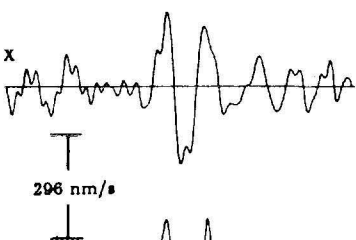
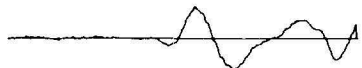


Figure 6-8 Low-Frequency Signals Recorded at 9,000 ft and 9,100 ft During Shut-In Stages of Mini-Frac No. 1

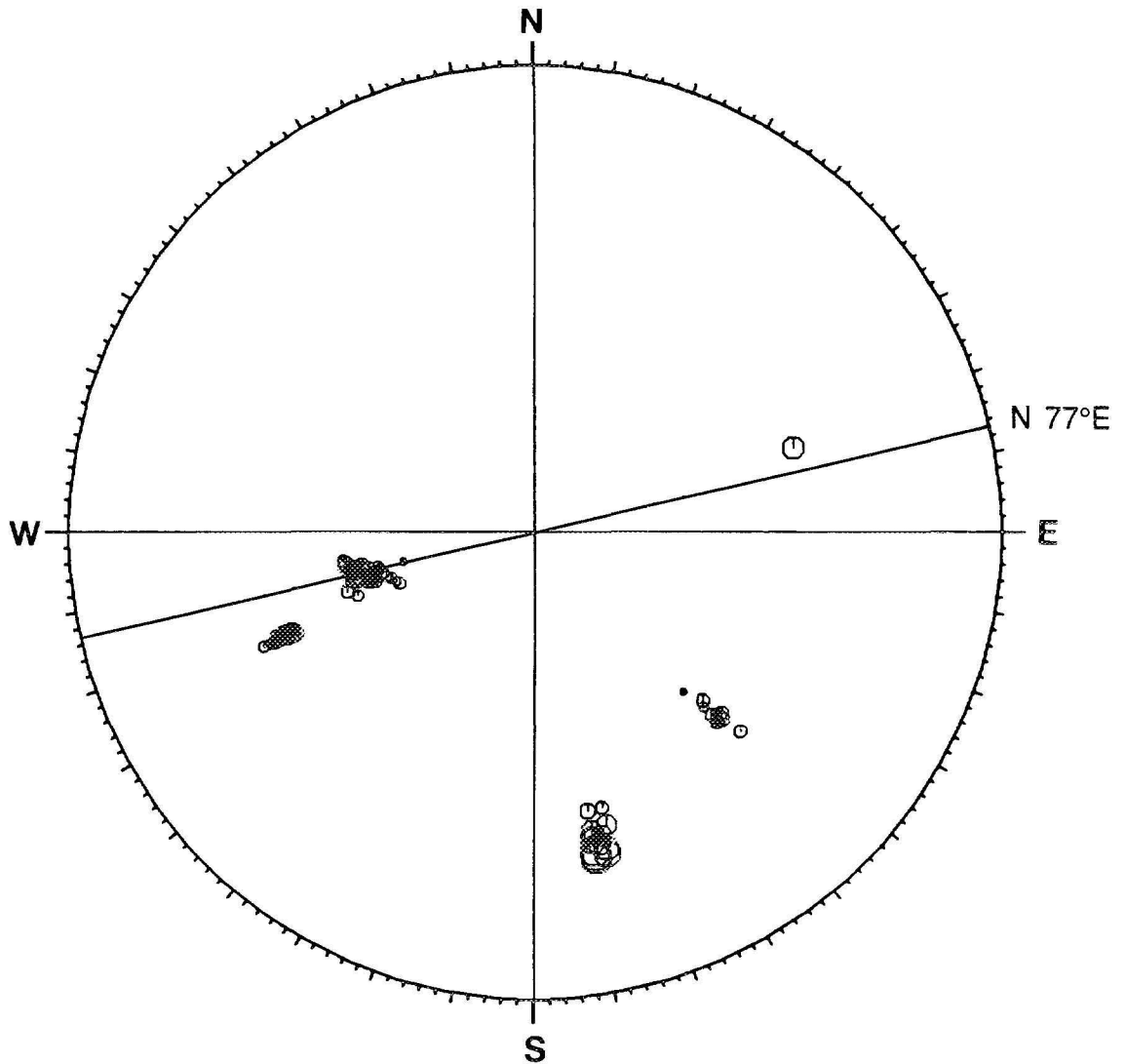


Figure 6-9 Upper Hemisphere Stereographic Projection of Particle Motion Orientations for Low-Frequency Signals Recorded at 9,000 ft, 9100 ft and 9,590 ft During Shut-In

The SFE No. 3 well was flowed back at rates of 1 to 5 bbl/min for approximately 90 minutes, beginning approximately 2-1/2 hours after starting Stage 9. The flowback was stopped for 4 minutes, approximately 30 minutes after start of the flowback. Teledyne Geotech recorded 40 minutes of

three-component seismic data at a depth of 9,590 ft during the flowback. Although the background noise (CMR) was much stronger during the flowback, because of fluid noise resulting from the flowback, many low-frequency signals, with dominant frequencies of 17 to 25 Hz, were recorded during the

flowback. The time-domain signatures of these signals were very similar for all the signals and quite different from the signatures of high-frequency signals typically recorded during shut-in following hydraulic fracture operations.

One of the low-frequency signals recorded at 9,590 ft during flowback following Stage 9 is compared in Figure 6-10 to a typical high-frequency signal recorded at the same depth during shut-in of the mini-frac. The signal-to-noise ratio (S/N) of the low-frequency signals was much higher during the interval when the flowback was temporarily halted. The low-frequency signals tended to occur in swarms. Four of the low-frequency flowback signals are shown in Figure 6-11. Separate distributions are given for non-swarm and swarm events. The two

signals depicted in the top row on this figure were recorded during the interval when the flowback was temporarily halted, while the two signals in the bottom row were recorded while the flowback was in progress.

Amplitude and interval distributions of the low-frequency signals recorded at 9,590 ft during flowback are shown in Figure 6-12, for swarm events and non-swarm events. Included for comparison is one low-frequency signal from 9,550 ft measured during Stage 6. The amplitudes are root-mean-square (RMS) signal amplitudes over a 0.1-second time window, while the intervals are the time intervals between successive events. Both incremental and cumulative distributions are shown for the amplitudes and intervals. The incremental distributions represent the number of occurrences (amplitude or interval) within a specified range,

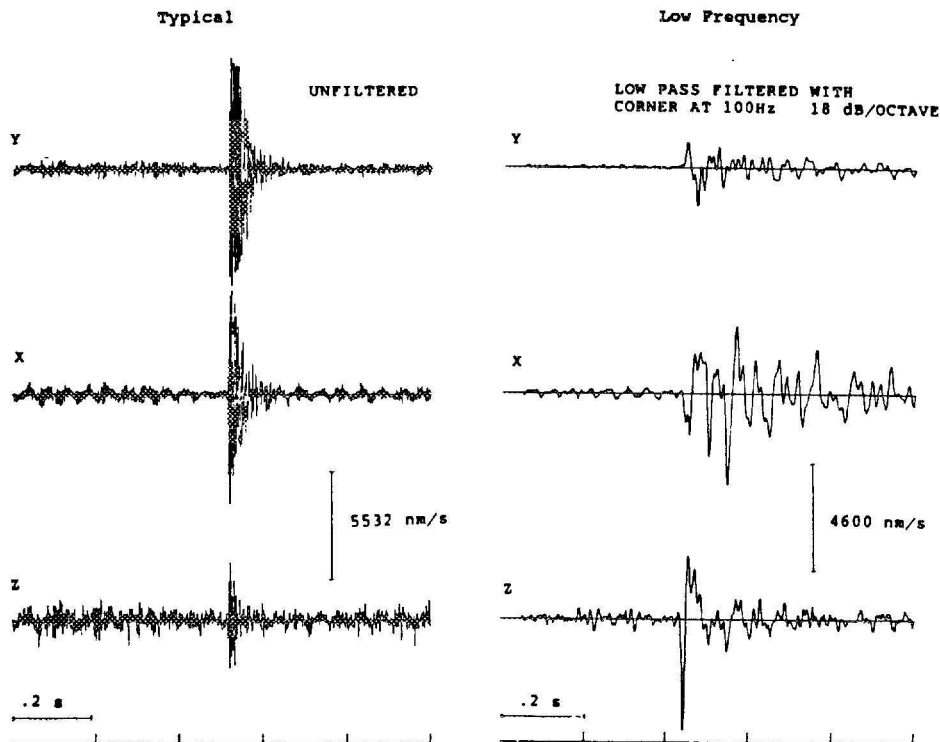
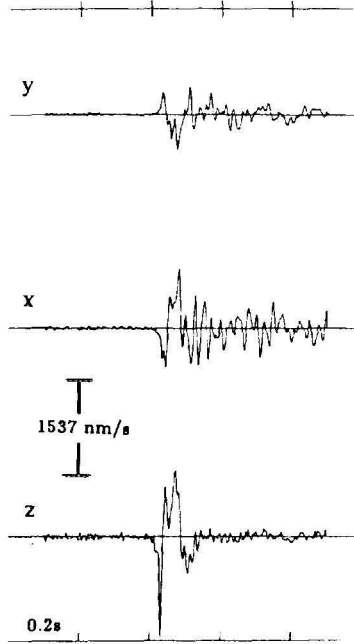
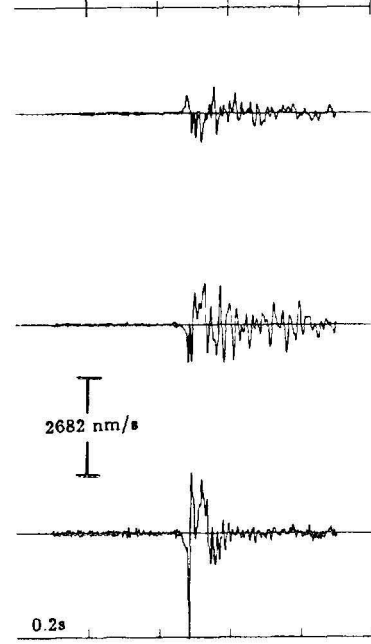


Figure 6-10 Comparison of Low-Frequency Signals Recorded at 9,590 ft During Flowback to Typical High-Frequency Signals Recorded at 9,590 ft During Shut-In

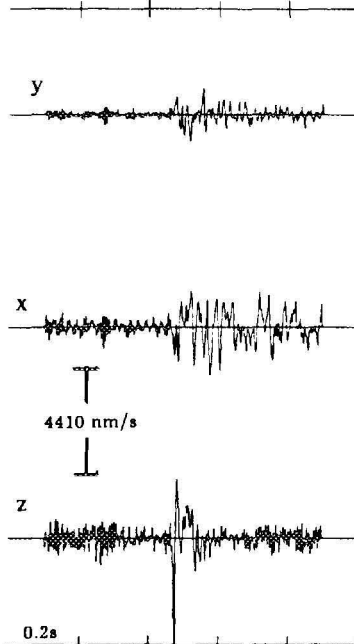
0 0:0:0.00
SFE3S3-FLBK4-25-LPNTCH.DAT
CTS/IN: 0.145E+04
SEC/IN: 0.200



0 0:0:0.00
SFE3S3-FLBK4-26-LPNTCH.DAT
CTS/IN: 0.253E+04
SEC/IN: 0.200



0 0:0:0.00
SFE3S3-FLBK-27-LPNTCH.DAT
CTS/IN: 0.416E+04
SEC/IN: 0.200



0 0:0:0.00
SFE3S3-FLBK-45-LPNTCH.DAT
CTS/IN: 0.294E+04
SEC/IN: 0.200

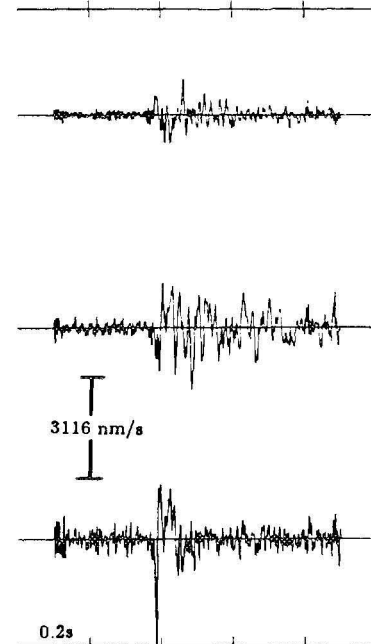


Figure 6-11 Typical Low-Frequency Signals Recorded at 9,590 ft During Flowback Following Stage 9 of Mini-Frac No. 1

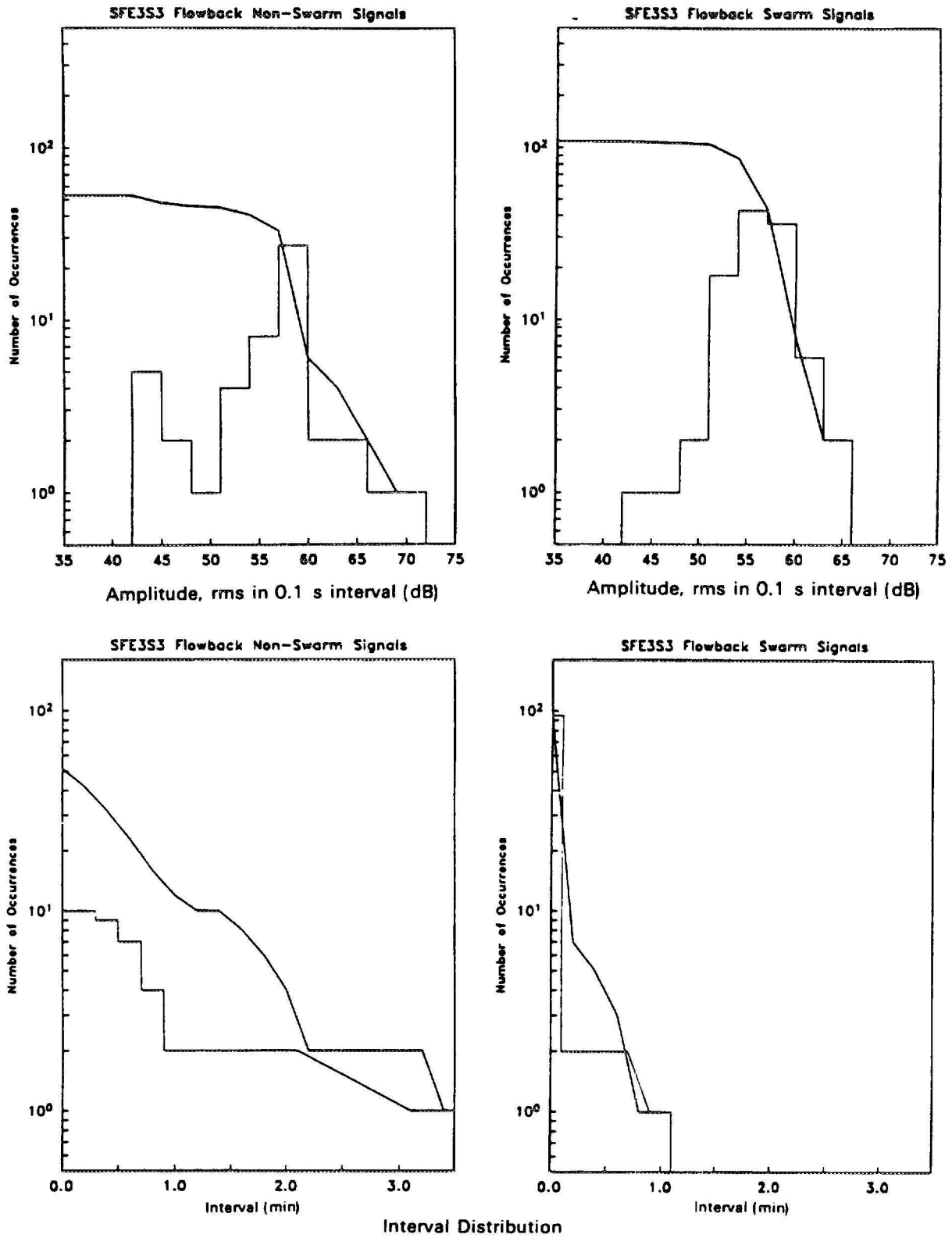


Figure 6-12 Amplitude and Interval Distributions of Low-Frequency Signals Recorded at 9,590 ft During Flowback Following Stage 9 of Mini-Frac No. 1

while the cumulative distributions represent the number of occurrences (amplitude or interval) greater than a specified value. The amplitudes exhibit a power law distribution, similar to amplitude distributions observed for naturally-occurring seismic events, such as earthquakes. The interval distribution for the non-swarm events is consistent with a Poisson process (events equally likely to occur at any time, i.e., no time dependence among the events). The overall occurrence rate for the flowback low-frequency signals was approximately two per minute, twice the rate observed for low-frequency signals recorded during shut-in of the mini-frac.

Particle motion orientations of a selection of the low-frequency signals are shown in Figure 6-13. The particle motion orientation of the one low-frequency signal recorded at 9,590 ft during Stage 6 of the mini-frac is included on this figure for comparison. The particle motions of the low-frequency flow-

back signals are oriented 77° relative to North. The low-frequency character of these signals implies a source dimension of a few tens of feet to a few hundred feet, consistent with the expected dimensions of the induced fracture at the SFE No. 3 well. The orientation of the particle motion of the signals is consistent with that expected for the seismic radiation from a vertically-oriented tensile fracture whose strike is in the direction of the fracture induced by the hydraulic stimulation. Therefore, the azimuth of the mini-frac-induced fracture at the SFE No. 3 well is interpreted to be $N77^\circ E$.

6.2.3.2 Fracture Height Results and Analyses

Introduction and Summary

Teledyne Geotech has determined, both empirically and theoretically, that the background seismic motion induced within a

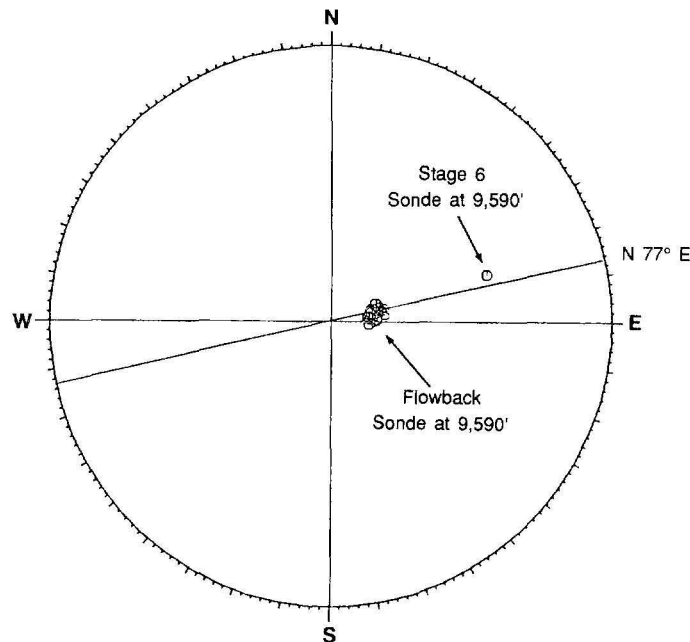


Figure 6-13 *Upper Hemisphere Stereographic Projection of Particle Motion Orientations for Low-Frequency Signals Recorded at 9,590 ft During Flowback*

hydraulically-fractured region can be used to determine hydraulic fracture height. It has been shown (e.g., Fix and Others, 1989) that the data shows a profound difference when recorded in the treatment well within and outside (i.e., above or below) the treatment-altered region. This change in data character is demonstrated when an average of the background horizontal component of motion, H, is directly compared to background vertical component of motion, Z, through a ratio, H/Z. Data recorded above or below the treatment-affected zone show Z greater than H; data recorded within the zone show either H greater than Z or a marked and consistent reduction in Z compared to H. It has been found that a single, average value of H/Z for each recording depth shows the change and/or inversion of the H/Z ratio. The ratio is used because it has the advantage of reducing time-dependent source effects which have been linked to pressure and temperature diffusion of the treatment fluid. To define the change in H/Z, data must be recorded at a suite of depths whose overall expanse exceeds the extent of the treatment altered zone.

Prior to the main hydraulic fracture treatment, microseismic data were recorded in the SFE No. 3 well on three separate occasions. These microseismic surveys were performed pre-perforation, pre-mini-frac but post-perforation, and during shut-in stages of a nine stage mini-frac treatment. Cumulatively, the surveys spanned from 8,700 ft to 9,610 ft with the perforation interval between 9,225 ft and 9,330 ft. The result of an H/Z analysis of the data showed the following:

- no seismic evidence of a hydraulic fracture before the treatment;
- Post-Stage 2 of Mini-Frac No. 1, top of the fracture at $9,175 \pm 25$ ft and bottom at $9,475 \pm 25$ ft; and

- Post-Stage 8 of Mini-Frac No. 1, top of the fracture at $9,125 \pm 25$ ft and bottom at $9,425 \pm 25$ ft.

Seismic data collected during and after the main hydraulic fracture treatment will be discussed in Sections 7.0 and 8.0.

Field Operation and Data Acquisition

In early December 1988, Teledyne Geotech recorded a pre-perforation baseline seismicity survey (see Section 2.2.1.1). Data were taken at 24 depths between 9,610 and 8,700 ft along an ascending traverse within the pressurized well. The pressure at the wellhead was fixed at 2,000 psi immediately prior to data recording at each depth. The 24 depths were sufficient to determine a reliable background baseline. Table 6-4 shows the recording depths and the occupation times at each depth. Although not specifically shown in Table 6-4, typically 6 minutes of 2,000 sample/sec data were recorded at each depth. For ease of reporting and because of the consistency in the analysis of these data, only the results from a representative portion of this data set will be reported.

On February 12, the post-perforation, pre-mini-frac microseismic data set was recorded (see Section 2.2.1.2). Twelve depths were monitored. The "Pre-Frac" column of Table 6-4 indicates the depths occupied and the local (military clock) time of the recordings. Note that the recording session consisted of interleaved ascending and descending traverses. At each depth, 4 minutes of 2,000 sample/sec data were recorded.

On February 17th, the actual mini-fracturing operation was performed. The operation was divided into six pumping stages and three shut-in stages. During each pumping stage, the sonde was locked at the bottom of the hole.

Table 6-4 Depths (Relative to KB at 21.5 ft Above Ground Level) and Data Recording Inception Times (Local Military Clock Time) at the SFE No. 3*

Depth, ft	Pre-Perf Traverse	Pre-Frac Traverse	Mini-Frac Stage 3 Traverse	Mini-Frac Stage 6 Traverse	Mini-Frac Stage 7 Traverse	Post-Main Massive Traverse
8,700	-	-	-	-	-	03:50
8,750	-	-	-	-	-	03:37
8,800	-	-	-	-	-	03:18
8,850	-	-	-	-	-	02:43
8,900	-	-	-	-	-	22:24
8,925	-	-	-	-	-	02:56
8,950	-	-	-	-	-	22:41; 02:28
8,975	-	-	-	-	-	22:48; 02:18
9,000	02:02	18:21	09:22	12:00	18:04	22:58; 02:06
9,025	01:41	-	-	13:50	-	23:10; 01:22
9,050	01:31	18:32	09:30	12:11	18:15	01:11
9,075	01:21	-	-	13:41	-	-
9,100	00:58	18:13	09:10	11:52	17:54	23:20
9,125	00:45	-	-	13:32	-	-
9,150	00:25	18:39	09:38	12:20	18:30	00:57
9,175	00:25	-	-	13:24	-	00:48
9,200	00:14	18:05	09:02	11:43	17:35	23:33
9,225	00:02	-	-	13:58	-	-
9,250	23:52	18:46	-	-	-	-
9,260	-	-	-	-	-	23:47
9,270	-	-	09:46	12:29	18:38	-
9,275	23:43	-	-	-	-	-
9,300	23:33	-	-	-	-	-
9,325	23:23	-	-	-	-	-
9,350	23:13	18:45	09:53	12:37	18:46	00:34
9,375	23:02	-	-	13:16	-	-
9,400	22:52	17:56	08:47	11:30	17:21	23:53
9,425	22:34	-	-	14:06	-	00:22
9,450	19:56	19:02	10:02	12:44	18:55	00:07
9,475	19:44	-	-	13:07	-	-
9,500	19:33	17:48	08:35	11:16	17:08	-
9,525	-	-	-	14:14	-	-
9,550	19:21	-	10:11	12:51	19:02	-
9,575	-	-	-	12:59	-	-
9,590	-	17:38	08:20	11:03	16:56;19:18	-
9,600	19:07	-	-	-	-	-
9,610	18:51	-	-	-	-	-

*for the Mini-Frac pump stages, time is relative to shut-in

During the first shut-in (Stage 3), a 12-depth microseismic survey was performed. Like the pre-frac survey the day before, this survey consisted of interleaved ascending and descending traverses with 4 minutes of 2,000 sample/sec data recorded at each depth. The "Stage 3" column of Table 6-4 indicates the depths occupied and the clock time of the recording. Stage 6 microseismic monitoring consisted of 22 depth stations divided into 2 ascending and 2 descending traverses. The "Stage 6" column of Table 6-4 indicates the depths occupied and the clock time of the recording.

During the final mini-frac shut-in stage (No. 9), a 12-depth microseismic survey was performed. At the first three recording depths, 8 minutes of 2,000 sample/sec data were recorded; at the remaining depths, 4 minutes of data were recorded. The "Stage 3" column of Table 6-4 indicates the depths occupied and the clock time of the recording. Like the Stage 3 monitoring, the Stage 9 monitoring was an interleaved ascending and descending traverse.

Data Analysis and Results

The first step in the SFE No. 3 height determination data analysis is shown in Figure 6-14. The figure shows a comparison of average values of the RMS, or root-mean-square, of the background level of the data recorded before and during the mini-frac. These values were calculated from data sets in which the identifiable, discrete signals were removed and used 0.1-second windows on the sans signals data. As will be discussed below, some of the data sets recorded at SFE No. 3 had a very high level of electrical (60 Hz, harmonic) noise contamination. For this reason, all of the data used in the Figure 6-14 have been 60-hertz comb-filtered (radius = 1.05). Because of the large variation in the data values, Figure 6-14 has been plotted in decibels (dB) relative to ground particle velocity of 1

nm/s. For reference, a wellbore with the perforation interval indicated by the heavy lines is shown at the left in the figure.

Some very interesting features are shown in Figure 6-14. First, note the very high background level of about 52 dB for the pre-mini-frac, post-perforation data. Since the motion data were taken with the well pressurized and taking fluid, this level is probably indicative of the fluid motion from the well into the formation. Note also, the extremely low level of about 25 dB of the mini-frac Stage 3 and Stage 6 data above the perforations. At some of the stations, these data are below the pre-perforation RMS level, which should be the lowest baseline level for any of these data. The reason for the low level at these depths is not known. As a result of the analysis, only the data from post Stage 3 and Stage 9 were deemed reliable and were used for determining the height.

Figure 6-15 is comparable to Figure 6-14 with the exception that these data were calculated from the post-main fracture data set. Because the data were segmented, a number of values are given for various levels. The raw data used here did not have the 60-hertz noise problem; hence, Figure 6-15 was calculated from unfiltered, 0.1-second RMS data.

The apparently large variations seen in Figure 6-15 between 8,950 and 9,050 ft can be easily understood in conjunction with Table 6-4. The table shows these depths were repeat-observation depths, with the second monitoring occurring a minimum of 2 hours after the first. The higher level values in Figure 6-15 (solid dots) were recorded after the backfilling of the well that began at approximately 24:00. The higher background level was probably due to the subsequent fluid motion and tube wave noise. Note also above the 9,050-ft depth, the amplitude is about 20/25 dB comparable

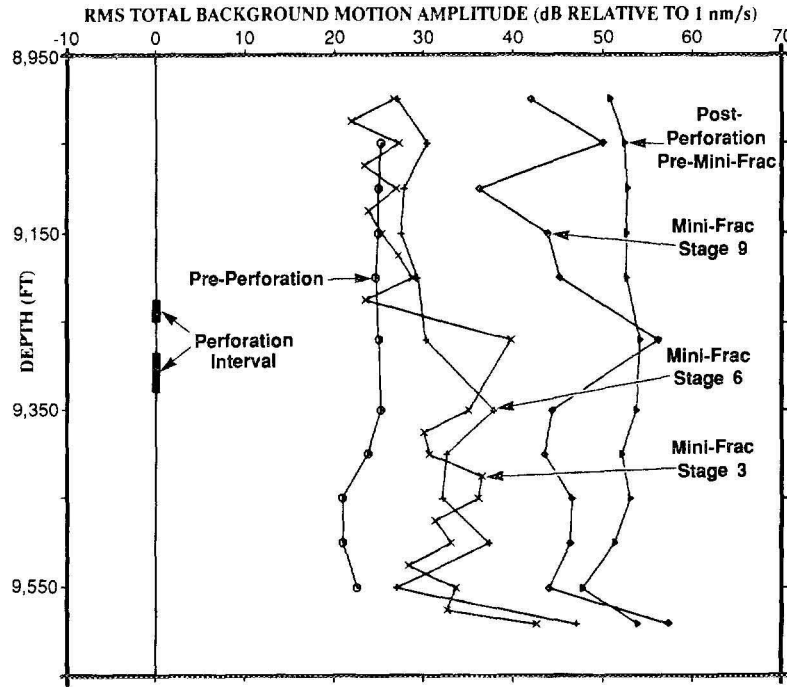


Figure 6-14 Total Background Particle Velocity Before and During Mini-Frac No. 1 (Average RMS, 60 Hz comb filtered) Versus Depth

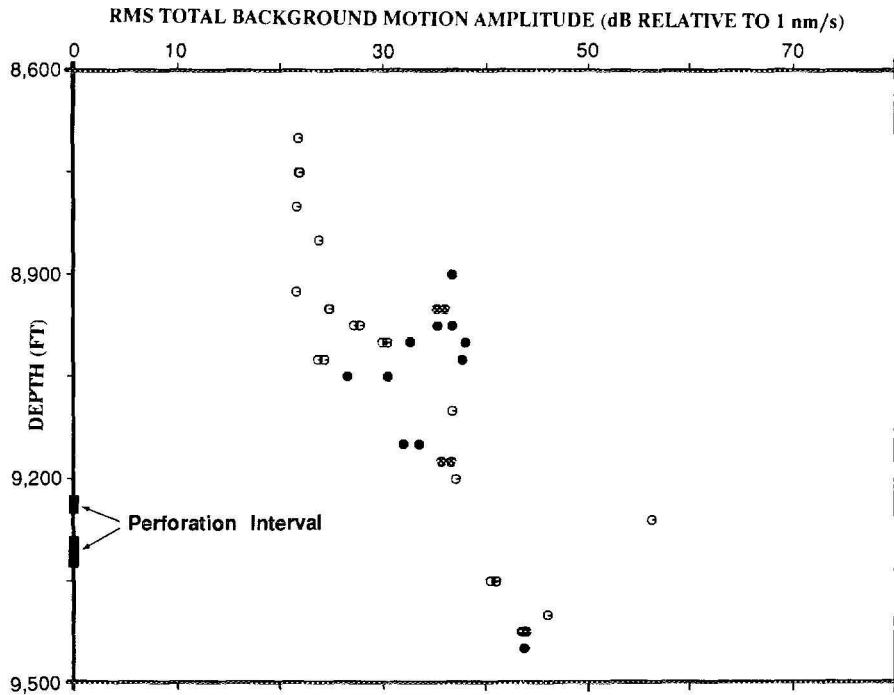


Figure 6-15 Total RMS Background Particle Velocity After Main Fracture and Production Versus Depth (Solid dots taken during backfilling operations)

to the Stage 3 and Stage 6 data plotted in Figure 6-14.

As discussed above and previously (Fix and Others, 1989), the basis for the height determination is the determination and analysis of the H/Z ratio as a function of depths, where H is the average of the RMS level of the horizontal motion component and Z is the same for the vertical component. The following figures show the values of H/Z calculated from the data at the various monitorings.

Figure 6-16 shows the H/Z ratios as a function of depth using the unfiltered motion data from the pre-perforation recording traverse. For reference, the ResTech-determined stress profile is also included in the figure. The main hydraulic fracture treatment data, which will be discussed in Section 7.0, have been high-pass filtered to eliminate the primary tool resonance pass-band below approximately 75 Hz. For comparison, Figure 6-17 shows pre-perforation H/Z ratios after 75-hertz high-pass filtering.

The most important characteristic in Figures 6-16 and 6-17 is that no structure or height characteristic is evident in the data. The H/Z ratios are consistently horizontal, showing H greater than Z with no abrupt change or inversion. This characteristic is expected since no fracturing had occurred when the data were recorded and since it has been seen consistently in pre-treatment data as described previously (Fix and Others, 1989). Figure 6-16 does show one interesting feature. The amplitude of the unfiltered H/Z ratios seems to follow the lithology and the stress amplitude profile. The reason for this is not known. It may simply be a coincidence or it may be a demonstration of how the lithology affects ambient earth motion.

Figure 6-18 shows the H/Z ratio as a function of depth for the pre-mini-frac, post-perforation data. These ratios were calculated

from unfiltered data. H/Z ratios calculated using a variety of bandpass and combing filters produced essentially identical results. The unique and very unusual characteristic of Figure 6-18 is the consistency of H less than Z (i.e., H/Z negative in dB). This type of behavior in pre-frac data had never been seen prior to this data set. However, the reason for this behavior is easily explained in light of Figure 6-14.

Figure 6-14 shows the background level of the pre-mini-frac, post-perforation data was uncharacteristically high considering the well had a minor amount of fracturing from the injection/ballout treatment. During this monitoring, the well was pressured at approximately 2,000 psi (wellhead pressure) and the formation was taking fluid. Under these circumstances, Z greater than H at all depths was, probably, a signature of the fluid motion and associated tube waves. What is significant about this data set is that it does not contain much, if any, useful information. It is interesting to note that even though Z was greater than H, the amplitude of H/Z was very nearly constant.

Figure 6-19 shows the H/Z ratios as a function of depth for the mini-frac Stage 3 data. Because of noise contamination, especially a very high electrical noise (60 Hz plus odd harmonics), these ratios were calculated from data that was band passed between 75 and 450 Hz and combed filtered for the 60 Hz (comb radius = 1.05) noise.

As described in previous data sets (Fix and Others, 1989), the data in Figure 6-19 show the characteristic signature of the fracturing: an inversion in the H/Z ratio as a function of depth. Interpreting the H/Z inversion gives the top of the fracturing at $9,175 \pm 25$ ft and the bottom of the fracturing at $9,475 \pm 25$ ft.

The analysis of the mini-frac Stage 6 data was inconclusive. The data were very noise

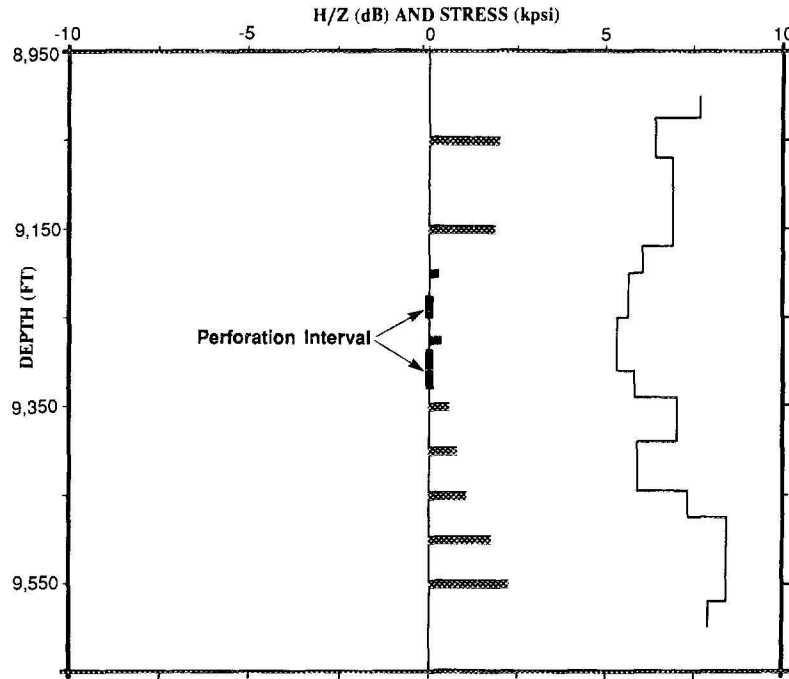


Figure 6-16 Pre-Perforation H/Z Ratio Using Unfiltered Motion Data (Histogram) and Stress Profile (Line) Versus Depth

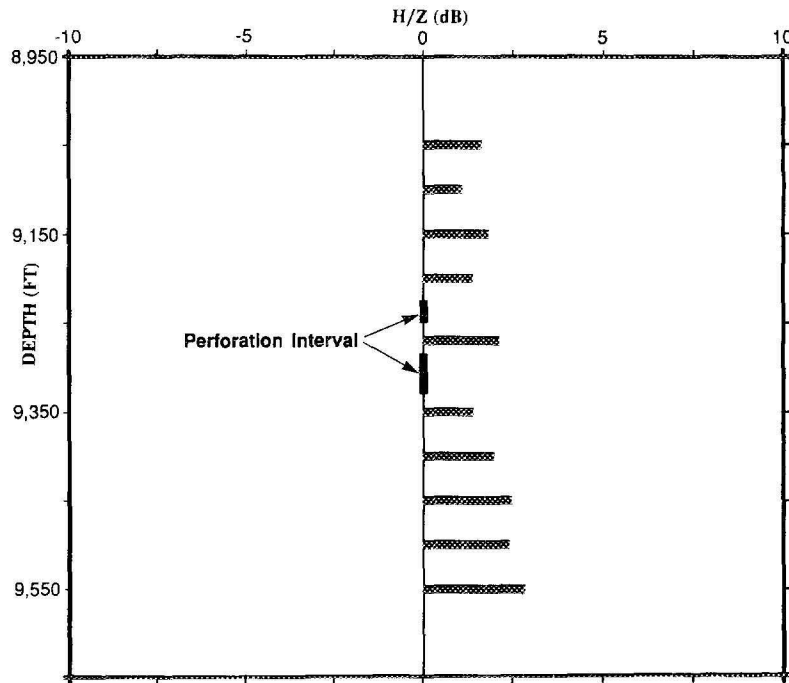


Figure 6-17 Pre-Perforation H/Z Ratio With 75 Hz High-Pass Filter Versus Depth

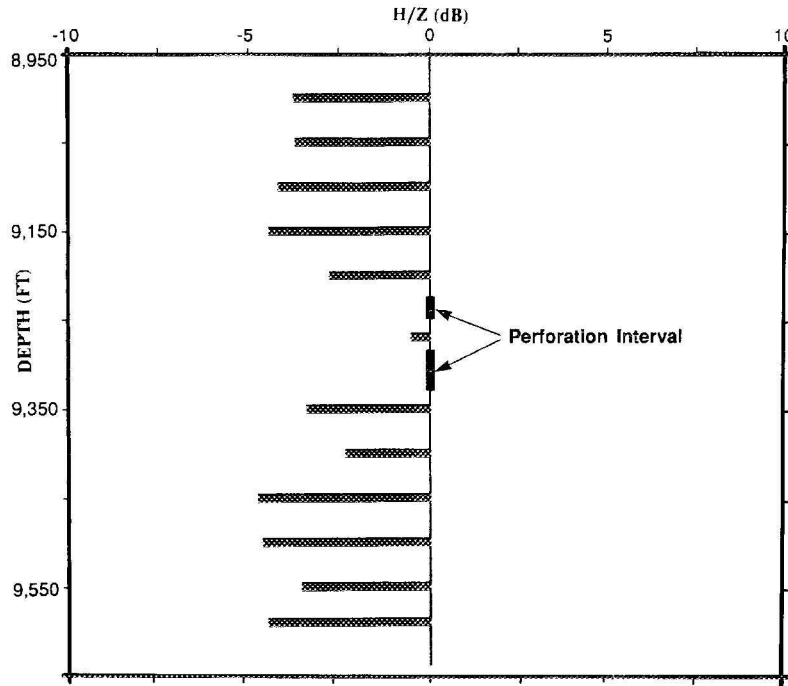


Figure 6-18 Pre-Mini-Frac, Post-Perforation H/Z Ratios (Unfiltered) Versus Depth

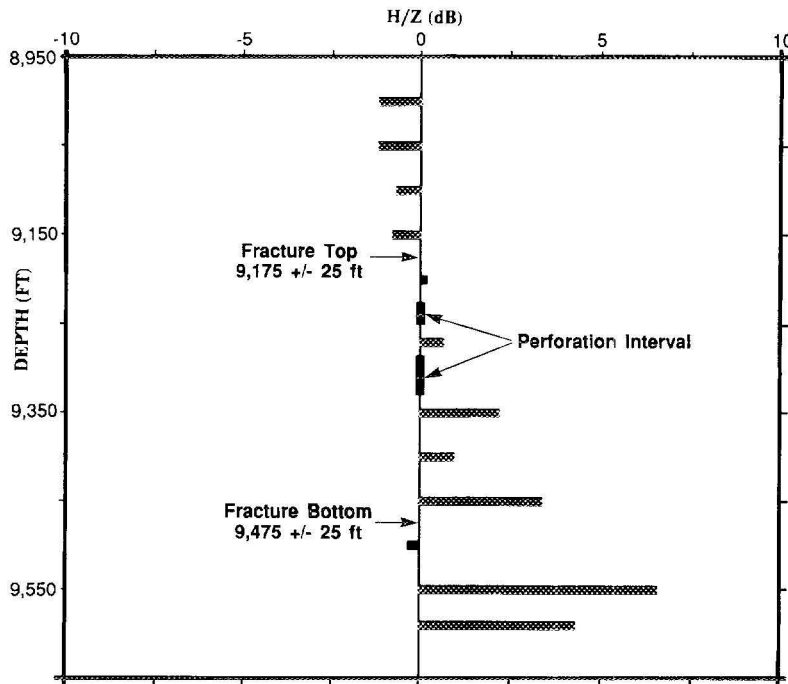


Figure 6-19 Mini-Frac Stage 3 H/Z Ratios Versus Depth

contaminated and could not be filtered to give any consistency in the H/Z ratio. There was, however, a hint in the data that the top of the fracture was effectively the same as the Stage 3 results. As a result, there will be not further discussion of the Stage 6 data.

Like the Stage 6 data, the Stage 9 data were very noisy. However, filtering of the data was effective in noise removal to give a consistent H/Z inversion. Figure 6-20 shows the H/Z for the post Stage 9 monitoring. The data used in these calculations were low pass filtered at 450 Hz and notched (notch radius = 1.02) at 60 Hz and higher harmonics. Despite the anomalous H/Z value between the perforations, the H/Z inversion in Figure 6-20 gives the top of the fracture at $9,125 \pm 25$ ft and the bottom of the fracture at $9,425 \pm 25$ ft. These values of top and bottom indicate between Stages 3 and 9, the top of the fracture grew up and the bottom of the fracture seemed to

close resulting in a shallower depth. Since the mini-frac did not include proppant, these dimensions are for the hydraulic size of the fracture.

6.2.4 Analysis of Mini-Frac No. 1 With 3-D Fracture Simulator

Mini-Frac No. 1 data were analyzed by FRACPRO in three ways: net pressure matches were obtained, the mini-frac dimensions were evaluated, and the main-frac dimensions were predicted. Each of these analyses are discussed in the following sections.

6.2.4.1 Net Pressure Analysis

Two matches of net pressure (bottomhole treating pressure minus closure pressure) were performed. One match, shown in Figure 6-21, utilized reservoir stresses taken from the calibrated well log. Figure 6-22

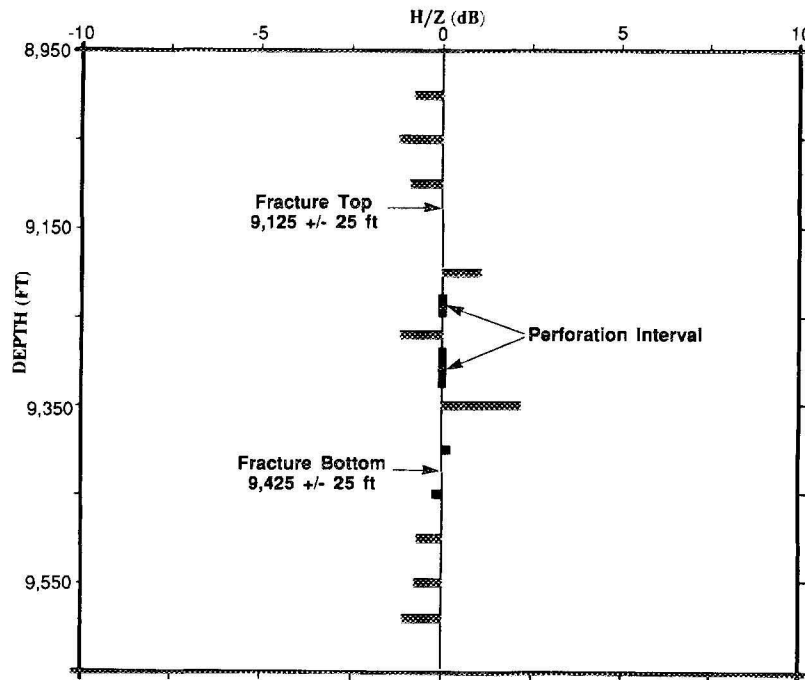


Figure 6-20 Mini-Frac Stage 9 H/Z Ratios Versus Depth

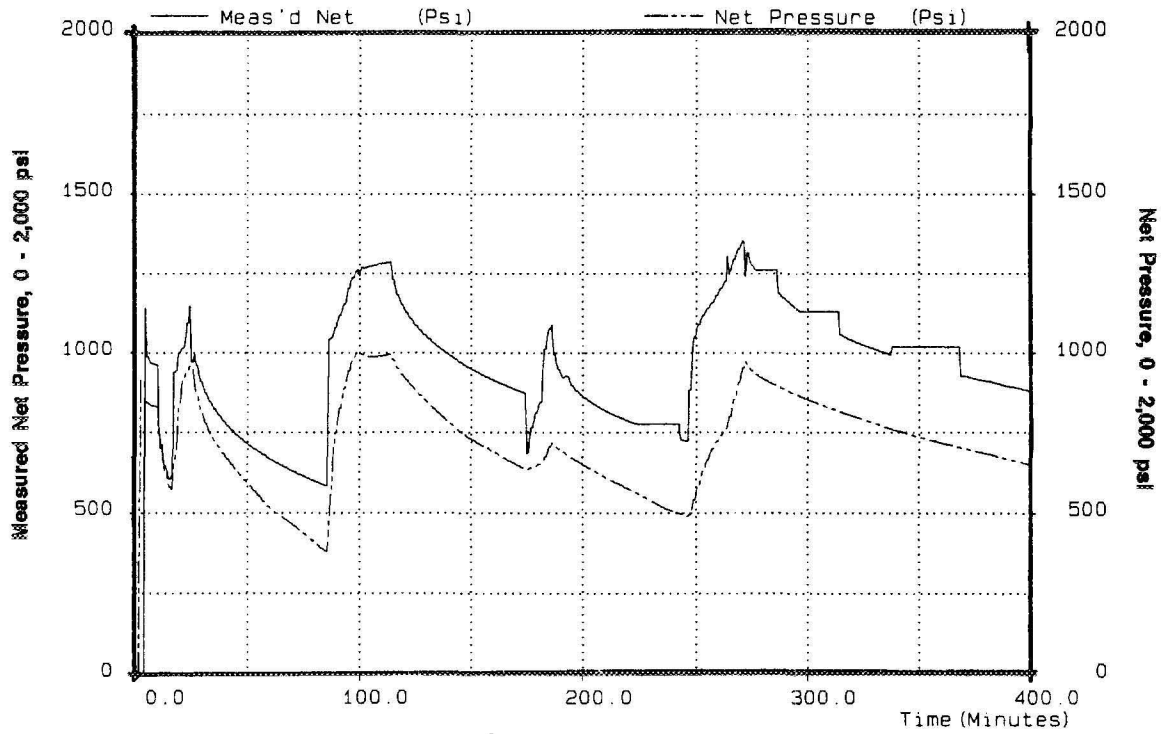


Figure 6-21 Mini-Frac No. 1 Pressure Match With Stresses From Logs

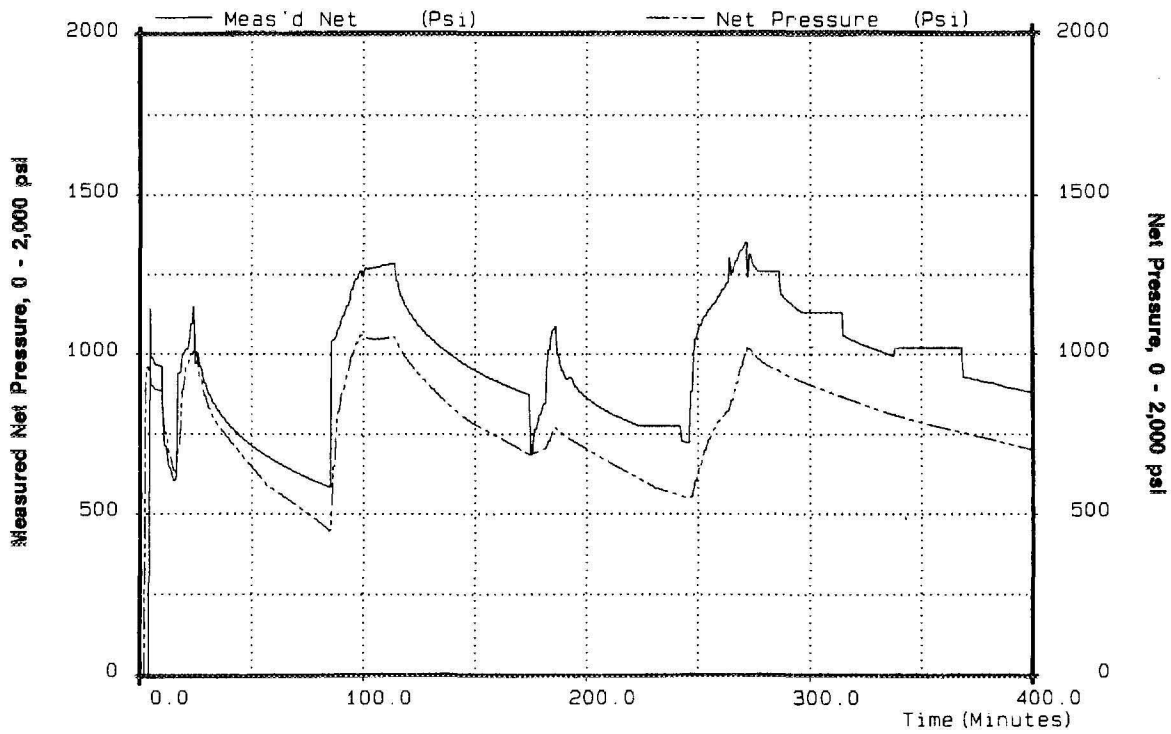


Figure 6-22 Mini-Frac No. 1 Pressure Match With Modified Stresses

illustrates the other match in which stresses were modified slightly to match more closely the measured net pressure response.

A comparison of the log-derived stress with the modified stress for particular zones is given in Table 6-5. As seen in the "delta stress" column, some zones were not modified at all. For zones in which stress was measured, the modifications resulted in stresses within 200 psi of the original, log-derived stresses. The maximum difference between values in zones without measurements was 400 psi. All stress modifications were positive, thereby creating higher stress

contrasts between the perforated interval and layers above and below. The modified stresses are discussed again in Sections 6.2.5 and 7.4.

Frac fluid rheological properties for both matches, listed in Table 6-6, were based upon on-site rheometer measurements. These rheology data were modified to reflect the potential effects of temperature and water-shedding by gels (especially near the fracture perimeter). Leakoff parameters used in both matches are given in Table 6-7, while the reservoir mechanical properties are given in Table 6-8.

Table 6-5 Comparison of Stress Input for Each Layer for the FRACPRO Analysis

Top of Zone, ft	Log Stress, psi	Modified Stress, psi	Delta Stress, psi
9,030	7,300	7,300	0
9,070	7,800	8,200	400
9,115	7,150	7,350	200
9,155	6,600	6,600	0
9,170	6,050	6,050	0
9,200	5,600	5,800	200
9,250	5,250	5,250	0
9,310	5,850	6,050	200
9,340	6,550	6,550	0
9,360	7,300	7,300	0
9,380	5,800	6,200	400
9,435	6,400	6,700	300
9,455	7,550	7,950	400
9,475	8,400	8,400	0
9,575	7,850	7,850	0

Table 6-6 Viscous Properties of the Fracture Fluid

Gel Type	2% KCl	40-lbm Linear	40-lbm X-Link	50-lbm X-link	Slickwater	50-lbm Linear
Unlinked n'	1.00000	0.56000	0.430000	0.43000	0.75000	0.43000
Unlinked k'	0.00002	0.01300	0.004400	0.06270	0.00010	0.06270
Xlinked n'	1.00000	0.56000	0.771000	0.72300	0.75000	0.43000
Xlinked k'	0.00002	0.01300	0.044000	0.06270	0.00010	0.06270
Wbore Xlink	0.00000	0.00000	0.000000	0.00000	0.00000	0.00000
Frac Xlink	0.00000	0.00000	1.000000	1.00000	0.00000	0.00000
Vol Frac H ₂ O	1.00000	0.98000	0.980000	0.98000	0.99000	0.98000
Fric P1*, ppt	25.0000	25.6000	22.00000	20.0000	40.0000	10.0000
Fric Q1*, bbl/min	20.0000	20.0000	20.00000	20.0000	10.0000	10.0000
Fric P2*, ppt	70.0000	40.0000	65.00000	55.0000	100.000	100.000
Fric Q2*, bbl/min	40.0000	40.0000	40.00000	40.0000	20.0000	20.0000

* Fric P1 = psi/1000-ft of friction at flowrate Fric Q1

Fric P2 = psi/1000-ft of friction at flowrate Fric Q2

Table 6-7 Mini-Frac No. 1 Leakoff Parameters Used for the FRACPRO Analysis

Formation Permeability, md	0.0065
Initial Total Leakoff Coefficient, ft $\sqrt{\text{min}}$	0.0010
Reservoir Fluid to Filtrate Permeability Ratio	10.0
Reservoir to Filter Cake Permeability Ratio	100.0
Leakoff Interval	Entire Fracture

Table 6-8 Reservoir Mechanical Properties Used for the FRACPRO Analysis

Top of Zone, ft	Modulus, psi	Poisson's Ratio
0*	6,500,000	0.30
9,180	8,700,000	0.18
9,335	6,000,000	0.26

* Although the interval from 0 to 9,180 ft was assigned the same mechanical properties, only the section from about 8,900 to 9,180 ft was actually felt by the fracture.

Perforation friction or other near-wellbore friction was calibrated by adjusting the number of perforations taking fluid so as to remove discontinuities from the measured net pressure at rate changes. This resulted in 52 perforations, each 0.33 inches in diameter (an initial given value).

Despite the treatment design which allowed for closure between stages, both matches indicated that closure did not occur between stages. Nevertheless, this fact did not significantly affect the microseismic data col-

lected by Teledyne Geotech during Mini-Frac No. 1.

6.2.4.2 Mini-Frac Dimensions

FRACPRO was used to evaluate the growth of Mini-Frac No. 1. Figure 6-23, generated with log-derived stress data, traces the change in width, length, upper height and lower height over time. Similarly, Figure 6-24 shows the dimensions that result using modified stresses. Dimensions at the end of each mini-frac stage are given for both

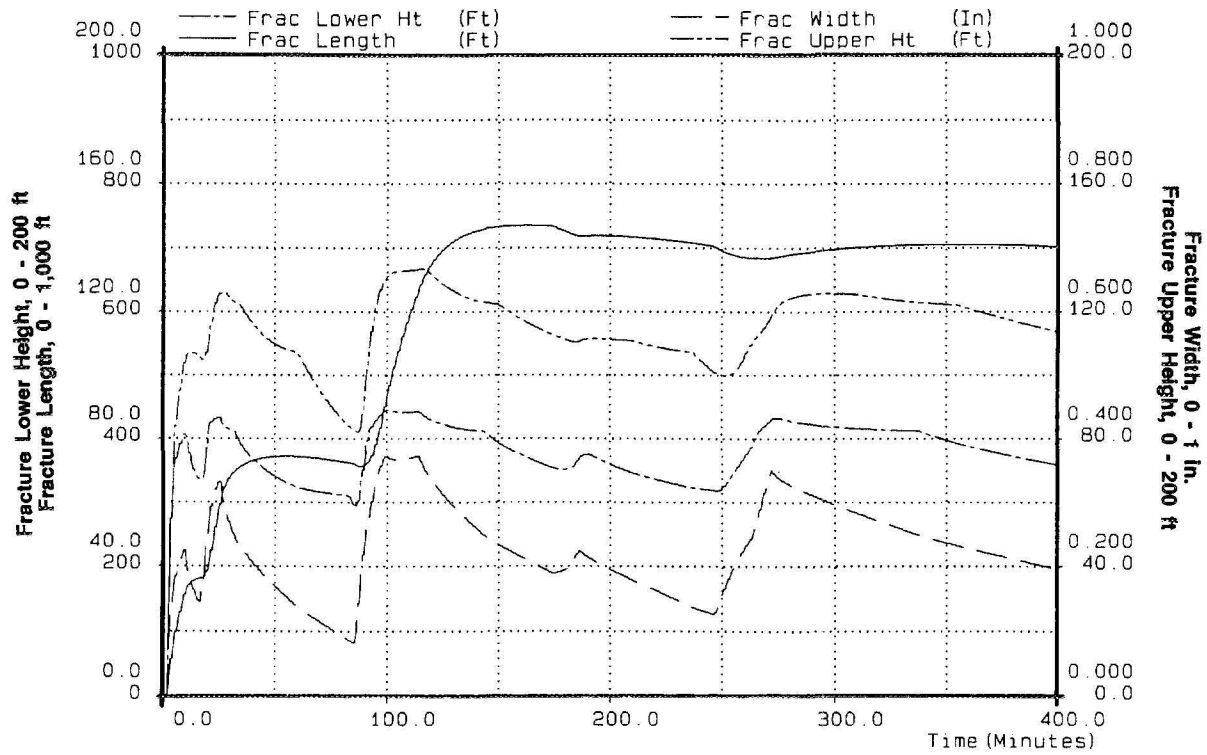


Figure 6-23 Mini-Frac No. 1 Dimensions With Stresses From Logs

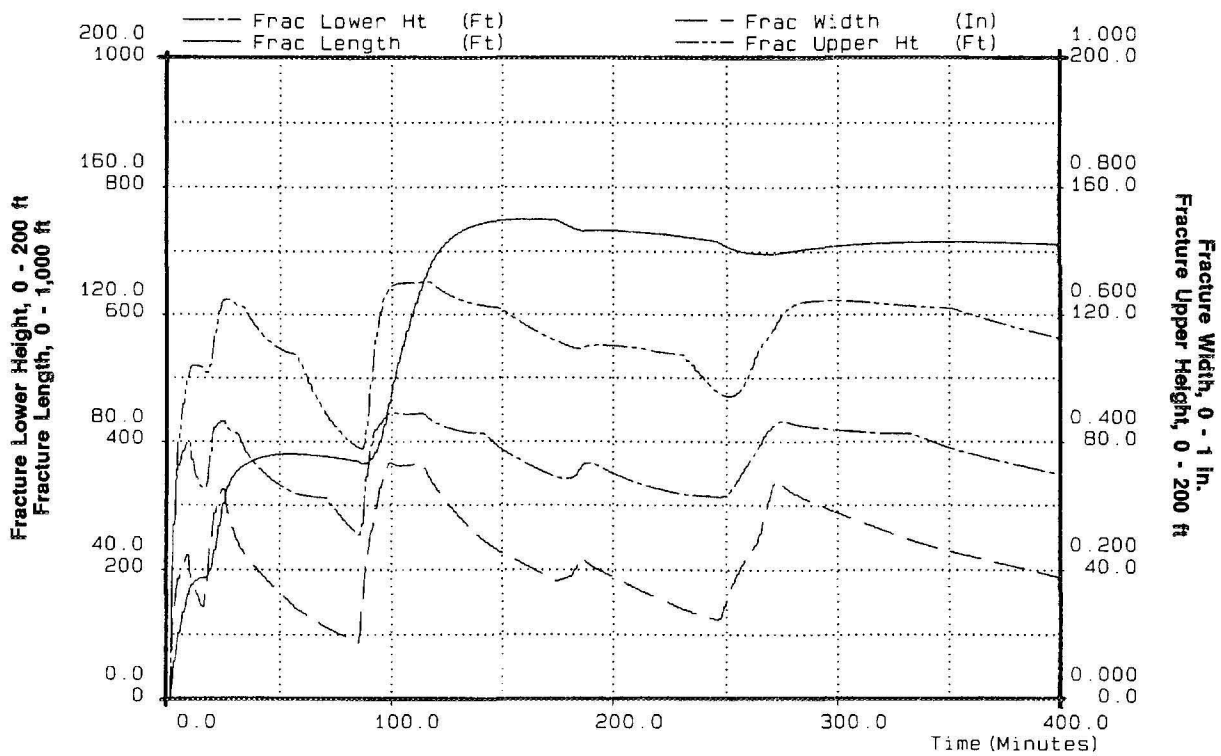


Figure 6-24 Mini-Frac No. 1 Dimensions With Modified Stresses

log-derived and modified stresses in Table 6-9.

With log-derived stresses, the maximum growth in upper and lower height was 137 ft and 91 ft, respectively, or an interval from 9,140 to 9,368 ft. Thus, the apparent permeable zone from 9,225 to 9,325 ft was covered by the mini-frac.

The maximum growth in upper and lower height using modified stresses was 133 ft and 91 ft, respectively, or an interval from 9,144 to 9,368 ft. The calculated mini-frac dimensions covered the apparent permeable zone. As expected, the larger stress contrasts in the modified stress profile gave correspondingly greater vertical confinement and greater length.

In either case, the low stress zone from 9,380 to 9,455 ft could not be confirmed nor denied from the analysis of data obtained during Mini-Frac No. 1.

6.2.4.3 Prediction of Main-Fracture Pressures and Dimensions

Based on the analysis conducted on Mini-Frac No. 1 with associated best-fit parameters (Tables 6-5 and 6-7), RES predicted the pressures and dimensions which would be associated with various main-fracture designs. RES postulated that a very small pad (about 5 percent) following Mini-Frac No. 2 would be sufficient, the idea being to get rapid fracture closure. However, the general consensus of the fracture design team tended toward larger pads. In particular, the design shown in Figure 6-25, favored early in the planning stages, involved a large pad as a "shadow frac." The purpose of the shadow frac was to aid in differentiating between the reservoir response behavior with and without proppant.

Subsequent to the completion of SFE No. 3, FRACPRO's ability to calculate and display proppant distribution was upgraded

Table 6-9 Mini-Frac No. 1 Dimensions at End of Pumping as Determined by FRACPRO Analysis

Dimension	Stage 1	Stage 2	Stage 3	Stage 4
Using Stresses From Log:				
Fracture Wing Length, ft	312	643	718	686
Fracture Upper Height, ft	126	133	111	120
Fracture Lower Height, ft	85	88	75	86
Fracture Width (Max), in.	0.31	0.36	0.22	0.35
Using Modified Stresses:				
Fracture Wing Length, ft	318	658	732	697
Fracture Upper Height, ft	125	131	110	118
Fracture Lower Height, ft	85	89	73	86
Fracture Width (Max), in.	0.30	0.36	0.22	0.34

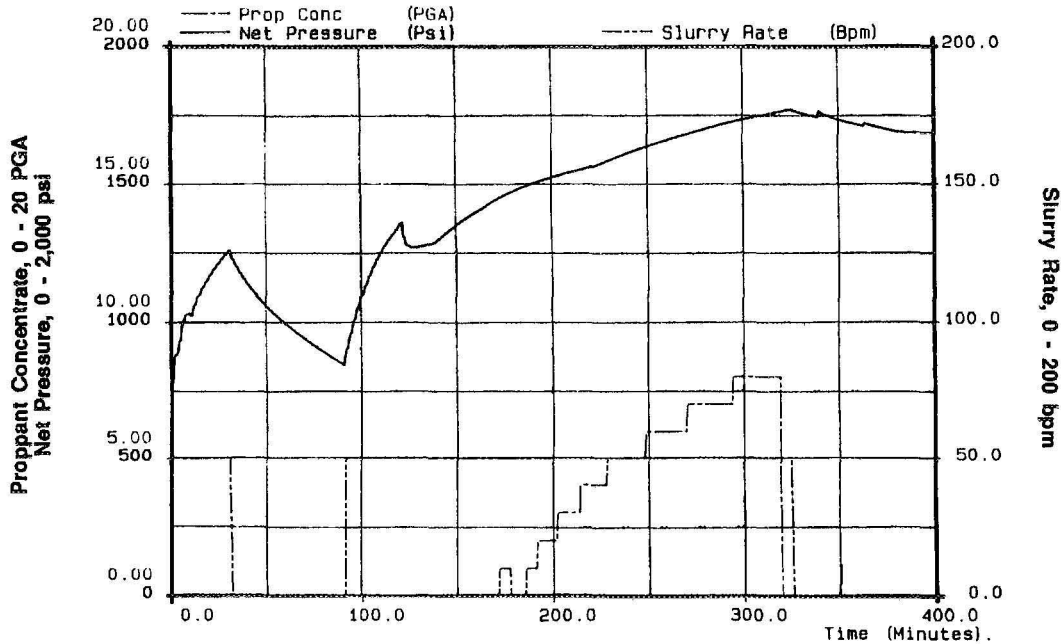


Figure 6-25 Net Pressure Prediction for Main Frac Based on Early Treatment Design

substantially, the greatest impact being on calculations for treatments with optimized pad volumes. However, these changes did not significantly affect the calculations for SFE No. 3 because the pressure response was dominated by the in-situ stress distribution; in comparison, the effect of proppant distribution was relatively minor.

Based on information from Mini-Frac No. 1, the predicted dimensions of the main fracture are shown in Figure 6-26; the propped dimensions are shown in Figure 6-27. As will be seen in Section 7.0, the final dimensions deduced from the main-fracture treatment data are quite close to those predicted on the basis of Mini-Frac No. 1. Thus, a well-conducted mini-frac may yield the data required for fracture treatment optimization, while also serving to minimize leakoff during the main treatment.

6.2.5 Analysis of Mini-Frac No. 2 With 3-D Fracture Simulator

6.2.5.1 Net Pressure Analysis

Since Mini-Frac No. 2 bottomhole pressure data was acquired with a gauge in the dead tubing string, this data was used to calculate net pressure for the Mini-Frac No. 2 and main-frac pressure matches. A dead string specific gravity of 0.998, measured for the main frac, was used for both matches.

Frac fluid rheological properties, shown in Table 6-6, were taken from on-site measurements and used for both the mini- and main fracs. These data were modified to reflect the potential effects of temperature and water-shedding by gels (especially near the fracture perimeter). Leakoff parameters for Mini-Frac No. 2 and the main frac are given

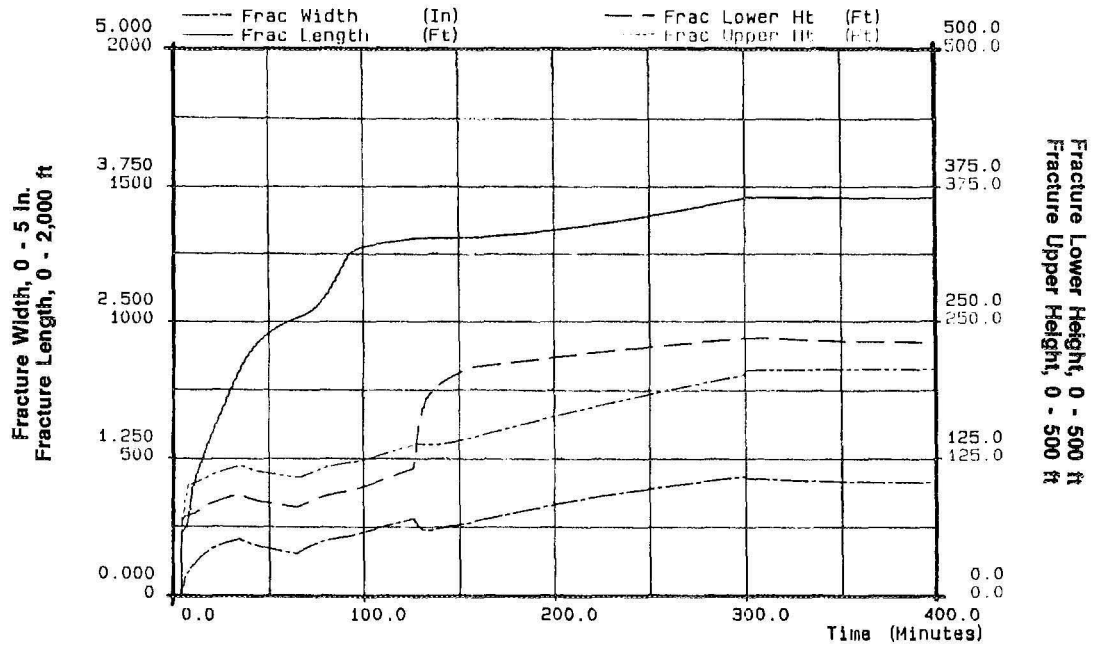


Figure 6-26 Dimensions Prediction for Main Frac Based on Early Treatment Design

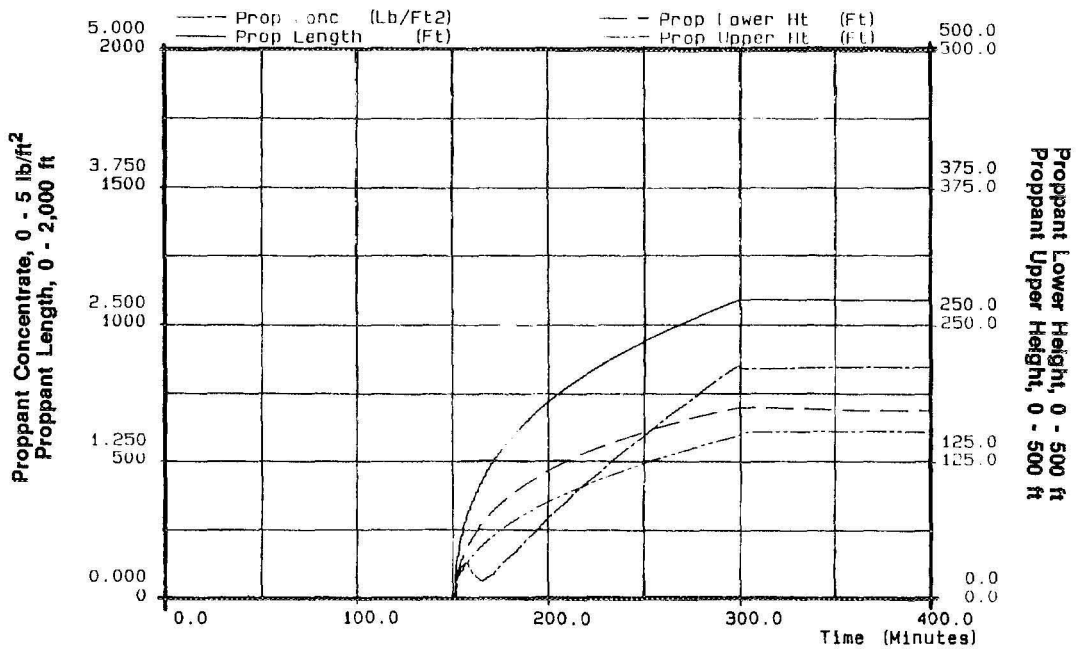


Figure 6-27 Propped Dimensions Prediction for Main Frac Based on Early Treatment Design

in Table 6-10; they are comparable to those for Mini-Frac No. 1 listed in Table 6-7.

The net pressure matches for Mini-Frac No. 2 and main frac are located in Section 7.3.1. Like the Mini-Frac No. 1 analysis, this analysis yields one match generated with log-derived stresses and another match with modified stresses. These stresses, found in Table 6-5, were discussed previously.

For Mini-Frac No. 2, the pressure falloff after shut-in was characterized by an initial rapid decline, followed by an extended period of slow decline. A simple leakoff coefficient alone (i.e., with constant fracture area or uniform stress) was not sufficient to match this behavior. Either the early or late shut-

in time portion of the falloff would have to be ignored. The close-in stress contrasts influence the late time shut-in, a period when the net pressure curve declines very slowly. Thus, when analyzing pressure falloff data to determine leakoff coefficient, one should include the effects of stress contrasts and of continued fracture growth/contraction.

6.2.5.2 Mini-Frac Dimensions

Dimensions of Mini-Frac No. 2 calculated with both log-derived and modified stresses are located in Section 7.3.2 on the same figures as those for the main frac. Mini-Frac No. 2 dimensions at the end of pumping are given by Table 6-11.

Table 6-10 Mini-Frac No. 2 and Main Frac Leakoff Parameters Used for the FRACPRO Analysis

Formation Permeability, md	0.0065
Initial Total Leakoff Coefficient, ft ² /min	0.0010
Reservoir Fluid to Filtrate Permeability Ratio	10.0
Reservoir to Filter Cake Permeability Ratio	100.0
Leakoff Interval	Entire Fracture

Table 6-11 Mini-Frac No. 2 Dimensions at End of Pumping as Determined by FRACPRO Analysis

Dimension	Using Stresses From Log	Using Modified Stresses
Fracture Wing Length, ft	967	985
Fracture Upper Height, ft	132	129
Fracture Lower Height, ft	87	87
Fracture Width (Max), in.	0.34	0.34

7.0 Hydraulic Fracture Treatment of the Lower Cotton Valley Formation (Taylor Sandstone)

7.1 TREATMENT OBJECTIVES AND DESIGN

In SFE Nos. 1 and 2, GRI researchers attempted to control fracture height growth by manipulating the pump rate and the viscosity of the fluids. Unfortunately, there was insufficient stress contrast to successfully limit fracture height even with these methods. As a consequence, a near-circular fracture was created during most treatments.

One goal of SFE No. 3 was to test the fracture diagnostic tools and techniques on a long, elliptical fracture. Afterwards, researchers could draw some conclusions regarding the real-time prediction for a variety of fracture geometries. For SFE No. 3, the Taylor section of the Cotton Valley sand was chosen for the treatment because it was believed to be bounded by significant stress barriers. Such barriers make the growth of a long, elliptical fracture more likely. The main treatment was designed to create a propped fracture half-length of about 900 to 1,000 ft.

The treatment design, along with the actual execution, is described in Table 7-1. The treatment consisted of 15 separate stages, the first being Mini-Frac No. 2. The main distinction between Mini-Frac No. 2 and the rest of the treatment was the presence of proppant in the main frac. The fracture treatment was pumped on March 16, 1989.

After a short shut-in, the design called for a 1,000-bbl slickwater pre-pad to be pumped. The purpose of the slick pad was to initiate the hydraulic fracture and to propagate it using thin fluid. The thin fluid was to be followed by a 3,700-bbl thick pad (Stages 4 to 6). The early portions of the pad were designed for a 50-lbm/1000 gal

delayed crosslink system. In Stage 5, 12,600 lbs of 100-mesh sand were to be added to evaluate the effects of sand on fluid entry pressures. Because substantial pressure increases were observed on previous SFE wells when 100 mesh sand was used in the pad, it was important to determine if similar pressure responses occurred in the Cotton Valley.

Following the thick pad, 5,500 bbl of gel were scheduled to be pumped while carrying 1,184,000 lbm of 20/40-mesh Ottawa sand at concentrations up to 8 lbm/gal. The last stage was to consist of 300 bbl of slick-water as flush.

In Staged Field Experiment No. 2, one of the major concerns was to limit fracture height growth by minimizing fluid viscosity. For SFE No. 3, no attempt was made to minimize viscosity. Instead, the design called for pumping a high viscosity fluid (1,000 cp). Researchers then strived to keep viscosity constant downhole so that its effect on fracture height growth in the presence of suspected barriers could be determined. A liquid gel concentrate (LGC) system was used to adjust the viscosity as required.

Using this design, the size of the thick pad was 40 percent of the total volume. If one included the pre-pad fluid, the total pad volume was designed to be 46 percent of the total fluid volume. Based on estimated values of pump time, shear rate and bottom-hole temperature, the fluid was designed to maintain apparent viscosity of between 900 and 1,200 cp. According to the fracture treatment design model, a fluid viscosity in this range should have been sufficient to create a fracture wide enough to accept the

07

Table 7-1 Fracture Treatment Design and Actual Treatment Volumes for SFE No. 3

Stage	Fluid Volume, bbi		Fluid Type	Proppant Conc., lbm/gal	Proppant Volume, lbm		Proppant Type
	Design	Actual			Design	Actual	
1	1,500	1,571	40-lbm linear	0	0	0	none
2	0	0	Shut-in	0	0	0	none
3	1000	576	Slickwater	0	0	0	none
4	3000	2,908	50-lbm x-link	0	0	0	none
5	300	293	50-lbm x-link	1	12,600	11,110	100-mesh sand
6	400	477	40-lbm x-link	0	0	0	none
7	400	337	40-lbm x-link	1	16,800	14,150	20/40 Ottawa sand
8	500	500	40-lbm x-link	2	42,000	41,120	20/40 Ottawa sand
9	500	437	40-lbm x-link	3	63,000	54,910	20/40 Ottawa sand
10	600	623	40-lbm x-link	4	100,800	105,330	20/40 Ottawa sand
11	800	755	40-lbm x-link	5	168,000	133,630	20/40 Ottawa sand
12	900	807	40-lbm x-link	6	226,800	227,250	20/40 Ottawa sand
13	900	934	40-lbm x-link	7	264,600	300,100	20/40 Ottawa sand
14	900	935	40-lbm x-link	8	302,400	292,420	20/40 Ottawa sand
15	300	240	Slickwater	0	0	0	none

Table 7-2 Viscosity at 300 RPM of Batch-Mixed Fluid, SFE No. 3

Tank No.	Gel Concentration, lbm/1,000 gal	Temperature, °F	Viscosity, cp
4	50	60.0	50.0
5	50	59.6	50.5
6	50	66.8	45.0
7	50	64.0	50.0
8	50	64.4	44.0
9	50	62.4	56.5
10	50	63.0	56.0
11	40	64.4	37.0
12	40	64.8	35.0
13	40	66.0	38.0
14	40	64.8	34.0

Table 7-3 Viscosity at 300 RPM of Continuous-Mix, 40-lbm Fluid, SFE No. 3

Tank No.	Temperature, °F	Viscosity, cp
15	63.4	32.0
16	64.8	40.0
17	64.4	35.0
18	65.4	33.0
19	64.8	36.0
20	66.2	30.0
21	66.4	33.0
22	65.6	33.0
23	66.6	28.5

proppant concentrations designed for SFE No. 3 fracture treatment.

7.2 TREATMENT MONITORING AND QUALITY CONTROL

The hydraulic fracture treatment on SFE No. 3 was pumped March 16, 1989. It was the focus of two different GRI research efforts: (1) measurement of fracture fluid rheology using the Rheology Van, and (2) 3-D fracture modeling utilizing the TAU. Each research project had its own requirements and needs with respect to monitoring. The treatment requirements were met and each contractor obtained the data necessary for their analysis. The following sections discuss in more detail the types of data measured and the analysis results.

7.2.1 Quality Control of the Fracturing Fluids

The GRI Rheology Van was on location to measure fracture fluid properties both before and during the actual treatment. In addition to the measurement of fluid properties, a total inventory of all materials and fluids was taken before and after the treatment. An analysis of each water tank, including total chlorides, iron content, bacteria culture, pH, phosphates and temperature, was conducted.

For SFE No. 3, the fracturing service company was allowed to batch mix approximately one-half of the fluid prior to the treatment. Afterwards, they utilized a liquid gel concentrate to mix fluids semi-continuously for the remainder of the treatment.

As illustrated in Table 7-2, considerable variation in linear gel viscosity of the batch-mixed fluids was observed. As shown in Table 7-3, there were also considerable variations in the linear gel viscosity of the continuously mixed fluids. Because the same LGC blender was used for batch

mixing and the semi-continuous mixing, it is reasonable that variations observed in one would also be observed in the other. Nonetheless, variations of this magnitude should not have been present at all. The LGC system should have provided tighter control over the mixing process. From these observations, it is apparent that additional work will be required by the service industry to help minimize these problems.

Prior to the treatment, actual crosslinked viscosities at downhole temperature were measured for each tank of batch-mixed gel using the Model 50 viscometers in the Rheology Van. These tests help to ensure the actual gel mixed in the field would behave as expected during the treatment. Figure 7-1 presents the viscosity behavior of two samples of 50-lbm gel at a reservoir temperature of 250° F. These pre-mixed samples contained all the additives used during the actual treatment. In general, the viscous behavior of this fluid is very consistent.

Figure 7-2 shows data measured on two samples of 40-lbm gel. The difference in viscosity shown with these samples is often observed in the field because it is very difficult to mix precisely and test each sample in an identical manner. Therefore, the field data are usually normalized by averaging the results from two to three tests.

Figure 7-3 is a plot of viscosities at bottom-hole temperature conditions for 40-lbm fluid (continuous mix) samples taken during the actual treatment. Again, similar variations in viscosities were observed. These variations are likely due to the effect of crosslinker on variable gel concentration.

Generally, job execution during SFE No. 3 was satisfactory, and service company efforts were probably typical of those expended on a routine fracture treatment. Most researchers working to define fracture geometry understand that there will be varia-

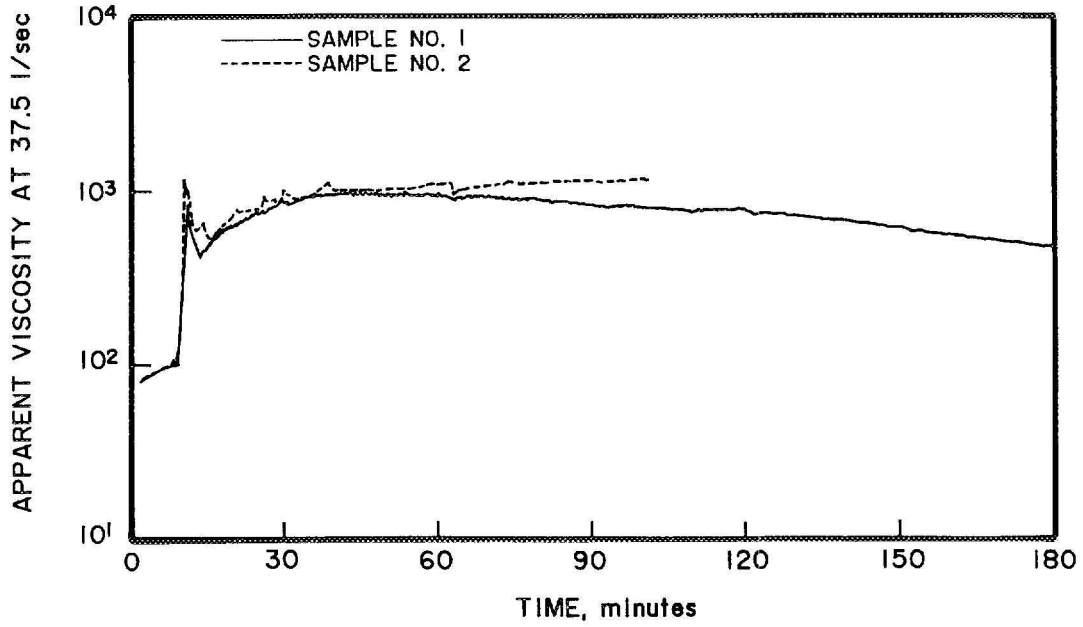


Figure 7-1 Viscosity of Pre-Mixed 50-lbm Gel at Downhole Temperature, SFE No. 3

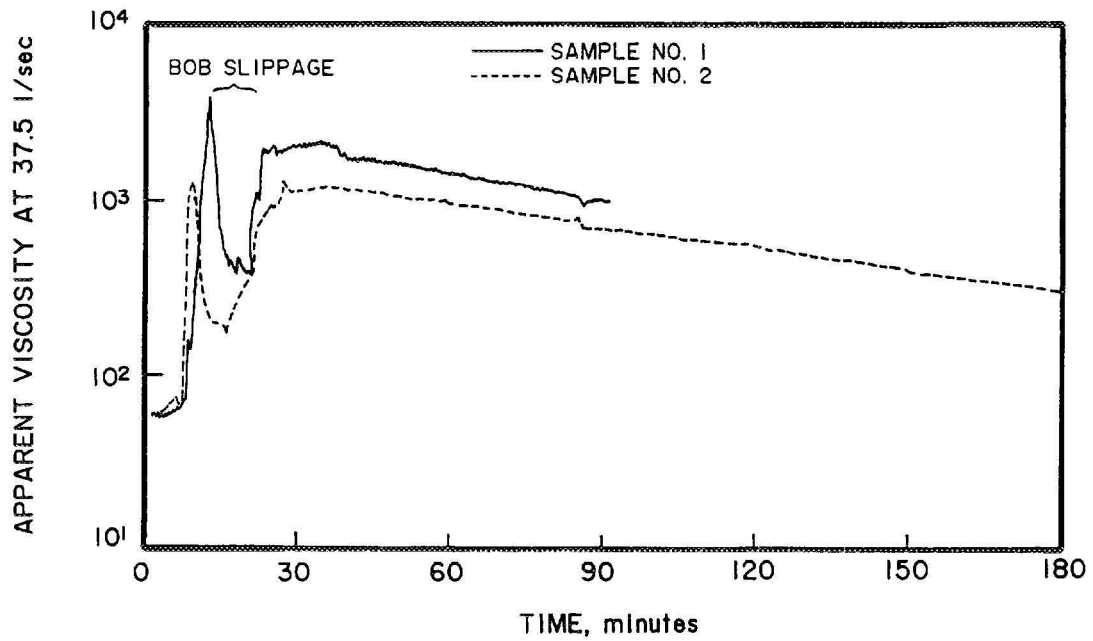


Figure 7-2 Viscosity of Pre-Mixed 40-lbm Gel at Downhole Temperature, SFE No. 3

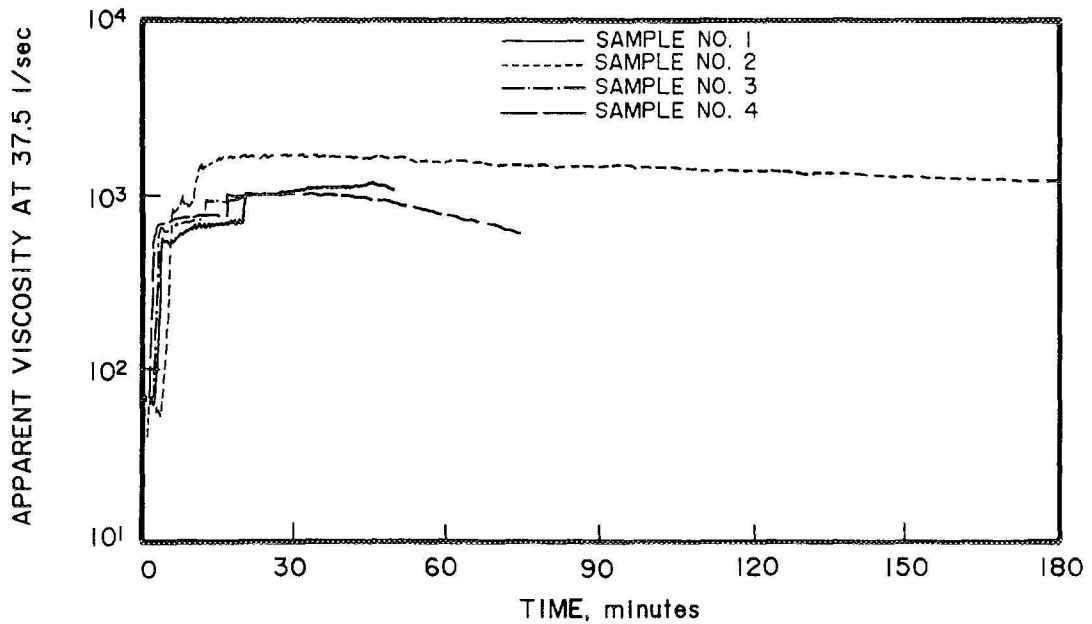


Figure 7-3 Viscosity of 40-lbm Gel (Continuous Mix) at Downhole Temperature, SFE No. 3

tions in downhole viscosity caused by the mixing process. If service companies improve their ability to mix gels during the treatment, then such variations in fluid properties may become less of a factor in real-time analysis of fracture treatments.

7.2.2 Measurement of Fracture Treatment Data

The treatment was pumped down the casing-tubing annulus so that the bottomhole injection pressures could be recorded by a pressure gauge run inside the tubing. Bottomhole treating pressures, as well as casing and tubing pressures, are illustrated in Figure 7-4. Figure 7-5 profiles the proppant concentration as well as the cross-linker, LGC, slurry and diesel flowrates. Traces of the base gel viscosity, the clean and slurry pH levels, and the downhole and fluid temperatures are provided by Figure 7-6.

As can be seen by the comparison of design and actual volumes in Table 7-1, the fracture treatment was pumped essentially as designed. A total of 9,006 bbl of 50- and 40-lbm fracturing fluid were pumped during the main fracture treatment. This volume was in addition to 1,281 bbl of 40-lbm linear gel pumped in the mini-frac just prior to the main frac. A total of 1,168,910 lbm of 20/40 Ottawa sand was pumped at a maximum proppant concentration of 8 lbm/gal.

The average treating pressure was approximately 3,000 psi with an injection rate of 50 bbl/min. A more detailed record of the treatment can be found in Appendix 3.

There were rate changes during the main treatment that indicated that the perforations were probably eroding. The impact of this erosion on the net pressure analysis is discussed in the following section.

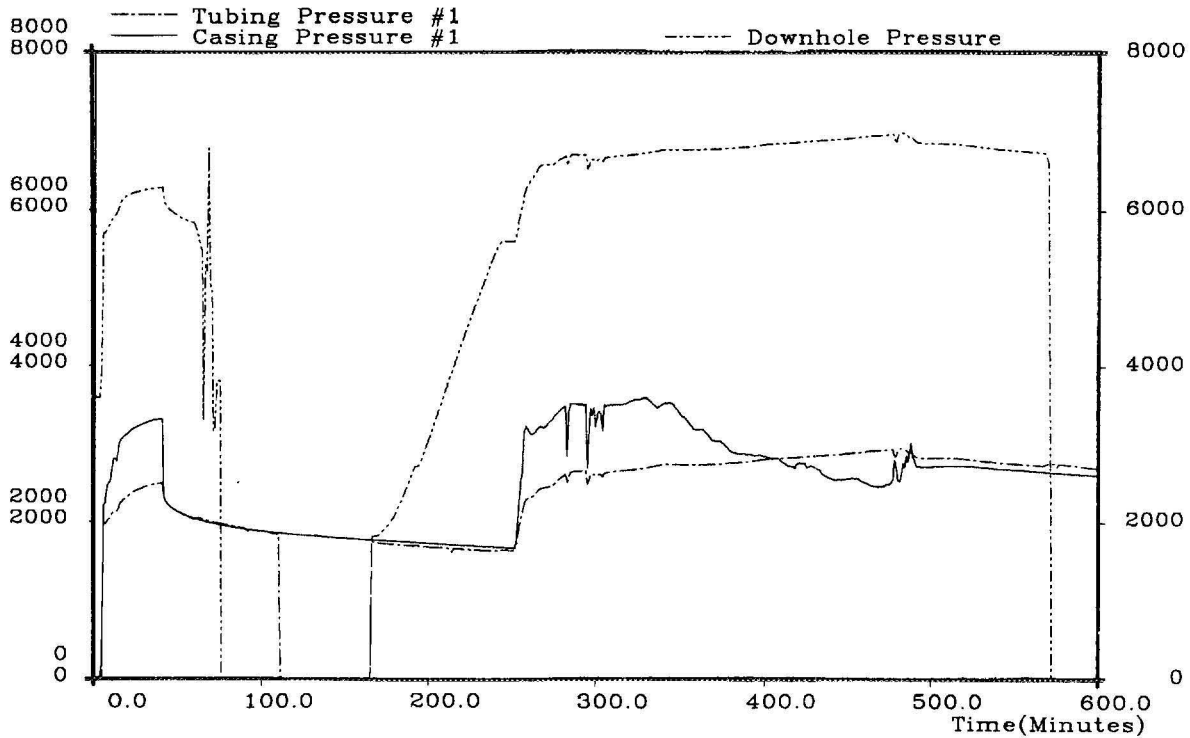


Figure 7-4 Profile of Bottomhole Treating Pressures, Casing Pressures and Tubing Pressures During Treatment

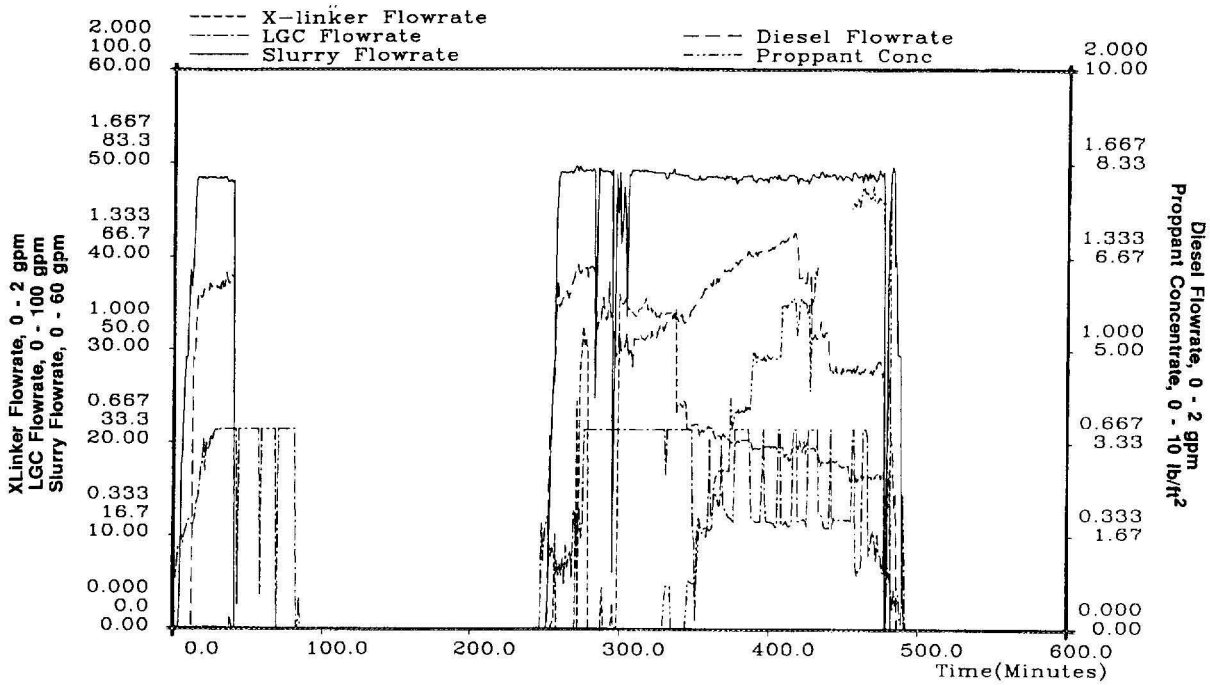


Figure 7-5 Profiles of Proppant Concentration and Cross-Linker, LGC, Slurry and Diesel Flowrates During Treatment

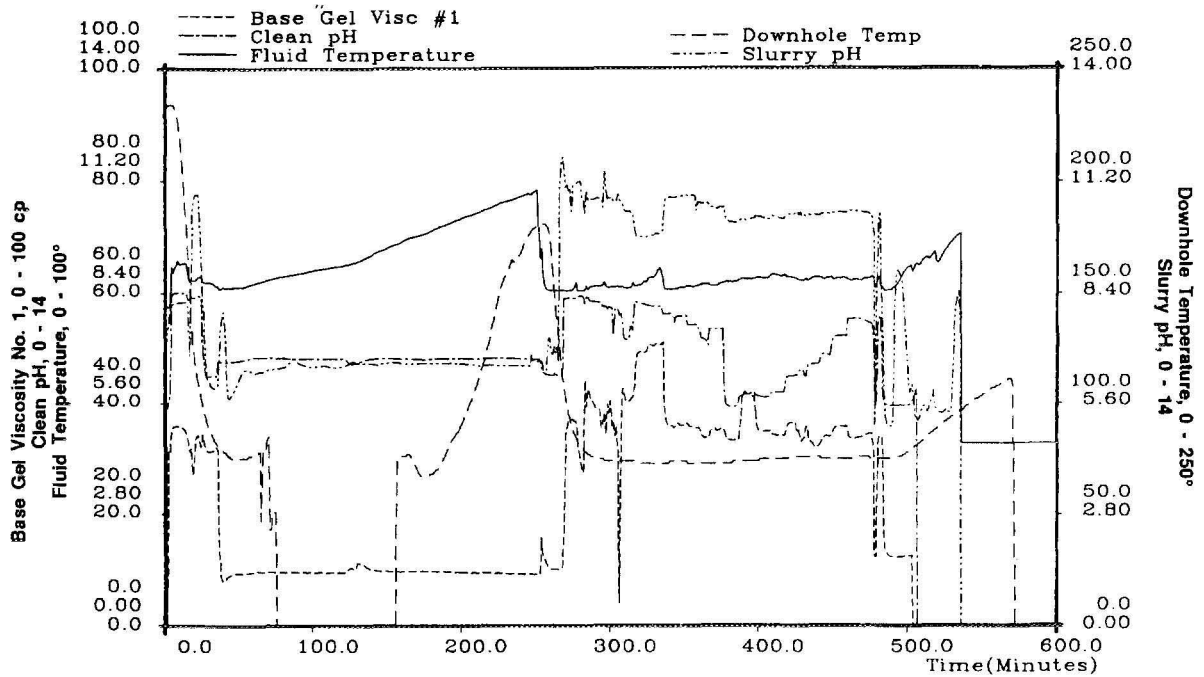


Figure 7-6 Profiles of the Base Gel Viscosity, the Clean and Slurry pH Levels, and the Downhole and Fluid Temperatures During Treatment

7.3 ANALYSIS WITH 3-D FRACTURE SIMULATOR

7.3.1 Net Pressure Analysis

The main-frac net pressure match that is generated with log-derived stresses (Table 6-5) is given in Figure 7-7. The pressure match using modified stresses (Table 6-5) is shown in Figure 7-8. The main frac treatment actually begins just after 250 minutes; the time before corresponds to Mini-Frac No. 2 and the subsequent shut-in. For both matches, the curves for measured net pressure have been corrected for the measured reduction in near-wellbore friction.

Fracture fluid rheological properties were taken from on-site rheometer measurements and were given in Table 6-6. As was discussed previously, the fluid rheological prop-

erties were modified somewhat to account for temperature effects and, more importantly, for the details of leading edge response (i.e., most of the pressure drop occurs near the fracture perimeter). Leakoff parameters (Table 6-9) are the same as those for Mini-Frac No. 2.

Comparison of Figures 7-7 and 7-8 reveals that Figure 7-8 (modified stresses) contains the better match. In Figure 7-7, the rapid drop in calculated net pressure at approximately 300 minutes corresponds with the point when the fracture reached the low stress zone indicated by the log-derived stress data at 9,380 to 9,455 ft. However, the measured net pressure curve shows a much smaller drop. This discrepancy was the rationale for increasing stress in this zone, an interval in which no measured stresses were taken.

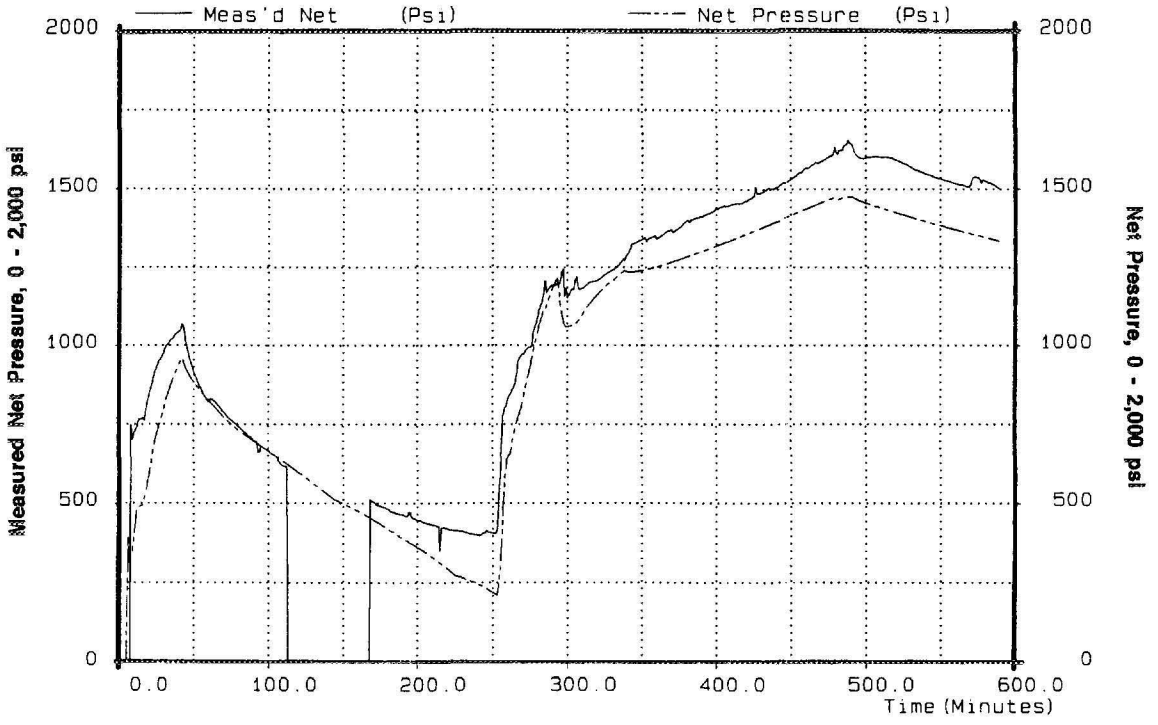


Figure 7-7 Net Pressure Match of Mini-Frac No. 2 and Main Fracture Using Log-Derived Stresses

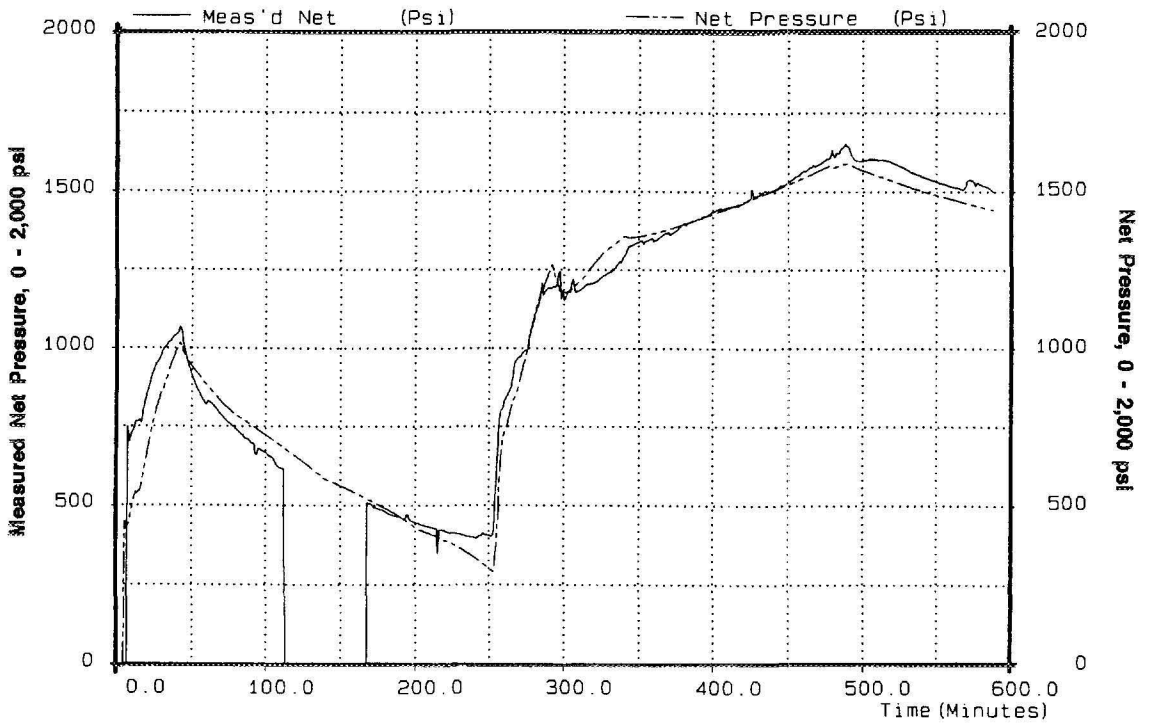


Figure 7-8 Net Pressure Match of Mini-Frac No. 2 and Main Fracture Using Modified Stresses

As was mentioned previously, the measured net pressure curves were corrected for perforation erosion (or other reduction in near-wellbore friction) indicated by the bottomhole pressure response to changes in slurry rate during the main treatment. Consider Figure 7-9 which presents three curves: the slurry rate, the measured net pressure with constant perforation friction, and the model net pressure using modified stresses. The measured net pressure has a discontinuity upon shut-in at about 480 minutes. This behavior indicates that, at the end of the job, excessive perforation friction was subtracted from the bottomhole pressure to arrive at measured net pressure.

Table 7-4 shows the perforation erosion history calculated on the basis of bottomhole pressure response to rate changes during the main frac. From 330 to 480 minutes (shut-in), the average perf diameter changed from 0.330 in. to 0.444 in. Zero pump time is the same as zero time on the pressure match plots.

To reconcile the mini- and main-frac shut-in pressure declines, the entire fracture was assumed to be leaking off. Nonetheless, there were a number of early events after the main-frac shut-in at 480 minutes. A short-time rapid drop (which could be just equilibration in the fracture) is followed by a very slow pressure falloff (which could correspond to pinching by barriers). The subsequent acceleration of falloff at about 525 to 570 minutes (thought perhaps to be associated with break-out into a permeable stratum above) was just stabilizing when flow-back was initiated at 570 minutes. Thus, the match -- which missed many of the above details -- can be viewed only as indicative of an onsetting trend, perhaps consistent with Mini-Frac Nos. 1 and 2. A much longer post-fracture falloff period would certainly have provided for a more definitive interpretation.

7.3.2 Main-Fracture Dimensions

The created dimensions of the main fracture, based on fracture modeling, are given in Figures 7-10 and 7-11 for log-derived stresses and modified stresses, respectively. The change in upper and lower height, the length and the width are shown over the course of the mini- and main frac treatments. Similarly, the propped dimensions with both log-derived and modified stresses are illustrated by Figures 7-12 and 7-13. Table 7-5 lists the main-frac dimensions at the end of the shut-in. Fracture height interpretations based on microseismic data are presented in Section 8.4.

The predicted dimensions calculated by using either log-derived or modified stresses were similar. For example, the fracture wing length using log-derived stresses was 1,751 ft; it was 1,819 ft using modified stresses. The propped length estimates were 1,403 ft and 1,441 ft for log-derived and modified stresses, respectively. The modified stress profile gave lengths approximately 4 percent greater and total heights approximately 3 percent smaller than the stress log profile.

Proppant profiles for the main frac at shut-in are the subjects of Figures 7-14 through 7-17. In Figures 7-14 and 7-15, different shadings and patterns represent the concentration (in lbm/ft^2) of proppant in the fracture. The corresponding stress profiles are also indicated: log-derived stresses for Figure 7-14 and modified stresses for Figure 7-15.

The next two figures give similar information except that the proppant is shown in terms of the volume fraction of proppant within the slurry. Figures 7-16 and 7-17 are for log-derived and modified stresses, respectively. Because the slurry becomes immobile at volume fractions of roughly 0.5 and above, figures of this type can indicate whether there is any possibility of screenout.

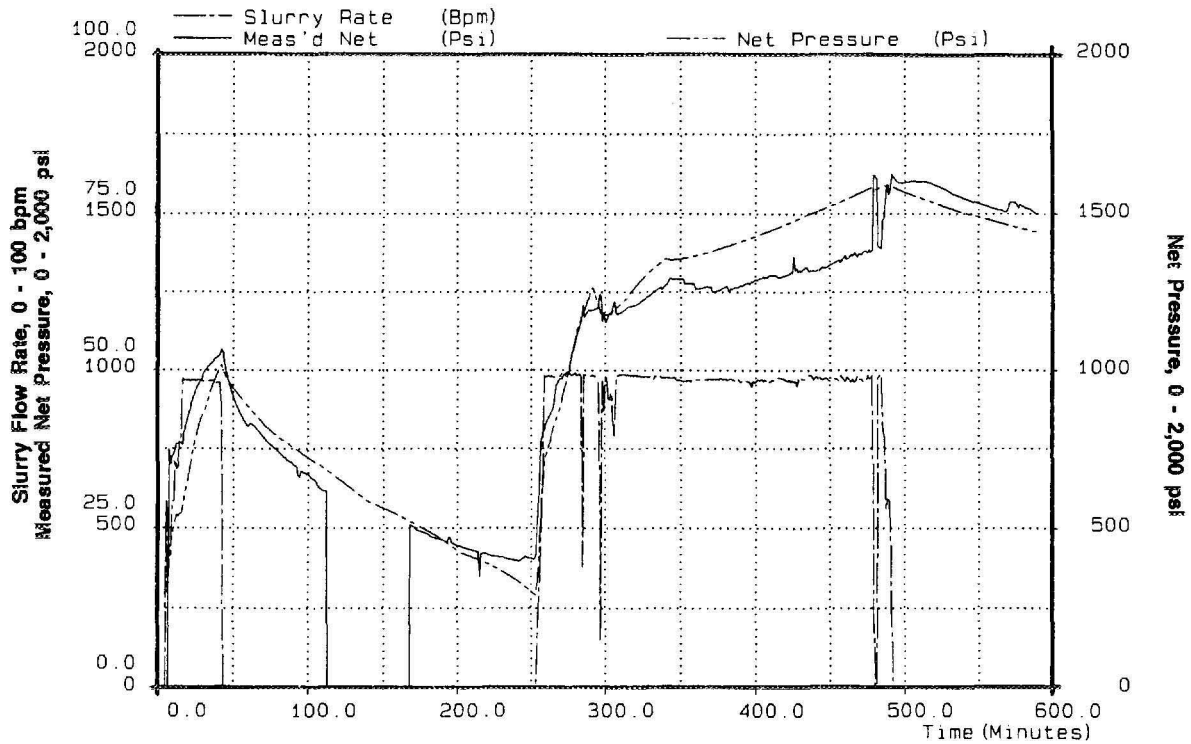


Figure 7-9 Profiles of Slurry Rate, Measured Net Pressure Without Erosion Correction, and Model Net Pressure Using Modified Stresses

Table 7-4 Main-Frac Perforation Erosion History

Pump Time, min	Perf Diameter, in.	Number of Perfs
0.0	0.330	52
330.0	0.330	52
380.0	0.394	52
410.0	0.394	52
480.0	0.444	52

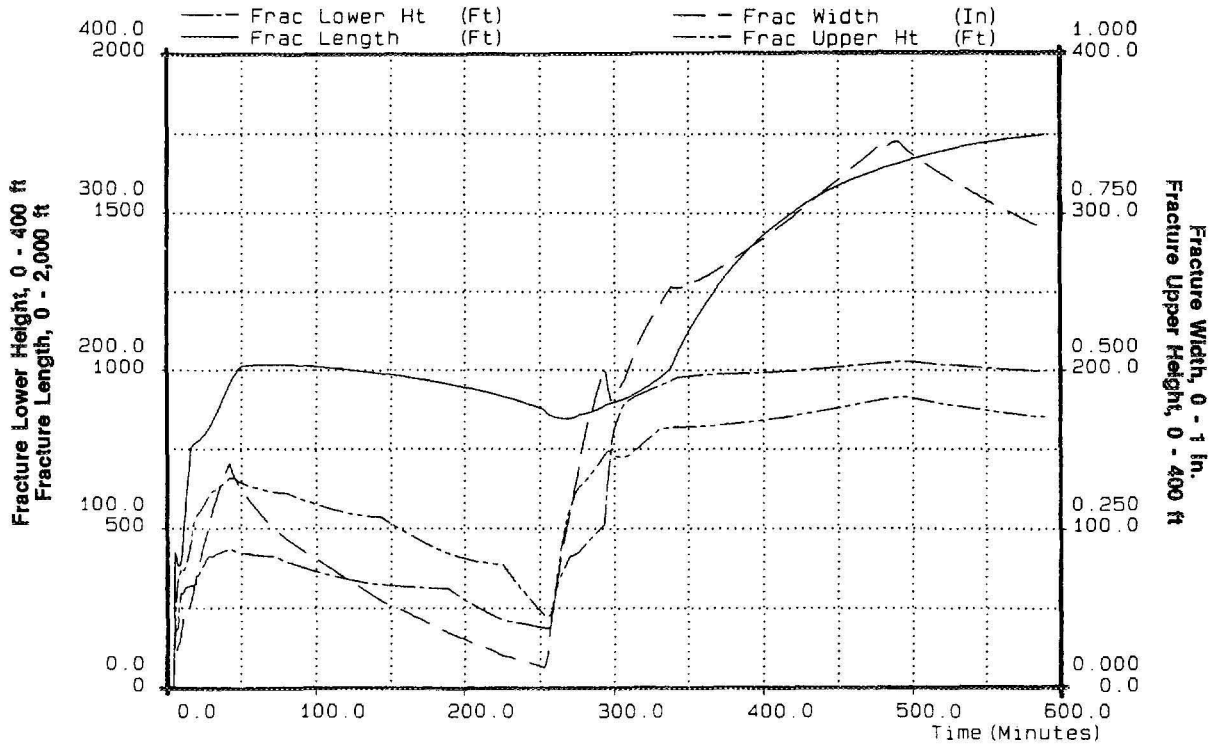


Figure 7-10 Main Fracture Created Dimensions During Treatment Using Log-Derived Stresses

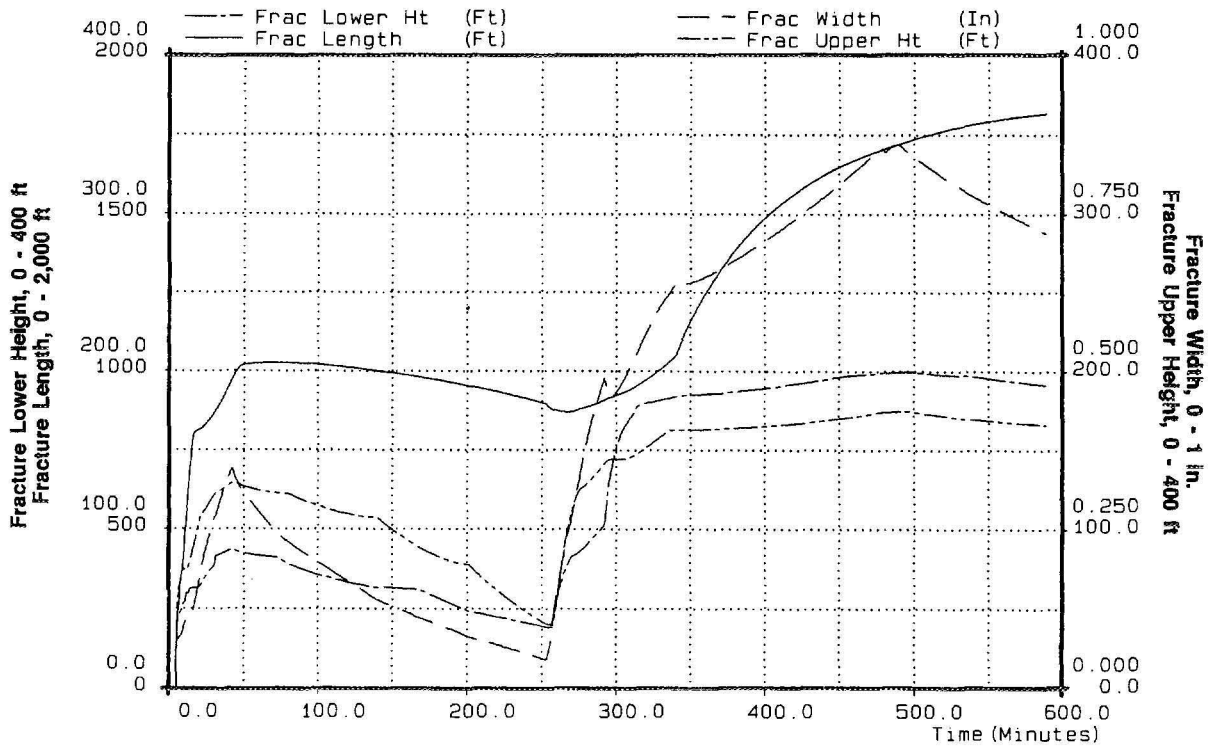


Figure 7-11 Main Fracture Created Dimensions During Treatment Using Modified Stresses

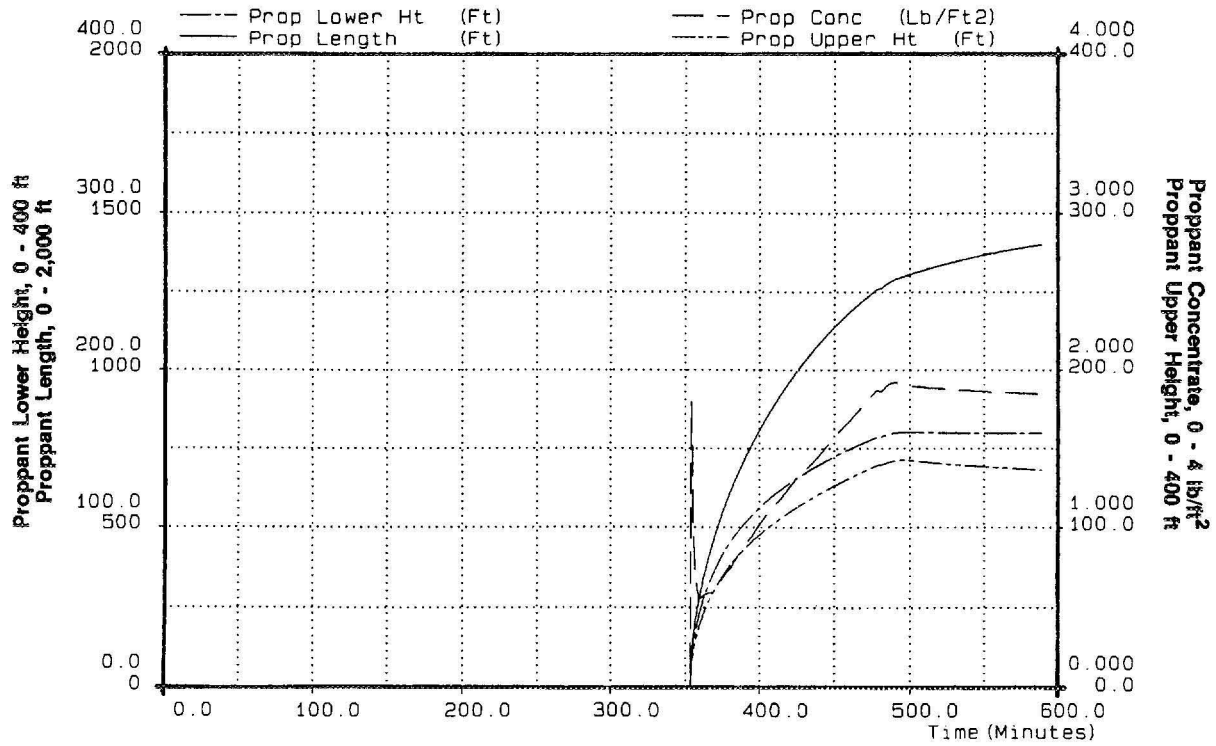


Figure 7-12 Main Fracture Propped Dimensions During Treatment Using Log-Derived Stresses

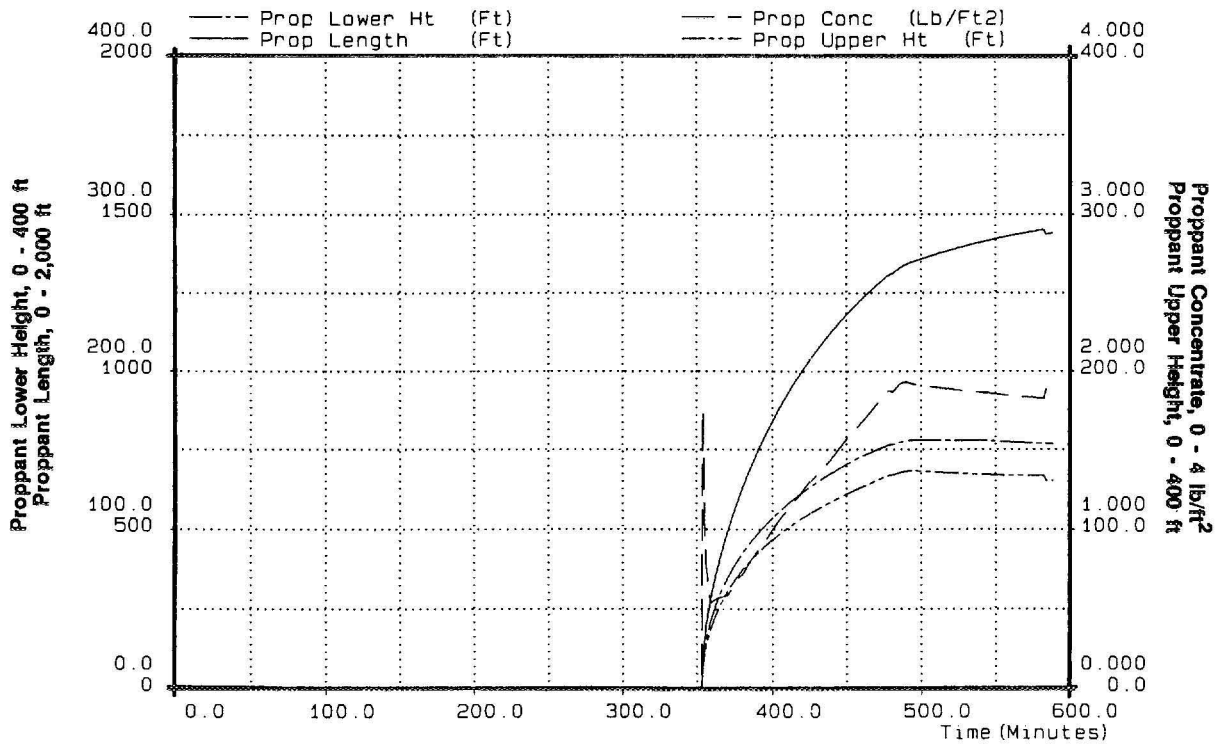


Figure 7-13 Main Fracture Propped Dimensions During Treatment Using Modified Stresses

Table 7-5 Main Fracture Dimensions at End of Shut-In as Determined by FRACPRO Analysis

Parameters	Stresses From Log	Modified Stresses
Fracture Wing Length, ft	1,751	1,819
Fracture Upper Height, ft	170	166
Fracture Lower Height, ft	200	192
Fracture Width (Max), in.	0.72	0.72
Fracture Aspect Ratio	9.46	10.2
Propped Length, ft	1,403	1,441
Propped Upper Height, ft	136	130
Propped Lower Height, ft	160	154
Proppant Concentration, lbm/ft ²	1.85	1.88
Propped Aspect Ratio	9.48	10.1

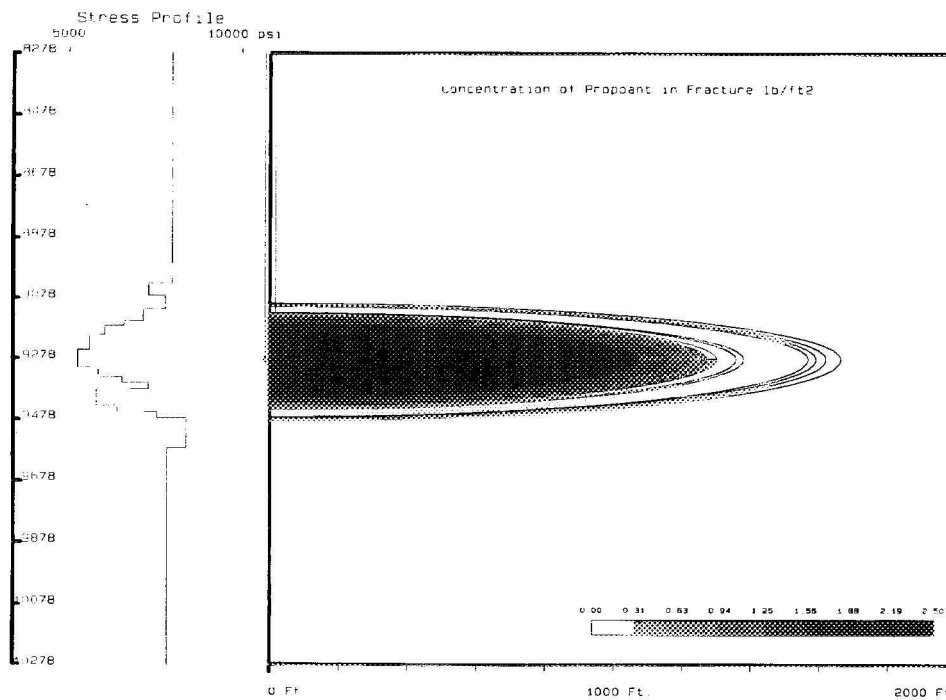


Figure 7-14 Proppant Concentration Profile at Treatment Shut-In Using Log-Derived Stresses

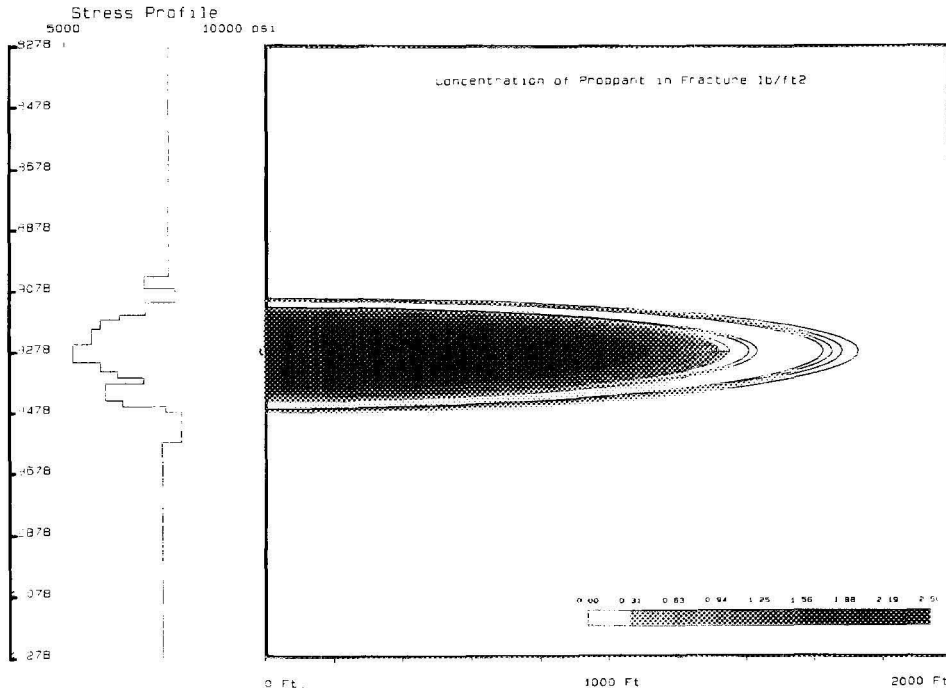


Figure 7-15 Proppant Concentration Profile at Treatment Shut-In Using Modified Stresses

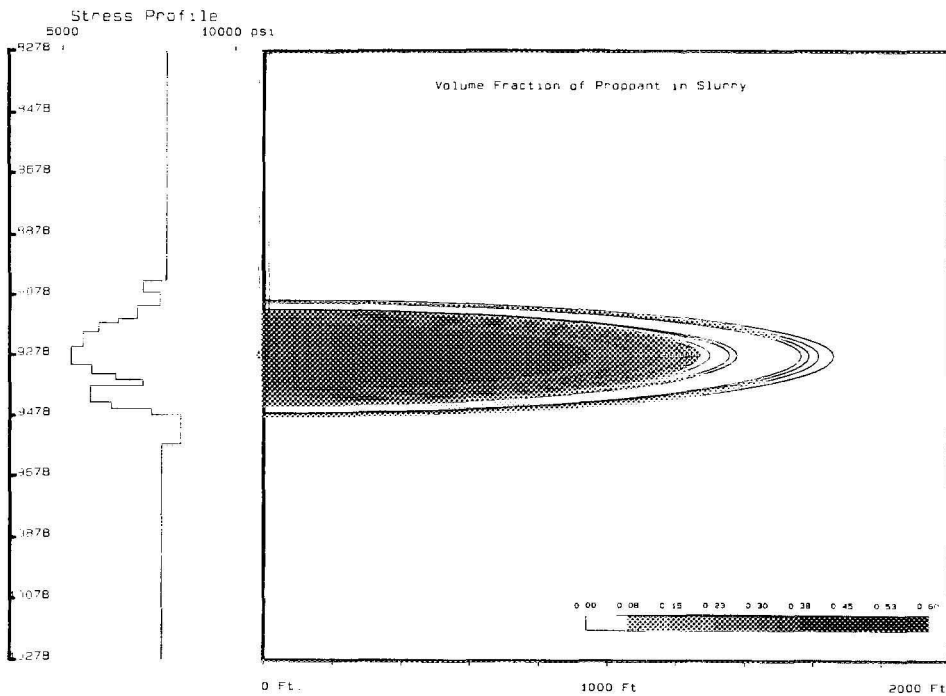


Figure 7-16 Volume Fraction of Proppant in Slurry at Treatment Shut-In Using Log-Derived Stresses

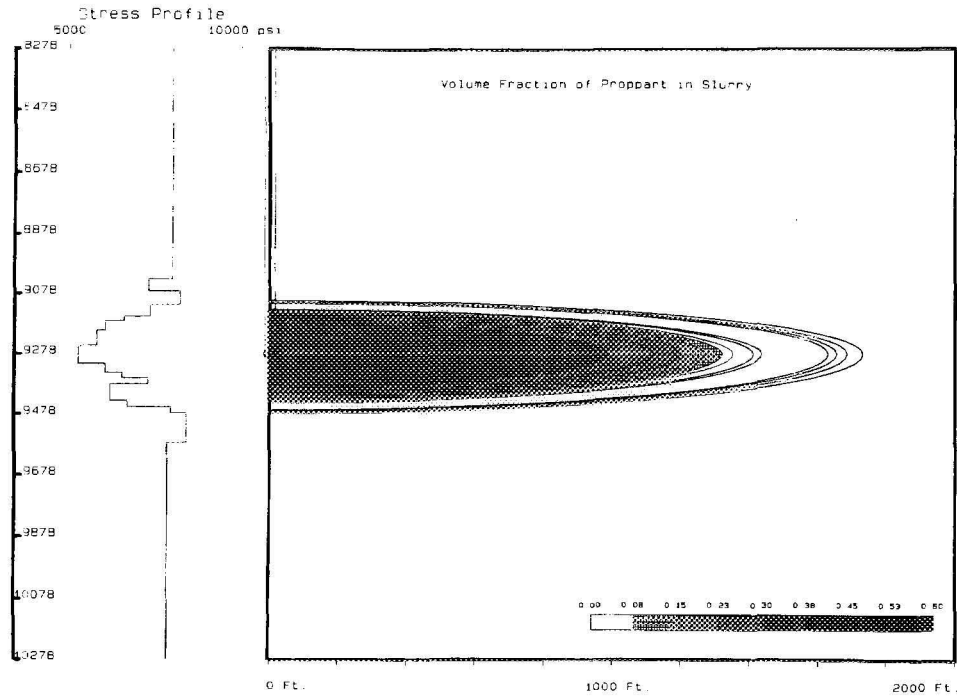


Figure 7-17 Volume Fraction of Proppant in Slurry at Treatment Shut-In Using Modified Stresses

Figures 7-16 and 7-17 reveal that there was little or no risk of screen-out. In addition, the concentration results using the two stress profiles were quite similar, as they

were for the dimensions. The average proppant concentration for the modified stress profile was about 2 percent less than for the log-derived stress profile.

8.0 Post-Fracture Analysis

8.1 PRODUCTION PERFORMANCE

SFE No. 3 was fracture treated on March 16, 1989, and post-frac production began the following day. It continued for 89 days at which time a post-frac pressure buildup test was performed.

Figure 8-1 illustrates the post-frac production history up to the time of the pressure buildup test. Gas production began after approximately four days of flow during which 1,890 bbl of water were produced prior to gas breakthrough. As illustrated, the gas rate steadily increased until it eventually stabilized at approximately 500 MCFD. Meanwhile, the water rate continuously decreased before leveling off at approximately 25 BPD. On April 22, the well was opened to the sales line. The gas rate dropped to its final

value of about 325 MCFD, flowing against a line pressure of 775 psi.

On June 16, the well was shut in for an extended pressure buildup test. Total post-frac production at that point was 34,127 MCF of gas, 8,992 bbl of water and 244 bbl of condensate. The final flow rates prior to shut-in were 320 MCFD, 24 BWPD and 2 BCPD.

8.2 CONVENTIONAL WELL TEST AND PRESSURE BUILDUP ANALYSIS

Following the post-fracture production period, SFE No. 3 was shut in for an extended pressure buildup test on June 16, 1989 and it remained shut in until July 14, 1989. Total shut-in time was 661 hours. A sur-

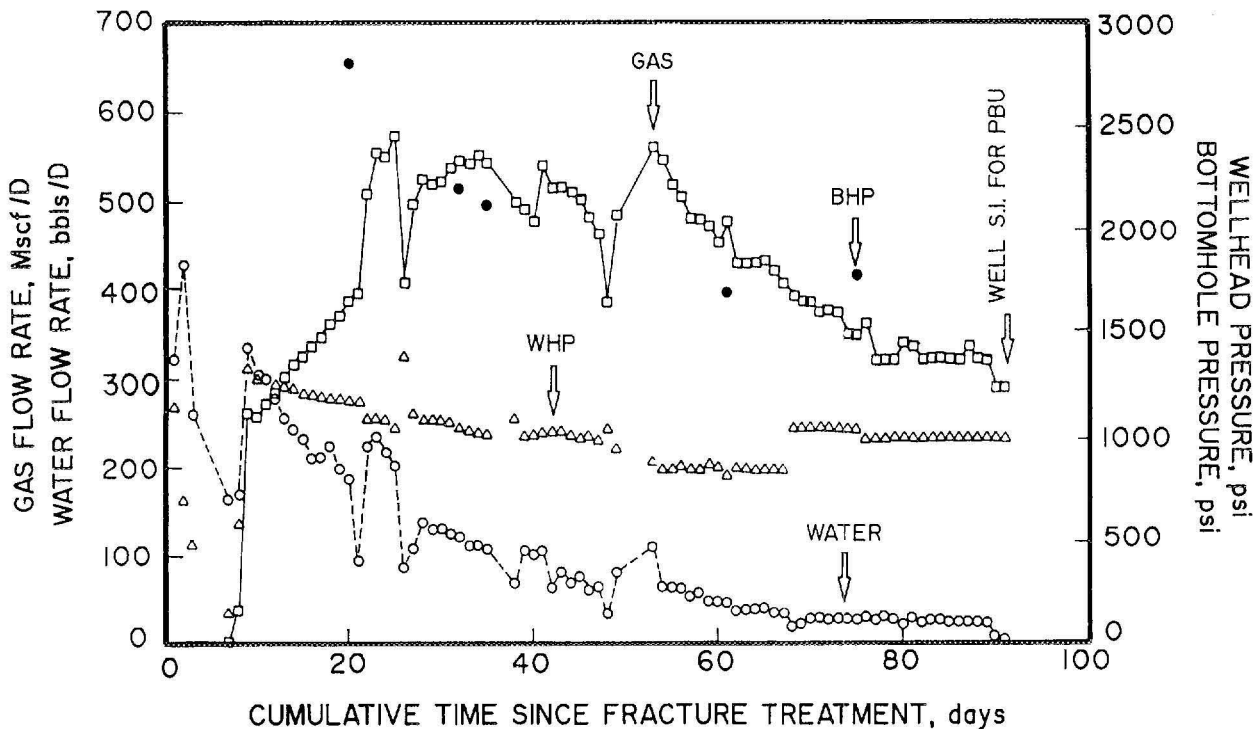


Figure 8-1 Post-Fracture Production History



face-readout quartz pressure gauge was used to monitor the bottomhole pressures during the buildup test. The flowing bottomhole pressure at the start of shut-in was 1,871 psia. By the end of the shut-in period, the bottomhole pressure increased to 2,731 psia.

Figure 8-2 shows a logarithmic plot of shut-in time vs. change in pressure during the pressure buildup test. Qualitative analysis of this plot shows that pseudo-radial flow was not reached and, therefore, a semi-log analysis was not applicable. As a result, this buildup test was evaluated quantitatively using type curves and linear flow analysis.

Cinco type curves (Cinco, 1978) were used to obtain the match shown in Figure 8-2. An acceptable match of the late-time data was obtained which indicated that a short, high conductivity fracture was achieved.

The calculated reservoir and fracture properties are listed in Table 8-1a. The same values for net gas pay (40 ft), total porosity (9.2 percent) and water saturation (30.0 percent) used for the post-mini-frac pressure buildup test were also used for this analysis since the fracture treatment analysis indicated that the fracture stayed contained mainly within the Taylor interval.

To verify the Cinco type-curve analysis, a similar analysis was performed using the Ramey-Barker type curves (Barker and Ramey, 1978). Unlike the Cinco curve, the Ramey-Barker curve used assumes infinite conductivity fractures; it also takes into account wellbore storage. A good match of the actual data was obtained, as shown in Figure 8-3. The results of the Ramey-Barker type-curve analysis, which assumed the same values for the formation properties, are given in Table 8-1b.

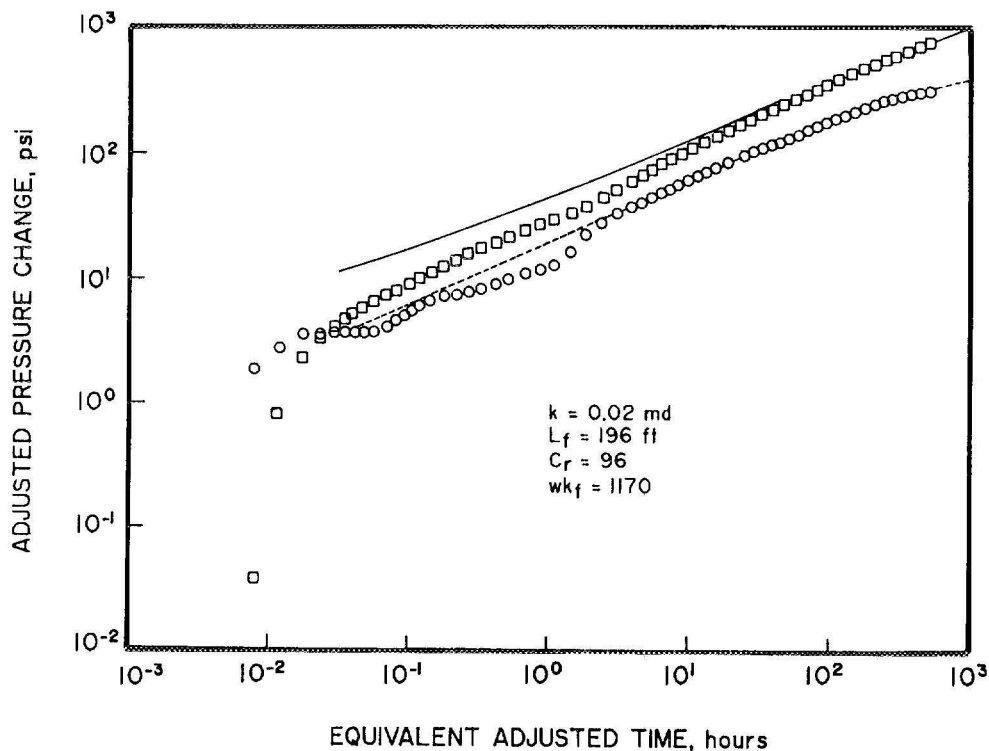


Figure 8-2 Cinco Type-Curve Analysis Assuming Finite Conductivity Hydraulic Fracture

Table 8-1a Results of Cinco Type-Curve Match of Post-Fracture PBU Data

In-Situ Permeability to Gas (k_g), md	0.020
Fracture Conductivity (ωk_f), md-ft	1,170
Dimensionless Fracture Conductivity (Cr)	96
Propped Fracture Half-Length (L_f), ft	196

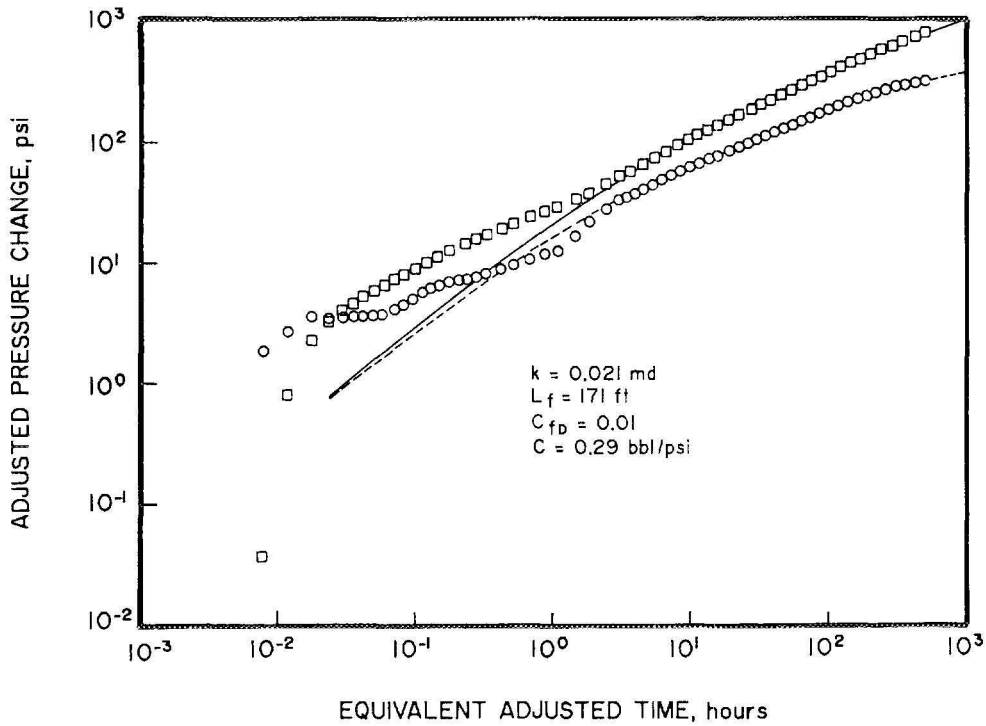


Figure 8-3 Ramey-Barker Type-Curve Analysis Assuming Infinite Conductivity Hydraulic Fracture With Wellbore Storage

Table 8-1b Results of Ramey-Barker Type-Curve Match of Post-Fracture PBU Data

In-Situ Permeability to Gas (k_g), md	0.021
Fracture Conductivity (ωk_f), md-ft	1,100
Dimensionless Fracture Conductivity (Cr)	> 100
Propped Fracture Half-Length (L_f), ft	171

Figure 8-4 presents a linear flow analysis of the pressure buildup test. The straight line portion of the curve at square-root-of-time less than 10 represents an early linear flow period. Based on the gas permeability from the type-curve analyses (0.020 md) and the slope of this early straight line, the propped fracture length was calculated to be 206 ft.

Although the type-curve analysis indicated that the semi-log, or Horner, plot could not be used to estimate the actual permeability, the semi-log plot could be used to approximate the maximum permeability as well as the reservoir pressure. Figure 8-5 presents the results from the semi-log analysis.

If one used the apparent straight line through the last few data points, the estimated permeability would be 0.042 md with a skin factor of -4.9. However, had the shut-in been continued until the proper straight-line portion was reached, the pres-

sure curve would have continued to bend upwards so that the slope of the later data points continuously increased. Of course, this behavior assumes there are no mitigating factors such as a boundary. An increase in slope translates into a decrease in the estimated permeability. Therefore, the estimated permeability based on the slope of the last data points is a maximum value.

To approximate reservoir pressure, a straight line was drawn from the last data point. Its slope was that which would result in a permeability of about 0.020 md. Extrapolating this straight line to infinite shut-in time (Horner time = 1) indicates a P' of at least 3,600 psia. This extrapolation, which probably results in a good estimate for average reservoir pressure, assumes the following: the flow time was chosen correctly; the flow would have settled into radial flow during the extrapolated period; and there are no significant boundary or interference effects.

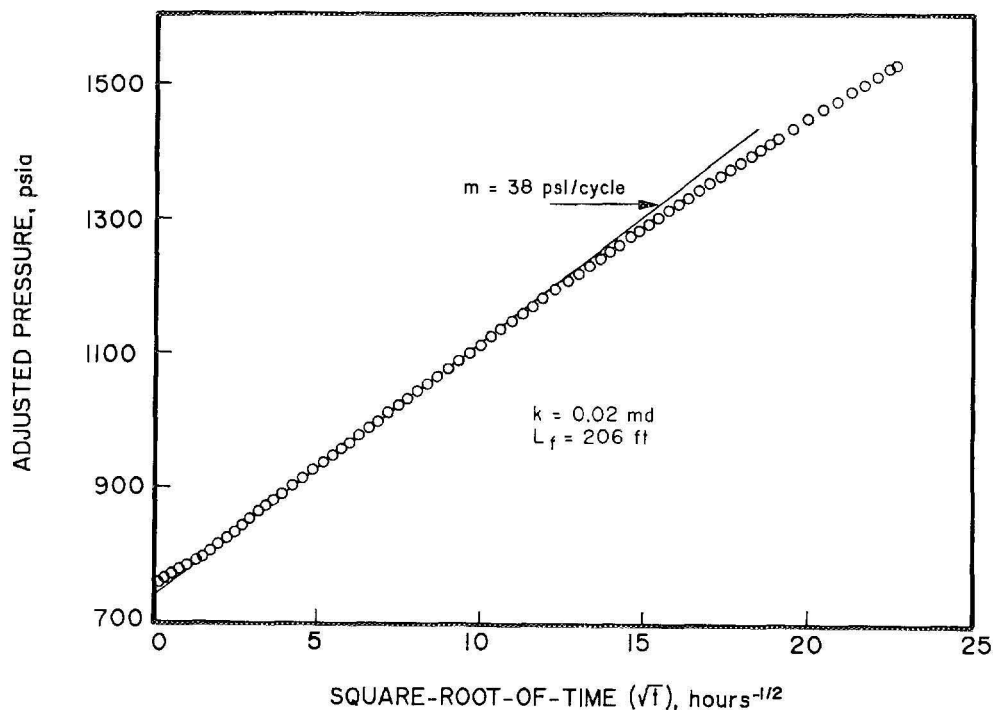


Figure 8-4 Linear Flow Analysis of Post-Fracture Buildup Test

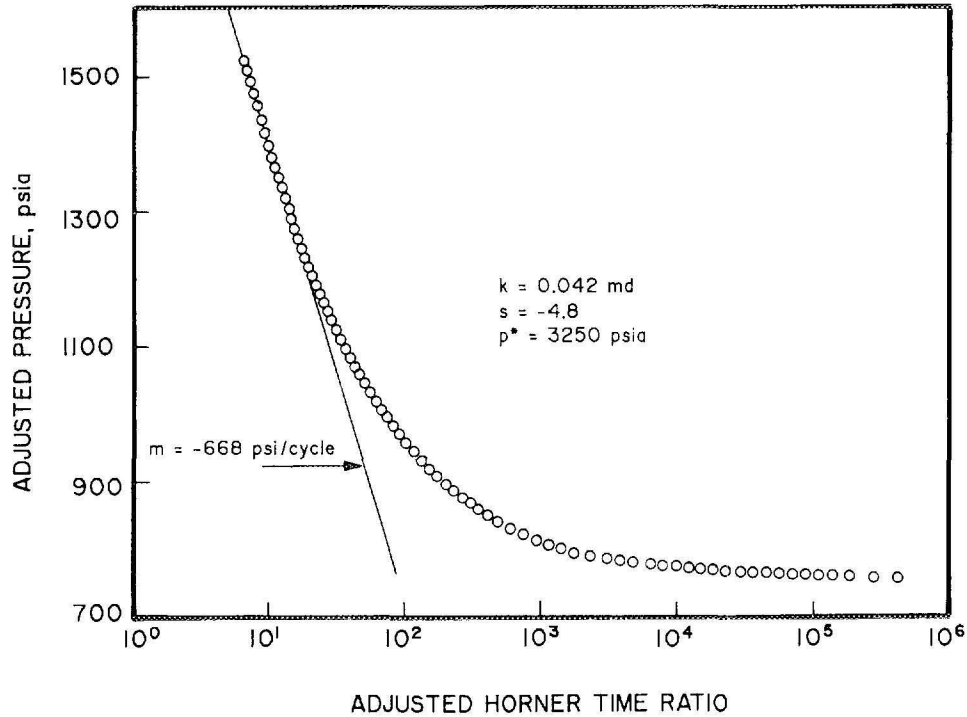


Figure 8-5 Horner Analysis of Post-Fracture Buildup Test

All of the different analysis methods agreed well. A summary of each analysis and a listing of the plotting functions and input parameters are included in Appendix 3. The combined results of the various conventional analyses are given by Table 8-1c.

Even though the conventional analyses of the post-fracture pressure buildup data provided consistent results, it is not believed that the results accurately describe the reservoir. The estimates of $kh = 0.8 \text{ md-ft}$ and $k = 0.02 \text{ md}$ are probably accurate. The estimates of $L_f = 200 \text{ ft}$ and $\omega k_f = 1,170 \text{ md-ft}$ only depict the portion of the hydraulic fracture that has "cleaned-up" and is affecting gas flow at the time of the pressure buildup test.

Based upon both the size of the hydraulic fracture treatment pumped on SFE No. 3 and upon previous experience gained primarily during the GRI Tight Sands Research

project during the past six years, it was obvious to researchers that a fracture longer than 200 ft was created and propped. The fracture was there, but the majority of it had not cleaned up enough to affect either the gas production or the pressure buildup test data.

The conventional analyses methods assume single-phase flow of a constant viscosity, constant compressibility fluid. The methods also assume the fracture conductivity is constant in time and space. To overcome these assumptions, numerical simulation models must be used to history match the production and pressure buildup data.

8.3 RESERVOIR SIMULATION

8.3.1 Description of Models

Reservoir simulation can account for numerous factors that cannot be adequately

Table 8-1c Combined Results of Analytical Analyses of Post-Fracture PBU Data

Net Gas Pay (h), ft	40
Total Porosity (ϕ), %	9.2
Water Saturation (S_w), %	30.0
In-Situ Permeability (k_g), md	0.020
Fracture Conductivity (ωk_f), md-ft	1,170 ($\sim\infty$)
Dimensionless Fracture Conductivity (Cr)	93
Propped Fracture Half-Length (L_f), ft	200

modeled by conventional analytical techniques. Examples include the following:

- multi-phase (gas-water) flow;
- fracture cleanup and gas breakthrough behavior;
- reservoir heterogeneity; and
- multi-layered reservoirs.

These factors can significantly impact the evaluation of post-fracture well performance. In SFE No. 3, multi-phase flow and fracture fluid cleanup are particularly important. Following the main fracture treatment, SFE No. 3 produced only water for several days. Moreover, water rates of at least 100 BPD were recorded for over two months. During the remaining producing period, the well produced at a water/gas ratio of about 0.1 bbl/MCF. To properly simulate the effects of fracture fluid cleanup and subsequent water production, a multi-phase model must be used.

Several models have been used to simulate flow from the Taylor sandstone completion in SFE No. 3. The models can be grouped

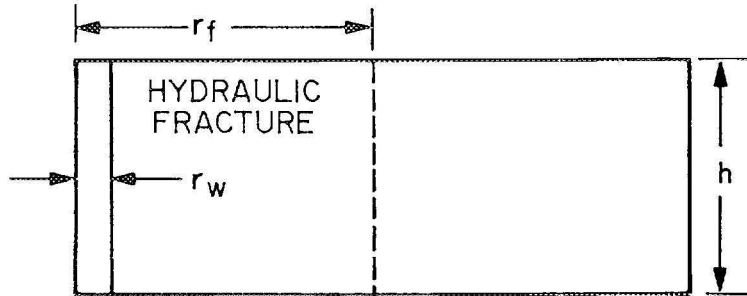
into three categories, presented below in Table 8-2.

Table 8-2 Description of Models Used in SFE No. 3 History Matching

Model Type	Model Geometry	Phase Configuration
I	1-D Radial	Single-Phase Gas
II	2-D Areal	Single-Phase Gas
III	3-D Areal	Two-Phase Gas-Water

Schematics of the model geometries, radial and areal, are presented in Figure 8-6. When analyzing post-fracture performance, S.A. Holditch & Associates, Inc. generally starts with simpler models, then proceeds to more complex models to increase the accuracy of the results. The simplest models are the single-phase radial systems, such as Type I. Type II models add complexity by modeling the fracture, but these are also considered relatively simple be-

ONE-DIMENSIONAL RADIAL
MODEL TYPE I



TWO-DIMENSIONAL AND
THREE-DIMENSIONAL AREAL MODEL
MODEL TYPES II AND III

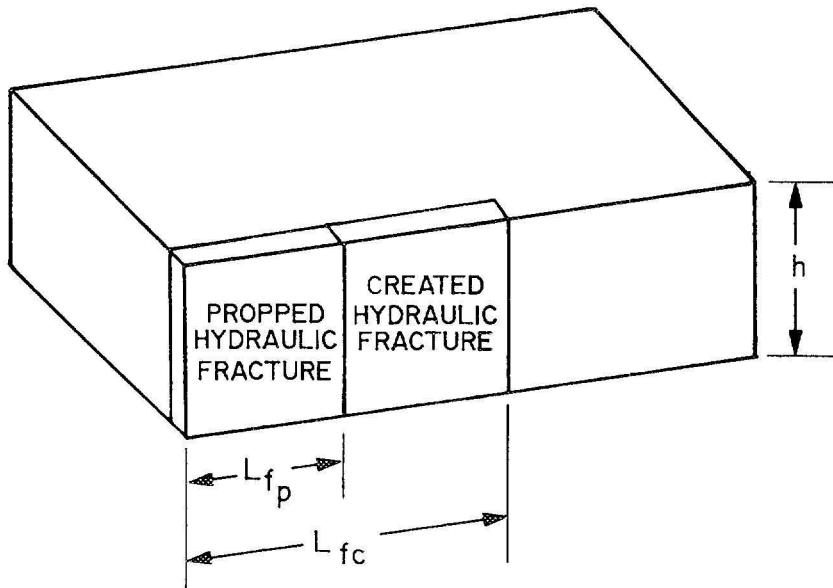


Figure 8-6 Reservoir Simulation Model Types

cause multi-phase flow is not taken into account. Model complexity is further increased by moving from a radial geometry to an areal geometry. The final increase in complexity occurs when moving to a three-dimensional model and adding the water phase to the problem, as in Model Type III.

The primary advantage of the simple models is speed. Radial models and single-phase models require considerably less computer time. Therefore, these models can be used to obtain qualitative and, to a limited degree, quantitative estimates of the fracture and reservoir properties required to match the post-fracture well history. Once an acceptable estimate of reservoir and fracture properties is obtained with the simple models, more sophisticated models can be used to obtain a final history match of the reservoir performance.

The use of radial models in history matching a hydraulically-fractured reservoir requires the transformation of fracture properties from a linear flow system to a radial flow system. In a radial model, the fracture is modeled by using a hydraulic fracture radius (r_f) that is related to the fracture half-length (L_f) by the following equation:

$$r_f = \frac{4L_f}{2\pi} \quad \text{Eq. 8-1}$$

This equation simply assumes that the cross-sectional area of the radial fracture system at a radial distance of r_f is equal to the cross-sectional area of the four sides of a hydraulic fracture with a half-length of L_f . Once a hydraulic fracture radius is obtained, the storage volume of the radial fracture system (ϕ_r) can be equated to the volume of the hydraulic fracture (ϕ_f) using the Equation 8-2:

$$\phi_r = \frac{2L_f\omega\phi_f}{\pi r_f^2} \quad \text{Eq. 8-2}$$

where ω = fracture width. Using these two equations, a hydraulic fracture can be simulated in a radial model (Type I).

8.3.2 Analysis Using Type I Model

Results of the radial model history matching, shown in Figure 8-7, were very similar to the conventional analytical results. An excellent match of the observed bottomhole pressures during the post-fracture pressure buildup test was obtained. The input parameters appear in Table 8-3a.

8.3.3 Analysis Using Type II Model

The next step in the history matching process was to use a 2-D, single-phase, finite-difference reservoir simulator so that the propped fracture could be more accurately modeled. Initial input to this model was based on the results of the conventional analyses and the 1-D, single-phase model. Reservoir and fracture properties, such as permeability and fracture length, were varied as necessary to obtain the best match possible.

Figure 8-8 presents the results of the first match obtained using this model. The match was based on the properties listed in Table 8-3b. These results were very similar to those achieved with both the conventional analyses (i.e., Horner analysis and type-curve analysis) and the Type I model simulation. However, the calculated fracture half-length was much less than the original design value of 1,000 ft as well as the results of the fracture treatment analysis (Section 7.3). Based on previous results from the GRI Tight Gas Sands Research Program, it was suspected that the single-phase analyses results would not be indicative of the actual propped fracture length because of the water that still remained both in the fracture and in the reservoir when the pressure buildup test was run.

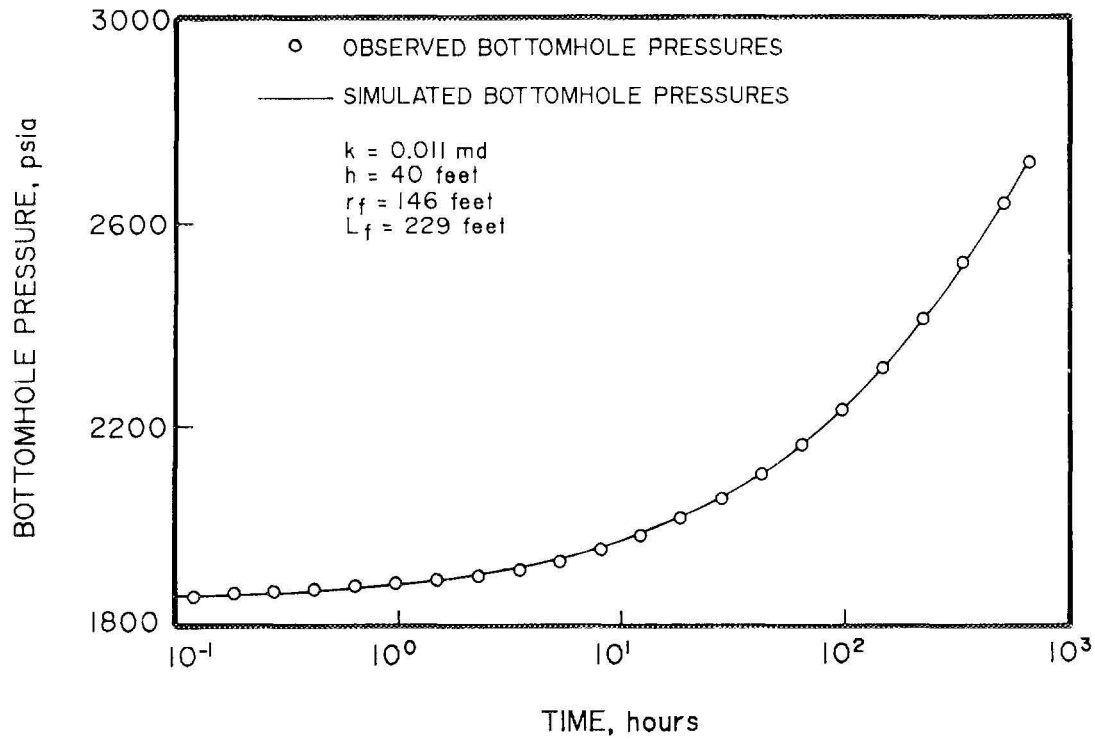


Figure 8-7 Results of 1-D, Single-Phase, Radial Model History Match

Table 8-3a Parameters for 1-D, Radial, Single-Phase Model (Type I)

Net Gas Pay (h), ft	40
Formation Permeability (k), md	0.011
Fracture Conductivity (ωk_f), md-ft	$\sim\infty$
Dimensionless Fracure Conductivity (Cr)	$\sim\infty$
Hydraulic Fracture Radius (r _f), ft	146
Equivalent, Infinite Conductivity, Fracture Half-Length (L _f), ft	229

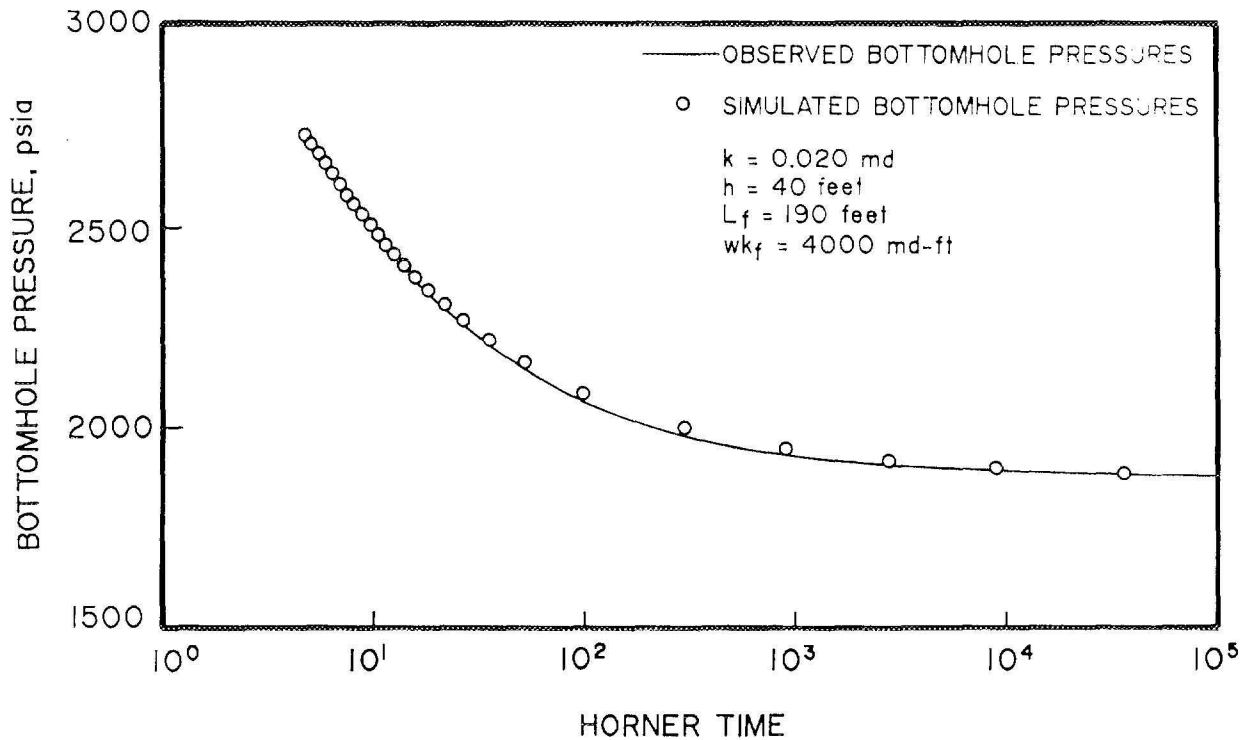


Figure 8-8 Results of 2-D, Single-Phase, Areal Model With Single-Conductivity-Function History Match

Table 8-3b Parameters for 2-D, Areal, Single-Phase Model (Type II)

Net Gas Pay (h), ft	40
Formation Permeability (k), md	0.020
Fracture Conductivity (ωk_f), md-ft	4,000
Dimensionless Fracture Conductivity (Cr)	335
Fracture Half-Length (L _f), ft	190

Attempts were made at simulating a much longer fracture and accounting for the "unseen" portion of the fracture by varying the fracture conductivity down the length of the fracture; thus, the conductivity would be high near the wellbore, decreasing out to the tip. Initially, very long fractures were simulated with no success. Reasonable matches of the production data and the pressure buildup data could not be obtained until the fracture length was reduced.

The final match using this approach is shown in Figure 8-9. Reservoir and fracture properties used to obtain the match are presented in Table 8-3c. Although the curvature of the simulated data in Figure 8-9 is not exactly that of the observed data, this match is sufficient to show that a longer total fracture length may be present. If so, the fracture conductivity away from the wellbore is apparently much less than the conductivity near the wellbore.

8.3.4 Analysis Using FAST

The final single-phase analysis performed on the SFE No. 3 post-fracture tests was accomplished using FAST. This model, which uses semi-analytic solutions, is being developed for GRI by Texas A&M University. FAST is designed to run much faster than a finite difference reservoir simulator and to give accurate results when history matching actual data or predicting future production. Figure 8-10 presents the graphical results of this history match. Analysis results used to generate this match are shown in Table 8-3d.

This match yielded an acceptable estimate of the reservoir and fracture properties. Moreover, FAST was much easier and faster to use than the more complicated, finite difference models. Still in the developmental phase, this model should be completed in 1990, thus providing a useful tool for analyzing gas reservoirs.

8.3.5 Analysis Using a Type III Model

Because of the water introduced into the system via the fracture treatment, this problem should actually be treated as a two-phase flow situation. Correct modeling of the gas and water flow is essential to determine the actual fracture and reservoir parameters. A two-phase analysis (Model Type III) will also result in a better prediction of reserves and future flow rates for SFE No. 3.

The simulator used in this portion of the study (SABRE) was a three-dimensional, three-phase reservoir simulator. Only two-phase (gas-water) flow was considered in this work because the well produced only gas and water with negligible amounts of condensate. A two-dimensional areal model was deemed sufficient for this study. Assuming a symmetrical drainage area and two equal wing-lengths of the fracture, only a quarter of the total area was simulated. Volumetric consistency was accounted for by using an interval thickness four times the actual thickness of the reservoir.

The total number of grids (or blocks) for the model was 23 x 15 x 1 (in the x, y and z axes, respectively), where the x-axis was along the fracture and the z-direction was the thickness. Twenty out of 23 grids were assigned for the fracture. Permeability and porosity were varied within the fracture grids to represent the propped and created fracture zones. Finer grids were used near the transitions between the propped and created fracture zones and between the created fracture and the matrix. Figure 8-11 shows a diagram of the model grid system.

Reservoir data and rock properties used for the initial estimates came from core analyses, log analyses and the single-phase, post-fracture, pressure buildup analysis. History matching in this study was divided into three stages: (1) water injection; (2)

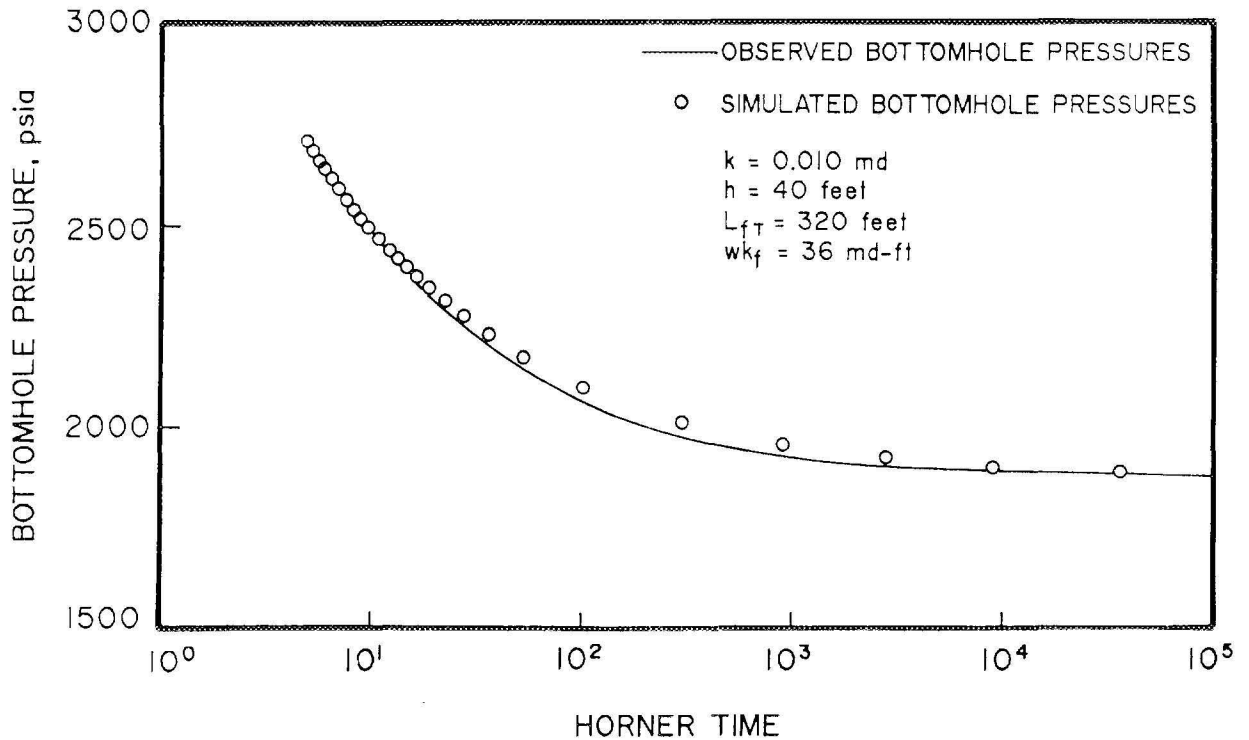


Figure 8-9 Results of 2-D, Single-Phase, Areal Model With Variable-Conductivity-Function History Match

Table 8-3c Parameters for 12, Areal, Single-Phase Model (Type II) With Variable Fracture Conductivity

Net Gas Pay (h), ft	40
Formation Permeability (k), md	0.010
Average Fracture Conductivity (ωk_f), md-ft	36.0
Average Dimensionless Fracture Conductivity (C_r)	3.58
Total Fracture Half-Length (L_f), ft	320
Fracture Segment Length for Variable Conductivity Calculations, ft	80
Fracture Conductivity of First Fracture Segment (ωk_{f1}), md-ft	10,000
Fracture Conductivity of Second Fracture Segment (ωk_{f2}), md-ft	1,000
Fracture Conductivity of Third Fracture Segment (ωk_{f3}), md-ft	100
Fracture Conductivity of Fourth Fracture Segment (ωk_{f4}), md-ft	10

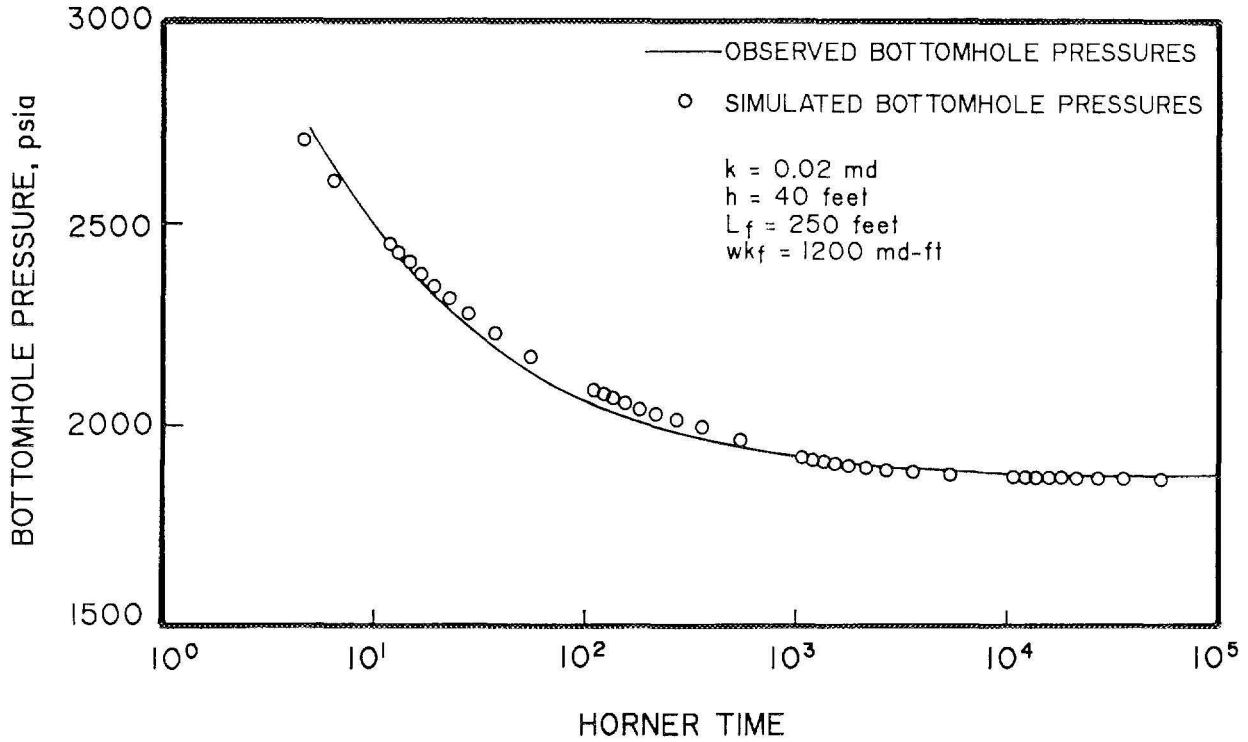


Figure 8-10 Results of Semi-Analytic Reservoir Model (FAST) History Match

Table 8-3d Parameters for 2-D, Single-Phase, Semi-Analytic Model (FAST)

Net Gas Pay (h), ft	40
Formation Permeability (k), md	0.02
Fracture Conductivity (ωk_f), md-ft	1,200
Dimensionless Fracture Conductivity (Cr)	76
Fracture Half-Length (L _f), ft	250

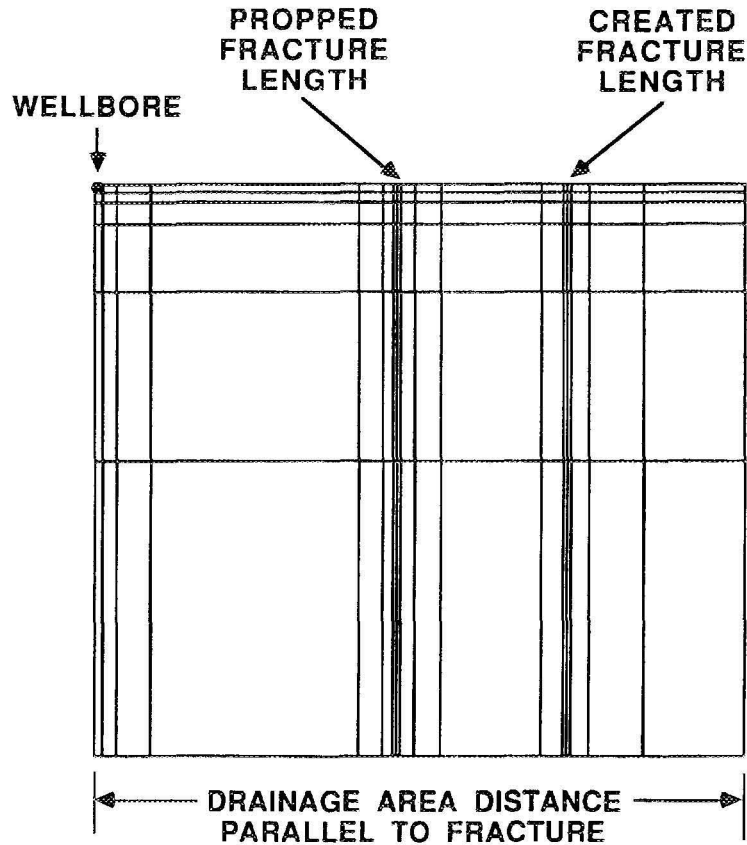


Figure 8-11 Model Grid System for Analysis of SFE No. 3

production-pressure buildup; and (3) production after the pressure buildup test.

The important parameter to be modeled in the injection stage was the total volume of water injected. When a half-fracture length of 200 ft was used (based on the pressure buildup analysis assuming single-phase flow in the reservoir), the formation could not take 12,247 bbl of fluid injected from SFE No. 3 with the constraints of a maximum injection pressure of 10,000 psi and total injection time of 3 days.

When a created fracture length of over 1,000 ft and essentially infinite fracture conductivity were used, the total volume of water injected (12,247 bbl) during all injections could be placed into the reservoir. The primary purpose of modeling the water

injection was to obtain the proper saturation profile around the fracture.

Figure 8-12 illustrates the gas and water production from SFE No. 3 before and after the post-fracture pressure buildup test. Gas flow rates were generally given as input data to the simulator when the well produced both gas and water. The calculated values of water flow rate and bottomhole pressures were used as the history matching parameters. The exception was when the well produced only water. In that case, the water flow rate was input to the simulator, and gas breakthrough and bottomhole pressures were calculated.

Sensitivity studies were conducted before trying to match the production data. The most sensitive parameters were found to be

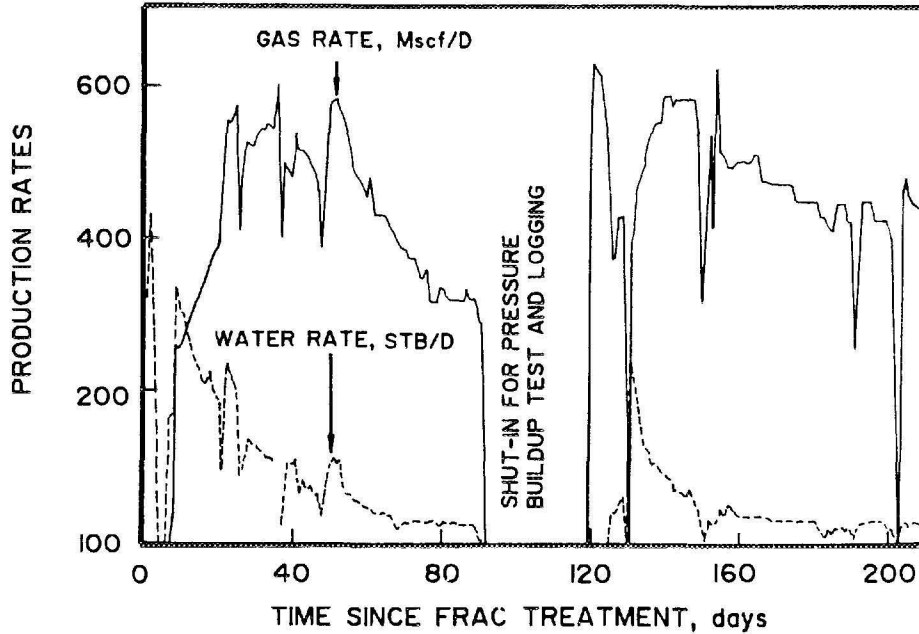


Figure 8-12 Production History of SFE No. 3

formation relative permeabilities, fracture permeabilities and formation permeability. In trying to model the correct gas breakthrough time, hysteresis effects on the gas relative permeability in the formation, as shown in Figure 8-13, were found to be extremely important. The hysteresis effects account for the differences between imbibition and drainage relative permeability curves. The imbibition curve shown on Figure 8-13 was generated by trial and error in order to obtain a good match on gas breakthrough time.

When restarting the model to simulate the production period, the total created fracture length obtained from modeling the injection period was divided into propped and unpropped segments. This was simulated by changing the permeabilities and porosities within the fracture. Once the model was set up, history matching of the rates and pressures was attempted by varying formation and fracture properties. Figures 8-14 and 8-15 show the final matches of water rates and bottomhole pressures,

respectively. No match of the gas flow rates is shown since the actual gas flow rates were used as input data. Excellent matches were obtained with the exception of the water rates in the first three weeks following the fracture treatment. This is probably due to either the incorrect modeling of the viscosity of the fracture fluid or the fact that fracture closure was not modeled. The properties used to obtain the matches shown in Figures 8-14 and 8-15 also resulted in an excellent match of the post-fracture pressure buildup test, shown in Figure 8-16.

Figure 8-17 shows the reservoir schematic obtained from the history matching of the production and pressure buildup tests. Total created fracture length was 1,515 ft, which was very similar to the fracture length determined by RES's fracture modeling. Propped fracture length determined from the two-phase modeling was 1,100 ft. This was much longer than the 200 ft determined from the single-phase analysis. However, the first 600 ft had a conductivity of 1,400

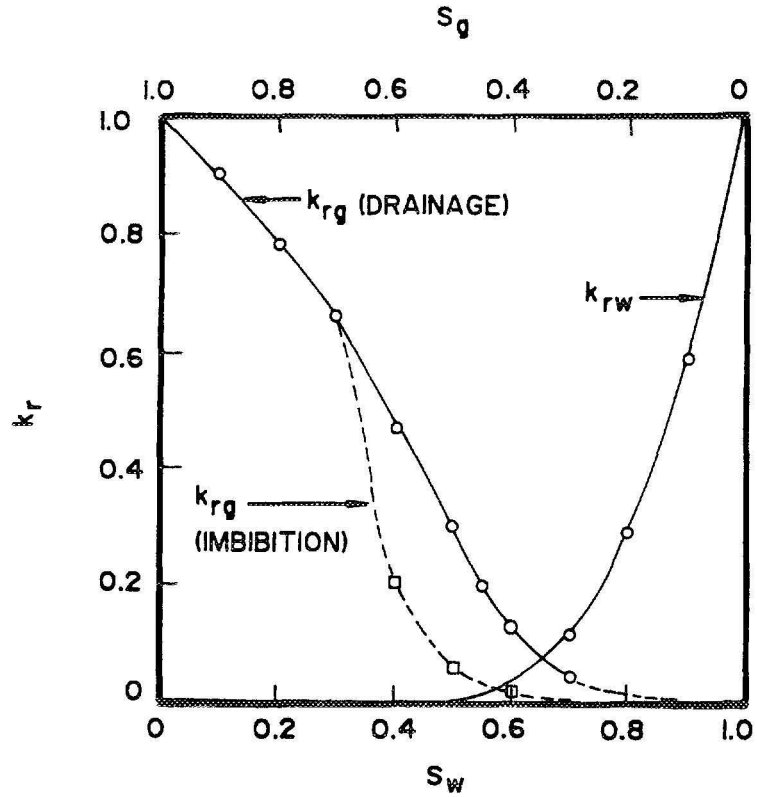


Figure 8-13 Relative Permeability Curves for SFE No. 3

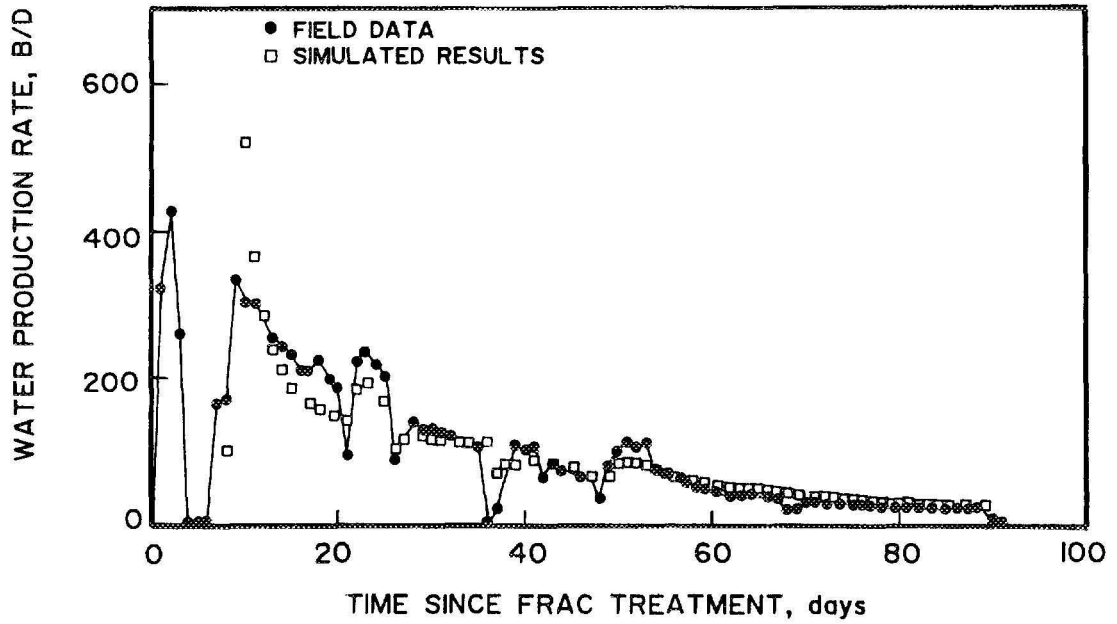


Figure 8-14 History Match of Water Production Prior to PBU Test, SFE No. 3

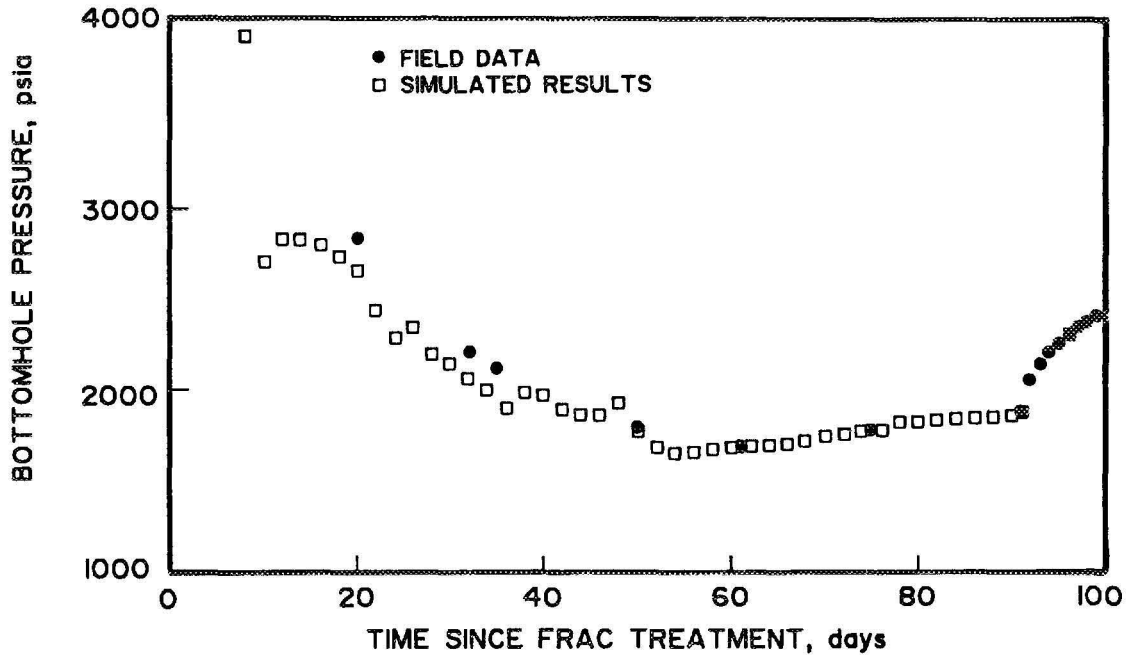


Figure 8-15 History Match of Flowing Bottomhole Pressures, SFE No. 3

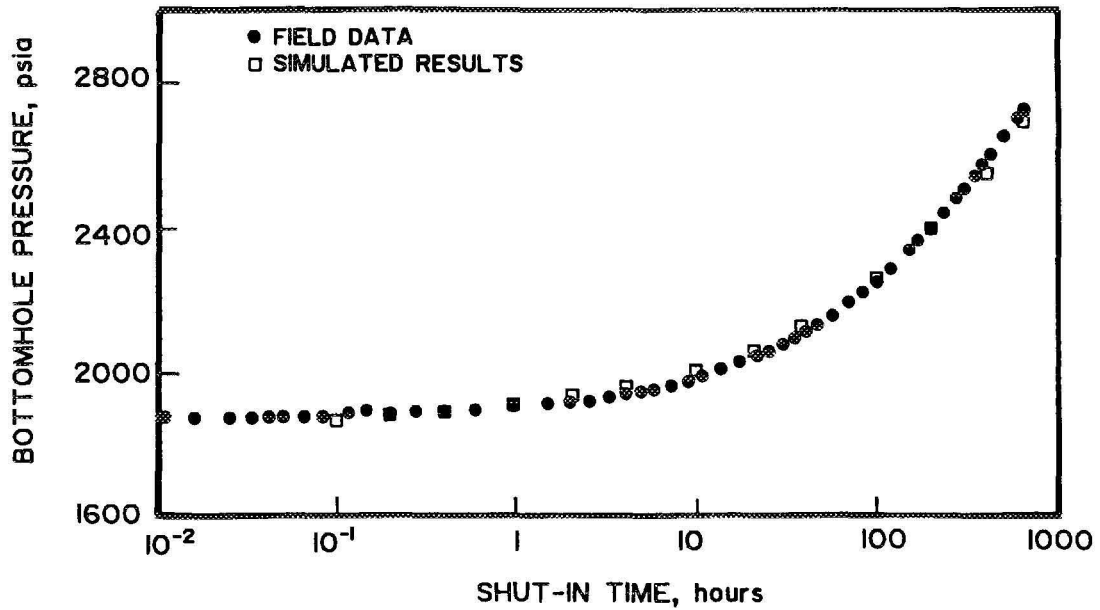


Figure 8-16 History Match of Post-Fracture PBU Tests, SFE No. 3

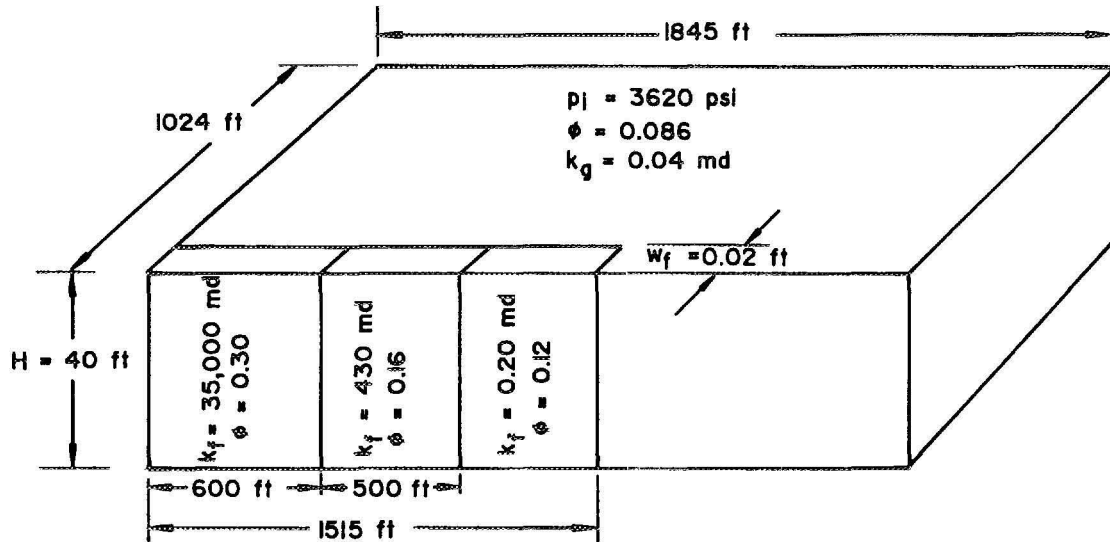


Figure 8-17 Reservoir Model for Initial History Match, SFE No. 3

md-ft ($k_f = 35,000$ md) while the last 500 ft had a conductivity of only 17 md-ft ($k_f = 430$ md). Thus, the segment of the fracture away from the wellbore was contributing little to the production from the well.

Although the higher conductivity segment of the fracture is much longer than the fracture length determined from the single-phase analysis, it is important to remember that much of the injected water still remains in the fracture and the formation. By the end of the production period, water rate had stabilized at about 25 BPD, which might indicate that the well had "cleaned up." However, inspection of the water saturation profile from the final simulation showed that water saturations greater than 80 percent still existed around most of the fracture. In fact, only the first 200 ft of the propped fracture length actually cleaned up and had water saturations near the initial water saturation. This would account for the single-phase analysis resulting in a fracture length of only 200 ft when a much longer fracture actually existed.

After the pressure buildup test was completed, SFE No. 3 was killed so the tubing

could be pulled and post-fracture logging could be performed. During this process, all fluid introduced into the wellbore and reservoir contained an additive designed to remove gel residue which remained in the fracture. It was hoped that this would increase the fracture conductivity and increase production. As was shown in Figure 8-12, gas rates after the buildup were indeed higher than before the PBU test.

Using the reservoir and fracture properties determined in the previous stage, the simulator calculated water rates after the buildup test very similar to those actually observed. Only one bottomhole pressure (BHP) measurement was made during this period, but it was much higher than the calculated (simulator) BHP at the corresponding time. After several simulation runs were made, pressure was shown to be sensitive to a change in fracture permeabilities, but water rate was not. After increasing fracture permeability, a good match of water rate remained, as shown in Figure 8-18, and the simulator bottomhole pressures were much closer to the measured pressure, as shown in Figure 8-19. Figure 8-20 shows the schematic used in this phase of the study. The only

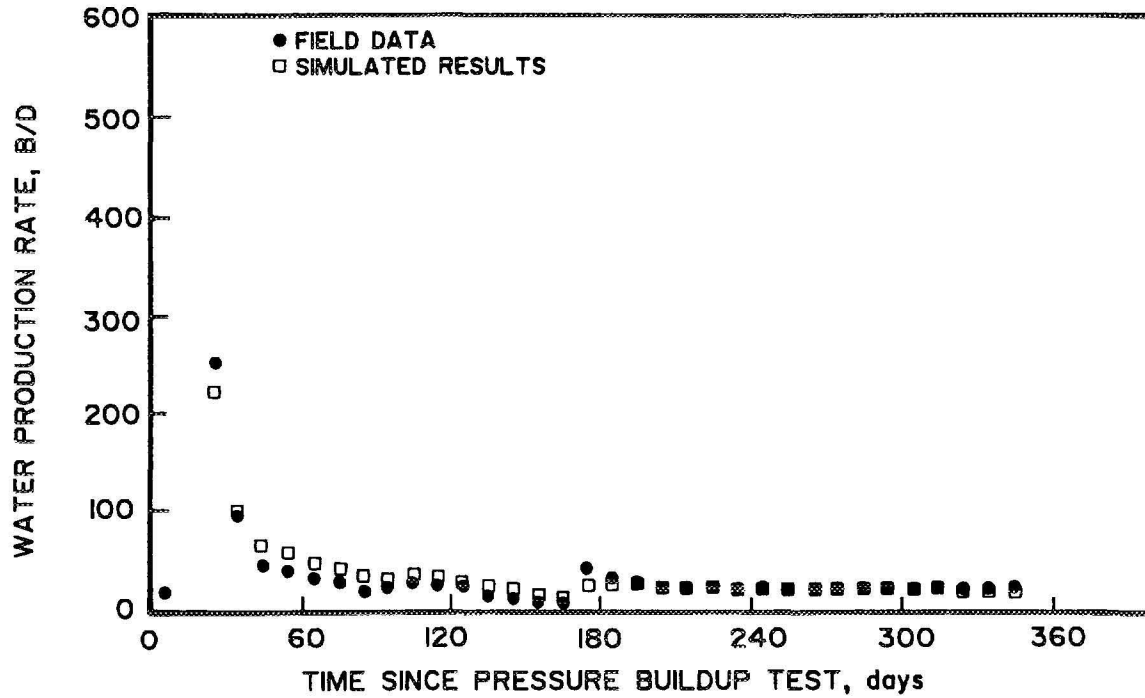


Figure 8-18 History Match of Water Production After PBU Test and Cleanup Treatment, SFE No. 3

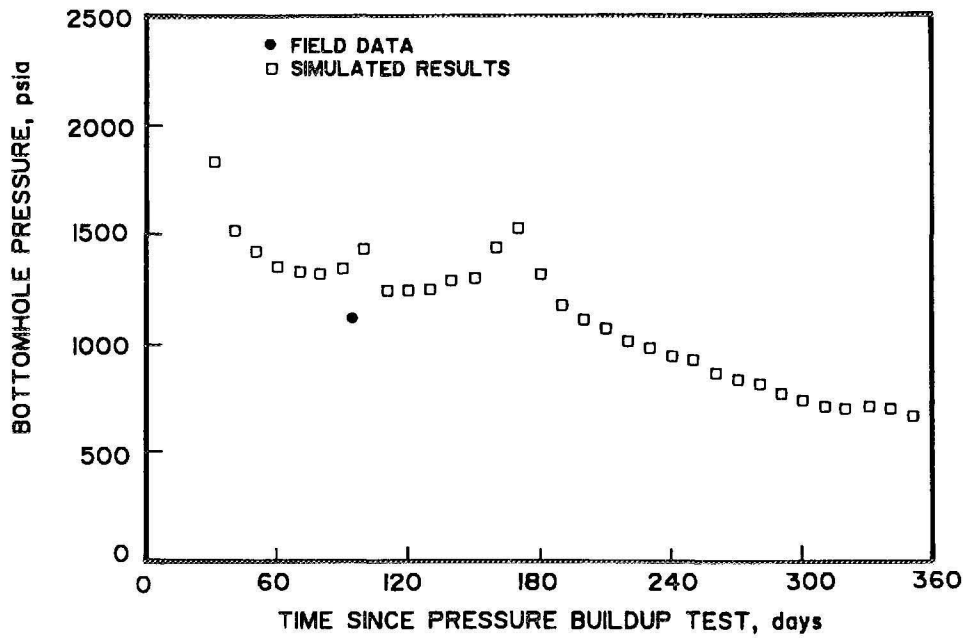


Figure 8-19 Flowing Pressure Match After PBU Test and Cleanup Treatment, SFE No. 3

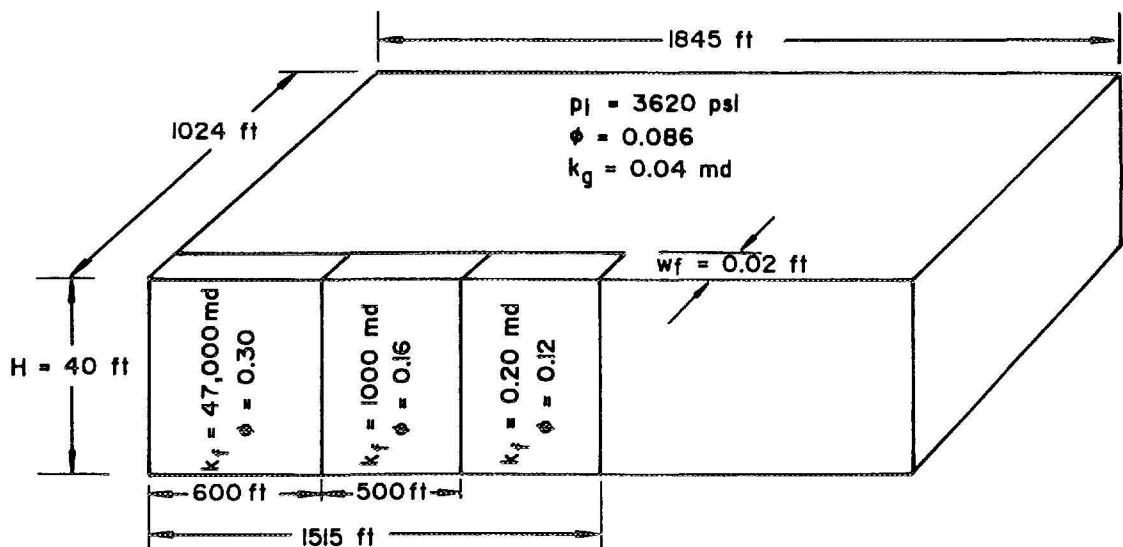


Figure 8-20 Reservoir Model for Final History Match, SFE No. 3

differences between the two different models were the fracture conductivities in the two segments of the propped fracture. Simulation showed that fracture conductivity did increase after the treated water was pumped into the formation. This was the cause of gas production increasing after the pressure buildup test.

Using the estimated reservoir and fracture properties determined from this analysis, a forecast of future performance was projected for SFE No. 3. The forecast indicates the well should produce 1,140 MMCF of gas over the next 20 years. An ultimate flowing BHP of 500 psia and an economic limit of 50 MCFD were used to determine the reserves forecast. Drainage area was assumed to be 160 acres, which makes the original GIP approximately 2.13 BCF.

8.4 MICROSEISMIC ANALYSIS OF THE TREATMENT-INDUCED FRACTURE AFTER FOUR MONTHS OF PRODUCTION

8.4.1 Objectives

The objective of the microseismic survey and analysis after four months of post-main-

frac production was to repeat a similar successful experiment performed after the SFE No. 2 main fracture treatment. The SFE No. 2 survey had successfully determined height, but the orientation was ambiguous. If microseismic data can be successfully acquired by reoccupying previously fractured wells, then a new research tool could be established. Fracture height and/or orientation could then be determined in production wells at any convenient time during a work-over when the tubing had been removed from the well.

8.4.2 Field Operations and Data Acquisition

After the main hydraulic fracture treatment on March 16, 1989, post-fracture well testing was performed. After completing the flow and pressure buildup testing, the well was killed, tubing was pulled, and a microseismic survey was performed in the well on July 25 and 26 (see Section 2.2.1.4). This post-main fracture monitoring consisted of 24 stations, including 20 depths and 4 reoccupied depths. The "Post-Main" column of Table 6-4 indicates the stations occupied and the clock time of the recording. Similar to the mini-frac monitorings, the post-main

monitoring was an interleaved ascending and descending traverse. Unlike the mini-frac monitorings, the post-main monitoring had some unique features.

During the previous SFE No. 3 microseismic surveys, the data had been recorded at the surface using Teledyne Geotech's Surface Digital Data Acquisition System (SDDAS). At the post-main fracture monitoring, the SDDAS system served as a backup to an Seismographic Services Ltd. (SSL) recording system. The SSL system was able to record 16 continuous seconds of 1,000-sample/sec data. After each 16-second recording, there was an approximate 8-second recording hiatus required to retrigger the system to record the next 16 seconds. This segmenting of the data posed some processing adjustments but did not affect the final analysis or interpretation of the data.

8.4.3 Hydraulic Fracture Orientation

Observations of seismic activity were made at 21 depths, from 6,350 ft to 9,450 ft, in the SFE No. 3 well, approximately four months after the main fracturing operation. Low-frequency signals were observed only at depths of 8,950 ft and above and at 9,400 ft and below. Particle motion orientations of these signals, determined by application of the SMART processor to the first half-cycle of each signal were inconsistent, both relative to the sensor axes and relative to North.

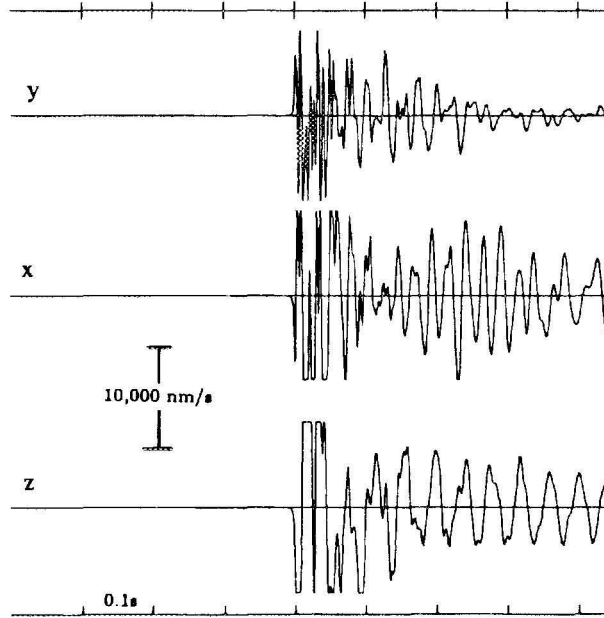
Another class of signals was observed in the post-main frac data. These are 12 very large signals with strong low-frequency energy in the initial part of the vertical component, recorded at 7 depths from 8,800 ft to 9,450 ft. Data recorded by the SSL recording system were used to analyze these signals because of the greater dynamic range provided by the SSL system. Orientations of the initial particle motions of 10 of the 12 large signals did not yield a consis-

tent azimuth, either relative to the sensors or relative to North.

For two of the signals, recorded at 8,925 ft and at 9,400 ft, very small amplitude, short duration precursors were discernible, approximately 30 to 80 ms preceding the large signals. These two large signals are shown in Figure 8-21. A noise-conditioned Pure-State Filter was applied to the time intervals preceding the 12 large signals to search for additional precursors. No additional precursors could be identified with confidence. The precursors to the two large signals which had visible precursors in the unprocessed data are shown in Figure 8-22, both unprocessed and after application of the noise-conditioned Pure-State Filter. The dominant frequency of the precursors was 100 to 200 Hz. Orientations of the initial particle motions of the precursors are given in Figure 8-23. For the signal recorded at 8,925 ft, both precursors are oriented 40° relative to North, while for the signal recorded at 9,400 ft, the earlier precursor is oriented 61°, and the later precursor is oriented perpendicular to this direction.

These large signals and precursors are interpreted to represent fluid-path and rock-path, respectively, propagation from discrete sources within the fractured zone, the sources having dimensions significantly smaller than the dimensions of the induced fracture. The relative amplitudes of the precursors and the large signals are consistent with this interpretation. The large signals result from propagation through the fractured zone to the wellbore, probably as acoustic waves, and then along the wellbore to the sensors, probably as tube waves. The polarization of the initial arrivals of the large signals should therefore be controlled by the locking arrangement of the tool and by the coupling between the tool and the formation. The coupling can vary significantly with position in the borehole, thus accounting for the variations in particle motion orientation observed for the large signals.

0 0:0:0.30
SFE3M-T4F45-8925-BIG.DAT
CTS/IN: 0.224E+09
SEC/IN: 0.100



0 0:0:0.45
SFE3M-T1F123-9400-BIG.DAT
CTS/IN: 0.224E+09
SEC/IN: 0.100

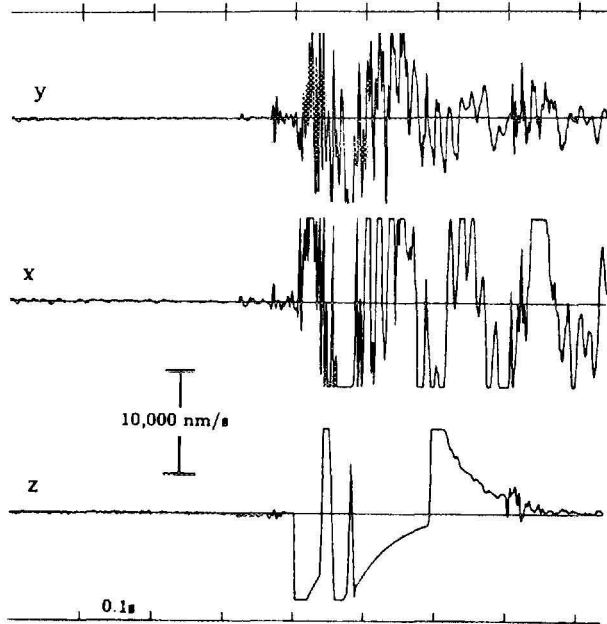
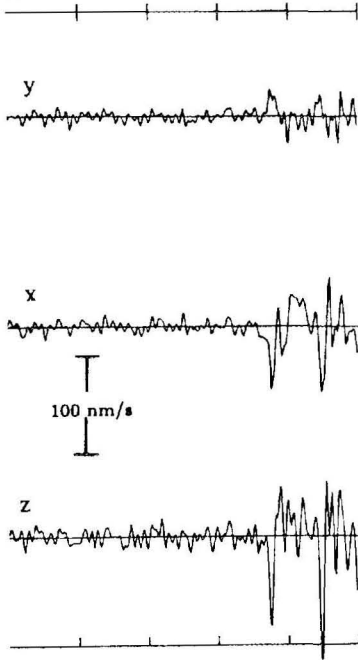
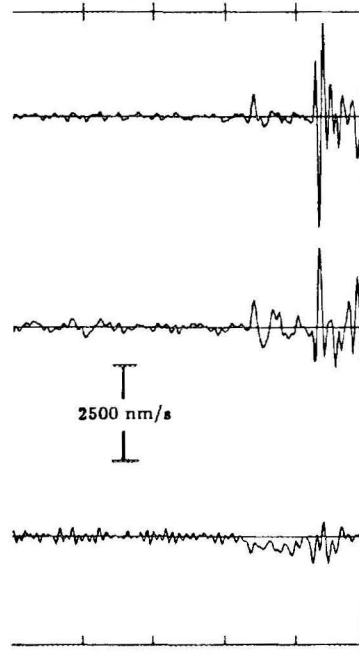


Figure 8-21 Very Large Signals With Apparent Precursors Recorded at 8,925 ft and 9,400 ft Approximately Four Months After Main Fracturing Operation

0 0:0:0.44
SFE3M-T4F45-8925-BIG.DAT
CTS/IN: 0.150E+07
SEC/IN: 0.500E-01

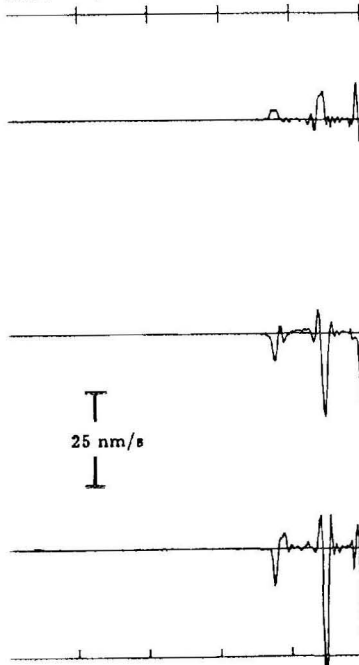


0 0:0:0.60
SFE3M-T1F123-9400-BIG.DAT
CTS/IN: 0.500E+08
SEC/IN: 0.500E-01

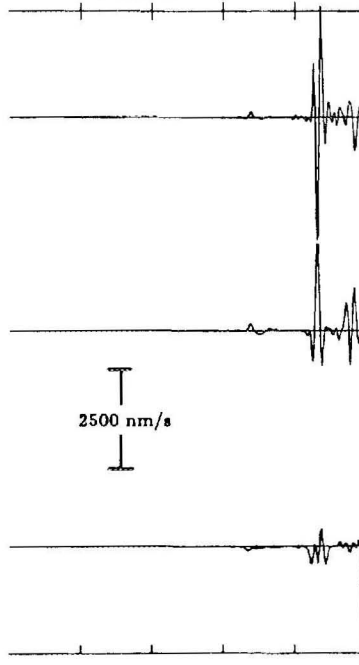


Unprocessed

0 0:0:0.52
SFE3M-T04-F45-8925-01-20.PSF
CTS/IN: 0.500E+06
SEC/IN: 0.500E-01



0 0:0:0.60
SFE3M-T01-F123-9400-01-20.PSF
CTS/IN: 0.350E+08
SEC/IN: 0.500E-01



Noise-conditioned Pure-State Filter Applied

Figure 8-22 Unprocessed Apparent Precursors After Use of Noise-Conditioned Pure-State Filter

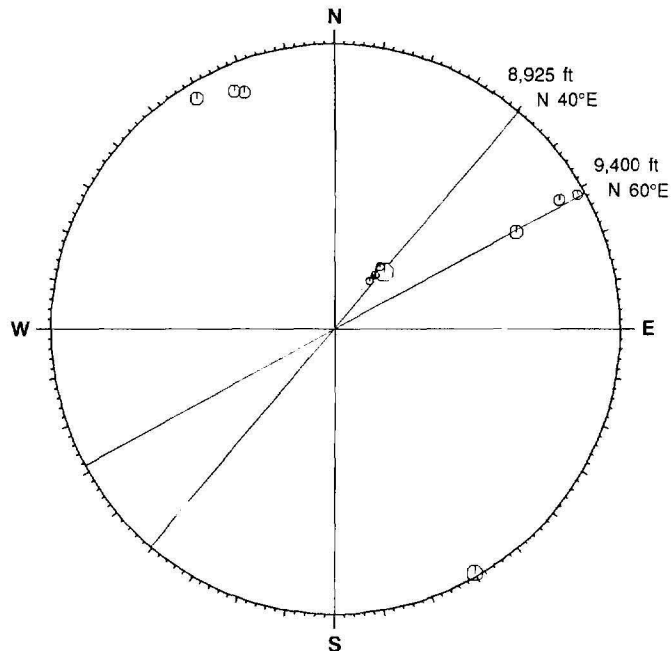


Figure 8-23 Upper Hemisphere Stereographic Projection of Particle Motion Orientations of Precursors to Very Large Signals Recorded at 8,925 ft and 9,400 ft

The precursors, on the other hand, result from propagation of body waves from the sources through the rock to the tool. The inclination from vertical of the precursors, 35° for the signal recorded at 8,925 ft (200 ft above the top of the fracture) and 77° for the signal recorded at 9,400 ft (25 ft below the bottom of the fracture), are consistent with this interpretation. Using a velocity of 4,800 ft/sec for both the acoustic wave and the tube wave as well as a compressional wave velocity of 15,000 ft/sec, the estimated location for the signal recorded at 9,400 ft is 426 ft from the borehole at a depth of 9,302 ft. The location for the signal recorded at 8,925 ft is 154 ft from the borehole at a depth of 9,145 ft. The different azimuths observed for the two depths, 40° for the 8,925-foot signal and 61° for the 9,400-foot signal, imply that the fractured zone has significant width.

8.4.4 Hydraulic Fracture Height

Figure 8-24 shows the results of the H/Z analysis on the post-main fracture data. These values were calculated from 70-hertz

high-pass and 60-hertz comb-filtered data. As with the Mini-Frac No. 1 Stage 3 and Stage 9 data, the inversion in the H/Z ratio was found and interpreted as indicating the top and bottom of the fracturing at $9,125 \pm 25$ ft and $9,375 \pm 25$ ft, respectively. These values are comparable to the height values determined from Mini-Frac No. 1 Stage 3 and 9 and, considering the volume of fluid pumped into the formation, probably indicate the propped height with the fluid height propped extending over a larger range. By the time these data were taken, the unpropped fracture was probably closed and only the propped fracture remained. Note also in Figure 8-24, the anomalous H/Z value in the middle of the perforation interval as seen in the Mini-Frac No. 1 Stage 9 data. This anomaly between perforations has been seen in several wells.

8.5 FRACTURE HEIGHT PROOF-OF-CONCEPT EXPERIMENT

The apparent success of the microseismic height determination led to an interest on the part of GRI to demonstrate by other

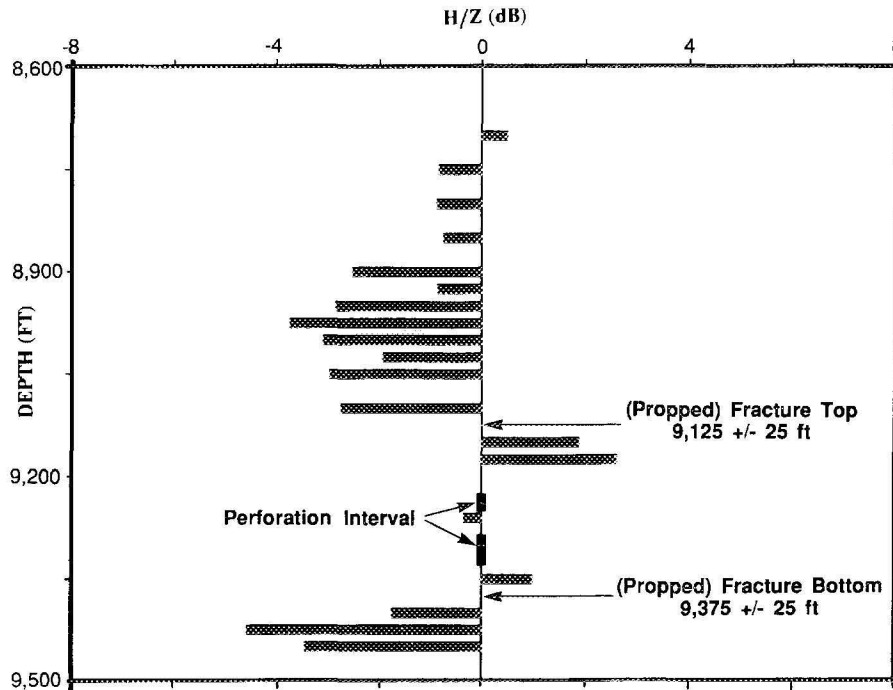


Figure 8-24 H/Z Ratios After Main Fracture Treatment Versus Depth

Independent measurements that the technique was, in fact, measuring true fracture dimensions. This section describes the experiment that was designed to provide a proof-of-concept for the height measurement and presents the results.

8.5.1 Experiment Design

A committee composed of staff members of S.A. Holditch & Associates, Inc., CER Corporation, ResTech, Teledyne Geotech and Mobil R&D formulated an experiment designed to compare results from various fracture height techniques -- some of which are routinely run and some which are experimental -- to results derived from Continuous Microseismic Radiation (CMR). The change in the CMR that accompanies a fracture is either the result of a change in the elastic properties of the rock in the treatment zone or a change in the seismic radiation function. A set of logs was recommended to try to measure the change of rock elastic prop-

erties in the immediate vicinity of the wellbore resulting from the treatment. These methods involve repeated measurement of a particular physical property before and after several stages of the completion and fracturing sequences. With the repeated measurements, changes can be detected in the physical property to which the log is responding. The recommended procedure started with measurements after casing cement had cured but before the perforations were made. Additional measurements were to be taken before Mini-Frac No. 1, after the last stage of Mini-Frac No. 1, and after the main fracture treatment.

The recommended techniques were: 1) vertical traverses to passively measure CMR, to calculate horizontal-to-vertical (H/Z) filtered rms ratios and to estimate depths of fracture top and bottom (this is the method being verified); 2) digital full wave-form sonic logs; 3) shear-wave logs; 4) cement bond logs; and 5) radioactive tracer tagging with differ-

ent elements for all stages of the fractures. In the planned experiment, traverses and logs were to be run from borehole total depth (TD) to well above the expected top of the hydraulic fracture. Table 8-4 provides a summary of the log type, log date, well status and responsible company. Appendix 1 includes a detailed list of the log data that was actually acquired in the proof-of-concept experiment.

8.5.2 Results and Interpretation

The logs available to Teledyne Geotech were studied for changes from one pass to the other. The character of the logs and physical parameters that were interrogated by the logs were considered in making the interpretations. The top and bottom of the changed intervals were noted. These changes were interpreted in terms of the vertical extent of any disturbance generated by the several completion processes. The depth of penetration of all the logs except the microseismic is shallow. Therefore, any changes may indicate changes in the cement annulus of the wellbore rather than the top and bottom of an induced fracture. The logs reviewed included the final stress log calculated by ResTech, the cement bond log/variable density display (CBL/VDL), the natural gamma ray log (GR), the cement evaluation tool (CET), tracer scan and microseismic height log (H/Z). The interpretations included in this section were abstracted from Fix and Others (1990). Other interpretations are made by Hunt (1990). Readers are encouraged to review these documents for details of the evaluations.

A summary of the estimated fracture dimensions from post-mini-frac information is presented by Figure 8-25. Depth in feet is the vertical scale. The bars represent the interpreted results from the following logs: CBL/VDL, GR, CET, AU¹⁹⁸ tracer scan, H/Z log from Mini-Frac No. 1 Stage 3, and H/Z log from Mini-Frac No. 1 Stage 9. In addition,

the perforation depths are included for reference. These results should be compared with the stress log in Figure 5-8; both figures have approximately the same depth scale.

The interpretation of the conventional logs is that the bottom of the fracture is in the vicinity of the bottom of the perforations, not far from the intermediate stress barrier at 9,340 ft. The microseismic log indicates that the fracture broke through to the lower barrier at 9,475 ft after Mini-Frac No. 1 Stage 3 and then closed to the middle of the lower pay zone after Mini-Frac No. 1 Stage 9. The CBL, GR and one interpretation of the gold tracer log indicate changes well above two stress barriers. Consequently, they are interpreted as being the result of microfractures in the cement annulus between the casing and the formation. The other interpretation of the gold tracer log and the CET log both agree with the top of the fracture as detected by the microseismic log for both stages. All four of these tops are in the vicinity of the stress barrier at 9,170 ft.

Similar to Figure 8-25, Figure 8-26 displays fracture top and bottom interpretations; the data were taken using the CBL/VDL, GR, CET, SC⁴⁶ and IR¹⁹² tracer scan, and H/Z. However, by the time the measurements were made, the main fracture had been completed and four months of production had occurred. Accordingly, the depths shown in Figure 8-26 correspond to those for a propped fracture.

The bottom of the fracture as interpreted from the logs, including the best interpretation of the CET log, is at the bottom of the perforations at 9,330 ft. The other possible CET log interpretation agrees with that of the microseismic height log. They place the bottom of the disturbed zone at about 9,375 ft. Referring to the calculated stress log (not the blocked log) in Figure 5-8, there is

Table 8-4 Proof-of-Concept Logging at SFE No. 3 -- Well Status, Actual Logging Date, Responsible Company and Log Data Acquired

Status and Date	Mobil Research	CER Corporation	Teledyne Geotech
Pre-Perforation November 30, 1988	TWRL ASWL SWAL LSAL	CBL/CET VAL	Microseismic
Pre-Minifrac No. 1 February 11, 1989	TWRL	CBL/CET Tracer	Microseismic
Post-Minifrac No. 1 February 18, 1989	TWRL	CBL/CET Tracer	Microseismic
Post-Main Fracture July 25, 1989	TWRL	CBL/CET VAL Tracer	Microseismic

Description of Logs

ASWL	Anisotropy Shear-Wave Log (Mobil Proprietary)
CBL	Cement Bond Log
CET	Eight Path Cement Bond Log
LSAL	Long-Spaced Acoustic Log (Digital Full-Waveform Log)
SWAL	Dipole Shear-Wave Log (Mobil Proprietary)
Tracer	Spectral Gamma Ray to Detect Selected Tracers
TWRL	Tube Wave Reflection Log (Mobil Proprietary)
VAL	Petro Data Shear Wave Log, Quadrapole Source -- 3 Dipole Receivers at 120°

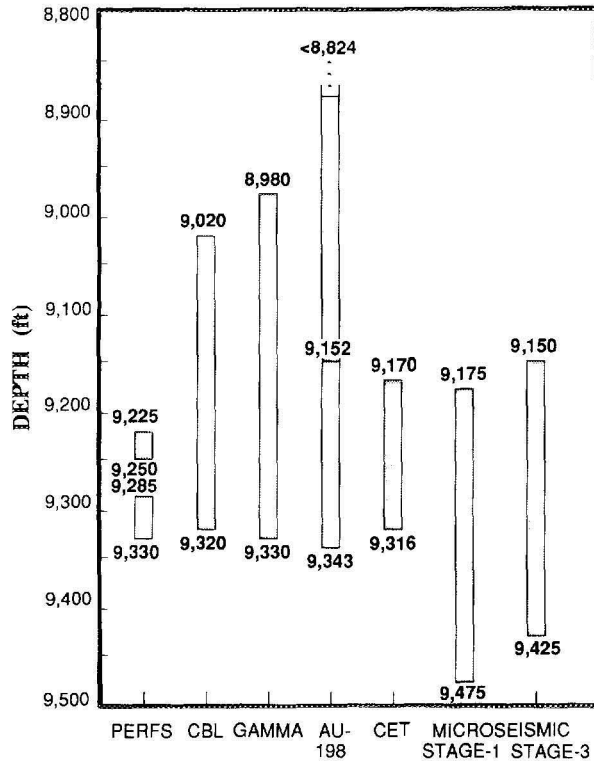


Figure 8-25 Summary of Mini-Frac Top and Bottom Interpretations From Proof-Of-Concept Experiment (Perforation depths given for reference)

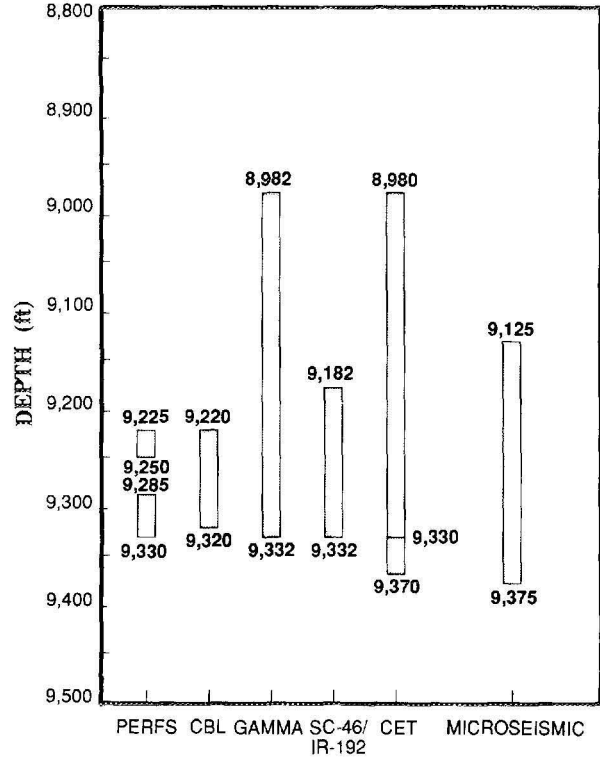


Figure 8-26 Summary of Main Frac Top and Bottom Interpretations From Proof-Of-Concept Experiment (Perforation depths given for reference)

a relatively high stress value of 7,800 psi at a 9,370-foot depth. This stress/depth combination may be fortuitous, but the 1,900 psi stress change on the stress log could be a very effective barrier to proppant.

The interpreted top of the main fracture from the logs is more variable due to the microfractures in the annulus. The GR and CET log interpreted tops (8,980 ft) are definitely the result of microfractures in the cement annulus. The CBL top is in agreement with the TWRL top (not shown); they are both at the top of the perforations. The tracer log top at 9,182 ft is below the stress barrier at 9,170 ft. The microseismic fracture top at 9,125 ft occurs at another high stress value in the calculated stress log. A

thin, high stress value of 8,200 psi is at a depth of 9,120 ft. This upper log segment is not as convincing as the lower log segment, but it does lend support to the proof-of-concept of the microseismic height log.

In general, the conventional cased-hole logs (e.g., CBL/VDL, GR, CET, tracers) were not suited for fracture height determination in this well. As a result, they should not be used individually for fracture height determination. The microseismic method has an advantage in that it penetrates the formation at dimensions of tens to a few hundred feet. Conventional cased-hole logs only penetrate a few inches. In some instances, the logs were in agreement with the microseismic method. However, in no case did any of

these logs indisputably contradict the microseismic height determination.

The microseismic height log yielded an excellent estimate of the top and bottom of a hydraulically stimulated fracture. As expected, different dimensions were measured

for fractures conducted with and without proppant. The top and bottom of the microseismic height log showed satisfactory agreement with calibrated calculated stress profiles. Thus, the proof-of-concept experiment is considered a success for the microseismic method.

9.0 References

SECTION 1.0 INTRODUCTION AND SUMMARY

Bundy, Thomas E., 1982: "Pre-Fracture Injection Surveys: A Necessity for Successful Fracture Treatments," *J. Pet. Tech.* (May) 995-1001.

CER Corporation and S.A. Holditch & Associates (Eds.), 1988: "Advancements in Travis Peak Formation Evaluation and Hydraulic Fracture Technology, Staged Field Experiment No. 1, Waskom Field, Harrison County, Texas," Report No. GRI-88/0077, prepared for GRI under Contract No. 5086-211-1306 (April).

CER Corporation and S.A. Holditch & Associates (Eds.), 1989: "Staged Field Experiment No. 2, Application of Advanced Geological, Petrophysical and Engineering Technologies to Evaluate and Improve Gas Recovery from Low Permeability Sandstone Reservoirs, Travis Peak Formation, North Appleby Field, Nacogdoches County, Texas," Report No. GRI-89/0140, prepared for GRI under Contract No. 5088-211-1682 (June) I.

CER Corporation and S.A. Holditch & Associates (Eds.), 1990: "Staged Field Experiment No. 2, Application of Advanced Geological, Petrophysical and Engineering Technologies to Evaluate and Improve Gas Recovery from Low Permeability Sandstone Reservoirs, Travis Peak Formation, North Appleby Field, Nacogdoches County, Texas," Report No. GRI-90/0093, prepared for GRI under Contract No. 5088-211-1682 (April) II.

Cooke, Claude E. Jr., 1979: "Radial Differential Temperature (RDT) Logging -- A New Tool for Detecting and Treating Flow Behind Casing," *J. Pet. Tech.* (June) 676-682.

Dobkins, Terrell A., 1981: "Improved Methods to Determine Hydraulic Fracture," *J. Pet. Tech.* (April) 719-726.

Finley, R.J., 1984: "Geological and Engineering Characteristics of Selected Low Permeability Gas Sandstones: A National Survey," The University of Texas at Austin, Bureau of Economic Geology Report of Investigations No. 138.

Gadeken, L.L., M.L. Gartner and D.E. Shurbak, 1989: "Improved Evaluation Techniques for Multiple Radioactive Tracer Applications," Paper presented at 12th International Logging Symposium of SAIG, Paris France, October 1989.

SECTION 2.0 SFE NO. 3 DATA ACQUISITION OBJECTIVES AND RESULTS

CER Corporation and S.A. Holditch & Associates (Eds.), 1990: "Staged Field Experiment No. 2, Application of Advanced Geological, Petrophysical and Engineering Technologies to Evaluate and Improve Gas Recovery from Low Permeability Sandstone Reservoirs, Travis Peak Formation, North Appleby Field, Nacogdoches County, Texas," Report No. GRI-90/0093, prepared for GRI under Contract No. 5088-211-1682 (April) II.

SECTION 3.0 GEOLOGICAL ANALYSIS OF THE TRAVIS PEAK FORMATION AND COTTON VALLEY SANDSTONE

Baumgardner, R.W. and S.E. Laubach, 1987: "Wellbore Ellipticity in East Texas: In-Situ Stress or Fracture-Related Spalling?" (abs.): *EOS, Trans., AGU*, **68**, No. 44, 1460.

Bushaw, D.J., 1968: "Environmental Synthesis of the East Texas Lower Cretaceous,"



Trans., Gulf Coast Association of Geological Societies, **18**, 416-438.

Collins, E.W., D.K. Hobday and C.W. Kreitler, 1980: "Quaternary Faulting in East Texas," The University of Texas at Austin, Bureau of Economic Geology Geological Circular 80-1.

de Waal, J.A., K.J. Bil, J.D. Kantorowicz and A.I.M. Dicker, 1988: "Petrophysical Core Analysis of Sandstones Containing Delicate Illite," *The Log Analyst*, **29**, No. 5, 317-331.

Dutton, S.P., 1987: "Diagenesis and Burial History of the Lower Cretaceous Travis Peak Formation, East Texas," The University of Texas at Austin, Bureau of Economic Geology Report of Investigations No. 164.

Dutton, S.P. and Others, 1988: "Geologic Analysis of the Travis Peak Formation," *Advancements in Travis Peak Formation Evaluation and Hydraulic Fracture Technology, Staged Field Experiment No. 1, Washkom Field, Harrison County, Texas, CER Corporation and S.A. Holditch & Associates (Eds.)*, Report No. GRI-88/0077, prepared for GRI under Contract No. 5086-211-1306 (April) 35-62.

Finley, R.J., S.P. Dutton, Z.S. Lin and A.E. Saucier, 1985: "The Travis Peak (Hosston) Formation: Geologic Framework, Core Studies, and Engineering Field Analysis," The University of Texas at Austin, Bureau of Economic Geology, contract report prepared for GRI under Contract No. 5082-211-0708.

Folk, R.L., 1974: *Petrology of Sedimentary Rocks*, Hemphill, Austin, Texas.

Holditch, S.A., B.M. Robinson and W.S. Whitehead, 1987: "The Analysis of Complex Travis Peak Reservoirs in East Texas," SPE Paper 16427; *Trans.*, SPE/DOE Joint Symposium on Low Permeability Reservoirs, 381-399.

Kosters, E.C. and Others, 1989: "Atlas of Major Texas Gas Reservoirs," The University of Texas at Austin, Bureau of Economic Geology.

Kulander, B.R., C.C. Barton and S.L. Dean, 1979: "The Application of Fractography to Core and Outcrop Fracture Investigations," Morgantown Energy Technology Center, Report prepared for U.S. DOE, METC/SP 79/3.

Laubach, S.E. and E.R. Monson, 1988: "Drilling-Induced Fractures: Indicators of Hydraulic Fracture Propagation Direction in a Naturally Fractured Reservoir," SPE Paper No. 18164, *Proc.*, 1988 SPE Annual Technical Conference and Exhibition, 587-596.

Laubach, S.E., R.S. Tye, S.P. Dutton and K. Herrington, 1989: "Geological Analysis of the Travis Peak Formation," *Staged Field Experiment No. 2, Application of Advanced Geological, Petrophysical and Engineering Technologies to Evaluate and Improve Gas Recovery from Low Permeability Sandstone Reservoirs, Travis Peak Formation, North Appleby Field, Nacogdoches County, Texas, CER Corporation and S.A. Holditch & Associates (Eds.)*, Report No. GRI-89/0140, prepared for GRI under Contract No. 5088-211-1682, June, I, 42-90.

Luffel, D.L., W.E. Howard and E.R. Hunt, 1989: "Relationships of Permeability, Porosity, and Overburden Stress Derived From an Extensive Core Analysis Database in the Travis Peak Formation," SPE Paper No. 18964, *Proc.*, 1989 SPE Joint Rocky Mountain Regional Meeting and Low-Permeability Reservoir Symposium, Denver, 729-740.

Pallatt, N., J. Wilson and B. McHardy, 1984: "The Relationship Between Permeability and the Morphology of Diagenetic Illite in Reservoir Rocks," *J. Pet. Tech.*, 2225-2227.

Presley, M.W. and C.H. Reed, 1984: "Jurassic Exploration Trends of East Texas," *The Jurassic of East Texas*, M.W. Presley (Ed.), East Texas Geological Society, 11-22.

Saucier, A.E. and R.J. Finley, 1984: "The Travis Peak/Hosston Formation of East Texas and North Louisiana: a Laboratory of Tight Gas Technology Development," *In Focus - Tight Gas Sands*, Gas Research Institute, 1, 15-25.

Saucier, A.E., R.J. Finley and S.P. Dutton, 1985: "The Travis Peak (Hosston) Formation of East Texas and North Louisiana," SPE Paper 13850, *Trans.*, SPE/DOE Joint Symposium on Low Permeability Reservoirs, 15-22.

Seni, S.J. and M.P.A. Jackson, 1983: "Evolution of Salt Structures, East Texas Diapir Province, Part 1: Sedimentary Record of Halokinesis," *Bull.*, AAPG, 67, No. 8, 1219-1244.

Thomas, W.A. and C.J. Mann, 1966: "Late Jurassic Depositional Environments, Louisiana and Arkansas," *Bull.*, AAPG, 50, 2194-2224.

Tye, R.S., 1989: "Stratigraphy and Depositional Systems of the Lower Cretaceous Travis Peak Formation, East Texas Basin," The University of Texas at Austin, Bureau of Economic Geology, contract report prepared for GRI under Contract No. 5082-211-0708.

Tye, R.S. and Others, 1989: "Preliminary Geologic Description, Mobil Cargill No. 15," The University of Texas at Austin, Bureau of Economic Geology, well report prepared for GRI under Contract No. 5082-211-0708.

Van Alstine, D.R., 1988: "Paleomagnetic Core Orientation Results From the Cargill No. 15 (SFE No. 3) Well, Harrison Co., Texas," *Applied Paleomagnetism*, Redmond,

Washington, Report prepared for CER Corporation.

Wescott, W.A., 1983: "Diagenesis of Cotton Valley Sandstone (Upper Jurassic), East Texas: Implications for Tight Gas Formation Pay Recognition," *Bull.*, AAPG, 67, No. 6, 1002-1013.

SECTION 4.0 WELL LOG AND CORE ANALYSES IN THE COTTON VALLEY FORMATION

Alger, R.P., L.L. Raymer, Jr., W.R. Hoyle and M.P. Tixier, 1963: "Formation Density Log Applications in Liquid Filled Holes," *J. Pet. Tech.* (March) 321-332.

CER Corporation and S.A. Holditch & Associates (Eds.), 1988: "Advancements in Travis Peak Formation Evaluation and Hydraulic Fracture Technology, Staged Field Experiment No. 1, Waskom Field, Harrison County, Texas," Report No. GRI-88/0077, prepared for GRI under Contract No. 5086-211-1306 (April).

CER Corporation and S.A. Holditch & Associates (Eds.), 1989: "Staged Field Experiment No. 2, Application of Advanced Geological, Petrophysical and Engineering Technologies to Evaluate and Improve Gas Recovery from Low Permeability Sandstone Reservoirs, Travis Peak Formation, North Appleby Field, Nacogdoches County, Texas," Report No. GRI-89/0140, prepared for GRI under Contract No. 5088-211-1682 (June) I.

Clavier, C., G. Coates and J. Dumanior, 1984: "The Theoretical and Experimental Bases for the Dual Water Model for the Interpretation of Shaly Sands," *Soc. Pet. Eng. J.* (April) 153-168; *Trans.*, AIME, 277.

Connolly, E. T., 1974: "Digital Log analysis Recognition and Treatment of Field Recording Errors," Paper S presented at 1974

SPWLA Logging Symposium, McAllen, Texas, June 2-5.

Corey, A.T., 1954: "The Interrelation Between Gas and Oil Relative Permeabilities," *Producers Monthly* (November) 38-41.

de Waal, J.A., K.J. Bil, J.D. Kantorowicz and A.I.M. Dicker, 1988: "Petrophysical Core Analysis of Sandstones Containing Delicate Illite," *The Log Analyst* (September-October) 317-331.

Howard, W.E. and E.R. Hunt, 1986: "Travis Peak: An Integrated Approach to Formation Evaluation," SPE Paper 15208 presented at the 1986 Unconventional Gas Technology Symposium, Louisville, KY, May 18-21.

Hubbert, M.K. and D.G. Willis, 1957: "Mechanics of Hydraulic Fracturing," *Trans., AIME*, **210**, 153-166.

Kenyan, W.E. and P.L. Baker, 1984: "EPT Interpretation in Carbonates Drilled with Salt Muds," SPE Paper 13192 presented at the 1984 SPE Annual Technical Conference and Exhibition, Houston, Sept. 16-19.

Kukal, G.C. and Others, 1983: "Critical Problems Hindering Accurate Log Interpretation of Tight Gas Sand Reservoirs," SPE Paper 11620 presented at the 1983 SPE/DOE Symposium, Denver, May 19-22.

Luffel, D.L., W.E. Howard and E.R. Hunt, 1989: "Relationships of Permeability, Porosity, and Overburden Stress Derived From an Extensive Core Analysis Database in the Travis Peak Formation," SPE Paper 19008 presented at the Denver Low Permeability Symposium, March.

Nolte, K.G. and M.B. Smith, 1979: "Interpretation of Fracturing Pressures," SPE Paper 8297 presented at the 1979 SPE Annual Technical Conference and Exhibition, September 23-26.

Pallat, N., J. Wilson and B. McHardy, 1984: "The Relationship Between Permeability and the Morphology of Diagenetic Illite in Reservoir Rocks," *J. Pet. Tech.*, **12**, 2225-2227.

Patchett, J.G. and E.B. Coalson, 1982: "The Determination of Porosity in Sandstone and Shaly Sandstone: Part II, Effects of Complex Mineralogy and Hydrocarbons," Paper T presented at the 1982 SPWLA Logging Symposium, Corpus Christi, Texas, July 6-9.

Raymer, L.L., E.R. Hunt and J.D. Gardner, 1980: "An Improved Sonic Transit Time-to-Porosity Transform," Paper presented at the 1980 SPWLA Annual Logging Symposium.

ResTech Houston, 1988: "Development of Petrophysical Techniques for Evaluating Tight Gas Sands," Final report prepared for GRI under Contract No. 5084-211-1062.

Schlumberger, 1985: *Log Interpretation Charts*, Ridgefield, 47.

Tixier, M.P., G.W. Loveless and R.A. Anderson, 1973: "Estimation of Formation Strength From the Mechanical Properties Log," SPE Paper 4532 presented at the 1973 Annual Meeting.

Tye, R.S., S.E. Laubach and K.L. Herrington, 1989: "The Role of Geology in Characterizing Low-Permeability Sandstones, North Appleby Field, East Texas Basin," SPE Paper 18964 presented at the Denver Low Permeability Symposium, March 6-8.

Tye, R.S. and Others, 1989: "Preliminary Geologic Description, Mobil Cargill No. 15," The University of Texas at Austin, Bureau of Economic Geology, Report prepared for GRI.

Western Atlas International Core Lab, 1989a: "Core Analysis Report for Mobil Exploration & Production Company, Cargill Unit No. 15, SFE No. 3, Waskom Field, Harrison County, Texas," (April 17).

Western Atlas International Core Lab, 1989b: "Core Analysis Report for Mobil Exploration & Production Company, Cargill Unit No. 15, SFE No. 3, Waskom Field, Harrison County, Texas," (June 23).

Western Atlas International Core Lab, 1989c: "Special Core Analysis Study on Samples from the Travis Peak and Cotton Valley Formations, Mobil E & P Cargill Unit #15 (SFE #3)," (October 20).

Western Atlas International Core Lab, 1989d: "Effects of Cleaning and Drying on Electrical Properties, Relative Permeability, and Capillary Pressure of Samples from the Travis Peak Formation, Mobil E & P, Cargill Unit #15 Well (SFE #3)," (July 14).

Whitehead, W.S., E.R. Hunt and S.A. Holditch, 1987: "The Effects of Lithology and Reservoir Pressure on the In-Situ Stresses in the Waskom (Travis Peak) Field," SPE/DOE Paper 16403 presented at Symposium on Low Permeability Reservoirs, Denver, Colorado, May 18-19.

SECTION 5.0 IN-SITU STRESS TESTING AND STRESS PROFILING

CER Corporation and S.A. Holditch & Associates (Eds.), 1988: "Advancements in Travis Peak Formation Evaluation and Hydraulic Fracture Technology, Staged Field Experiment No. 1, Waskom Field, Harrison County, Texas," Report No. GRI-88/0077, prepared for GRI under Contract No. 5086-211-1306 (April).

CER Corporation and S.A. Holditch & Associates (Eds.), 1989: "Staged Field Experiment No. 2, Application of Advanced Geological, Petrophysical and Engineering Technologies to Evaluate and Improve Gas Recovery from Low Permeability Sandstone Reservoirs, Travis Peak Formation, North Appleby Field, Nacogdoches County, Texas," Report No. GRI-89/0140, prepared for GRI under Contract No. 5088-211-1682 (June) I.

SECTION 6.0 ANALYSES AND INTERPRETATIONS OF PRE-FRACTURE DATA

Fix, J.E. and Others, 1989: "Development of Microseismic Methods to Determine Hydraulic Dimensions," Teledyne Geotech, Annual report (December 1987 - November 1988) prepared for GRI, GRI Report No. 89/0116, Teledyne Geotech Technical Report No. 88-11.

Lee, W.J., 1982: *Well Testing*, Society of Petroleum Engineers of AIME, New York.

SECTION 7.0 HYDRAULIC FRACTURE TREATMENT OF THE LOWER COTTON VALLEY FORMATION (TAYLOR SANDSTONE)

No specific references.

SECTION 8.0 POST-FRACTURE ANALYSIS

Barker, B.J. and H.J. Ramey, Jr., 1978: "Transient Flow to Finite-Conductivity Vertical Fractures," SPE Paper 7489 presented at the 1978 SFE Annual Technical Conference and Exhibition, Houston, October 1-3.

Cinco, H., F. Samaniego and N. Dominquez, 1978: "Transient Pressure Behavior for a Well with a Finite-Conductivity Vertical Fracture," *J. Pet. Tech.* (August) 253-264.

Fix, J.E. and Others, 1989: "Development of Microseismic Methods to Determine Hydraulic Dimensions," Teledyne Geotech, Annual report (December 1987 - November 1988) prepared for GRI, GRI Report No. 89/0116, Teledyne Geotech Technical Report No. 88-11.

Hunt, E.R., 1990: "Summary of Independent Analysis of Fracture Heights as Compared to the Continuous Microseismic Radiation Survey on GRI's SFE No. 3 (Mobil Cargill No. 15)," Prepared for GRI, Report No. GRI-90/0087 (February).

GENERAL REFERENCES

Cleary, M.P., 1980: "Analysis of Mechanisms and Procedures for Producing Favorable Shapes of Hydraulic Fractures," SPE Paper 9260, 1980 SPE Annual Technical Conference and Exhibition, Dallas, September.

Crockett, A.R., N.M. Okusu and N.P. Cleary, 1986: "A Complete Integrated Model for Design and Real-Time Analysis of Hydraulic Fracturing Operations," SPE Paper 15069, SPE 56th California Regional Meeting, Oakland, California, April.

Crockett, A.R., R.M. Willis and M.P. Cleary, 1989: "Improving Hydraulic Fracture Predictions by Real-Time History-Matching on Observed Pressures", *Production Engineering*, 4, 408-416.

Willis, R.M., T.B. Wright and A.M. Buhrli, 1987: "Monitoring and Analysis of Coal-Bed Fracturing Operations Using the GRI Mobile Test and Control Facility," Presented at Coal-Bed Methane Symposium, Tuscaloosa, Alabama, November.

Cleary, M.P., D.T. Barr and R.M. Willis, 1988: "Enhancement of Real-Time Hydraulic Fracturing Models with Full 3-D Simulation," SPE Paper No. 17713 presented at SPE Gas Technology Symposium, Dallas, Texas, June; *Production Engineering*, in press.

Cleary, M.P., 1988: "The Engineering of Hydraulic Fractures - State of the Art and Technology of the Future," *J. Pet. Tech.*, Distinguished Author Series (January) 13-21.

Nomenclature

a_0	coefficient for hyperbolic relationship given in Equation 4-18
a_1	coefficient for hyperbolic relationship given in Equation 4-18
a_2	coefficient for hyperbolic relationship given in Equation 4-18
Cr	dimensionless fracture conductivity
c	a units constant for Equation 4-20
c_b	bulk compressibility
E	Young's modulus
F	formation resistivity factor
G	shear modulus
H	average background horizontal component of motion
h	thickness
K_b	bulk modulus
k	permeability
k_a	permeability to air
k_b	permeability to brine
k_g	permeability to gas
k_w	permeability to water
k_∞	Klinkenberg-corrected gas permeability
L_f	fracture half-length
m	cementation factor
n	saturation exponent
P_c	capillary pressure
P_g	formation pressure gradient
P'_g	effective formation pressure gradient
P^*	extrapolated Horner pressure (Horner time = 1)
R	ratio of compressional and shear velocities
R_O	resistivity at $S_w = 100$ percent
R_T	resistivity at each S_w
r	correlation coefficient
r_f	hydraulic fracture radius
S_h	minimum horizontal stress gradient (also closure stress gradient)
S_{iw}	irreducible water saturation

S_p	stress gradient from internal pore pressure
S_v	vertical (overburden) stress gradient
S_w	water saturation
S_x	stress gradient in the x direction
S_y	stress gradient in the y direction
S_z	stress gradient in the z direction
s	skin effect
V_{sh}	shale volume
X	empirical stress factor
Z	average background vertical component of motion
β	biot constant - ratio of compressibility of solid rock to that of drained porous rock
Δ	delta
ϵ_x	elastic strain in the x direction
ν	Poisson's ratio
π	pi, 3.141592
ρ_b	bulk density
σ_c	in-situ stress gradient
σ_x	stress in the x direction
ϕ	porosity
ϕ_D	porosity derived from density log
ϕ_{De}	effective porosity from density log
ϕ_{Dsh}	shale correction factor for density log calculations
ϕ_e	effective porosity
ϕ_f	storage volume of hydraulic fracture
ϕ_N	porosity derived from neutron log
ϕ_{Ne}	effective porosity from neutron log
ϕ_{Nsh}	shale correction factor for neutron log calculations
ϕ_{nls}	neutron porosity in limestone units
ϕ_r	storage volume of radial fracture system
ϕ_s	porosity derived from sonic log
ϕ_{sh}	shale correction factor
ω	fracture width

Appendix 1

LOGGING OPERATIONS

APPENDIX 1

Results of Run No. 1 (Surface) Logging Operations

Results of Run No. 2 (Intermediate) Logging Operations

Results of Run No. 3 (First TP/CV) Logging Operations

Results of Run No. 4 (Second TP/CV) Logging Operations

Results of Run No. 5 (Third TP/CV) Logging Operations

Results of Run No. 6 (Final) Logging Operations

Results of Run No. 7 (Pre-Perforation) Logging Operations

Results of Run No. 8 (Post Perforation/Pre-Mini-Frac) Logging Operations

Results of Run No. 9 (Post Mini-Frac Treatment) Logging Operations

Results of Run No. 10 (Post Main Fracture Treatment) Logging

Results of Run No. 1 (Surface) Logging Operations

Date Logged: September 9, 1988
Run Number: 1
Logger's TD: 1,481 ft
Logging Service Company: Western Atlas

Descent No.	Service	Interval, ft	Notes
1	Dual Induction/Gamma Ray (GR)/ Spontaneous Potential (SP)		1
2	Dual Induction/GR/SP	0 - 1,481	2

Note 1: Could not get below 700 ft on this descent. Hole conditioning trip was made before Descent No. 2.

Note 2: Excellent quality log data. However, certain borehole conditions caused some data to be unusable.

Results of Run No. 2 (Intermediate) Logging Operations

Date Logged: September 22, 1988
Run Number: 2
Logger's TD: 6,311 ft
Logging Service Company: Western Atlas

Descent No.	Service	Interval, ft	Notes
1	Dual Induction Focused Log/GR/SP	1,470-6,311	1
1	Long Spaced Sonic/Caliper	1,470-6,311	1
2	Z-Density (Photoelectric Effect)	1,470-6,311	1
3	Formation Multitester/GR	5,934-6,300	1,2

Note 1: Excellent quality log data. However, certain borehole conditions caused some data to be unusable.

Note 2: Formation pressure data acquired at 5,934 ft, 6,004 ft, 6,017 ft, 6,144 ft and 6,152 ft.

Results of Run No. 3 (First TP/CV) Logging Operations

Date Logged: September 29-30, 1988
 Run Number: 3
 Logger's TD: 7,354 ft
 Logging Service Company: Western Atlas

Descent No.	Service	Interval, ft	Notes
1	Dual Induction Focused Log/ GR/SP	6,310-7,354	1
2	MicroLaterolog/Caliper/GR		2
3	MicroLaterolog/Caliper/GR	6,310-7,354	1
4	MicroLaterolog/Caliper/GR		3
5	MicroLaterolog/Caliper/GR	6,310-7,354	1
6	Proximity Log/Caliper/ GR/MiniLog	6,310-7,354	1

Note 1: Excellent quality log data. However, certain borehole conditions caused some data to be unusable.

Note 2: Surface data acquisition software program not compatible with Microlaterolog tool.

Note 3: MicroLaterolog tool failed downhole.

Results of Run No. 4 (Second TP/CV) Logging Operations

Date Logged: October 4-5, 1988
Run Number: 4
Logger's TD: 7,868 ft
Logging Service Company: Western Atlas

Descent No.	Service	Interval, ft	Notes
1	Dual Induction Focused Log/ Z-Density (Photoelectric)/GR/SP		2
2	Dual Induction Focused Log/ GR/SP	6,310-7,868	1
3	Z-Density (Photoelectric)/ Caliper/GR	6,310-7,868	1
4	Proximity Log	6,310-7,868	3
5	Proximity Log	6,310-7,868	1

Note 1: Excellent quality log data. However, certain borehole conditions caused some data to be unusable.

Note 2: Adapter between Dual Induction and Z-Density failed downhole, requiring separate descents for each tool.

Note 3: Proximity Log resistivity read low in shales.

Results of Run No. 5 (Thrd TP/CV) Logging Operations

Date Logged: October 14-17, 1988
 Run Number: 5
 Logger's TD: 9,018 ft
 Logging Service Company: Western Atlas

Descent No.	Service	Interval, ft	Notes
1	Dual Induction Focused Log/GR/SP	6,310-9,018	1
2	Proximity Log/GR		2
3	Proximity Log/GR		3
4	Proximity Log/GR	6,310-9,018	3
5	Proximity Log/GR		3
6	Z-Density (Photoelectric)/GR/Caliper	6,310-9,018	1
7	Proximity Log/GR	7,700-9,018	2,4
8	Proximity Log/GR		2
9	Proximity Log/GR	7,700-9,018	2
10	Proximity Log/GR	6,310-9,018	3,5
11	Proximity Log/GR		2
12	Proximity Log/GR	6,310-8,300	1

Note 1: Excellent quality log data. However, certain borehole conditions caused some data to be unusable.

Note 2: Proximity tool failed downhole.

Note 3: Proximity resistivity reading low.

Note 4: Open-hole stress test performed between Descent Nos. 6 and 7.

Note 5: A 30-ft core was cut between Descent Nos. 9 and 10.

Results of Run No. 6 (Final) Logging Operations

Date Logged November 2-11, 1988
 Run Number: 6
 Logger's TD: 9,690 ft
 Logging Service Companies: Western Atlas [WA]
 Schlumberger Well Services [SWS]
 Halliburton Logging Services [HLS]

Research Logging
 Organizations: Schlumberger Doll Research [SDR]
 Mobil Dallas Research Lab [MDRL]
 Amoco Production Research [APR]
 PetroData Systems, Inc. [PSI]

Descent No.	Service	Interval, ft	Notes
1	Proximity Log/GR [WA]		2
2	Proximity Log/GR [WA]		2
3	Proximity Log/GR [WA]	6,310-9,690	1
4	Dual Induction Focused Log/GR/SP[WA]	6,310-9,690	1
4	Z-Density (Photoelectric Measurement)/Caliper/GR [WA]	6,310-9,690	1
4	Compensated Neutron [WA]	4,550-9,690	1
5	Long Spaced Sonic/Waveforms [APR]	5,500-9,600	1
6	Borehole Televiewer [APR]		2
7	Digital Sonic/Waveforms [SWS]	6,310-9,692	1
8	Electromagnetic Propagation Log/LithoDensity Log/Caliper [SWS]	6,310-9,692	1
8	Compensated Neutron Log/GR [SWS]	5,800-9,692	1
9	Formation Microscanner/GR/4-Arm Caliper [SWS]	7,340-9,630	1,3

10	Modular Reservoir Testing Tool (RFT)/ GR [SWS]	6,350-9,414	1
11	Digital Sonic Waveform Tool/ Waveforms [SDR]	7,300-7,400	1
12	Borehole Televierer [SDR]		2
13	Borehole Televierer [SDR]	7,320-9,620	1,4
14	Stratigraphic High Resolution Dipmeter/4-Arm Caliper [SWS]	6,310-9,678	1
15	Dipole Sonic/GR [SWS]	7,300-9,400	1,3
16	Geochemical Log/Natural GR [SWS]	6,310-9,660	1
17	Rotary SideWall Coring Tool (RSCT)/ GR [HLS]	9,600	1,5
18	RSCT/GR [HLS]	8,359-9,414	1,5
19	RSCT/GR [HLS]	8,211-8,352	1,2
20	Borehole Televierer [MDRL]	7,330-9,630	1
21	Borehole Televierer [MDRL]	9,330-9,630	1,2
22	Shear Wave Sonic Log [MDRL]	5,800-9,690	1
22	P-Wave Sonic Log [MDRL]	5,800-9,690	1
22	Stonely Wave Sonic Log [MDRL]	6,310-9,700	1
23	High Resolution Induction [HLS]		2
24	6-Arm Microsonic Dipmeter [HLS]		2,3
25	Quadra Pole Sonic Log - Large Source [PSI]	6,300-9,690	1
26	Quadra Pole Sonic Log - Small Source [PSI]	8,800-9,690	1
27	Sonic Echo Log [PSI]	7,800-9,690	1
28	RSCT/GR [HLS]		2
29	RSCT/GR [HLS]	6,405-7,522	1,5

30	RSCT/GR [HLS]	7,732	1,5
----	---------------	-------	-----

Note 1: Excellent quality log data. However, certain borehole conditions caused some data to be unusable.

Note 2: Equipment failure downhole resulted in discontinuance of descent.

Note 3: Hole conditioning tripe made between Descent No. 24 and 25.

Note 4: Certain tool measurements inoperative, preventing acquisition of all data.

Note 5: RSCT coring bit jammed, descent discontinued.

Results of Run No. 7 (Pre-Perforation) Logging Operations

Date Logged: November 29-December 4, 1988
 December 8-10, 1988

Run Number: 7

Logger's TD: 9,650 ft

Logging Service Companies: Schlumberger Well Services [SWS]
 Edcon Logging

Research Organizations: Mobil Dallas Research Labs [MDRL]
 Amoco Production Research [APR]
 PetroData Services Inc. [PSI]
 Teledyne Geotech [TG]

Descent No.	Service	Interval, ft	Notes
1	Tube Wave Reflection Log [MDRL]	8,500-9,640	1
2	Cement Bond Log/Variable Density Log/ GR/Casing Collar Locator (CCL)	5,300-9,640	1
3	Cement Evaluation Log/CCL/GR [SWS]	6,300-9640	1
4	Borehole Gravimeter [Edcon]/GR [SWS]/ Pressure Gauge [CER]	250-9,330	1
5	BHGM [APR]		2
6	Continuous Microseismic Radiation Survey (CMR) [TG]	9,000-9,600	1,2
7	Anisotropic Shear Wave Log [MDRL]	8,500-9,640	1
8	Long Spaced Acoustic Log [MDRL]	8,500-9,640	1
9	Shear Wave Acoustic Log [MDRL]	8,500-9,640	1
10	Temperature Log [SWS]	8,500-9,640	1,3
11	CMR [TG]		1
12	CMR [TG]	9,025-9,125	1
13	Quadra Pole Sonic [PSI]	8,500-9,460	1
14	Quadra Pole Sonic - Echo Mode [PSI]	8,500-9,460	1

- Note 1: Excellent quality log data. However, certain mechanical conditions, such as poor cement bonding, caused some data to be unusable.
- Note 2: Equipment failure resulted in discontinuance of descent.
- Note 3: Cased-hole stress tests and cement squeeze operation performed between this and subsequent descents.

Results of Run No. 8 (Post-Perforation/Pre-Mini-Frac) Logging Operations

Date Logged: January 26, 1989
 February 11-12, 1989

Run Number: 8

Logger's TD: 9,639 ft

Logging Service Companies: Schlumberger Well Services [SWS]
 Halliburton Logging Services [HLS]

Logging Research Organizations: Teledyne Geotech [TG]
 Mobil Dallas Research Labs [MDRL]

Descent No.	Service	Interval, ft	Notes
1	Tube Wave Reflection Log [MDRL]	8,800-9,600	1,3
2	Cement Evaluation Log/GR/CL [SWS]	8,800-9,620	1
3	Cement Bond Log/Variable Density Log/GR/CCL [SWS]	8,800-9,620	1
4	Continuous Microseismic Radiation [TG]	9,000-9,620	1,2
5	Tracer Scan Log [HLS]	8,900-9,640	1

- Note 1: Excellent quality log data. However, certain mechanical conditions, such as poor cement bonding, caused some data to be unusable.
- Note 2: Orienting equipment failed downhole, but did not interrupt operations.
- Note 3: Descent performed on January 26, 1989.

Results of Run No. 9 (Post-Mini-Frac Treatment) Logging Operations

Date Logged: February 15-19, 1989
 Run Number: 9
 Logger's TD: 9,590 ft
 Logging Service Companies: Schlumberger Well Services [SWS]
 Halliburton Logging Services [HLS]
 Research Logging Organizations: Mobil Dallas Research Labs [MDRL]
 Teledyne Geotech [TG]

Descent No.	Service	Interval, ft	Notes
1	CMR [TG]		2
2	CMR [TG]		2
3	CMR [TG]	9,000-9,590	1,3
4	CMR [TG]	9,000-9,590	1
5	Tube Wave Reflection Log [MDRL]	8,900-9,590	1
6	Cement Bond Log/Variable Density Log/GR/CCL [SWS]	8,900-9,590	1
7	Cement Evaluation Log/GR/CCL [SWS]	8,900-9,590	1
8	TracerScan Log [HLS]	8,800-9,590	1

Note 1: Excellent quality log data. However, certain mechanical conditions, such as poor cement bonding, caused some data to be unusable.

Note 2: Equipment failure resulted in discontinuance of descent.

Note 3: Orienting equipment failed downhole, but did not interrupt operations.

Results of Run No. 10 (Post-Main Fracture Treatment) Logging Operations

Date Logged: March 22, 1989
 July 24-28, 1989
 Run Number: 10
 Logger's TD: 9,516 ft
 Logging Service Companies: Halliburton Logging Services [HLS]
 Schlumberger Well Services [SWS]
 Research Logging Organizations: Mobil Dallas Research Labs [MDRL]
 Teledyne Geotech [TG]
 Petro Data Services, Inc [PSI]

Descent No.	Service	Interval, ft	Notes
1	Tracer Scan Log [HLS]		3,5
2	Sinker Bars [HLS]		4,5
3	Tracer Scan Log [HLS]	8,950-9,516	1,5
4	Cement Bond Log (CBL)/Variable Density Log (VDL)/GR/CCL [SWS]		2
5	CBL/VDL/GR/CCL [SWS]		2
6	CBL/VDL/GR/CCL [SWS]		2
7	Cement Evaluation Log/GR/CCL [SWS]	8,900-9,460	1
8	Tube Wave Reflection Log - Small Source [MDRL]	8,900-9,460	1
9	Tube Wave Reflection Log - Large Source [MDRL]	8,900-9,460	1
10	Continuous Microseismic Radiation Survey [TG]	8,700-9,440	1
11	CBL/VDL/GR/CCL [SWS]	8,900-9,460	1
12	QuadraPole Sonic [PSI]	8,900-9,460	2

Note 1: Excellent quality log data. However, certain mechanical conditions, such as poor cement bonding, caused some data to be unusable.

Note 2: Equipment failure resulted in discontinuance of descent.

- Note 3: Downward progress of tool halted at 8,000 ft inside tubing. Pulled tool out of hole. Released and reset packer with less weight on it prior to descent No. 2.
- Note 4: Tool string consisting only of sinker bars lowered into the well to determine ability of reaching TD.
- Note 5: Descent performed on March 22, 1989.

Appendix 2

ROUTINE CORE ANALYSIS RESULTS

A2

CORE LABORATORIES

Company : MOBIL EXPLORATION & PRODUCTION COMPANY
 Well : Cargill Unit No. 15
 Location :
 Co,State : Harrison County, Texas

Field : Waskom Field
 Formation : Travis Pk, Cotton Valley
 Coring Fluid : Water Base Mud
 Elevation :

File No.: 57151-15922
 Date : 30-Mar-1989
 API No. :
 Analysts: DEVIER, JR, BB, RG

CORE ANALYSIS RESULTS
 (HYDROSTATIC CONFINEMENT)

SAMPLE NUMBER	DEPTH ft	NOB (800 psi)		NOB (Reservoir)		POROSITY (HELIUM) %	SATURATION (PORE VOLUME)		GRAIN DENSITY gm/cc	DESCRIPTION	RES PRESS psi
		K _o	φ	K _o	φ		OIL	WATER			
		md	%	md	%		%	%			
CORE No. 1 7351.0 - 7397.7 ft											
1	7351.8	0.012	6.1	0.003			0.0	74.3	2.78	Sst lt rd v f/f gr pyr mic slily calc no flu	3823.
2	7352.7	0.021	7.2	0.015	6.9		0.0	52.7	2.66	Sst lt rd v f/f gr v slily calc no flu	3823.
3	7353.8					10.4	0.0	50.1	2.69	Sst lt rd v f/f gr sh lam no flu	
4	7354.7	0.050	8.5	0.041	8.2		0.0	61.3	2.68	Sst lt rd v f/f gr v slily calc no flu	3824.
5	7355.3	0.047	9.7	0.035	8.3		0.0	69.6	2.70	Sst lt rd v f/f gr sh lam pyr no flu	3825.
6	7356.7	0.309	9.7	0.238	9.5		0.0	43.6	2.66	Sst lt rd v f/f gr v slily calc no flu	3825.
* 7	7357.4					9.1	0.0	44.7	2.67	Sst lt rd v f/f gr v slily calc no flu	
8	7358.0	0.156	9.3	0.111	9.1		0.0	43.1	2.66	Sst lt rd v f/f gr cln no flu	3826.
9	7358.9	0.072	10.4	0.052	9.5		0.0	46.9	2.68	Sst lt rd v f/f gr occ pyr no flu	3827.
10	7360.1	0.002	4.5	<.001	4.2	5.0	0.0	65.2	2.74	Sst lt rd v f/f gr slily sh lam pyr slily calc no flu	
11	7360.9	0.071	9.0	0.038	8.7		0.0	59.4	2.59	Sst lt rd v f/f gr slily stly no flu	3828.
12	7361.5	0.187	9.1	0.095	8.8		0.0	63.5	2.67	Sst lt rd v f/f gr cln no flu	3828.
13	7362.4	0.055	7.3	0.029	7.0		0.0	61.6	2.66	Sst lt rd v f/f gr v slily calc no flu	3828.
14	7363.4	0.272	10.2	0.203	9.8		0.0	69.6	2.67	Sst lt rd v f/f gr v slily calc no flu	3829.
15	7363.9	0.032	7.5	0.008	7.0		0.0	73.5	2.68	Sst lt rd f/m gr sh lam occ pyr no flu	3829.
* 16	7364.5					6.9	0.0	58.7	2.66	Sst lt rd f/m gr sh no flu	
17	7365.4	0.035	7.3	0.012	7.1		0.0	64.4	2.66	Sst lt rd v f/f gr cln no flu	3830.
18	7366.3	0.046	7.0	0.017	6.7		0.0	63.8	2.66	Sst lt rd v f/f gr slily sh no flu	3830.
* 19	7367.1					9.4	0.0	72.8	2.67	Sst lt rd v f/f gr sh lam no flu	
20	7367.5	0.026	8.6	0.026	8.2		0.0	72.7	2.67	Sst lt rd v f/f gr cln no flu	3831.
21	7368.3	0.151	10.9	0.114	10.5		0.0	71.8	2.66	Sst lt rd v f/f gr cln no flu	3832.
22	7369.5	0.111	8.5	0.077	8.2		0.0	67.6	2.65	Sst lt brn v f/f gr occ pyr no flu	3832.
23	7370.3	0.037	10.2	0.035	9.0		0.0	65.9	2.67	Sst lt brn v f/f gr sh lam no flu	3833.
24	7371.1	0.347	8.1	0.244	7.7		0.0	57.7	2.65	Sst lt brn v f/f gr cln no flu	3833.

FINAL REPORT 1 - 1

CORE LABORATORIES

Company : MOBIL EXPLORATION & PRODUCTION COMPANY
 Well : Cargill Unit No. 15

Field : Waskom Field
 Formation : Travis Pk, Cotton Valley Date : 30-Mar-1989

File No.: 57151-15922

CORE ANALYSIS RESULTS

(HYDROSTATIC CONFINEMENT)

SAMPLE NUMBER	DEPTH ft	NOB (800 psi)		NOB (Reservoir)		POROSITY (HELIUM) %	SATURATION (PORE VOLUME)		GRAIN DENSITY gm/cc	DESCRIPTION	RES PRESS psi
		K _w	φ	K _w	φ		OIL	WATER			
		md	%	md	%		%	%			
25	7371.9	0.042	4.7	0.007	4.3	0.0	37.4	2.68	Sst lt brn v f/m hd sh lam no flu	3833.	
26	7372.5	0.083	8.8	0.048	8.4	0.0	73.2	2.66	Sst lt rd v f/f gr hd no flu	3834.	
27	7373.2	0.008	5.2	0.004		0.0	85.2	2.68	Sst lt rd v f/f gr hd no flu	3834.	
28	7374.6	0.019	8.0	0.019	7.8	0.0	61.2	2.66	Sst lt brn v f/f gr hd no flu	3835.	
29	7375.3	0.128	9.0	0.094	8.7	0.0	74.4	2.69	Sst lt brn v f/f gr hd no flu	3835.	
30	7376.9	0.591	9.7	0.510	9.4	0.0	65.1	2.65	Sst lt brn v f/f gr hd no flu	3836.	
31	7377.9	0.329	9.6	0.214	9.2	0.0	66.7	2.66	Sst lt brn v f/f gr hd no flu	3837.	
32	7378.9	0.029	7.5	0.018	6.8	0.0	68.6	2.67	Sst lt brn v f/f gr hd lam no flu	3837.	
33	7379.4	7.38	8.6	6.90	8.3	0.0	58.4	2.67	Sst lt brn v f/f gr hd no flu	3837.	
CORE No. 2 7381.9 - 7409.8 ft											
34	7381.3	17.5	9.3	16.7	9.0	0.0	58.2	2.65	Sst lt brn v f/m gr hd lam no flu	3838.	
35	7382.2	34.5	10.1	32.2	9.8	0.0	66.0	2.64	Sst lt brn v f/m gr hd lam no flu	3839.	
36	7384.2	73.0	12.4	68.4	12.1	0.0	59.4	2.65	Sst lt brn v f/m gr hd lam no flu	3840.	
37	7385.5	136.	13.2	130.	12.9	0.0	63.4	2.64	Sst lt brn v f/m gr hd lam no flu	3840.	
38	7386.5	146.	12.8	140.	12.5	0.0	47.6	2.65	Sst lt brn m/c gr hd occ sh lam no flu	3841.	
39	7391.5	72.8	12.1	69.1	11.8	0.0	53.0	2.65	Sst lt brn f/m gr hd no flu	3844.	
40	7392.1	78.0	12.8	74.0	12.5	0.0	60.1	2.65	Sst lt brn f/m gr hd no flu	3844.	
41	7393.1	24.2	9.7	22.7	9.3	0.0	45.3	2.64	Sst lt brn f/m gr hd no flu	3844.	
42	7393.5	0.056	7.1	0.013	6.5	0.0	80.3	2.67	Sst lt brn v f/f gr hd no flu	3845.	
43	7394.2	0.169	8.6	0.039	7.9	0.0	82.2	2.68	Sst lt rd v f/f gr hd hem no flu	3845.	
44	7395.4	0.053	9.5	0.028	8.8	0.0	88.3	2.66	Sst gry wh f/m gr hd no flu	3846.	
45	7396.0	0.010	4.8	0.006	4.6	0.0	92.9	2.68	Sst lt rd v f/f gr hd no flu	3846.	
46	7396.9	0.065	10.4	0.036	9.9	0.0	82.3	2.67	Sst lt rd v f/f gr hd no flu	3846.	
47	7397.5	0.023	7.9	0.007		0.0	91.1	2.71	Sst lt rd v f/f gr hd no flu	3847.	
48	7398.1	0.050	9.9	0.031	8.2	0.0	82.3	2.68	Sst lt rd v f/f gr hd no flu	3847.	
49	7398.9	0.028	9.3	0.012	7.2	0.0	88.6	2.68	Sst lt rd v f/f gr hd no flu	3847.	

CORE LABORATORIES

Company : MOBIL EXPLORATION & PRODUCTION COMPANY
Well : Cargill Unit No. 15

Field : Waskom Field
Formation : Travis Pk, Cotton Valley
File No.: 57151-15922
Date : 30-Mar-1989

CORE ANALYSIS RESULTS
(HYDROSTATIC CONFINEMENT)

SAMPLE NUMBER	DEPTH ft	NOB (800 psi)		NOB (Reservoir)		POROSITY (HELIUM) %	SATURATION		GRAIN DENSITY gm/cc	DESCRIPTION	RES PRESS psi
		K _w	φ	K _w	φ		(PORE VOLUME) OIL %	WATER %			
		md	%	md	%						
50	7399.9	0.090	2.2	0.009			0.0	85.4	2.73	Sst dk f/m gr v hd v hem no flu	3848.
51	7400.9	0.623	4.1	0.062	2.5		0.0	84.8	2.76	Sst dk f/m gr v hd v hem no flu	3848.
52	7401.9	0.039	7.3	0.018	6.8		0.0	84.1	2.67	Sst lt rd v f/f gr hd slty lam no flu	3849.
53	7402.9	0.040	7.0	0.024	6.6		0.0	81.3	2.67	Sst lt rd v f/f gr hd slty lam no flu	3850.
54	7403.8	0.096	7.5	0.052	7.3		0.0	65.7	2.66	Sst lt rd v f/f gr hd slty lam no flu	3850.
55	7404.9	0.267	8.6	0.127	8.3		0.0	72.4	2.66	Sst lt rd v f/f gr hd slty lam no flu	3851.
56	7405.9	0.067	7.9	0.029	7.4		0.0	74.8	2.66	Sst lt rd v f/f gr hd slty lam no flu	3851.
57	7406.9	0.201	6.2	0.118	6.0		0.0	55.5	2.65	Sst lt rd v f/f gr hd slty lam no flu	3852.
58	7407.9	0.360	7.9	0.255	7.6		0.0	66.2	2.65	Sst lt rd v f/f gr hd slty lam no flu	3852.
CORE No. 3 7868.0 - 7888.6 ft											
59	7869.1	0.016	2.2	<.001			0.0	79.7	2.83	Sst m gry v f/f gr hd calc v sh pyr no flu	4092.
60	7870.5	0.013	3.7	<.001			0.0	94.1	2.79	Sst m gry v f/f gr hd calc v sh pyr no flu	4093.
61	7871.5	0.083	4.7	0.007			0.0	89.7	2.77	Sst m gry v f/f gr hd calc v sh pyr no flu	4093.
62	7872.9						0.0	77.1	2.85	Sst m gry v f/f gr hd calc v sh pyr no flu	
63	7873.6	0.069	3.9	0.014	3.5	3.5	0.0	91.2	2.77	Sst m gry v f/f gr hd calc v sh pyr no flu	4095.
64	7874.8	0.016	3.9	<.001			0.0	78.5	2.80	Sst m gry v f/f gr hd calc v sh pyr no flu	4095.
65	7875.5	0.004	2.8	<.001			0.0	74.1	2.75	Sst m gry v f/f gr hd calc v sh pyr no flu	4095.
66	7876.4	0.068	5.9	0.020	5.1	5.1	0.0	42.5	2.65	Sst gry wh v f/f gr hd no flu	4096.
67	7877.6	0.308	7.9	0.225	7.5	7.5	0.0	52.9	2.65	Sst gry wh v f/f gr hd no flu	4096.
68	7879.3	1.28	9.1	1.13	8.8	8.8	0.0	47.8	2.65	Sst gry wh v f/f gr hd no flu	4097.
69	7880.3	1.53	8.8	1.39	8.5	8.5	0.0	48.9	2.69	Sst gry wh v f/m gr hd sh lam no flu	4098.
70	7881.4	0.657	9.1	0.546	8.6	8.6	0.0	55.9	2.70	Sst gry wh v f/m gr hd sh lam no flu	4098.
71	7882.4	0.220	7.8	0.176	7.6	7.6	0.0	59.4	2.65	Sst gry wh v f/m gr hd sh lam no flu	4099.
72	7883.2	0.189	9.2	0.127	8.8	8.8	0.0	66.3	2.67	Sst gry wh v f/f gr hd lam no flu	4099.
73	7884.5	0.015	8.1	0.010	7.8	7.8	0.0	82.1	2.69	Sst gry wh v f/f gr hd lam no flu	4100.
74	7884.8	0.068	6.4	0.004			0.0	88.3	2.71	Sst gry wh v f/f gr hd v sh lam no flu	4100.

FINAL REPORT 1 - 3

CORE LABORATORIES

Company : MOBIL EXPLORATION & PRODUCTION COMPANY
 Well : Cargill Unit No. 15

Field : Waskom Field
 Formation : Travis Pk, Cotton Valley
 File No.: 57151-15922
 Date : 30-Mar-1989

CORE ANALYSIS RESULTS
 (HYDROSTATIC CONFINEMENT)

SAMPLE NUMBER	DEPTH ft	NOB (800 psi)		NOB (Reservoir)		POROSITY (HELIUM) %	SATURATION (PORE VOLUME)		GRAIN DENSITY gm/cc	DESCRIPTION	RES PRESS psi
		K _o md	φ %	K _o md	φ %		OIL %	WATER %			
* 75	7886.0					6.1	0.0	87.6	2.70	Sh m gry blk y hd no flu	
76	7887.2	0.022	4.7	0.001			0.0	62.8	2.67	Sst gry wh v f/f gr hd calc no flu	4101.
CORE No. 4 7888.6 - 7912.5 ft											
77	7888.9	0.034	6.4	0.008			0.0	82.4	2.77	Sst gry wh v f/f gr hd sh calc no flu	4102.
78	7889.9	0.028	6.6	0.005			0.0	64.8	2.73	Sst gry wh v f/f gr hd sh calc no flu	4103.
79	7890.9	0.014	5.8	0.003			0.0	64.1	2.73	Sst gry wh v f/f gr hd calc no flu	4103.
80	7891.8	0.017	6.6	0.006			0.0	81.0	2.75	Sst lt gry v f/f gr hd v sh pyr v calc no flu	4104.
81	7892.8	0.018	5.0	0.004			0.0	81.5	2.77	Sst lt gry v f/f gr hd v sh pyr v calc no flu	4104.
82	7893.9	0.019	4.2	0.004			0.0	77.0	2.77	Sst lt gry v f/f gr hd v sh pyr v calc no flu	4105.
83	7894.8	0.048	3.4	0.008			0.0	87.7	2.79	Sst lt gry v f/f gr hd v sh pyr v calc no flu	
84	7896.4	0.174	5.3	0.052	4.9		0.0	63.7	2.81	Sst gry wh v f/f gr hd calc no flu	4106.
85	7897.0	0.154	6.9	0.061	6.5		0.0	62.9	2.67	Sst lt gry v f/f gr hd v sh pyr calc no flu	4106.
86	7898.3	0.033	5.6	0.006			0.0	84.6	2.80	Sst lt gry v f/f gr hd v sh pyr calc no flu	4107.
87	7899.3	0.032	5.8	0.005	4.8		0.0	87.5	2.78	Sst lt gry v f/f gr hd v sh pyr calc no flu	4108.
88	7900.2	0.021	3.6	0.003			0.0	80.7	2.80	Sst lt gry v f/f gr hd v sh pyr calc no flu	4108.
* 89	7901.5					1.9	0.0	85.0	2.67	Sltst m gry pity hd v sh calc no flu	
90	7902.2	0.344	3.0	0.016	2.6		0.0	86.8	2.78	Sst lt gry v f/f gr hd sh foss calc no flu	4109.
* 91	7903.2					4.9	0.0	80.2	2.80	Sst lt gry v f/f gr hd sh foss calc no flu	
* 92	7904.5					4.0	0.0	89.4	2.77	Sst lt gry v f/f gr hd sh foss calc no flu	
* 93	7905.3					2.9	0.0	89.9	2.71	Sst lt gry v f/f gr hd sh foss calc no flu	
* 94	7906.4					4.9	0.0	85.2	2.69	Sst lt gry v f/f gr hd v sh foss calc no flu	
* 95	7907.4					4.2	0.0	84.4	2.68	Sst lt gry v f/f gr hd sh foss calc no flu	
* 96	7908.4					4.8	0.0	86.7	2.69	Sst lt gry v f/f gr hd v sh foss calc no flu	
97	7909.1	0.070	7.7	0.013	6.8		0.0	92.2	2.69	Sst lt gry v f/f gr hd sh foss calc no flu	4113.
* 98	7910.3					6.6	0.0	89.9	2.73	Sst lt gry v f/f gr hd sh foss calc no flu	
99	7911.4	0.020	4.2	0.002			0.0	90.8	2.72	Sst lt gry v f/f gr hd sh foss calc no flu	4114.

CORE LABORATORIES

Company : MOBIL EXPLORATION & PRODUCTION COMPANY
Well : Cargill Unit No. 15

Field : Waskom Field
Formation : Travis Pk, Cotton Valley
File No.: 57151-15922
Date : 30-Mar-1989

CORE ANALYSIS RESULTS

(HYDROSTATIC CONFINEMENT)

SAMPLE NUMBER	DEPTH ft	NOB (800 psi)		NOB (Reservoir)		POROSITY (HELIUM) %	SATURATION (PORE VOLUME)		GRAIN DENSITY gm/cc	DESCRIPTION	RES PRESS psi
		K _o	φ	K _o	φ		OIL	WATER			
		md	%	md	%		%	%			
* 100	7912.1					4.8	0.0	94.5	2.71	Sst lt gry v f/f gr hd sh foss calc no flu	
CORE No. 5 7916.7 - 7943.3 ft											
* 101	7916.9					5.6	0.0	88.7	2.70	Sst gry wh v f/f gr hd sh lam calc no flu	
102	7917.9	0.019	3.7	<.001			0.0	69.4	2.68	Sst gry wh v f/f gr hd sh lam calc no flu	4117.
103	7918.4	0.035	5.7	0.007	5.1		0.0	90.4	2.68	Sst gry wh v f/f gr hd sh lam calc no flu	4118.
* 104	7919.9					6.3	0.0	90.4	2.74	Sh m gry plty hd pyr no flu	
* 105	7920.6					5.7	0.0	86.4	2.72	Sst gry v f/f gr hd v sh pyr calc no flu	
* 106	7921.9					7.9	0.0	91.4	2.79	Sh m gry plty hd pyr no flu	
* 107	7923.8					6.1	0.0	89.1	2.75	Sh m gry plty hd pyr no flu	
* 108	7924.6					6.2	0.0	91.6	2.79	Sst gry v f/f gr hd v sh pyr calc no flu	
109	7925.5	0.020	3.0	0.003			0.0	94.7	2.76	Sst gry v f/f gr hd v sh pyr calc no flu	4121.
* 110	7926.5					2.9	0.0	87.5	2.75	Sst gry v f/f gr hd v sh v foss pyr v calc no flu	
* 111	7927.5					6.3	0.0	87.7	2.72	Sst gry v f/f gr hd v sh v foss pyr calc no flu	
* 112	7928.2					4.4	0.0	65.8	2.66	Sst wh v f/f gr hd calc no flu	
* 113	7928.9					7.6	0.0	64.6	2.66	Sst wh v f/f gr hd calc no flu	
* 114	7930.5					7.0	0.0	38.6	2.65	Sst wh v f/f gr hd calc no flu	
* 115	7931.5					6.2	0.0	65.9	2.65	Sst wh v f/f gr hd calc no flu	
* 116	7932.2					4.8	0.0	69.4	2.66	Sst wh v f/f gr hd calc no flu	
117	7932.9	0.639	5.2	0.042	4.5		0.0	92.0	2.72	Sst lt gry v f/f gr hd v sh pyr calc no flu	4125.
* 118	7933.1					6.2	0.0	91.5	2.75	Sst lt gry v f/f gr hd intbd sh pyr calc no flu	
* 119	7934.5					5.6	0.0	90.5	2.73	Sst lt gry v f/f gr hd intbd sh pyr calc no flu	
* 120	7935.6					7.5	0.0	92.0	2.77	Sh m gry plty hd pyr no flu	
* 121	7937.5					6.0	0.0	90.9	2.78	Sst lt gry v f/f gr hd intbd sh pyr calc no flu	
* 122	7938.5					5.2	0.0	86.6	2.80	Sst gry brn v f/f gr hd v sh foss pyr calc no flu	
* 123	7939.5					6.9	0.0	90.1	2.77	Sh m gry plty hd pyr no flu	
* 124	7940.5					8.0	0.0	90.5	2.81	Sh m gry plty hd pyr no flu	

FINAL REPORT 1 - 5

CORE LABORATORIES

Company : MOBIL EXPLORATION & PRODUCTION COMPANY
 Well : Cargill Unit No. 15

Field : Maskom Field File No.: 57151-15922
 Formation : Travis Pk, Cotton Valley Date : 30-Mar-1989

CORE ANALYSIS RESULTS
 (HYDROSTATIC CONFINEMENT)

SAMPLE NUMBER	DEPTH ft	NOB (800 psi)		NOB (Reservoir)		POROSITY (HELIUM) %	SATURATION		GRAIN DENSITY gm/cc	DESCRIPTION	RES PRESS psi
		K _w	φ	K _w	φ		(PORE VOLUME) OIL	WATER			
		md	%	md	%						
* 125	7942.0					3.6	0.0	95.2	2.81	Sst gry brn v f/f gr hd sh foss calc no flu	
126	7943.2	0.017	1.8	<.001			0.0	74.5	2.82	Sst gry brn v f/f gr hd sh foss calc no flu	4130.
CORE No. 6 9017.8 - 9043.5 ft											
127	9018.0- 19.0									UNABLE TO OBTAIN SAMPLE	
* 128	9019.3					4.3	0.0	83.2	2.77	Sh dk gry hd pyr v foss v calc grad Ls no flu	
* 129	9021.5					1.9	0.0	74.5	2.72	Sh lt/dk gry blkly hd v foss pyr v calc no flu	
* 130	9021.4					2.0	0.0	76.5	2.72	Ls lt gry v f/f xln hd sh v foss no flu	
* 131	9022.6					2.5	0.0	76.3	2.73	Sh lt/dk gry plty v foss v calc no flu	
* 132	9023.5					5.3	0.0	95.1	2.78	Sh dl gry blkly foss pyr slily calc no flu	
* 133	9024.9					3.2	0.0	83.5	2.76	Sh dk gry blkly v foss pyr slily v calc no flu	
* 134	9025.7					1.7	0.0	75.7	2.72	Ls lt gry v f/f xln hd v foss no flu	
* 135	9026.7					1.9	0.0	84.2	2.72	Ls lt/dk gry microxin hd v foss no flu	
* 136	9027.6					2.5	0.0	78.9	2.76	Ls lt gry v f/f xln hd v foss pyr no flu	
* 137	9028.4					2.2	0.0	76.0	2.74	Sh lt gry plty hd v foss v calc no flu	
* 138	9029.3					3.5	0.0	89.4	2.74	Sh dk gry plty hd v foss v calc no flu	
	9030.0- 30.9									INTERVAL REMOVED BY CLIENT	
139	9033.5	0.058	2.9	0.002			0.0	90.6	2.75	Sh dk gry blkly hd slty foss pyr v calc no flu	4697.
* 140	9034.4					2.1	0.0	76.7	2.75	Ls lt gry v f/f xln hd v foss pyr no flu	
* 141	9035.5					1.9	0.0	82.1	2.73	Ls lt gry v f/f xln hd v foss pyr no flu	
* 142	9036.7					3.4	0.0	77.3	2.75	Ls lt gry v f/f xln hd v foss pyr no flu	
* 143	9037.5					2.4	0.0	79.2	2.76	Slstst lt gry plty hd v foss calc grad Ls no flu	
* 144	9038.5					4.4	0.0	74.4	2.78	Slstst dk gry plty hd v foss calc grad Ls no flu	
* 145	9039.5					4.3	0.0	83.2	2.80	Slstst dk gry plty hd v foss pyr calc grad Ls no flu	
* 146	9040.8					2.0	0.0	76.3	2.72	Slstst dk gry plty hd foss pyr slily calc no flu	
* 147	9041.9					5.1	0.0	92.5	2.77	Slstst dk gry plty hd foss pyr slily calc no flu	
* 148	9042.1					2.2	0.0	77.2	2.73	Ls lt gry v f/f xln hd sh v foss no flu	

CORE LABORATORIES

Company : MOBIL EXPLORATION & PRODUCTION COMPANY
Well : Cargill Unit No. 15

Field : Waskom Field File No.: 57151-15922
Formation : Travis Pk, Cotton Valley Date : 30-Mar-1989

CORE ANALYSIS RESULTS
(HYDROSTATIC CONFINEMENT)

SAMPLE NUMBER	DEPTH ft	NOB (800 psi)		NOB (Reservoir)		POROSITY (HELIUM) %	SATURATION (PORE VOLUME)		GRAIN DENSITY gm/cc	DESCRIPTION	RES PRESS psi
		K _w	φ	K _w	φ		OIL	WATER			
		md	%	md	%		%	%			
149	9043.3	0.277	3.6	0.008			2.6	83.0	2.71	Sltst lt gry pty hd foss calc no flu	4702.
CORE No. 7 9199.0 - 9229.0 ft											
* 150	9199.5					5.3	0.0	79.3	2.74	sltst dk gry blk y hd v foss pyr calc no flu	
* 151	9200.9					3.0	0.0	84.0	2.74	Ls lt gry v f/f xln hd sh foss no flu	
* 152	9202.6					2.6	0.0	73.0	2.73	Ls lt gry v f/f xln hd v sh foss pyr no flu	
153	9202.7	0.017	3.2	<.001			0.0	58.5	2.68	Sst gry brn v f/f gr hd calc no flu	4785.
* 154	9203.9					4.6	0.0	54.8	2.66	Sst gry brn v f/f gr hd sh lam calc no flu	
155	9204.5	0.105	6.2	0.024	5.7		0.0	65.9	2.67	Sst gry brn v f/f gr hd sh lam calc no flu	4786.
156	9205.6	0.016	7.2	0.002			0.0	42.9	2.66	Sst gry brn v f/f gr hd calc no flu	4787.
157	9206.6	0.021	8.3	0.003			0.0	41.7	2.66	Sst gry brn v f/f gr hd sh lam calc no flu	4787.
158	9207.2	0.023	7.7	0.011	7.1		0.0	38.7	2.65	Sst gry brn v f/f gr hd calc no flu	4788.
159	9208.2	0.032	8.1	0.008	7.6		0.0	38.2	2.65	Sst gry brn v f/f gr hd calc no flu	4788.
160	9209.6	0.034	8.3	0.009	7.8		0.0	39.3	2.65	Sst gry brn v f/f gr hd calc no flu	4789.
161	9210.6	0.035	8.6	0.010	8.1		0.0	36.1	2.65	Sst gry brn v f/f gr hd calc no flu	4789.
162	9211.5	0.026	7.9	0.011	6.9		0.0	47.9	2.65	Sst gry brn v f/f gr hd calc no flu	4790.
163	9212.8	0.013	1.9	<.001			0.0	60.4	2.68	Sst gry brn v f/f gr hd v calc no flu	4791.
164	9213.4	0.014	1.9	<.001			0.0	66.4	2.68	Sst gry brn v f/f gr hd v calc no flu	4791.
165	9214.8	0.024	8.5	0.015	7.6		0.0	43.5	2.66	Sst gry brn v f/f gr hd calc no flu	4792.
166	9215.2	0.026	8.2	0.014	7.5		0.0	48.5	2.66	Sst gry brn v f/f gr hd calc no flu	4792.
167	9216.4	0.025	7.5	0.013			0.0	48.2	2.66	Sst gry brn v f/f gr hd calc no flu	4793.
* 168	9217.4					1.6	0.0	75.6	2.69	Sst gry brn v f/f gr hd sh foss calc no flu	
* 169	9218.4					3.0	0.0	81.9	2.66	Sst gry brn v f/f gr hd calc no flu	
* 170	9219.6					1.1	0.0	59.1	2.66	Sst gry brn v f/f gr hd v calc no flu	
* 171	9220.6					1.0	0.0	74.0	2.68	Sst gry brn v f/m gr occ pbl hd calc no flu	
* 172	9221.2					1.0	0.0	77.1	2.68	Sst gry brn v f/m gr occ pbl hd calc no flu	
173	9222.4	0.027	6.4	0.004			0.0	80.0	2.69	Sst gry brn v f/f gr hd sh lam calc no flu	4796.

FINAL REPORT 1 - 7

CORE LABORATORIES

Company : MOBIL EXPLORATION & PRODUCTION COMPANY
 Well : Cargill Unit No. 15

Field : Waskom Field
 Formation : Travis Pk, Cotton Valley
 File No.: 57151-15922
 Date : 30-Mar-1989

CORE ANALYSIS RESULTS

(HYDROSTATIC CONFINEMENT)

SAMPLE NUMBER	DEPTH ft	NOB (800 psi)		NOB (Reservoir)		POROSITY (HELIUM) %	SATURATION (PORE VOLUME)		GRAIN DENSITY gm/cc	DESCRIPTION	RES PRESS psi
		K _w md	φ %	K _w md	φ %		OIL %	WATER %			
* 174	9223.5					5.0	0.0	87.2	2.76	Sst gry brn v f/f gr hd intbd sh calc no flu	
175	9224.4	0.025	6.4	0.005			0.0	73.7	2.69	Sst gry brn v f/f gr hd sh lam calc no flu	4797.
176	9225.3	0.001	1.7	<.001	1.3	1.7	0.0	77.4	2.70	Sst gry brn v f/f gr hd sh lam calc no flu	4797.
177	9226.3	0.010	1.5	<.001			0.0	76.3	2.69	Sst gry brn v f/f gr hd calc no flu	4798.
* 178	9227.5					1.7	0.0	81.3	2.69	Sst gry brn v f/f gr hd foss calc no flu	
* 179	9228.4					8.1	0.0	49.4	2.66	Sst gry brn v f/f gr hd calc no flu	
CORE No. 8 9229.4 - 9259.6 ft											
	9229.4- 31.0									UNABLE TO OBTAIN SAMPLE	
180	9231.6	0.059	8.9	0.018	8.3		0.0	27.6	2.65	Sst gry brn v f/f gr hd calc no flu	4800.
	9232.0- 34.0									UNABLE TO OBTAIN SAMPLE	
	9232.2- 33.1									INTERVAL REMOVED BY CLIENT	
* 181	9234.2					1.6	0.0	71.2	2.69	Sst gry brn v f/f gr hd sh lam calc no flu	
182	9234.7									UNABLE TO OBTAIN SAMPLE	
183	9235.6	0.060	3.8	0.006			0.0	70.9	2.69	Sst gry brn v f/f gr hd sh lam calc no flu	4802.
184	9236.7	0.010	2.8	<.001			0.0	69.9	2.66	Sst gry brn v f/f gr hd calc no flu	4803.
* 185	9237.5					1.1	0.0	69.2	2.69	Sst gry brn v f/f gr hd calc no flu	
* 186	9237.7					3.0	0.0	53.0	2.67	Sst gry brn v f/f gr hd calc no flu	
187	9239.6	0.008	1.5	<.001			0.0	60.1	2.69	Sst gry brn v f/f gr hd foss calc no flu	4805.
188	9240.9	0.052	7.7	0.007	7.3		0.0	39.7	2.67	Sst gry brn v f/f gr hd sh lam calc no flu	4805.
189	9241.6	0.040	6.7	0.007	4.7		0.0	36.3	2.66	Sst gry brn v f/f gr hd calc no flu	4806.
* 190	9242.9					7.6	0.0	43.5	2.67	Sst gry brn v f/f gr hd calc no flu	
* 191	9243.4					2.9	0.0	47.5	2.69	Sst gry brn m/v c gr pbl hd calc no flu	
* 192	9244.6					2.1	0.0	75.7	2.67	Sst gry brn v f/f gr pbl hd sh calc no flu	
* 193	9245.6					0.9	0.0	48.0	2.68	Sst gry brn f/v c gr pbl hd calc no flu	
194	9246.4	0.019	5.9	0.005	4.7		0.0	56.0	2.66	Sst gry brn v f/f gr hd sh lam calc no flu	4808.
* 195	9247.2					7.6	0.0	51.2	2.66	Sst gry brn v f/f gr hd calc no flu	

CORE LABORATORIES

Company : MOBIL EXPLORATION & PRODUCTION COMPANY
Well : Cargill Unit No. 15

Field : Waskom Field
Formation : Travis Pk, Cotton Valley
File No.: 57151-15922
Date : 30-Mar-1989

CORE ANALYSIS RESULTS
(HYDROSTATIC CONFINEMENT)

SAMPLE NUMBER	DEPTH ft	NOB (800 psi)		NOB (Reservoir)		POROSITY (HELIUM) %	SATURATION (PORE VOLUME) DIL WATER		GRAIN DENSITY gm/cc	DESCRIPTION	RES PRESS psi	
		K=	φ	K=	φ		%	%				%
		md	%	md	%							
196	9248.2	0.013	2.0	<.001			0.0	53.4	2.68	Sst gry brn v f/f gr hd calc no flu	4809.	
197	9249.3	0.186	8.9	0.117	8.7		0.0	27.7	2.66	Sst gry brn v f/f gr hd calc no flu	4810.	
198	9250.4	0.086	8.5	0.043	8.1		0.0	24.4	2.66	Sst gry brn v f/f gr hd calc no flu	4810.	
199	9251.3	0.064	8.4	0.027	8.0		0.0	27.6	2.66	Sst gry brn v f/f gr hd calc no flu	4811.	
200	9252.5	0.022	7.2	0.013	6.8		0.0	30.9	2.67	Sst gry brn v f/f gr hd sh lam calc no flu	4811.	
201	9253.6	0.014	5.9	0.008	5.1		0.0	36.9	2.67	Sst gry brn v f/f gr hd calc no flu	4812.	
202	9254.7	0.001	2.0	<.001	1.3	1.9	0.0	70.6	2.69	Sst gry brn v f/f gr hd sh lam calc no flu	4812.	
203	9255.6	0.008	5.8	0.005	4.0		0.0	38.8	2.67	Sst gry brn v f/f gr hd sh lam calc no flu	4813.	
204	9256.5	0.008	5.7	0.005	3.7		0.0	39.3	2.67	Sst gry brn v f/f gr hd sh lam calc no flu	4813.	
205	9257.8	0.009	4.4	0.003			0.0	39.7	2.66	Sst gry brn v f/f gr hd calc no flu	4814.	
* 206	9258.6					1.6	0.0	67.0	2.69	Sst gry brn v f/f gr hd occ pbl calc no flu		
207	9259.2	0.003	1.5	<.001	1.1	1.5	0.0	64.6	2.68	Sst gry brn v f/f gr hd v calc no flu	4815.	
CORE No. 9 9259.6 - 9282.9 ft												
208	9260.6	0.523	7.0	0.048	6.3		0.0	50.0	2.68	Sst gry brn v f/f gr hd sh lam calc no flu	4816.	
209	9261.5	0.009	4.3	0.002			0.0	40.3	2.66	Sst gry brn v f/f gr hd calc no flu	4816.	
210	9262.6	0.026	7.5	0.012	5.1		0.0	29.9	2.67	Sst gry brn v f/f gr hd calc no flu	4817.	
211	9263.4	0.003	2.9	0.001	2.5	3.0	0.0	30.4	2.65	Sst gry brn v f/f gr hd calc no flu	4817.	
* 212	9264.6					3.1	0.0	11.7	2.70	Ls gry brn micro/f xln pbl sdy no flu		
213	9265.3	0.007	1.4	<.001	1.0	1.4	0.0	50.4	2.68	Sst gry brn v f/f gr hd v calc no flu	4818.	
	9266.0- 68.0									UNABLE TO OBTAIN SAMPLE		
* 214	9268.7					5.3	0.0	19.5	2.70	Ls gry brn micro/f xln pbl sdy no flu		
215	9269.4	0.217	8.8	0.110	8.4		0.0	15.9	2.71	Ls gry brn micro/f xln pbl sdy no flu	4820.	
	9270.0- 73.0									UNABLE TO OBTAIN SAMPLE		
* 216	9273.7					3.8	0.0	28.2	2.65	Sst gry brn v rf/f gr hd calc no flu		
* 217	9274.4					1.5	0.0	63.1	2.69	Ls gry brn micro/v f xln hd pbl sdy sh lam foss no flu		
218	9275.6	0.004	3.2	<.001			0.0	30.2	2.65	Sst gry brn v f/f gr hd calc no flu	4823.	

FINAL REPORT 1 - 9

CORE LABORATORIES

Company : MOBIL EXPLORATION & PRODUCTION COMPANY
 Well : Cargill Unit No. 15

Field : Waskom Field
 Formation : Travis Pk, Cotton Valley
 File No.: 57151-15922
 Date : 30-Mar-1989

C O R E A N A L Y S I S R E S U L T S

(HYDROSTATIC CONFINEMENT)

SAMPLE NUMBER	DEPTH ft	NOB (800 psi)		NOB (Reservoir)		POROSITY (HELIUM) %	SATURATION (PORE VOLUME)		GRAIN DENSITY gm/cc	DESCRIPTION	RES PRESS psi
		K=	φ	K=	φ		OIL	WATER			
		md	%	md	%		%	%			
219	9276.2	0.023	6.6	0.018	5.6		0.0	21.0	2.65	Sst gry brn v f/f gr hd calc no flu	4824.
	9277.0- 78.0									UNABLE TO OBTAIN SAMPLE	
220	9278.1	0.012	5.3	0.005			0.0	22.0	2.65	Sst gry brn v f/f gr hd calc no flu	4825.
221	9279.6	0.010	3.8	0.002			0.0	43.6	2.66	Sst gry brn v f/f gr hd sh lam calc no flu	4825.
222	9280.6	0.015	3.9	0.003			0.0	70.0	2.67	Sst gry brn v f/f gr hd sh lam calc no flu	4826.
* 223	9281.1					7.9	0.0	25.7	2.72	Ls gry brn micro/v f xln hd pbl sdy foss no flu	
* 224	9282.6					5.4	0.0	27.8	2.65	Sst gry brn v f/f gr hd calc no flu	
CORE No. 10 9282.9 -9311.3 ft											
225	9283.5	0.010	4.6	0.003			0.0	29.9	2.65	Sst gry brn v f/f gr hd calc no flu	4827.
226	9284.8	0.008	4.3	0.002			0.0	34.9	2.65	Sst gry brn v f/f gr hd calc no flu	4828.
* 227	9285.6					3.5	0.0	38.3	2.71	Ls gry brn micro/f xln hd sdy foss no flu	
* 228	9286.6					2.7	0.0	35.2	2.70	Ls gry brn micro/f xln hd sdy foss no flu	
* 229	9287.5					6.7	0.0	45.3	2.65	Sst gry brn v f/f gr hd calc no flu	
230	9288.9	0.023	7.8	0.004			0.0	34.9	2.65	Sst gry brn v f/f gr hd sh lam calc no flu	4830.
231	9289.5	0.075	7.7	0.012	7.3		0.0	38.3	2.65	Sst gry brn v f/f gr hd sh lam calc no flu	4830.
232	9290.8	0.007	4.2	0.003	4.8		0.0	35.2	2.65	Sst gry brn v f/f gr hd calc no flu	4831.
233	9291.7	0.009	6.0	0.007	4.0		0.0	34.6	2.65	Sst gry brn v f/f gr hd calc no flu	4832.
234	9292.8	0.027	8.6	0.015	8.3		0.0	28.4	2.65	Sst gry brn v f/f gr hd calc no flu	4832.
235	9293.9	0.027	9.2	0.016	8.7		0.0	27.9	2.65	Sst gry brn v f/f gr hd calc no flu	4833.
236	9294.8	0.019	7.8	0.013	7.4		0.0	22.9	2.65	Sst gry brn v f/f gr hd calc no flu	4833.
237	9295.2	0.028	7.4	0.017	6.3		0.0	22.3	2.65	Sst gry brn v f/f gr hd calc no flu	4834.
* 238	9296.3					6.6	0.0	24.0	2.65	Sst gry brn v f/f gr hd calc no flu	
239	9297.5	0.010	4.8	0.005			0.0	42.6	2.65	Sst gry brn v f/f gr hd sh calc no flu	4834.
	9298.2- 02.0									INTERVAL REMOVED BY CLIENT	
240	9298.2	0.007	4.4	0.003			0.0	46.1	2.66	Sst gry brn v f/f gr hd sh calc no flu	4835.
* 241	9302.2					3.2	0.0	49.1	2.65	Sst gry brn v f/f gr hd calc no flu	

CORE LABORATORIES

Company : MOBIL EXPLORATION & PRODUCTION COMPANY
Well : Cargill Unit No. 15

Field : Waskom Field
Formation : Travis Pk, Cotton Valley
File No.: 57151-15922
Date : 30-Mar-1989

CORE ANALYSIS RESULTS
(HYDROSTATIC CONFINEMENT)

SAMPLE NUMBER	DEPTH ft	NOB (800 psi)		NOB (Reservoir)		POROSITY (HELIUM) %	SATURATION		GRAIN DENSITY gm/cc	DESCRIPTION	RES PRESS psi
		K _w md	φ %	K _w md	φ %		(PORE VOLUME) OIL %	WATER %			
242	9303.3	0.010	4.3	0.002			0.0	52.3	2.65	Sst gry brn v f/f gr hd calc no flu	4838.
243	9304.3	0.005	3.1	<.001	2.7	3.1	0.0	42.5	2.65	Sst gry brn v f/f gr hd calc no flu	4838.
244	9305.6	0.010	3.6	<.001			0.0	33.3	2.65	Sst gry brn v f/f gr hd calc no flu	4839.
245	9306.3	0.008	4.2	<.001			0.0	37.4	2.65	Sst gry brn v f/f gr hd calc no flu	4839.
246	9307.2	0.004	3.8	0.001	3.4	3.7	0.0	36.9	2.65	Sst gry brn v f/f gr hd calc no flu	4840.
* 247	9308.6					3.6	0.0	33.9	2.65	Sst gry brn v f/f gr hd calc no flu	
* 248	9309.5					3.8	0.0	43.0	2.65	Sst gry brn v f/f gr hd calc no flu	
249	9310.5	0.006	1.2	<.001	0.8	1.0	0.0	61.0	2.67	Sst gry brn v f/f gr hd calc no flu	4841.
* 250	9311.1					1.2	0.0	74.5	2.68	Sst gry brn v f/f gr hd calc no flu	
CORE No. 11 9313.0 - 9320.4 ft											
251	9313.8	0.005	3.8	<.001			0.0	76.0	2.73	Sst m gry brn v f/f gr hd v sh pyr calc no flu	4843.
252	9314.7	0.009	3.3	0.002	2.8	3.2	0.0	83.7	2.70	Sst m gry brn v f/f gr hd v sh pyr calc no flu	4844.
253	9315.6	0.015	5.9	0.008			0.0	88.6	2.68	Sst m gry brn v f/f gr hd v sh pyr calc no flu	4844.
254	9316.2	0.002	2.7	<.001	2.0	2.7	0.0	61.1	2.66	Sst gry brn v f/f gr hd calc no flu	4845.
255	9317.8	0.004	3.5	<.001	3.3		0.0	74.7	2.66	Sst gry brn v f/f gr hd calc no flu	4846.
256	9318.6	0.023	7.5	0.006	6.0		0.0	56.9	2.67	Sst gry brn v f/f gr hd sh lam calc no flu	4846.
* 257	9319.6					4.7	0.0	48.0	2.66	Sst gry brn v f/f gr hd sh lam calc no flu	
258	9320.2	0.010	5.3	0.004	5.0		0.0	40.8	2.66	Sst gry brn v f/f gr hd sh lam calc no flu	4846.
CORE No. 12 9321.1 - 9340.0 ft											
259	9321.4	0.005	3.7	<.001	3.1	3.8	0.0	41.2	2.66	Sst gry brn v f/f gr hd calc no flu	4847.
260	9322.9	0.015	3.6	0.002			0.0	78.7	2.70	Sst m gry brn v f/f gr hd v sh pyr calc no flu	4848.
261	9323.5	0.013	1.1	<.001	0.2	1.0	0.0	69.9	2.69	Sst m gry brn v f/f gr hd sh pyr calc no flu	4848.
* 262	9324.9					8.4	0.0	44.8	2.66	Sst gry brn v f/f gr hd sh pyr calc no flu	
263	9325.5	0.029	9.1	0.018	7.7		0.0	41.9	2.65	Sst gry brn v f/f gr hd calc no flu	4849.

FINAL REPORT 1 - 11

CORE LABORATORIES

Company : MOBIL EXPLORATION & PRODUCTION COMPANY
 Well : Cargill Unit No. 15

Field : Waskom Field File No.: 57151-15922
 Formation : Travis Pk, Cotton Valley Date : 30-Mar-1989

CORE ANALYSIS RESULTS
 (HYDROSTATIC CONFINEMENT)

SAMPLE NUMBER	DEPTH ft	NOB (800 psi)		NOB (Reservoir)		POROSITY (HELIUM) %	SATURATION (PORE VOLUME)		GRAIN DENSITY gm/cc	DESCRIPTION	RES PRESS psi
		K _o	φ	K _o	φ		OIL %	WATER %			
		md	%	md	%						
* 264	9326.5					10.5	0.0	40.2	2.65	Sst gry brn v f/f gr hd sh lam calc no flu	
265	9327.4	0.042	10.7	0.031	9.8		0.0	37.7	2.65	Sst gry brn v f/f gr hd calc no flu	4850.
* 266	9328.3					10.3	0.0	39.6	2.65	Sst gry brn v f/f gr hd calc no flu	
267	9329.1	0.036	10.8	0.030	8.8		0.0	38.8	2.66	Sst gry brn v f/f gr hd calc no flu	4851.
	9329.7- 30.1									INTERVAL REMOVED BY CLIENT	
268	9330.2	0.030	10.7	0.016	10.3		0.0	39.4	2.65	Sst gry brn v f/f gr hd calc no flu	4852.
	9330.8- 31.3									INTERVAL REMOVED BY CLIENT	
	9331.3- 32.2									PREVIOUSLY SAMPLED, NO PLUG POSSIBLE	
269	9333.2	0.006	5.6	0.001			0.0	41.7	2.65	Sst gry brn v f/f gr hd calc no flu	4853.
	9334.0- 34.3									PREVIOUSLY SAMPLED, NO PLUG POSSIBLE	
	9334.4- 35.0									INTERVAL REMOVED BY CLIENT	
270	9335.4	0.011	5.7	0.005			0.0	46.9	2.65	Sst gry brn v f/f gr hd calc no flu	4854.
271	9336.4	0.012	6.5	0.002			0.0	38.2	2.65	Sst gry brn v f/f gr hd calc no flu	4855.
272	9337.5	0.002	2.2	<.001	1.5	2.5	0.0	73.3	2.67	Sst gry brn v f/f gr hd calc no flu	4855.
273	9338.8	0.010	8.7	0.002			0.0	42.0	2.66	Sst gry brn v f/f gr hd sh lam calc no flu	4856.
* 274	9339.4					5.2	0.0	92.6	2.72	Sst m gry brn v f/f gr hd calc v sh pyr no flu	
CORE No. 13 9340.0 - 9367.9 ft											
275	9340.2	0.007	5.8	0.002			0.0	37.3	2.65	Sst gry brn v f/f gr hd calc no flu	4857.
* 276	9341.3					2.9	0.0	85.2	2.69	Sst gry brn v f/f gr hd v sh pyr calc no flu	
277	9342.7	0.010	4.8	0.004	2.3		0.0	86.9	2.68	Sst gry brn v f/f gr hd v sh pyr calc no flu	4858.
278	9343.5	<.001	2.4		0.9	2.4	0.0	66.0	2.66	Sst gry brn v f/f gr hd calc no flu	4859.
279	9344.4	0.016	5.7	0.003			0.0	85.6	2.73	Sst m gry v f/f gr hd v sh v pyr calc no flu	4859.
280	9345.6	0.188	6.9	0.010	6.1		0.0	88.5	2.72	Sst m gry v f/f gr hd v sh v pyr calc no flu	4860.
281	9346.5	0.156	6.5	0.009	5.6		0.0	96.2	2.75	Sst m gry v f/f gr hd v sh v pyr calc no flu	4860.
* 282	9347.9					4.7	0.0	90.5	2.72	Sst gry brn v f/f gr hd calc no flu	
283	9348.3					1.0	0.0	66.5	2.69	Sst gry brn v f/f gr hd calc no flu	4861.

CORE LABORATORIES

Company : MOBIL EXPLORATION & PRODUCTION COMPANY
Well : Cargill Unit No. 15

Field : Waskom Field
Formation : Travis Pk, Cotton Valley
File No.: 57151-15922
Date : 30-Mar-1989

C O R E A N A L Y S I S R E S U L T S
(HYDROSTATIC CONFINEMENT)

SAMPLE NUMBER	DEPTH ft	NOB (800 psi)		NOB (Reservoir)		POROSITY (HELIUM) %	SATURATION		GRAIN DENSITY gm/cc	DESCRIPTION	RES PRESS psi
		K _w	φ	K _w	φ		(PORE VOLUME)				
		md	%	md	%		OIL %	WATER %			
284	9349.5	0.003	0.8	<.001		0.9	0.0	72.5	2.69	Sst gry brn v f/f gr hd calc no flu	4862.
* 285	9351.2					4.9	0.0	88.8	2.75	Sh dk gry biky hd v foss pyr no flu	
* 286	9351.5					4.7	0.0	87.6	2.76	Sh dk gry biky hd v foss pyr no flu	
* 287	9352.8					4.3	0.0	84.1	2.76	Sh dk gry biky hd v foss pyr grad ls no flu	
* 288	9353.1					2.7	0.0	79.3	2.75	Sh dk gry biky hd v foss pyr grad ls no flu	
289	9354.5	0.024	6.7	0.005			0.0	83.8	2.71	Sst gry brn v f/f gr hd v sh v calc n1 flu	4864.
290	9355.8	0.121	4.8	0.009	4.6		0.0	67.4	2.69	Sst gry brn v f/f gr hd intbd sh calc no flu	4865.
291	9356.7					1.2	0.0	70.1	2.65	Sst gry brn v f/f gr hd calc no flu	4865.
292	9357.9	0.235	5.7	0.010	5.1		0.0	85.1	2.72	Sst dk gry v f/f gr hd v sh calc no flu	4866.
293	9358.5					1.3	0.0	52.4	2.67	Sst gry brn v f/f gr hd sh calc no flu	4866.
294	9359.8					2.8	0.0	92.9	2.78	Sst gry brn v f/f gr hd sh calc no flu	4867.
295	9360.3					2.5	0.0	79.8	2.79	Sst gry brn v f/f gr hd sh calc no flu	4867.
296	9361.4	0.100	6.6	0.009			0.0	82.7	2.73	Sst gry v f/f gr hd sh calc no flu	4868.
	9362.0- 65.2									SHALE, NO ANALYSIS	
										CORE No. 14 9449.0 - 9468.1 ft	
	9362.5- 67.9									INTERVAL REMOVED BY CLIENT	
297	9449.5	0.005	3.5	0.001			0.0	81.9	2.70	Sst gry v f/f gr hd sh v calc no flu	4914.
* 298	9450.6					2.0	0.0	79.1	2.70	Sst gry v f/f gr hd sh v calc no flu	
299	9451.2	0.021	6.7	0.005			0.0	58.6	2.69	Sst gry v f/f gr hd v sh v calc no flu	4915.
300	9452.9	0.029	4.9	0.003	3.7		0.0	84.2	2.71	Sst gry v f/f gr hd v sh v calc no flu	4916.
	9453.4- 55.2									SHALE, NO ANALYSIS	
301	9453.4					2.5	0.0	85.4	2.71	Sst gry v f/f gr hd sh foss calc no flu	4916.
302	9455.5	0.368	6.0	0.021	5.3		0.0	89.2	2.73	Sst gry v f/f gr hd sh foss calc no flu	4917.
303	9456.7	0.010	6.1	0.003			0.0	87.3	2.73	Sst gry v f/f gr hd sh foss calc no flu	4917.
304	9457.7					3.3	0.0	66.7	2.70	Sst gry v f/f gr hd v sh foss calc no flu	4918.
305	9458.7	0.016	4.6	0.002			0.0	77.1	2.70	Sst gry v f/f gr hd v sh foss calc no flu	4918.

FINAL REPORT 1 - 13

CORE LABORATORIES

Company : MOBIL EXPLORATION & PRODUCTION COMPANY
 Well : Cargill Unit No. 15

Field : Waskom Field
 Formation : Travis PK, Cotton Valley Date : 30-Mar-1989

File No.: 57151-15922

CORE ANALYSIS RESULTS

(HYDROSTATIC CONFINEMENT)

SAMPLE NUMBER	DEPTH ft	NOB (800 psi)		NOB (Reservoir)		POROSITY (HELIUM) %	SATURATION			GRAIN DENSITY gm/cc	DESCRIPTION	RES PRESS psi
		K _w md	φ %	K _w md	φ %		(PORE VOLUME)					
							OIL %	WATER %				
306	9459.4					4.3	0.0	81.4	2.70	Sst gry v f/f gr hd v sh foss calc no flu	4919.	
307	9460.3	0.046	6.0	0.006			0.0	83.5	2.72	Sst gry v f/f gr hd v sh foss calc no flu	4919.	
* 308	9461.5					5.5	0.0	83.7	2.72	Sst gry v f/f gr hd v sh foss calc no flu		
* 309	9462.1					4.1	0.0	84.1	2.71	Sst gry v f/f gr hd sh calc no flu		
	9463.0- 68.1									SHALE, NO ANALYSIS		
CORE No. 15 9469.0 - 9482.0 ft												
* 310	9469.5					5.9	0.0	98.6	2.74	Sh dk gry blkly hd sdy pyr no flu		
	9470.0- 73.0									SHALE, NO ANALYSIS		
* 311	9473.1					6.1	0.0	96.3	2.74	Sh dk gry blkly hd intbd sd pyr no flu		
	9474.0- 75.0									SHALE, NO ANALYSIS		
* 312	9475.2					5.6	0.0	95.4	2.76	Sh dk gry blkly hd sdy pyr no flu		
	9476.0- 79.0									SHALE, NO ANALYSIS		
313	9479.7	0.147	5.4	0.009	4.5		0.0	95.1	2.75	Sh dk gry blkly hd sdy v foss pyr no flu	4929.	
	9480.0- 82.0									SHALE, NO ANALYSIS		
CORE No. 16 94482.0 - 9500.0 ft												
314	9482.6	0.228	5.4	0.017	4.8		0.0	93.7	2.75	Sh dk gry blkly hd sdy v foss no flu	4931.	
* 315	9483.3					4.3	0.0	91.3	2.74	Sh dk gry blkly hd sdy foss no flu		
* 316	9484.9					6.6	0.0	93.9	2.77	Sh dk gry blkly hd sdy foss no flu		
	9485.0- 91.0									SHALE, NO ANALYSIS		
* 317	9491.5					6.5	0.0	95.8	2.76	Sh dk gry blkly hd sdy v foss no flu		
* 318	9494.2					5.8	0.0	92.8	2.76	Sh dk gry blkly hd sdy v foss no flu		
* 319	9495.1					1.8	0.0	81.3	2.74	Sh dk gry blkly hd sdy v foss v calc grad ls no flu		
	9495.5- 99.0									SHALE, NO ANALYSIS		
* 320	9499.3					3.1	0.0	93.2	2.73	Sh dk gry blkly hd sdy foss no flu		

CORE LABORATORIES

Company : MOBIL EXPLORATION & PRODUCTION COMPANY
 Well : Cargill Unit No. 15

Field : Waskom Field
 Formation : Travis Pk, Cotton Valley
 File No.: 57151-15922
 Date : 30-Mar-1989

CORE ANALYSIS RESULTS
 (HYDROSTATIC CONFINEMENT)

SAMPLE NUMBER	DEPTH ft	NOB (800 psi)		NOB (Reservoir)		POROSITY (HELIUM) %	SATURATION (PORE VOLUME)		GRAIN DENSITY gm/cc	DESCRIPTION	RES PRESS psi
		K _w	φ	K _w	φ		OIL	WATER			
		md	%	md	%		%	%			
* INDICATES FRACTURED SAMPLES: CMS-300 TESTING NOT PERFORMED @ INDICATES PERMEABILITY AT 800 PSI <.0005 md: CMS-300 UNABLE TO ANALYZE											

FINAL REPORT 1 - 15

Appendix 3

WELL TEST ANALYSIS AND FRACTURE TREATMENT SUMMARY

A3

W E L L T E S T A N A L Y S I S

Gas Well Analysis
 Buildup Test
 Test period preceded by one rate

Operator : GAS RESEARCH INSTITUTE
 Well : SFE NO. 3 (CARGILL UNIT WELL NO. 15)
 Location : WASKOM FIELD, HARRISON COUNTY, TEXAS
 Formation : COTTON VALLEY

Perforated Interval : 9225-9250, 9285-9330
 Analyst : S. A. HOLDITCH & ASSOCIATES
 Test Date : 6/16 - 7/14/89

Remarks : POST-FRACTURE PRESSURE BUILDUP TEST

RESERVOIR PARAMETERS

Net pay (ft)	40.00
Wellbore radius (ft)	.3650
Porosity (fraction)	.0920

Gas saturation (fraction)	.7000
Oil saturation (fraction)	.0000
Water saturation (fraction)	.3000
Formation compressibility (1/psi)	.0000040
Total compressibility (1/psi)	.0002467

RESERVOIR FLUID PROPERTIES

Bottom hole temperature (deg F)	246.00
Separator gas gravity	.6420
Mole percent hydrogen sulfide (%)	.0000
Mole percent carbon dioxide (%)	.0000
Mole percent nitrogen (%)	.0000
Gas-condensate ratio (scf/STB)	139578.
Condensate gravity (Deg API)	50.00
Gas equivalent of condensate (scf/STB)	751.590
Wet gas specific gravity	.6640
Water compressibility (1/psi)	.0000036

PRODUCTION PARAMETERS

Input pressure at t = 0 (psig)	1856.42
Initial drainage area pressure (psia)	3600.00
Corrected pressure at t = 0 (psia)	1871.12
Adjusted initial drainage area pressure (psia)	2457.95
Adjusted pressure at t = 0 (psia)	758.14
Atmospheric pressure correction (psi)	14.70
Total pressure correction (psi)	14.70
Time correction	.0000

FLUID PROPERTIES AT AVERAGE PRESSURE

Average pressure (psia)	2735.56
Gas viscosity (cp)	.01784
Total compressibility (1/psi)	.0002467
Z-Factor	.92066
Gas formation volume factor (RB/Mcf)	1.19645
Pressure adjustment factor (cp/psia)	.30019E-05
Time adjustment factor (cp/psia)	.44006E-05

SEMI-LOG ANALYSIS

Semi-log slope (psi/cycle)	-668.36
Permeability (md)	.0418
Permeability thickness, kh (md-ft)	1.6706
Skin factor	-4.859
Adjusted pressure at an adjusted time of one hour (psia)	-286.11
Pressure at an adjusted Horner time ratio of one, p* (psia)	3250.20
Radius of investigation (ft)	
End of test	268.1
End of production	601.9
Start of middle-time region	268.1

LINEAR FLOW ANALYSIS

Slope of linear flow (psi/sqrt(hr))	37.63
Permeability (md)	.0200
Fracture half-length (ft)	206.05
Permeability-fracture length (kLf) (md-ft)	849.15

TYPE CURVE ANALYSIS - FINITE CONDUCTIVITY VERTICAL FRACTURE

Permeability (md) .0198
 Permeability thickness, kh (md-ft) .791
 Fracture half-length (ft) 195.7
 Dimensionless fracture conductivity 96.38
 Fracture conductivity (md-ft) 1172.

MATCH POINT

Dimensionless pressure .8160
 Dimensionless time .3365E-03
 Adjusted Pressure Change (psi) 1000.
 Equivalent Adjusted Time (hr) 1.000

TYPE CURVE ANALYSIS - INFINITE CONDUCTIVITY VERTICAL FRACTURE WITH WELLBORE STORAGE

Permeability (md) .0210
 Permeability thickness, kh (md-ft) .838
 Fracture half-length (ft) 170.7
 Dimensionless wellbore storage coefficient .9784E-02
 Wellbore storage coefficient (bbl/psi) .2895

MATCH POINT

Dimensionless pressure .8643
 Dimensionless time .4685E-03
 Adjusted Pressure Change (psi) 1000.
 Equivalent Adjusted Time (hr) 1.000

RATE DATA

Input Rates		Calculated	
Cumulative Time (Day)	Gas Rate (Mscf/D)	Adjusted Cumulative Time (hr)	Gas Rate (Mscf/D)
1 106.65	320.00	3328.8	321.72

TIME AND PRESSURE DATA

	Time (hr)	Pressure (psia)	Equivalent Adjusted Time (hr)	Adjusted Horner Time Ratio	Adjusted Pressure (psia)
1	.11111E-01	1871.2	.78962E-02	.42157E+06	758.18
2	.16667E-01	1872.2	.11845E-01	.28102E+06	758.95
3	.25000E-01	1874.1	.17773E-01	.18729E+06	760.43
4	.33333E-01	1875.3	.23705E-01	.14042E+06	761.38
5	.41667E-01	1876.4	.29640E-01	.11231E+06	762.21
6	.50000E-01	1877.2	.35578E-01	93562.	762.82
7	.58333E-01	1878.0	.41518E-01	80176.	763.44
8	.66667E-01	1878.7	.47460E-01	70138.	763.94
9	.75000E-01	1879.3	.53404E-01	62332.	764.38
10	.83333E-01	1879.7	.59349E-01	56088.	764.73
11	.10000	1880.6	.71243E-01	46724.	765.44
12	.11667	1881.4	.83142E-01	40038.	766.02
13	.13333	1882.2	.95045E-01	35023.	766.62
14	.15000	1883.0	.10695	31124.	767.28
15	.15833	1883.5	.11291	29483.	767.63
16	.17972	1884.4	.12820	25966.	768.34
17	.20639	1885.6	.14727	22603.	769.22
18	.24639	1887.3	.17590	18925.	770.53
19	.28639	1888.5	.20454	16274.	771.49
20	.32639	1889.8	.23321	14274.	772.54
21	.38695	1891.4	.27663	12034.	773.77
22	.46028	1893.1	.32925	10110.	775.12
23	.59361	1895.9	.42502	7832.1	777.28
24	.72695	1898.3	.52090	6390.5	779.16
25	.97500	1902.3	.69953	4758.6	782.24
26	1.2417	1905.7	.89186	3732.4	784.91
27	1.5083	1908.7	1.0845	3069.5	787.23
28	2.0433	1913.9	1.4715	2262.1	791.31
29	2.5853	1918.4	1.8644	1785.5	794.76
30	3.3853	1928.1	2.4460	1360.9	802.43
31	4.1853	1936.6	3.0299	1098.6	809.10
32	4.9853	1944.1	3.6157	920.64	815.03
33	5.7853	1950.8	4.2032	791.96	820.38
34	6.5853	1957.2	4.7923	694.62	825.46
35	7.3853	1963.2	5.3827	618.42	830.17
36	8.1853	1968.8	5.9745	557.16	834.69
37	8.9853	1974.3	6.5676	506.85	839.11
38	9.7853	1979.5	7.1619	464.79	843.27
39	10.585	1984.7	7.7574	429.11	847.45
40	11.385	1989.8	8.3540	398.47	851.55
41	12.185	1994.7	8.9518	371.86	855.51
42	12.985	1999.3	9.5506	348.54	859.24
43	13.785	2003.8	10.150	327.95	862.89
44	14.585	2008.2	10.751	309.62	866.44
45	15.385	2012.4	11.353	293.21	869.90
46	16.185	2016.6	11.955	278.43	873.27
47	16.985	2020.6	12.559	265.05	876.51
48	17.785	2024.5	13.163	252.89	879.73
49	18.585	2028.3	13.768	241.78	882.84

50	19.385	2032.0	14.374	231.59	885.86
51	20.185	2035.7	14.980	222.21	888.81
52	21.077	2039.7	15.657	212.60	892.12
53	23.477	2049.9	17.483	190.40	900.61
54	25.877	2059.7	19.314	172.35	908.68
55	28.327	2069.2	21.189	157.10	916.48
56	30.727	2078.1	23.031	144.53	923.90
57	33.127	2086.5	24.878	133.81	930.97
58	35.527	2094.7	26.728	124.54	937.83
59	37.927	2102.6	28.583	116.46	944.41
60	40.327	2110.2	30.442	109.35	950.75
61	42.727	2117.6	32.304	103.05	957.03
62	45.127	2124.7	34.170	97.419	963.02
63	47.527	2131.6	36.039	92.367	968.88
64	49.927	2138.3	37.911	87.805	974.52
65	52.327	2144.8	39.786	83.667	980.05
66	54.727	2151.2	41.664	79.896	985.55
67	57.127	2157.4	43.545	76.446	990.87
68	59.527	2163.4	45.428	73.277	996.02
69	61.927	2169.3	47.313	70.357	1001.1
70	64.327	2175.1	49.201	67.657	1006.0
71	66.727	2180.8	51.091	65.154	1010.9
72	69.127	2186.3	52.983	62.828	1015.7
73	71.527	2191.7	54.877	60.659	1020.4
74	73.927	2197.0	56.773	58.633	1025.0
75	76.327	2202.2	58.671	56.737	1029.5
76	78.727	2207.4	60.570	54.958	1034.0
77	81.127	2212.4	62.471	53.285	1038.3
78	83.527	2217.3	64.374	51.710	1042.6
79	85.677	2221.7	66.080	50.376	1046.4
80	89.332	2228.9	68.982	48.256	1052.8
81	93.170	2236.4	72.034	46.212	1059.3
82	97.170	2244.0	75.217	44.256	1066.0
83	101.17	2251.4	78.404	42.457	1072.5
84	105.17	2258.6	81.594	40.797	1078.8
85	109.17	2265.7	84.786	39.261	1085.1
86	113.17	2272.6	87.981	37.835	1091.2
87	117.17	2279.3	91.178	36.509	1097.3
88	121.17	2286.0	94.377	35.271	1103.2
89	125.17	2292.5	97.578	34.114	1109.0
90	129.17	2298.9	100.78	33.030	1114.7
91	133.17	2305.1	103.99	32.012	1120.3
92	137.08	2311.1	107.12	31.076	1125.7
93	141.41	2317.7	110.59	30.100	1131.6
94	145.41	2323.7	113.80	29.251	1136.9
95	149.41	2329.6	117.01	28.449	1142.2
96	153.41	2335.3	120.22	27.690	1147.4
97	157.41	2341.0	123.43	26.969	1152.6
98	161.41	2346.6	126.64	26.285	1157.6
99	165.41	2352.1	129.85	25.635	1162.6
100	169.41	2357.5	133.06	25.017	1167.5
101	173.41	2362.8	136.28	24.427	1172.4
102	177.41	2368.1	139.49	23.864	1177.2
103	181.41	2373.3	142.70	23.327	1182.0
104	185.41	2378.5	145.91	22.814	1186.7
105	189.41	2383.5	149.12	22.322	1191.3
106	193.41	2388.6	152.34	21.852	1196.0
107	197.41	2393.5	155.55	21.401	1200.4

108	201.41	2398.3	158.76	20.968	1204.9
109	206.25	2404.1	162.64	20.467	1210.2
110	214.25	2413.5	169.06	19.690	1218.9
111	222.25	2422.7	175.47	18.971	1227.4
112	230.25	2431.6	181.88	18.302	1235.7
113	238.25	2440.4	188.29	17.679	1243.8
114	246.25	2448.9	194.69	17.098	1251.8
115	254.25	2457.3	201.08	16.555	1259.7
116	262.25	2465.5	207.47	16.045	1267.3
117	270.25	2473.4	213.85	15.566	1274.8
118	278.25	2481.2	220.22	15.116	1282.1
119	286.25	2488.9	226.59	14.691	1289.3
120	294.25	2496.4	232.95	14.290	1296.4
121	302.25	2503.7	239.30	13.911	1303.4
122	310.25	2510.9	245.64	13.552	1310.1
123	318.25	2518.0	251.97	13.211	1316.8
124	326.25	2524.9	258.29	12.888	1323.4
125	334.25	2531.6	264.60	12.581	1329.9
126	342.25	2538.3	270.90	12.288	1336.3
127	350.25	2544.9	277.19	12.009	1342.5
128	358.25	2551.3	283.47	11.743	1348.7
129	366.43	2557.7	289.89	11.483	1354.8
130	374.44	2563.9	296.14	11.241	1360.8
131	382.86	2570.3	302.71	10.996	1366.9
132	390.86	2576.3	308.95	10.775	1372.7
133	399.08	2582.3	315.34	10.556	1378.5
134	407.08	2588.1	321.54	10.353	1384.0
135	415.08	2593.7	327.74	10.157	1389.5
136	423.08	2599.2	333.92	9.9689	1394.9
137	431.34	2605.0	340.29	9.7823	1400.5
138	439.34	2610.3	346.44	9.6085	1405.6
139	447.34	2615.7	352.58	9.4412	1410.9
140	460.92	2625.9	362.98	9.1708	1420.8
141	484.08	2639.0	380.62	8.7458	1433.6
142	508.08	2653.4	398.76	8.3478	1447.8
143	532.08	2667.1	416.77	7.9871	1461.3
144	556.08	2680.3	434.65	7.6586	1474.2
145	580.08	2692.6	452.39	7.3583	1486.5
146	604.08	2704.7	469.98	7.0828	1498.4
147	628.08	2716.2	487.43	6.8293	1509.9
148	652.08	2727.3	504.73	6.5952	1521.0
149	660.58	2731.0	510.82	6.5166	1524.7

3/16/89

Date

S. A. HOLDITCH & ASSOCIATES, INC.

ACID AND FRACTURE TREATMENT SUMMARY SHEET

Company GRI

Well Name SFE No. 3

Tubing Size & Weight 2 3/8", 4.7# Tubing Volume 35 bbls

Packer Depth NA Casing Volume

Casing Size & Weight To Perfs 291bbls (Annulus)

Below Packer Total Flush Volume 291 bbls

Casing Size & Weight Perforations 9225-9250, 9285-9330

(If frac down casing) 7", 29#

annulus SITP SICP

Tested Frac Lines to 5500 psig

Pressured Tubing-Casing Annulus to

(Post-Frac)ISIP 2970 5 min 2950 10 min 2950 15 min 30 min

Time	Fluid Type	Stage Volume (gal)	Cum. Volume (gal)	Inj. Rate (BPM)	Tubing Pres. (psi)	Casing Pres. (psi)	Remarks
7:31	40# linear gel			21	2050	2300	(Wellbore fluid - 40# linear gel)
7:35	40# linear gel	4200	4200	30	2150	2560	
7:39	40# linear gel			40	2250	2920	pH = 6.7
7:43	40# linear gel	16200	16200	50	2350	3150	Start BA-40 (.8 gal/1000 gal)
7:48	40# linear gel			50.5	2460	3290	pH = 10.5
7:51	40# linear gel	34400	34400	50.0	2500	3320	cut BA-40
7:53	40# linear gel	40500	40500	50.0	2540	3380	pH = 8.8, start 3rd tank
7:57	40# linear gel	47500	47500	50.1	2560	3400	pH = 6.1, diesel = 1.2 BPM
8:02	40# linear gel	58010	58010	50.0	2590	3450	finish gel; flush w/slick
8:06	Slick Water	8490	66500	50.1	2610	3470	cut WAC-9 in flush
8:08	Slick water	12340	70350	50.2	2620	3460	Flush complete
					2400	2450	ISIP
Halliburton total on diesel = 36.5 bbls							
8:20					2190	2150	12 min SIP
Flush for mini-frac is first part of slick water pre-pad							
8:28					2090	2170	20 min SIP
11:38					1700	1820	3 1/2 hour SIP
11:38	Slick water	0	70250	10.6	1940	1940	
11:40	Slick water	1300	71550	20.2	2110	2320	pH = 6.4
11:42	Slick water	30000	73250	30.3	2280	2740	diesel - 0.8 BPM
11:43	Slick water	5200	75450	41.0	2430	3150	
11:46	Slick water	10550	80800	50.4	2470	3400	diesel - 1.2 BPM
11:47	Slick water	12320	82570	50	2500	3300	Slick on perfs

Time	Fluid Type	(Slurry) Stage Volume (gal)	Cum. Volume (gal)	Inj. Rate (BPM)	Tubing Pres. (psi)	Casing Pres. (psi)	Remarks
11:50	Slick water	19500	89750	50.4	2530	3320	Start BA-40
11:53	Slick water	25000	95250	50.3	2600	3380	pH = 11.2
11:54 1/2	Slick water						
11:55	Slick water	29670	99920				Start gel
12:00	50# Gel	11000	110920	50.2	2650	3490	pH = 11.0, XL = 1.1 gpm
12:01	50# Gel	12320	112240	50.3	2650	3520	Gel on perfs
12:11	50# Gel	33100	133020	50.2	2830	3700	Vis = 43 cps, pH = 10.7
12:28	50# Gel	66700	166620	49.1	2800	3600	problems with suction -
12:35	50# Gel	80500	180420	50.5	2830	3700	rate fluctuating
12:45	50# Gel	102800	202720	50.0	2860	3750	pH = 9.8, Vis = 49
12:56	50# Gel	126000	225920	50.4	2880	3800	Start 100 mesh
12:59	50# Gel	5500	231420	50.3	2900	3720	1.0 ppg
13:02 1/2	50# Gel	12320	238240	50.6	2910	3670	100 mesh on perfs
13:03	50# Gel	13170	239090	50.7	2920	3700	cut 100 mesh; start 40# gel
13:04	40# Gel	8500	247590	50.0	2930	3730	
13:08 1/2	40# Gel	11470	250560	50.0	2930	3730	100 mesh flushed
13:11	40# Gel	16800	255890	49.9	2930	3720	Start 1 ppg 20/40 sand
13:13	40# Gel	5000	260890	50.3	2920	3660	1.1 ppg
13:16 1/2	40# Gel	12320	268210	50.2	2920	3560	1# on perfs
13:19	40# Gel	17560	273450	50.3	2920	3500	Start 2 ppg stage
13:23	40# Gel	8200	281650	50.5	2920	3400	
13:25	40# Gel	12320	285770	50.0	2910	3360	2 ppg on perfs
13:30	40# gel	22910	296360	50.6	2930	3350	Start 3 ppg stage
13:32	40# Gel	5150	301510	50.5	2920	3300	3.0 ppg
13:35 1/2	40# Gel	12320	308680	50.1	2930	3210	3# on perfs
13:38 1/2	40# Gel	18500	314860	50.1	2930	3200	pH = 10.5, XL = 0.7 gpm
13:41	40# Gel	23870	320230	50.1	2930	3180	Start 4 ppg stage
13:42	40# Gel	3400	323630	50.1	2940	3140	3.7 ppg
13:43	40# Gel	4800	325030	50.1	2940	3120	4.0 ppg
13:47	40# Gel	12320	332550	50.0	2940	3050	4# on perfs
13:52	40# Gel	23650	343880	50.1	2950	3020	4.0 ppg
13:54	40# Gel	27500	347730	50.2	2950	3030	Start inc. sand to 5#
13:55	40# Gel	29790	350020	50.1	2950	3020	Start 5 ppg stage
13:58	40# Gel	6600	356620	50.3	2960	3000	
14:01	40# Gel	12320	362340	50.3	2970	2950	5.0 ppg, XL = 0.7 gpm, pH=10.2
14:07	40# Gel	26000	376020	50.4	2980	2970	
14:14	40# Gel	41260	391280	50.2	2980	2950	Start 6 ppg
14:16 1/2	40# Gel	4600	395880	50.3	2970	2920	5.9 ppg

Time	Fluid Type	Stage Volume (gal)	Cum. Volume (gal)	Inj. Rate (BPM)	Tubing Pres. (psi)	Casing Pres. (psi)	Remarks
14:20 1/2	40# X-L Gel	12320	403600	50.3	2970	2860	6 ppg on perfs
14:24	Lost suction - rate dropped - sand dropped to 3-4 ppg (only lasted approx. 1 minute)						
14:26	40# X-L Gel	26200	417480	50.1	2970	2900	5.9 ppg
14:35	40# X-L Gel	43900	435180	49.4	2980	2850	6.0 ppg
14:36	40# X-L Gel			50.3	2980	2820	Start inc sand (6 tanks of fluid remaining)
14:37	40# X-L Gel	48140	439420	50.6	2990	2750	Start 7 ppg stage (5600 SX left)
14:40	40# X-L Gel	7000	446420	50.6	2990	2750	6.8 ppg
14:43	40# X-L Gel	12320	451740	50.5	2990	2710	7 ppg on perfs
14:49	40# X-L Gel	25450	464870	50.1	3000	2680	6.9 ppg
14:55	40# X-L Gel	38500	477920	50.4	3010	2680	6.9 ppg
14:59	40# X-L Gel	46500	485920	50.3	3020	2700	7.0 ppg (start inc. sand)
15:01	40# X-L Gel	49860	489280	50.6	3030	2690	Start 8 ppg
15:02	40# X-L Gel	3450	492730	50.2	3030	2660	7.6 ppg
15:07	40# X-L Gel	12320	501600	50.6	3040	2630	8# on perfs (7.6 ppg - RES)
15:14	40# X-L Gel	29000	518280	50.0	3050	2570	8.4 ppg
15:20	40# X-L Gel	41500	530780	50.6	3070	2630	7.7 ppg-RES; 8.0 ppg Halliburton
15:23	40# X-L Gel	47800	537080	50.1	3080	2630	8.0 ppg
15:27	40# X-L Gel	56270	545550	50.4	3080	2630	8.0 ppg; cut sand; start flush
15:29	40# linear/Slick	4000	549550	50.3	3080	2800	drop rate
15:30	Slick water	6500	552050	40.0	3060	2950	
15:31	Slick water	7200	552750	30.3	3040	3020	drop rate
15:32	Slick water	9000	554550				
15:33	Slick water	10000	555550	30.3	3040	3200	drop rate - bring pumps down
15:36	Slick water	12280	557830	10.0	3000		finish flush
					2970	2870	ISIP
15:41					2950	2860	5 min SIP
15:46					2950	2860	10 min SIP

Note: Volumes are from Halliburton flow meters and include sand.

Halliburton total fluid = 487,480 gallons - since shut down
27,500 lbs extra sand pumped.

